

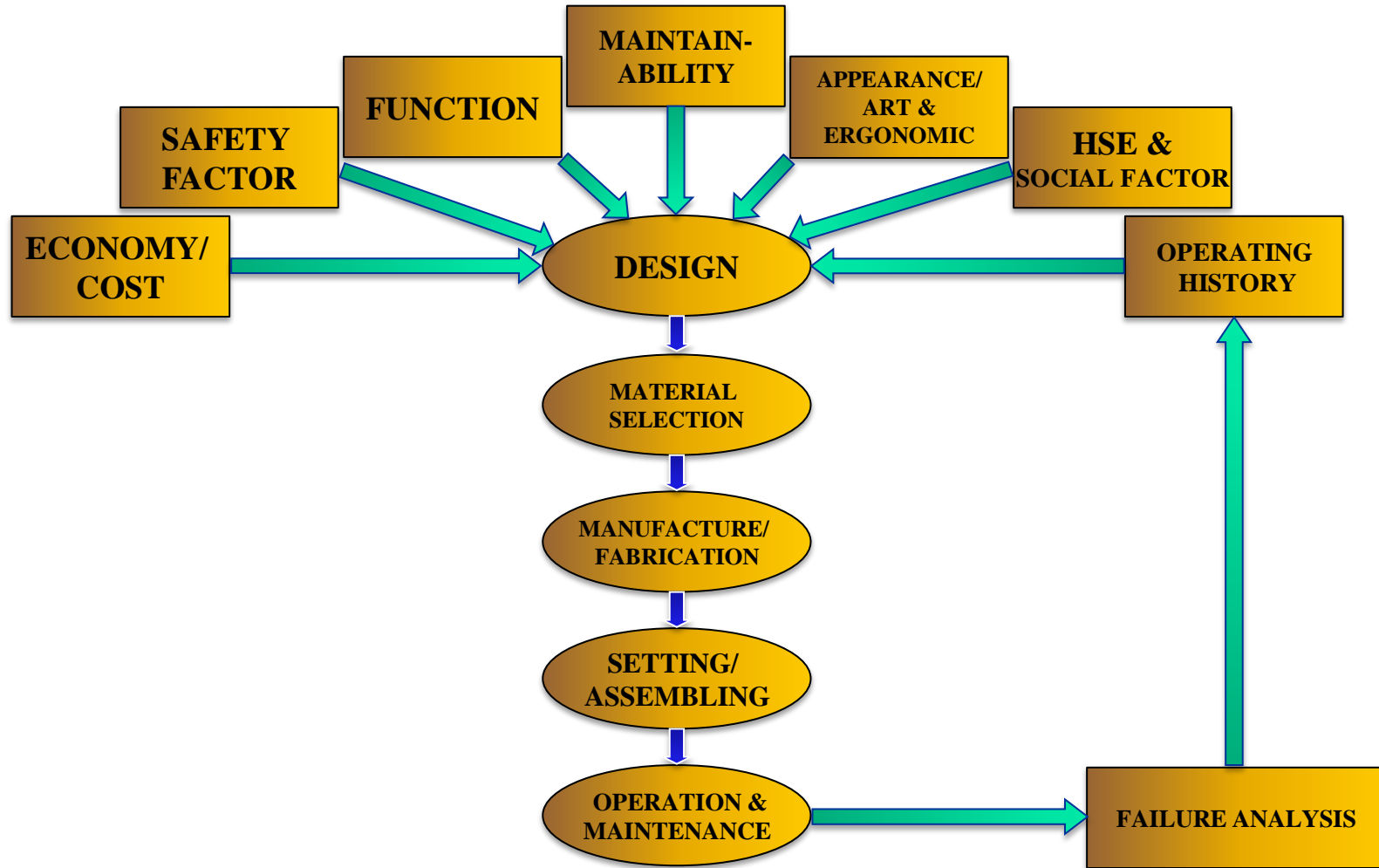
ENGINEERING SERVICES FOR VARIOUS INDUSTRIES

**(Oil&Gas, Chemical&Petrochemical, Power Generation,
Pulp&Paper, Mining&Cement, Agro&Palm Oil Processing,
Maritime, Transportation, Building&Construction,
Metal Manufacturing&Fabrication,
Loss Adjuster/Insurance, etc).**

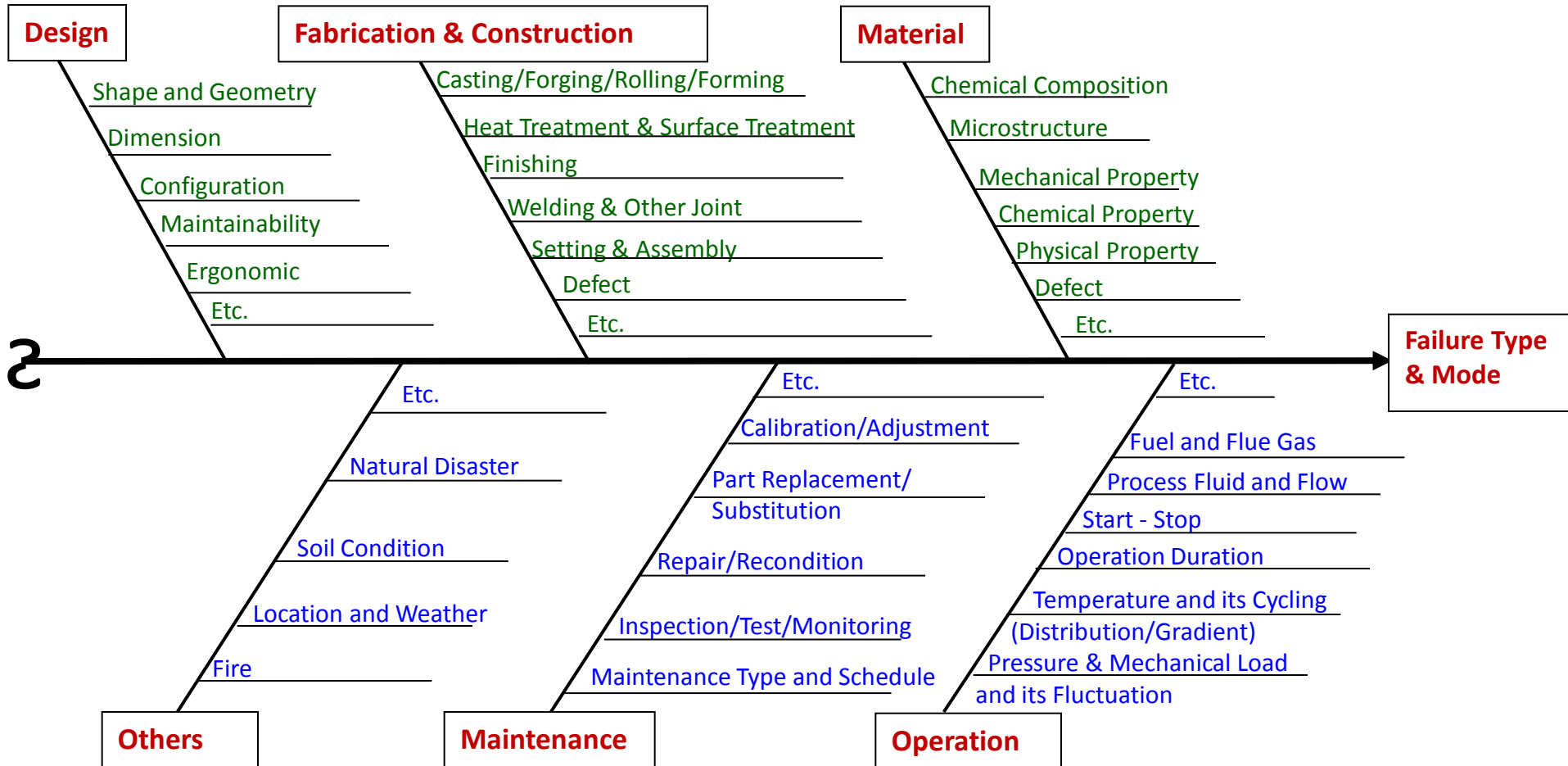
**BY
PT. EMPU AGUNG SAKTI**

I Engineering Services in the field of **ROOT CAUSE FAILURE ANALYSIS (RCFA)**

FACTORS AFFECTING TO THE FAILURE OF EQUIPMENT



CLASSIFICATION OF FACTORS AFFECTING FAILURE



**Deterioration and Damage Mechanisms that may reduce
the Component's Life or Cause its Failure**

(According to API RP 571)

A. Mechanical and Metallurgical Failure

B. Uniform or Localized Loss of Thickness

C. High Temperature Corrosion

D. Environment Assisted Cracking

Deterioration and Damage Mechanisms that may reduce the Component's Life or Cause its Failure

(According to API RP 571)

A. Mechanical and Metallurgical Failure Mechanisms

- Graphitization
- Softening (Spheroidization)
- Temper Embrittlement
- Strain Aging
- 885⁰F Embrittlement
- Sigma Phase Embrittlement
- Brittle Fracture
- Creep / Stress Rupture
- Thermal Fatigue
- Short Term Overheating - Stress Rupture
- Steam Blanketing
- Dissimilar Metal Weld (DMW) Cracking
- Thermal Shock
- Erosion / Erosion-Corrosion
- Cavitations
- Mechanical Fatigue
- Vibration-Induced Fatigue
- Refractory Degradation
- Reheat Cracking

Deterioration and Damage Mechanisms that may reduce the Component's Life or Cause its Failure

**(According to API RP 571)
(Continued)**

B. Uniform or Localized Loss of Thickness

- Galvanic Corrosion
- Atmospheric Corrosion
- Corrosion Under Insulation (CUI)
- Cooling Water Corrosion
- Boiler Water Condensate Corrosion
- CO₂ Corrosion
- Flue Gas Dew Point Corrosion
- Microbiologically Induced Corrosion (MIC)
- Soil Corrosion
- Caustic Corrosion
- Dealloying
- Graphitic Corrosion

Deterioration and Damage Mechanisms that may reduce the Component's Life or Cause its Failure

**(According to API RP 571)
(continued)**

C. High Temperature Corrosion [400⁰F (204⁰C)]

- Oxidation
- Sulfidation
- Carburization
- Decarburization
- Metal Dusting
- Fuel Ash Corrosion
- Nitriding

D. Environment – Assisted Cracking

- Chloride Stress Corrosion Cracking (Cl - SCC)
- Corrosion Fatigue
- Caustic Stress Corrosion Cracking (Caustic Embrittlement)
- Ammonia Stress Corrosion Cracking
- Liquid Metal Embrittlement (LME)
- Hydrogen Embrittlement (HE)

REFINING INDUSTRY DAMAGE MECHANISMS
(According to API RP 571)

- A. Uniform or Localized Loss in Thickness Phenomena**
- B. Environment-Assisted Cracking**
- C. Other Mechanisms**

REFINING INDUSTRY DAMAGE MECHANISMS (According to API RP 571)

A. Uniform or Localized Loss in Thickness Phenomena

- Amine Corrosion
- Ammonium Bisulfide Corrosion (Alkaline Sour Water)
- Ammonium Chloride Corrosion
- Hydrochloric Acid (HCl) Corrosion
- High Temp H₂/H₂S Corrosion
- Hydrofluoric (HF) Acid Corrosion
- Naphthenic Acid Corrosion (NAC)
- Phenol (Carbonic Acid) Corrosion
- Phosphoric Acid Corrosion
- Sour Water Corrosion (Acidic)
- Sulfuric Acid Corrosion

REFINING INDUSTRY DAMAGE MECHANISMS

**(According to API RP 571)
(continued)**

B. Environment–Assisted Cracking

- Polythionic Acid Stress Corrosion Cracking (PASCC)
- Amine Stress Corrosion Cracking
- Wet H₂S Damage (Blistering / HIC / SOHIC / SCC)
- Hydrogen Stress Cracking – HF
- Carbonate Stress Corrosion Cracking

C. Other Mechanisms

- High Temperature Hydrogen Attack (HTHA)
- Titanium Hydriding

EMAS's team of experts is skilled at investigating the proximate cause of failure in static and rotating plant equipment. Our staff employ a multidisciplinary approach to examining the full spectrum failure causes including design issues, materials of construction and manufacture, operational and maintenance regimes. Following a failure analysis investigation we will make recommendations aimed at preventing further failures and can assist clients with implementing corective procedures.

- ❑ Data Collection (Design, Dimension, Material Specification, Operation Condition and Maintenance and Inspection Records).**
- ❑ Preliminary Examination of the Failed Part such as: Visual Examination and Record Keeping, Dimensional Measurement, and/or Non-Destructive Tests (PT, MPI, UT, RT, ECT).**
- ❑ Preparation of Samples for Laboratory Examination.**
- ❑ Macroscopic Examination on Damaged/Fracture Surface by a Stereomicroscope.**
- ❑ Chemical Analysis using an Optical Spark Emission Spectrometer.**
- ❑ Metallographic Examination using an Optical Light Microscopy.**

- ❑ Hardness Test using Vickers Method or Other Methods.**
- ❑ Other Mechanical Tests if required (Tensile Test, Bend Test, Charpy V-Notch Test, Fatigue Test, Creep Test, etc).**
- ❑ Microfractographic Examination on Damaged/Fracture Surfaces by SEM (Scanning Electron Microscopy)**
- ❑ EDS (Energy Dispersive Spectroscopy) and XRD (X-Ray Diffraction) Analysis on Damaged/Fracture Surface Deposit to detect the presence of any corrosion by products or others.**
- ❑ Other Tests and Measurements (Stress/Fracture Mechanics Analysis, Corrosion Test, Vibration Measurement and Analysis, etc).**
- ❑ Analysis of All Data or Evidence, Formulation of Conclusions and Writing the Report (Including Recommendations).**

Highlights of Case Studies

in

ROOT CAUSE FAILURE ANALYSIS (RCFA)

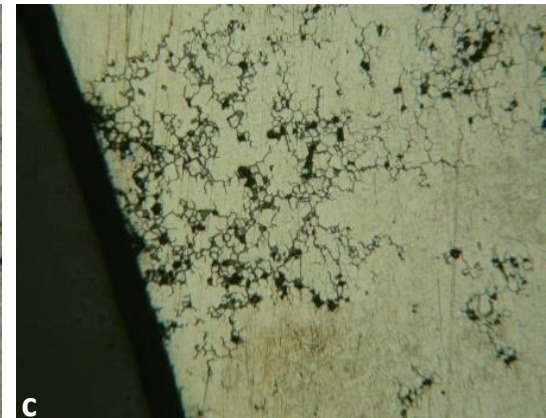
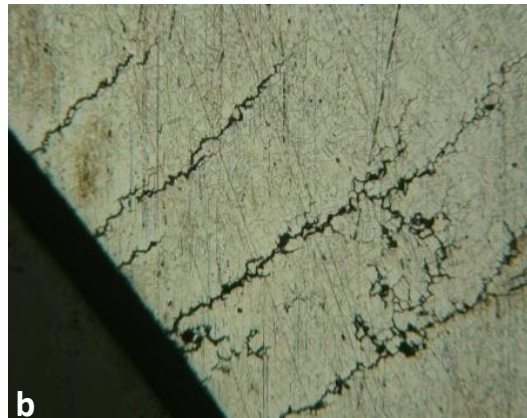
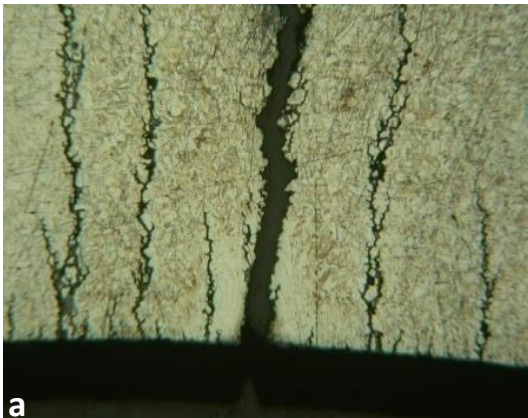
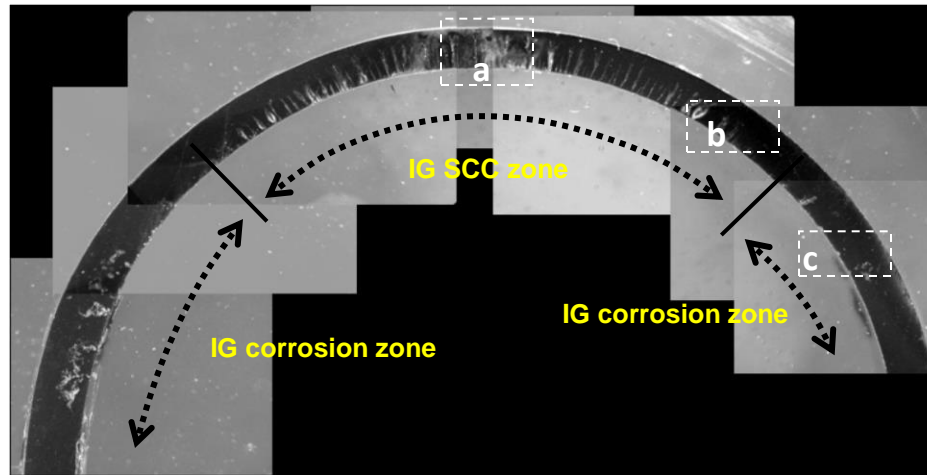


Photograph of a Pre-Heater equipped with an expansion bellows



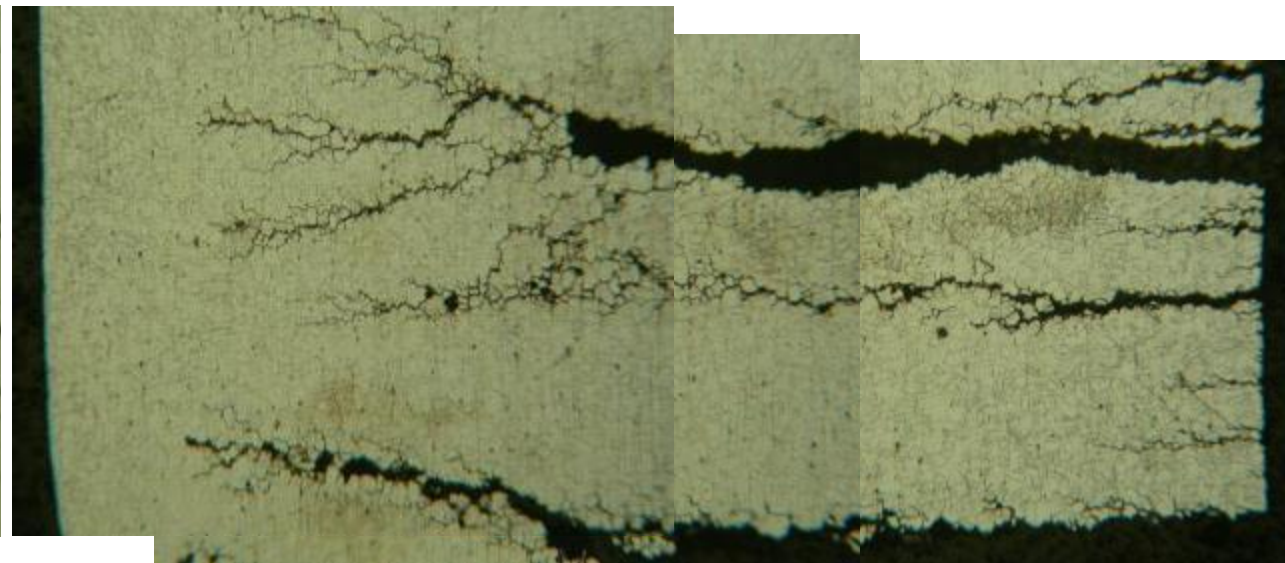
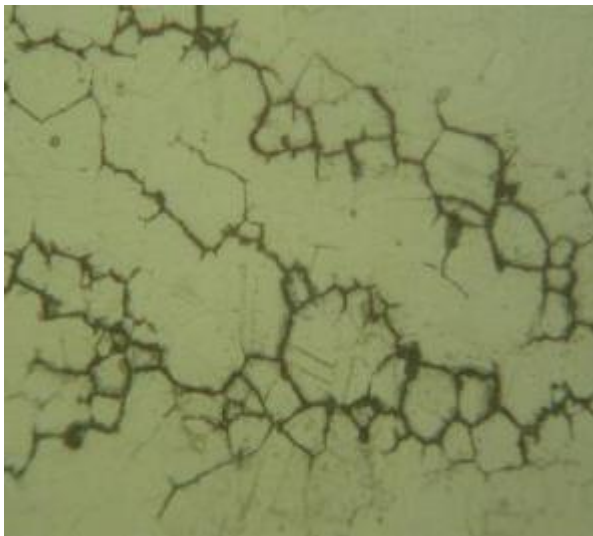
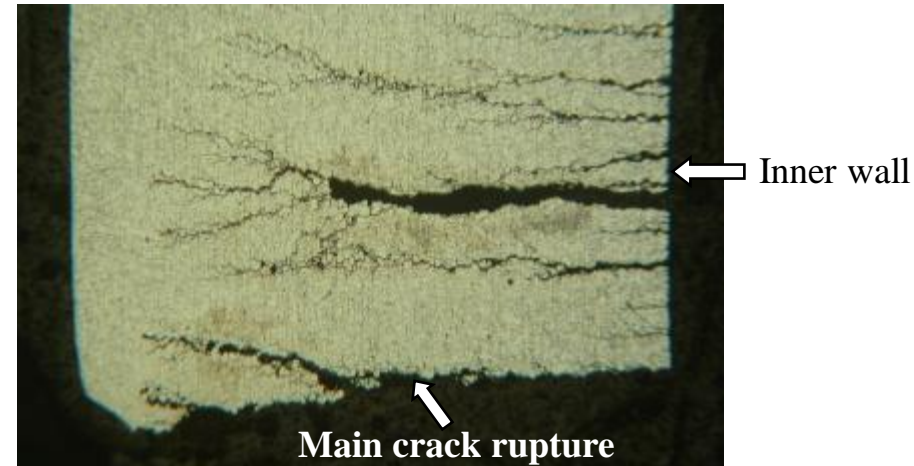
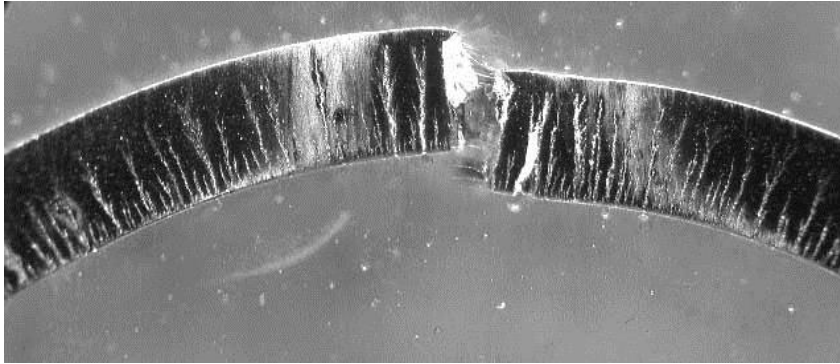
Close up view of a ruptured expansion bellows

FAILURE ANALYSIS ON A RUPTURED EXPANSION BELLOWS OF A PRE-HEATER DUE TO STRESS-CORROSION CRACKING (continued)



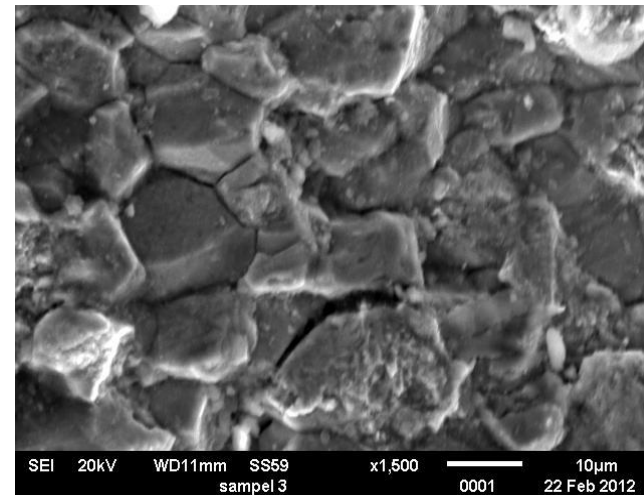
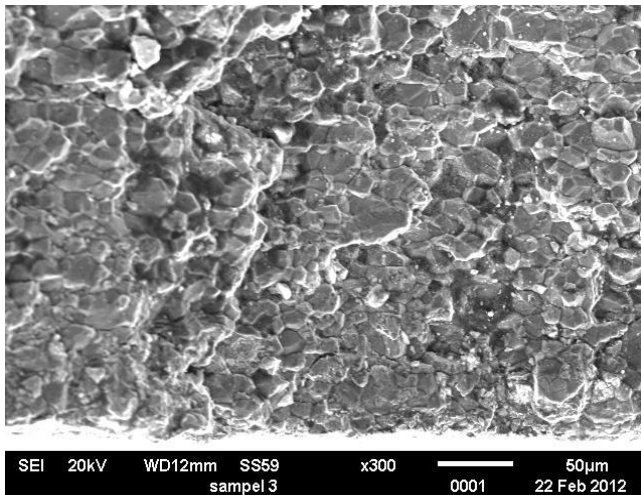
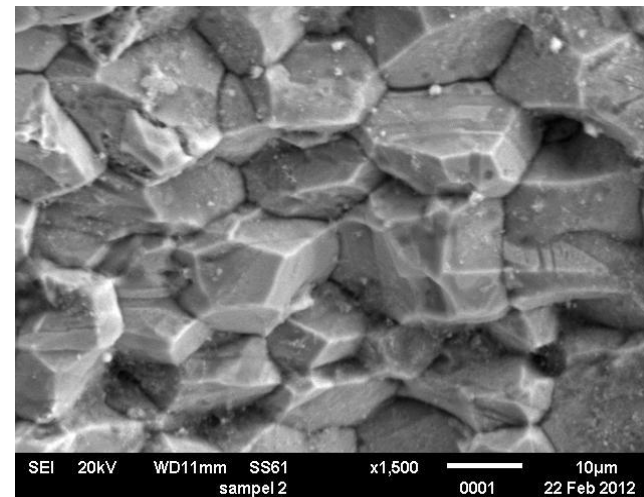
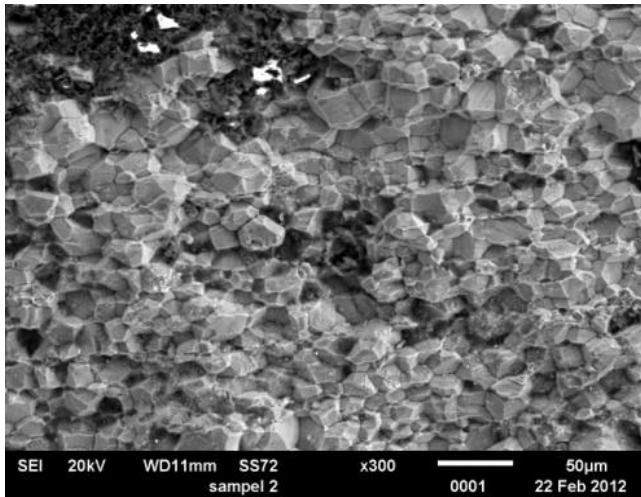
Macrostructures obtained from some specimen of the ruptured bellows convolution and the corresponding microstructures at different test locations as indicated.

FAILURE ANALYSIS ON A RUPTURED EXPANSION BELLOWS OF A PRE-HEATER DUE TO STRESS-CORROSION CRACKING (continued)



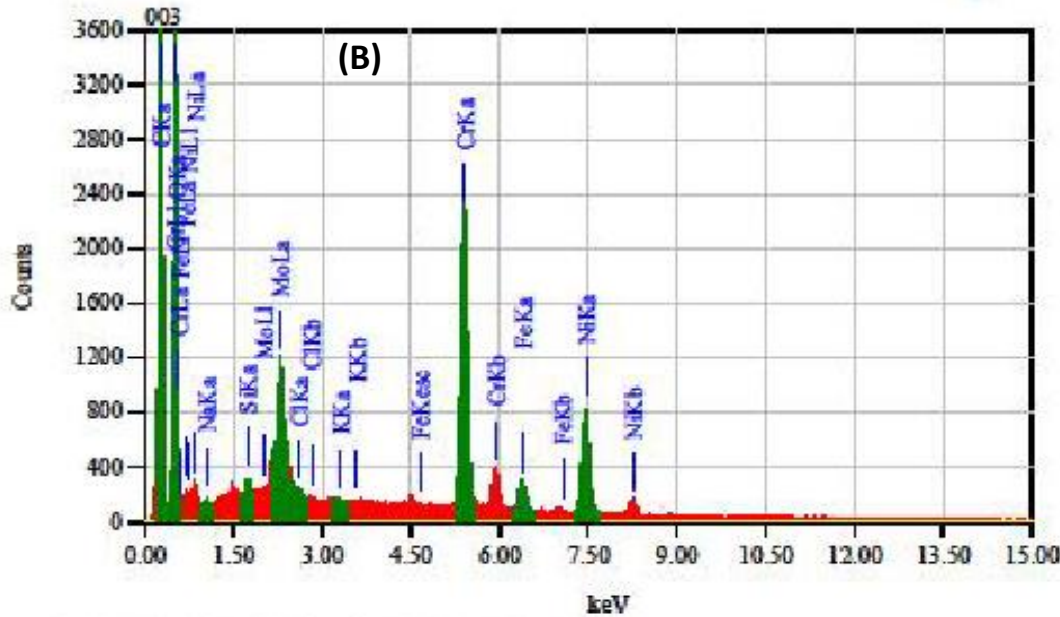
Microstructures of a ruptured expansion bellows showing multiple parallel caustic intergranular cracks

FAILURE ANALYSIS ON A RUPTURED EXPANSION BELLOWS OF A PRE-HEATER DUE TO STRESS-CORROSION CRACKING (continued)



SEM photofractographs obtained from the fracture surfaces of the ruptured bellows convolutions, showing the intergranular and brittle pattern of SCC .

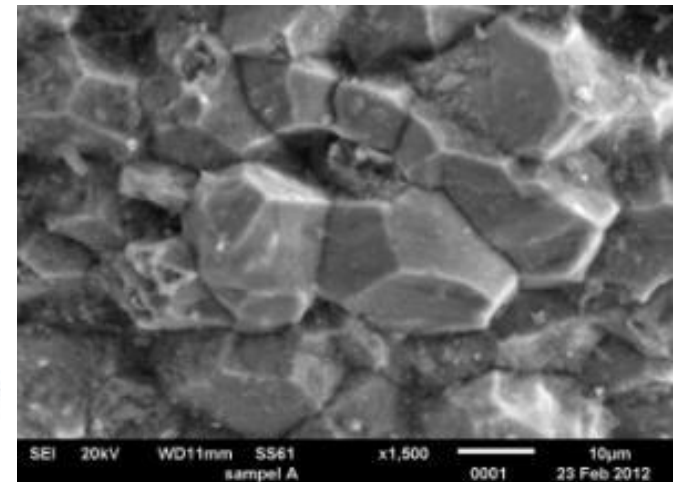
FAILURE ANALYSIS ON A RUPTURED EXPANSION BELLOWS OF A PRE-HEATER DUE TO STRESS-CORROSION CRACKING (continued)



ZAF Method Standardless Quantitative Analysis

Fitting Coefficient : 0.3593

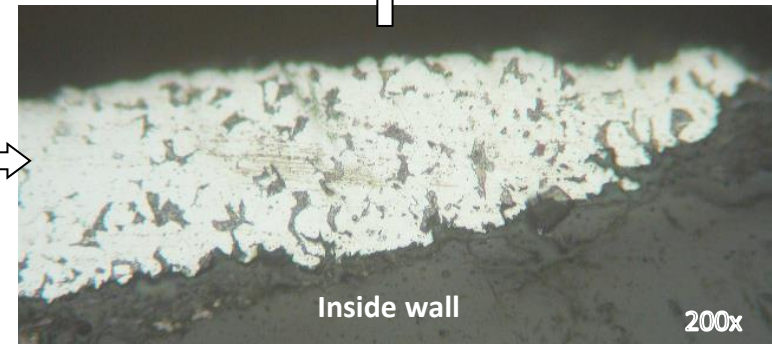
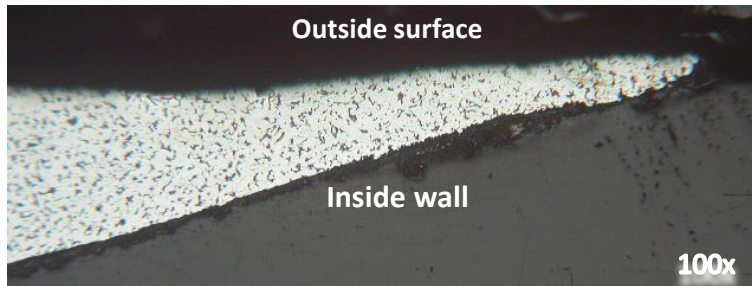
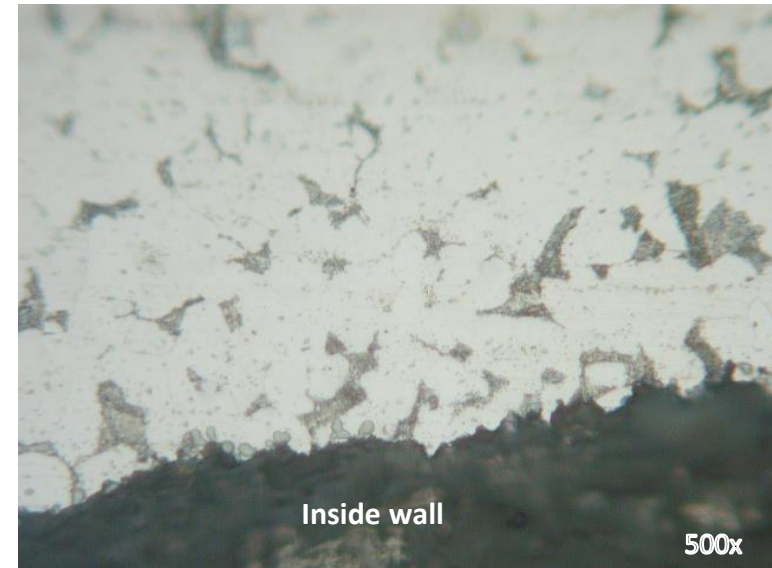
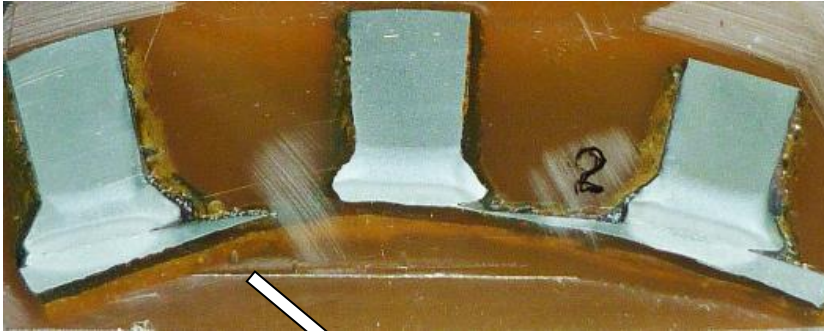
Element	(keV)	Mass%	Error%	Atom%	Compound	Mass%	Cation	K
C	0.277	41.21	0.10	58.91				24.1060
O	0.525	30.27	0.39	32.49				29.6483
Na	1.041	0.19	0.27	0.14				0.1570
Si	1.739	0.25	0.15	0.15				0.3223
Cl	2.621	0.11	0.12	0.05				0.1966
K	3.312	0.03	0.16	0.01				0.0613
Cr	5.411	12.81	0.33	4.23				21.4512
Fe	6.398	1.90	0.43	0.58				3.1073
Ni	7.471	9.31	0.67	2.72				15.0893
Mo	2.293	3.93	0.34	0.70				5.8607
Total		100.00		100.00				



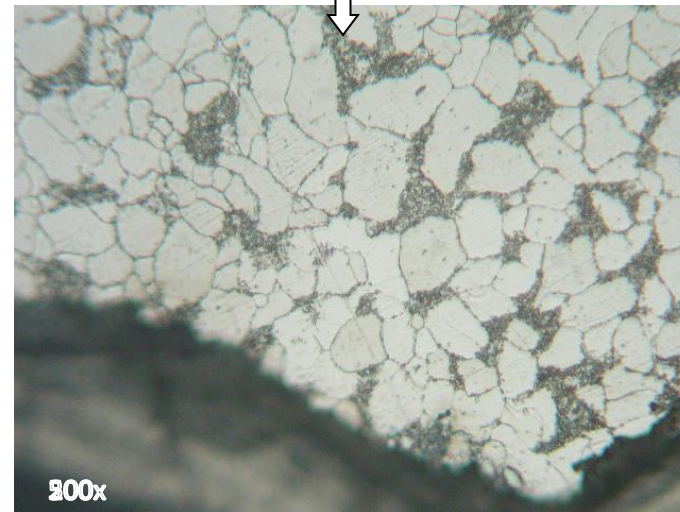
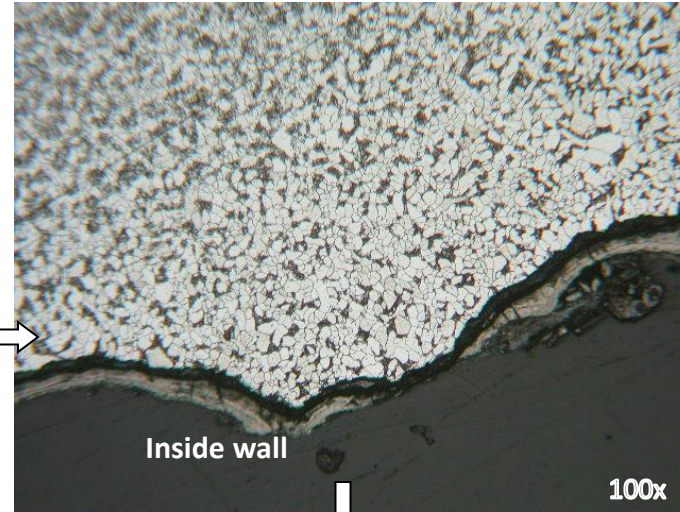
EDS spectrum of elements obtained from the fracture surface deposits of the ruptured bellows convolutions, showing caustic intergranular SCC due to sodium.

FAILURE ANALYSIS ON LEAKED CONVECTION HEATER TUBES DUE TO EROSION-CORROSION

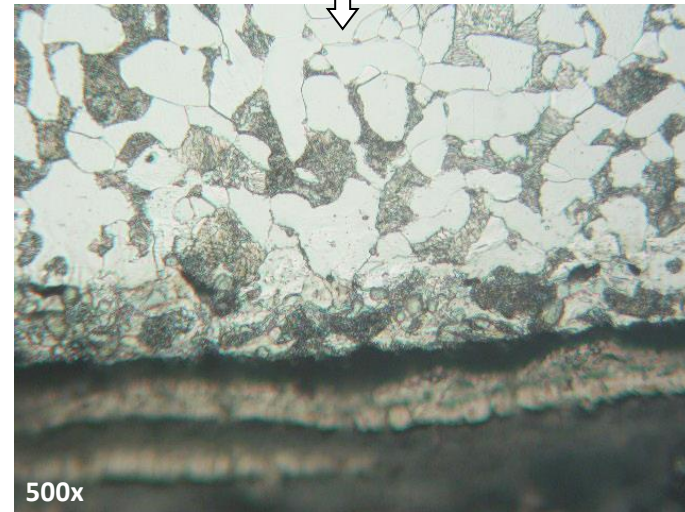
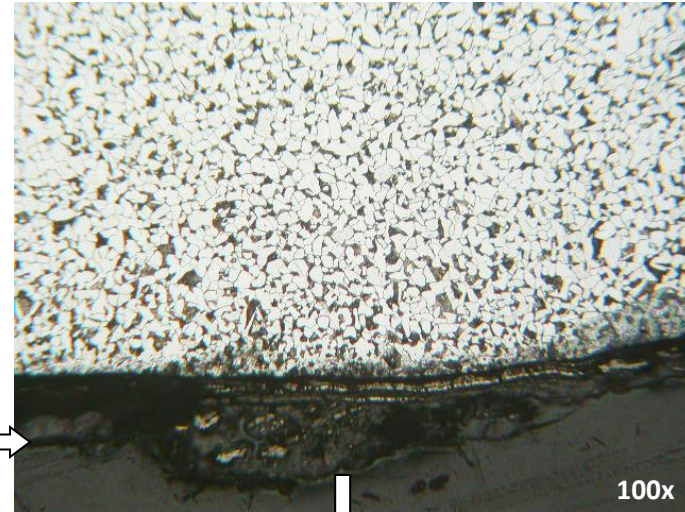
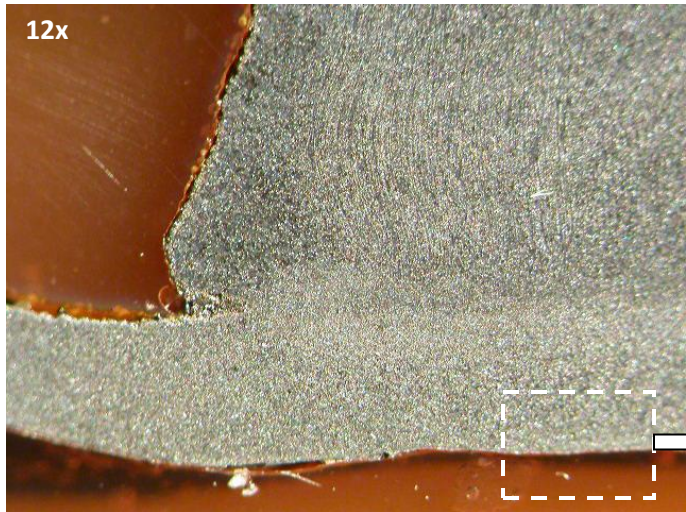




Microstructures obtained from some leaked area of the convection heater tube showing typical damage mechanism due to erosion corrosion

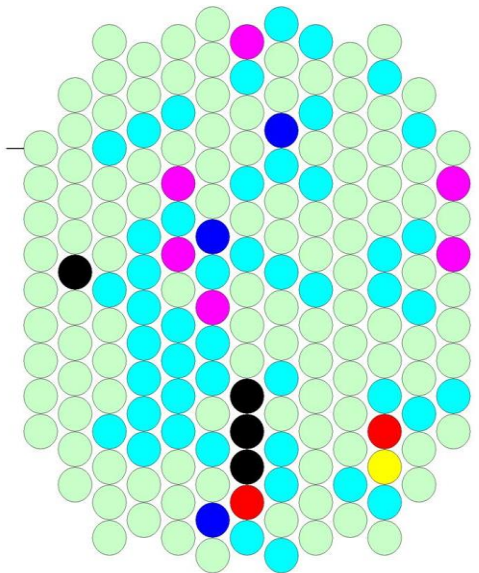
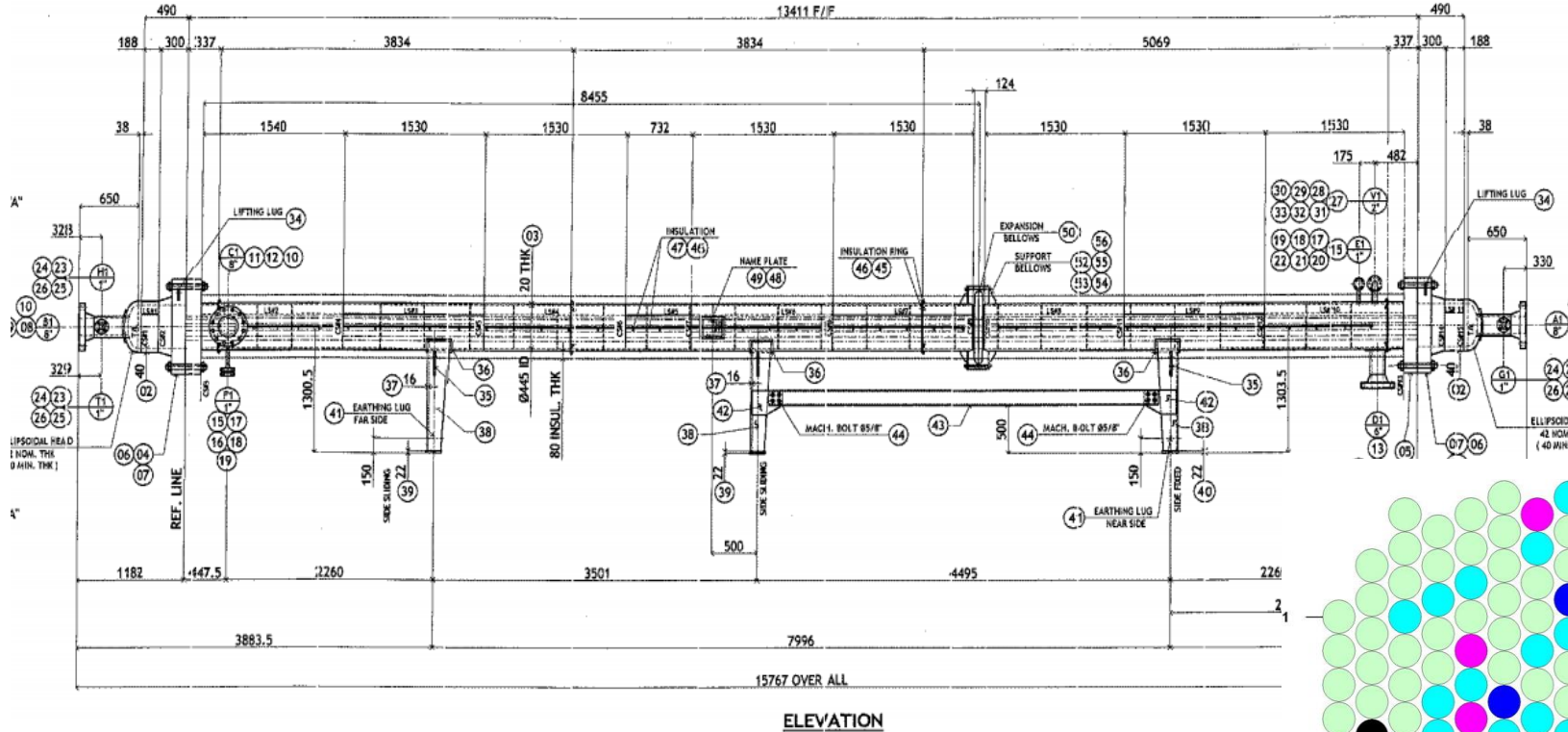


Microstructures obtained from some thinned area of the other convection heater tube showing typical damage mechanism due to erosion corrosion. The microstructures are remained unchanged, consisting of ferrite and pearlite.



Microstructures obtained from some thinned area of the other convection heater tube showing typical damage mechanism due to erosion corrosion. The microstructures are remained unchanged, consisting of ferrite and pearlite.

FAILURE ANALYSIS OF FEED PRE-HEATER TUBES DUE TO FATIGUE CORROSION AND STRESS-CORROSION CRACKING



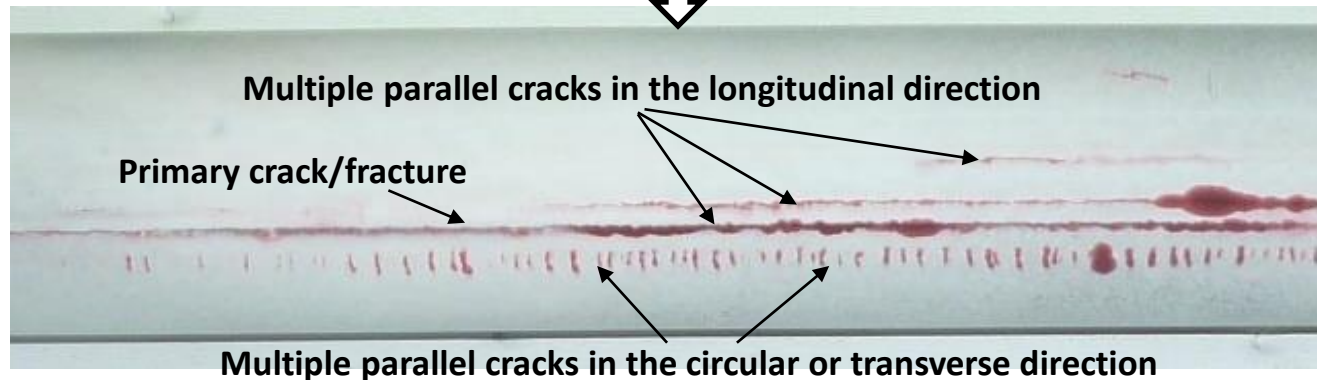
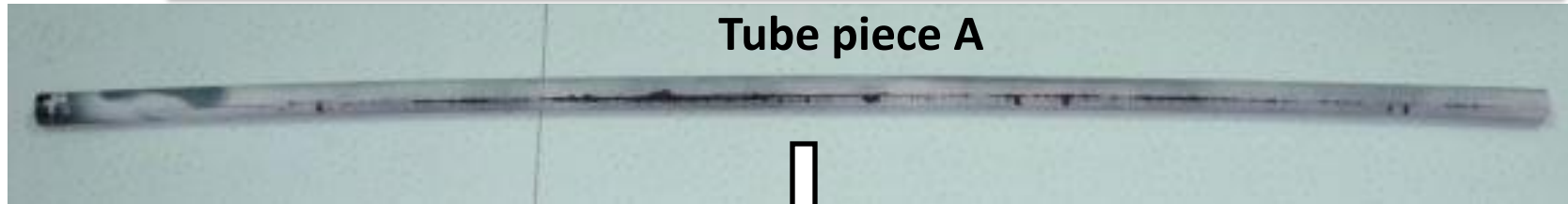
As built drawing of the Feed Pre-heater showing slurry inlet/outlet, steam inlet/outlet and location where a number of tubes were found leaks.

FAILURE ANALYSIS OF FEED PRE-HEATER TUBES DUE TO FATIGUE CORROSION AND STRESS-CORROSION CRACKING (continued)

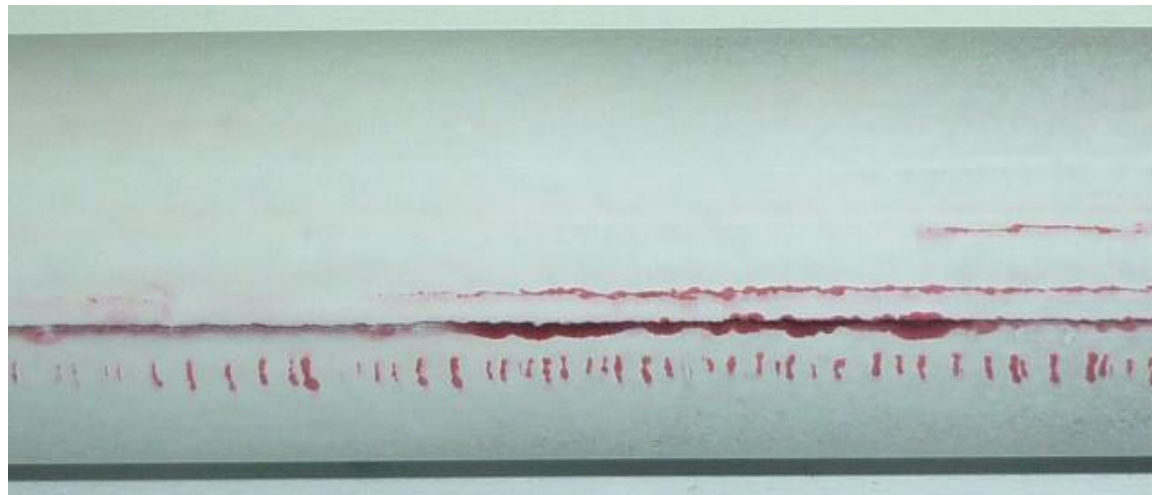


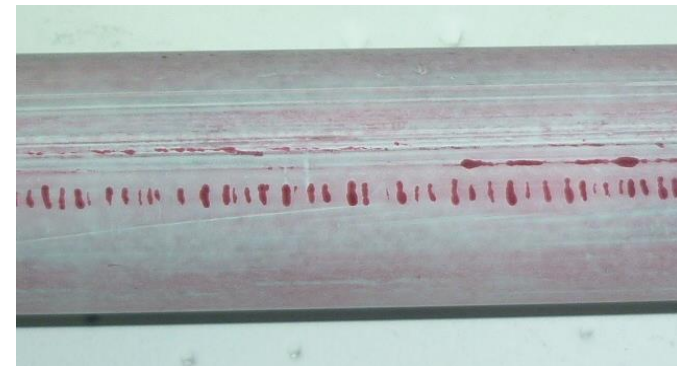
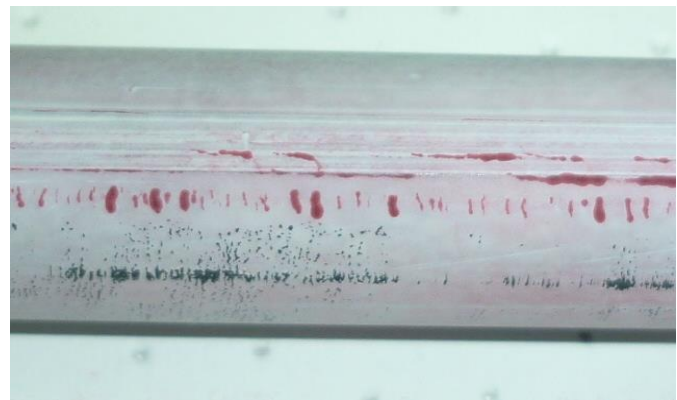
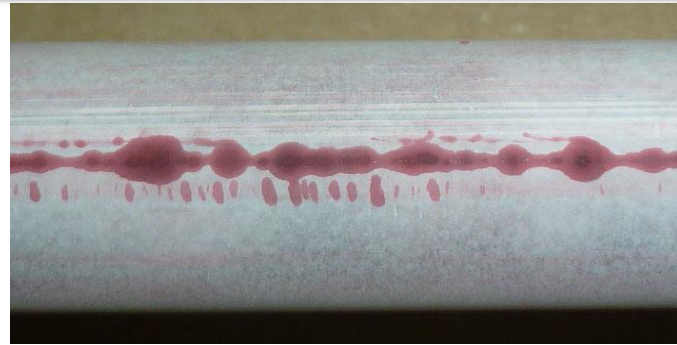
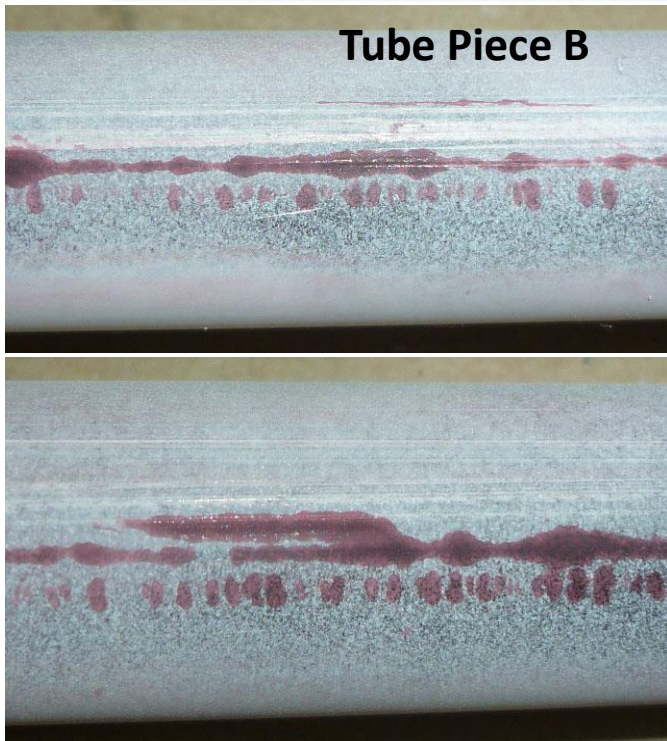
Three tube pieces (A, B and C) of about 750-800 mm in length were used for failure analysis. Tube piece A was located at a location in the Pre-heater showing one large primary crack or fracture and other multiple parallel cracks in the longitudinal direction. In addition other multiple parallel cracks in the circular or transverse direction were also found at the adjacent of the multiple longitudinal cracks. Tube piece B was the same as tube piece A but at a distance about 2-3 meters away from A showing no any visual cracks. Whereas tube piece C was a new tube similar to the tube pieces A and B.

FAILURE ANALYSIS OF FEED PRE-HEATER TUBES DUE TO FATIGUE CORROSION AND STRESS-CORROSION CRACKING (continued)



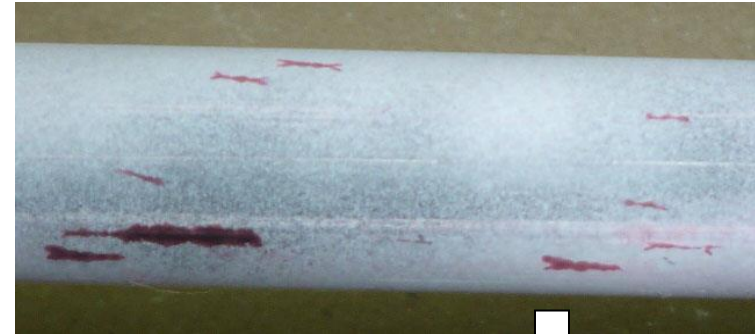
Dye penetrant test on the tube piece A showing a large primary crack along with other parallel cracks in the longitudinal direction and other multiple parallel cracks in the circular or transverse direction.





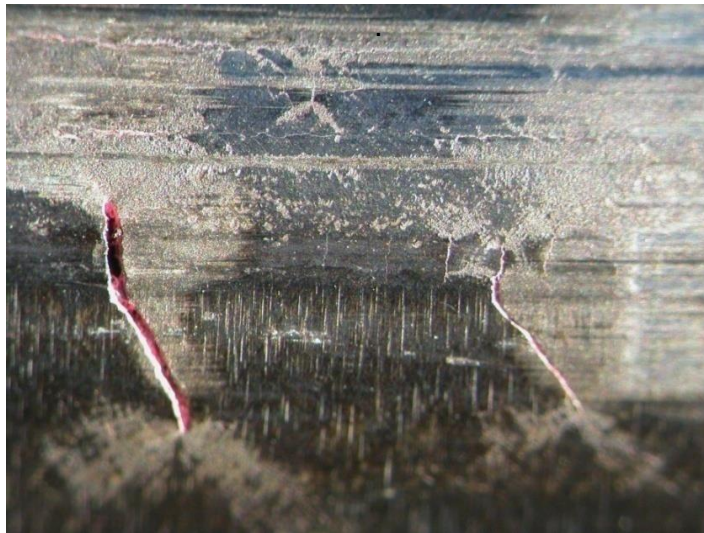
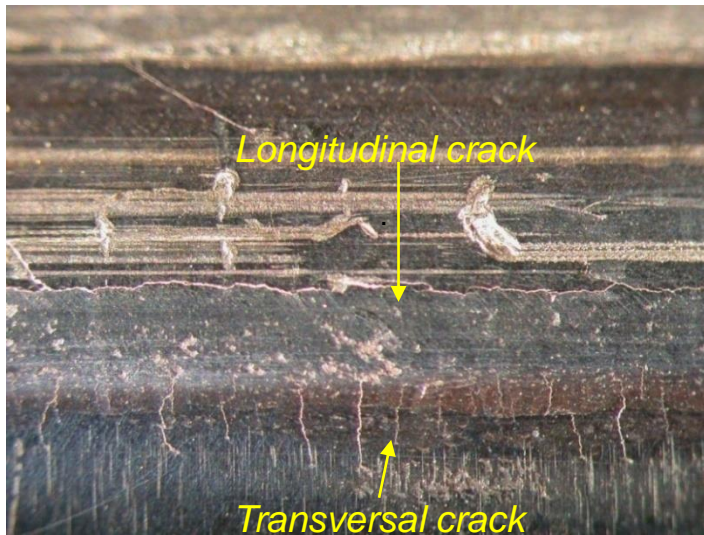
Dye penetrant test on the tube piece B showing similar cracks pattern as shown in the tube piece A, where one sort of cracks being as multiple parallel cracks in the longitudinal direction and the other being as multiple parallel cracks in the circular or transverse direction. All the cracks shown in the tube piece B were being as continued cracks connecting with those cracks formed in the tube piece A.

Tube Piece B

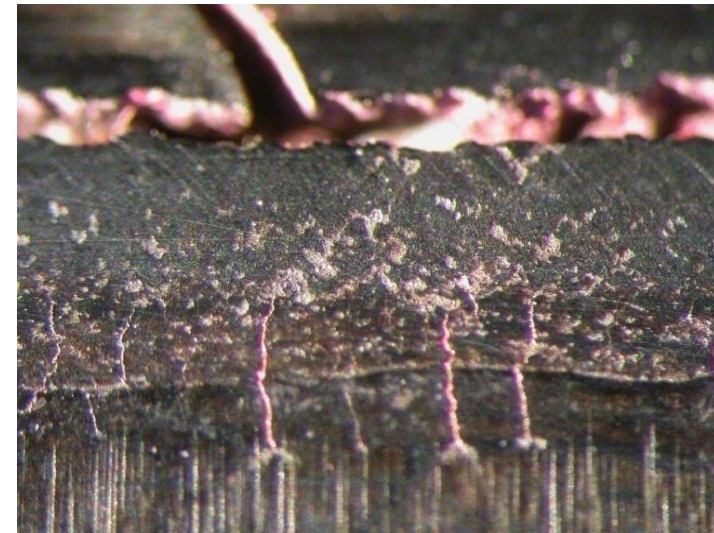
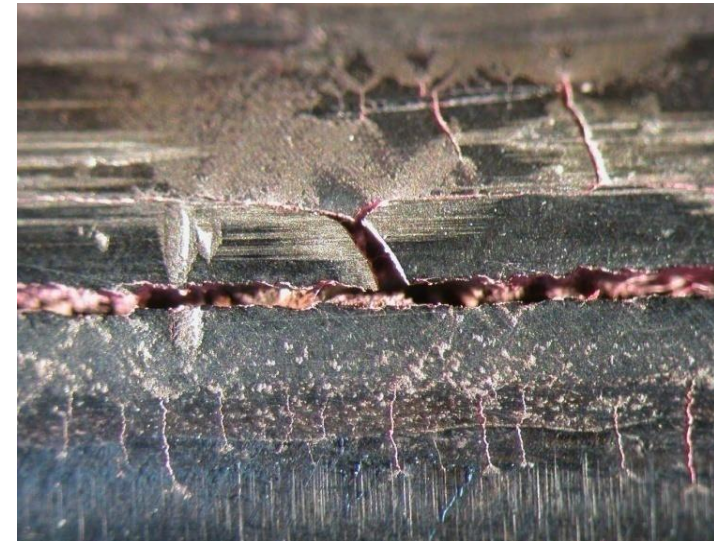


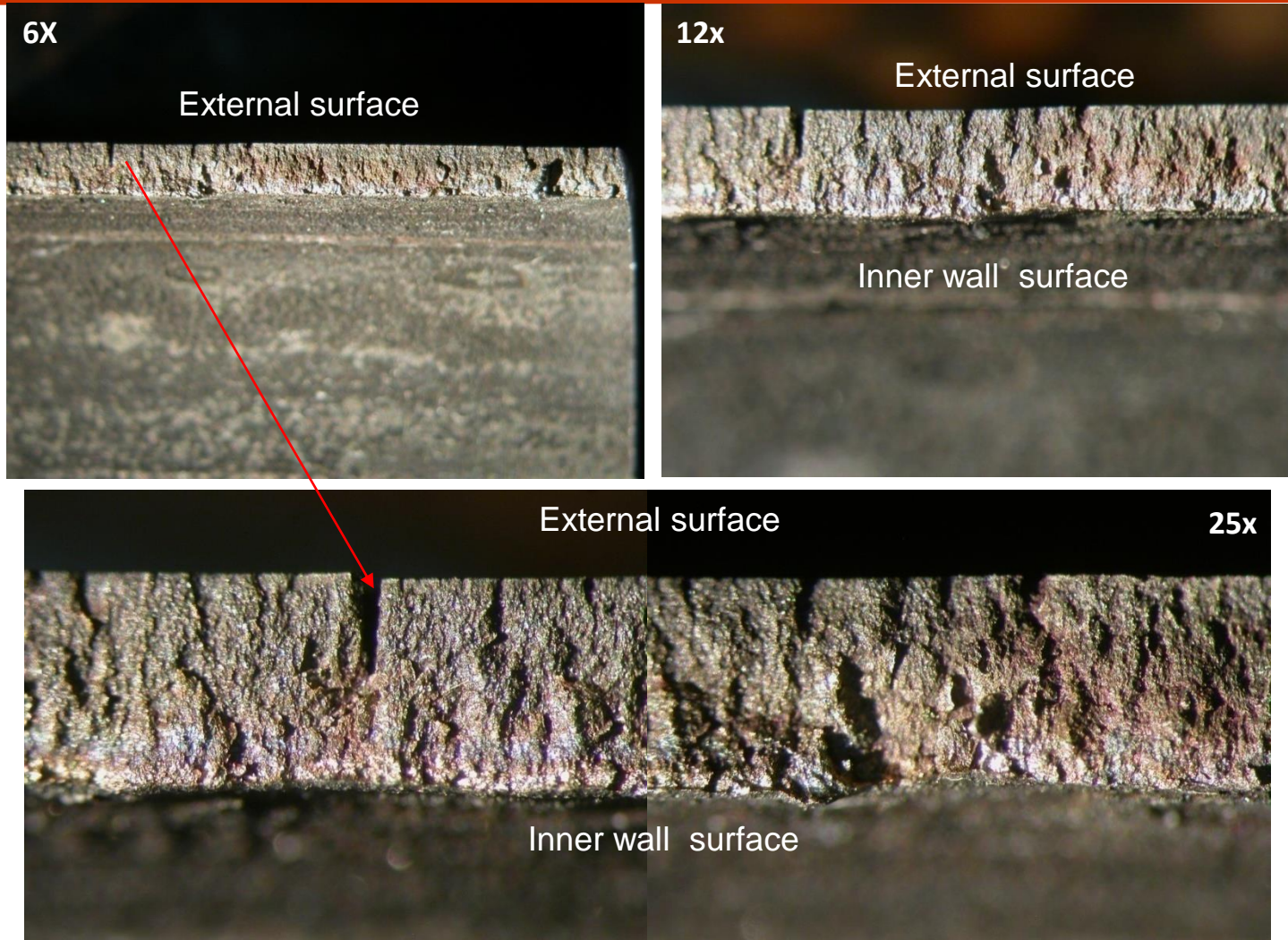
Dye penetrant test on the tube piece B located approximately at the opposite side or at 180° from the multiple cracks area of the tube showing some intermittent parallel cracks in the longitudinal direction. On this side of the tube B, no any circular or transverse cracks were observed.

FAILURE ANALYSIS OF FEED PRE-HEATER TUBES DUE TO FATIGUE CORROSION AND STRESS-CORROSION CRACKING (continued)

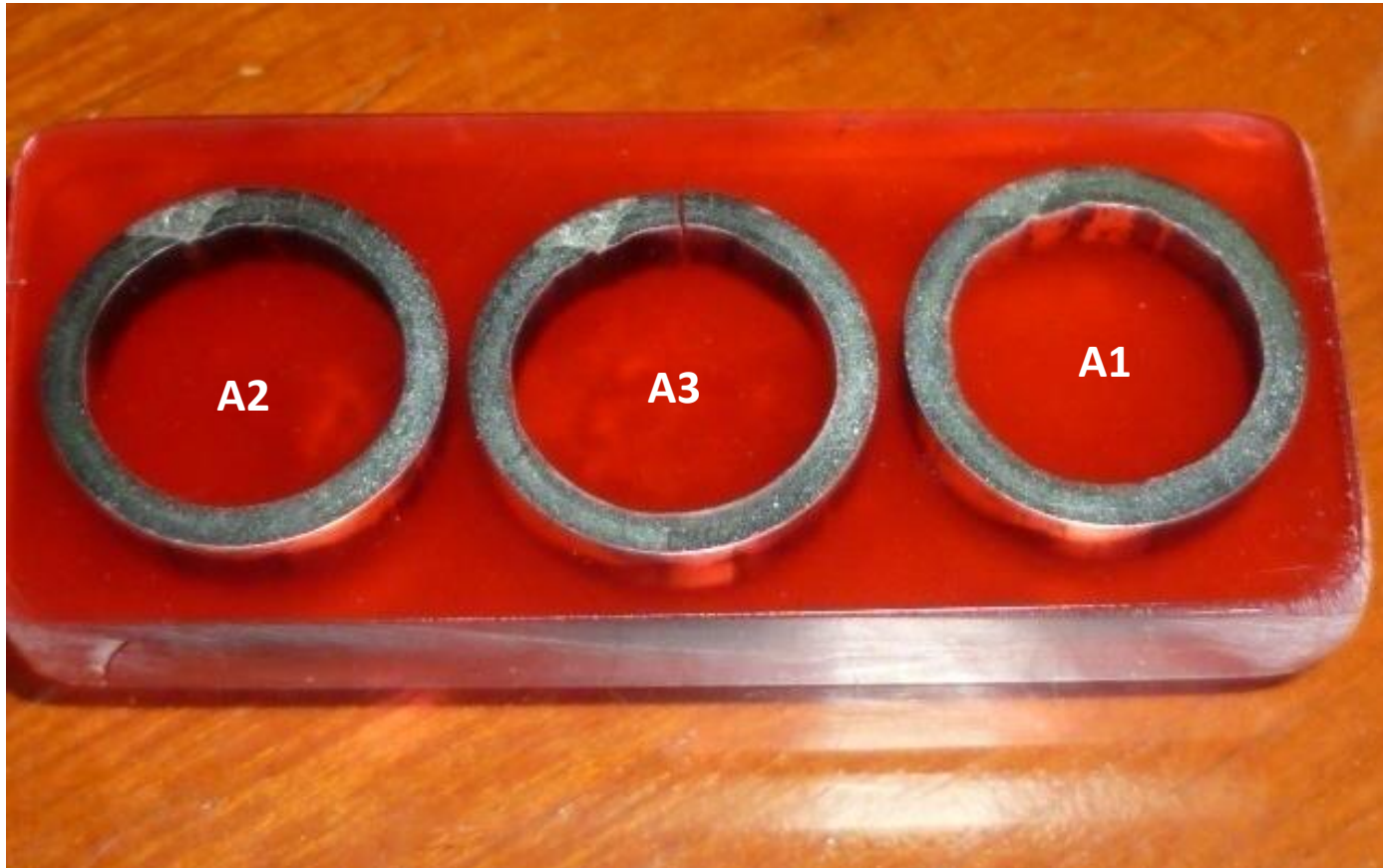


Cracks appearance on the tube piece A at location near to the crack ends or tips showing multiple parallel cracks in the longitudinal direction and other multiple parallel cracks around the circular or transverse direction of the tube. In addition, there were also other severe surface damages such as scratch, wear, cut, and/or bruise due to some possible fretting contact occurred between the tube and the adjacent tubes.

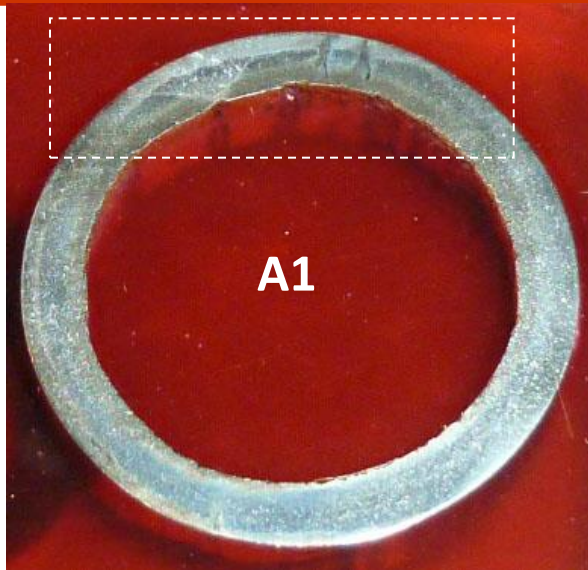




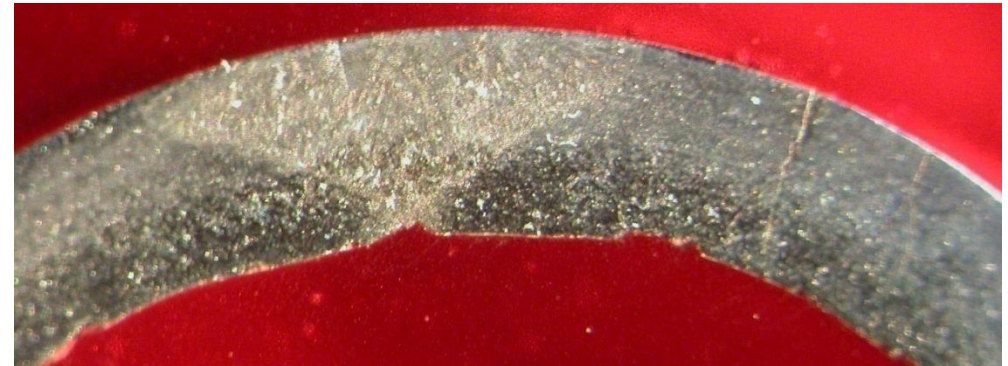
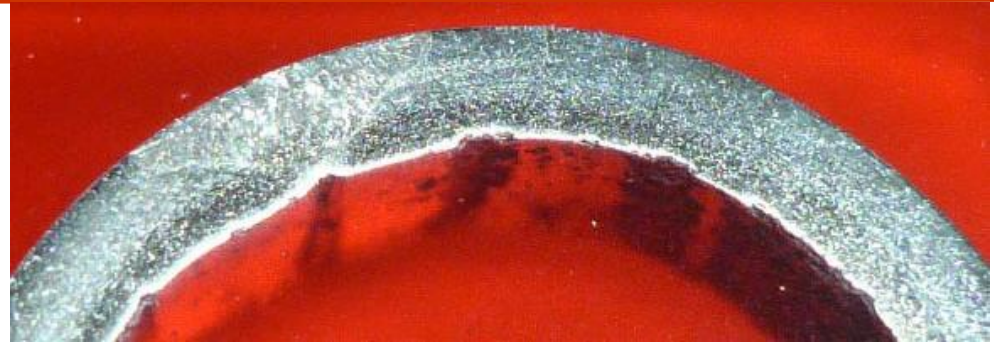
Fracture surface obtained from some of the tube piece A showing crack pattern topography through the tube wall from the external surface to the internal surface of the tube with brittle fracture appearance.



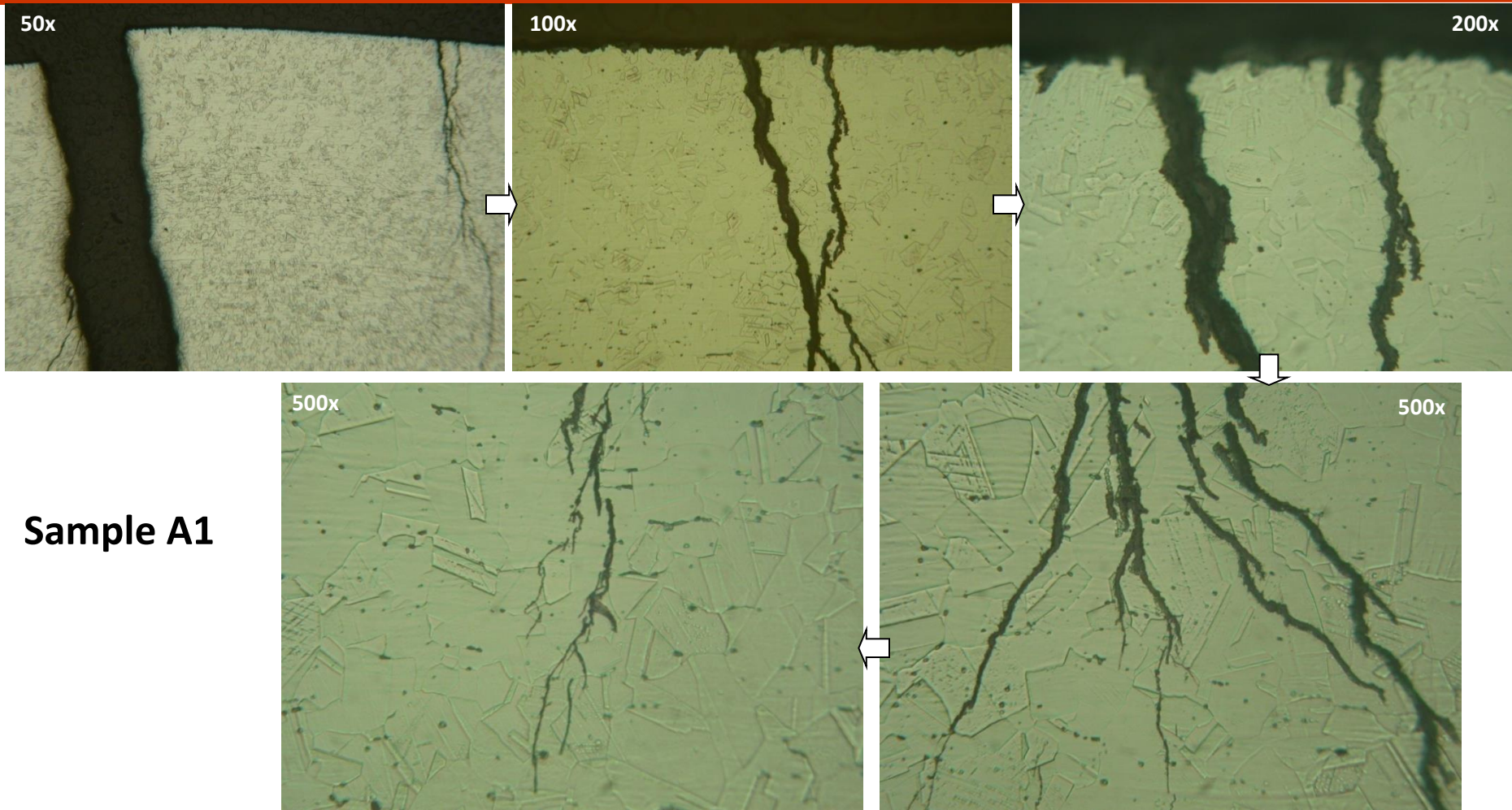
Three specimens in transverse cross section (A1, A2 and A3) were prepared from the tube piece A at three different locations for metallographic examination.



Sample A1



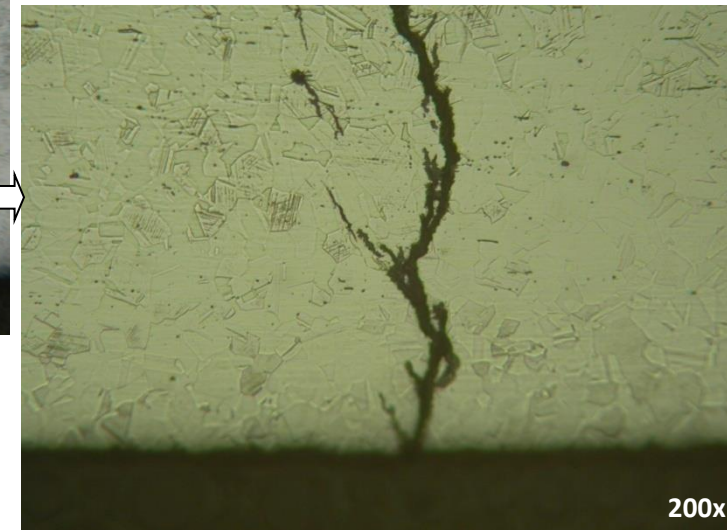
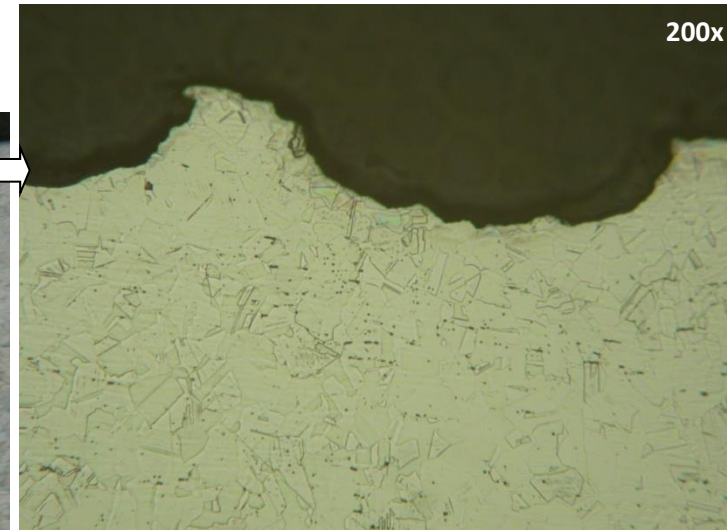
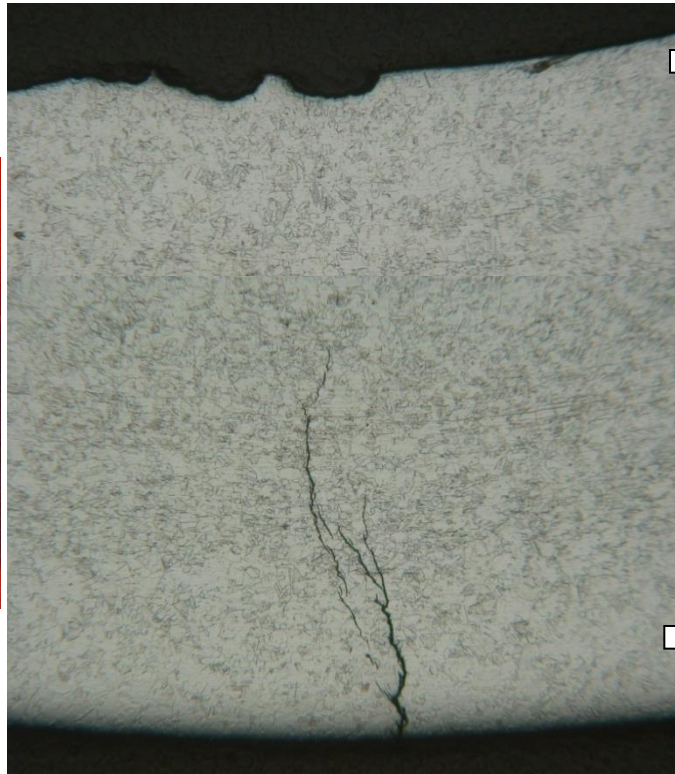
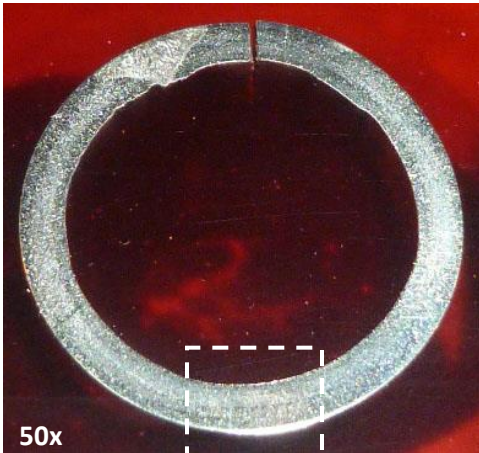
Macrostructures obtained from specimen A1, showing the primary fracture located approximately 2 mm apart from the weld seam of the tube. Adjacent to the primary crack, other parallel fine cracks were also formed.



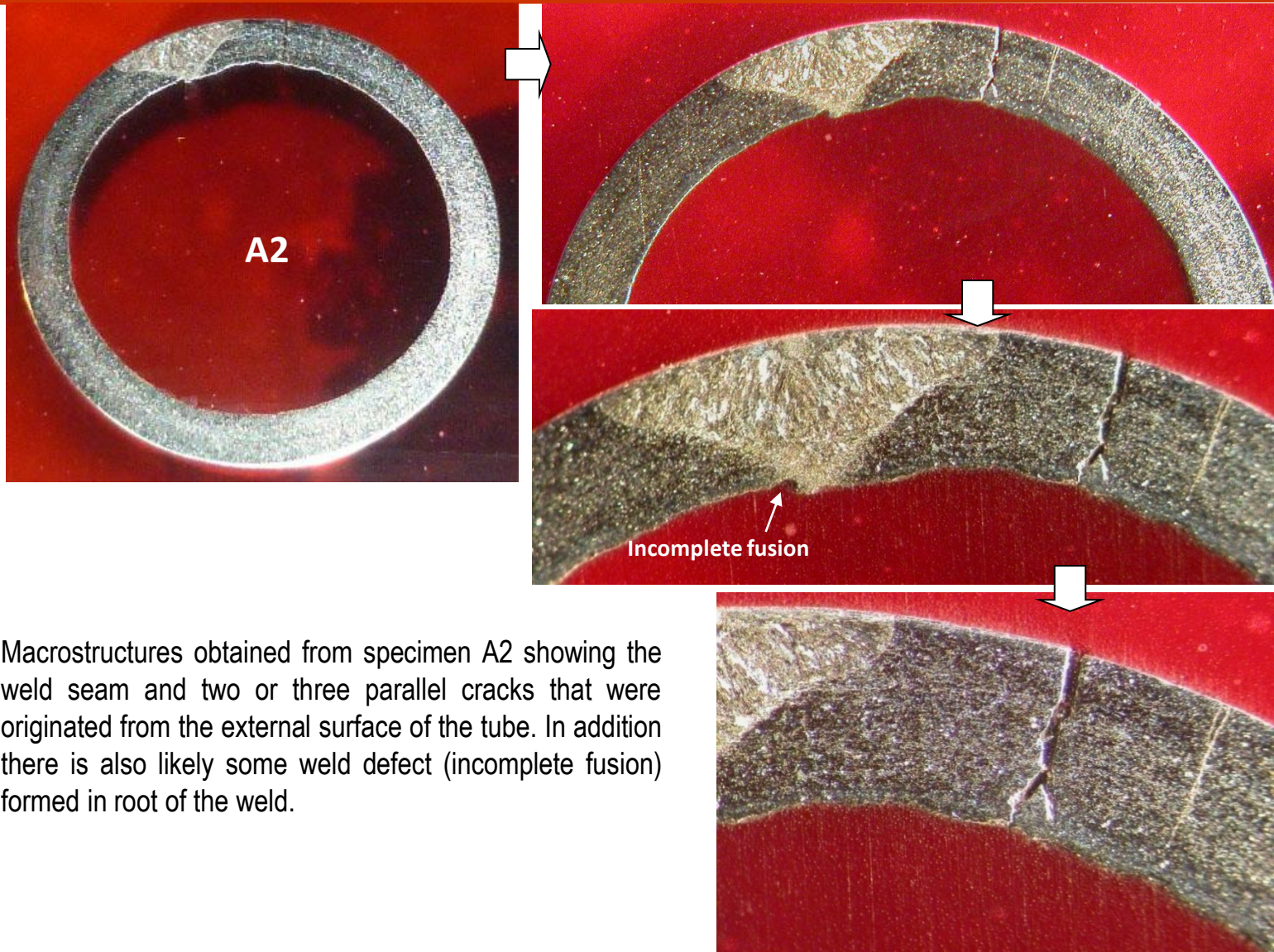
Sample A1

Microstructures of specimen A1 obtained around the primary crack and other fine parallel cracks. It is also obviously seen that the other parallel cracks were initiated from the corrosion pits and propagated by fatigue cracking, and later continued by stress-corrosion cracking (SCC). It is clearly seen that the SCC occurred in this material had propagated in transgranular manner with some branching.

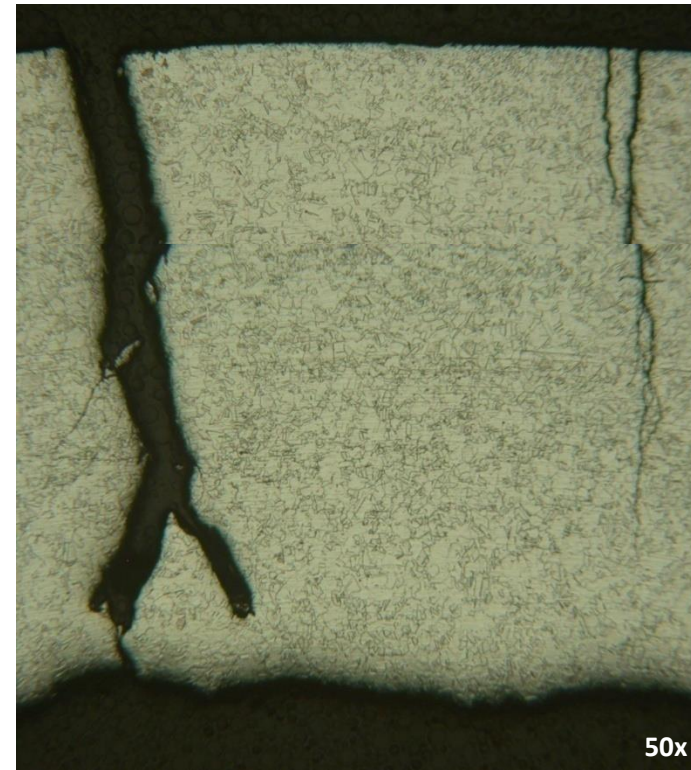
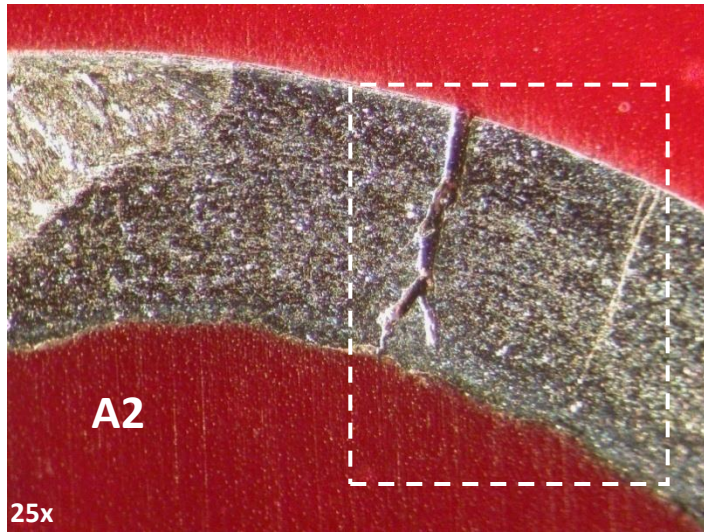
Sample A1



Microstructures obtained from specimen A1 at location approximately around 180° or at the opposite side of the primary crack showing some formation of cracks originated from the tube external surface and a number of erosion corrosion formed on the tube internal wall, respectively.

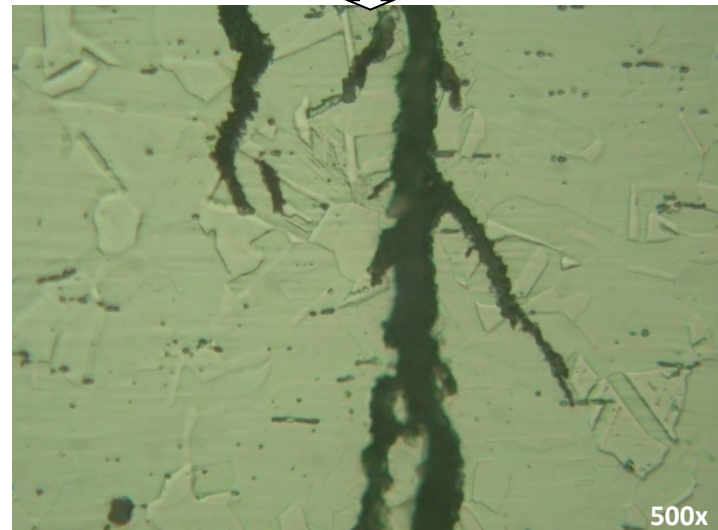
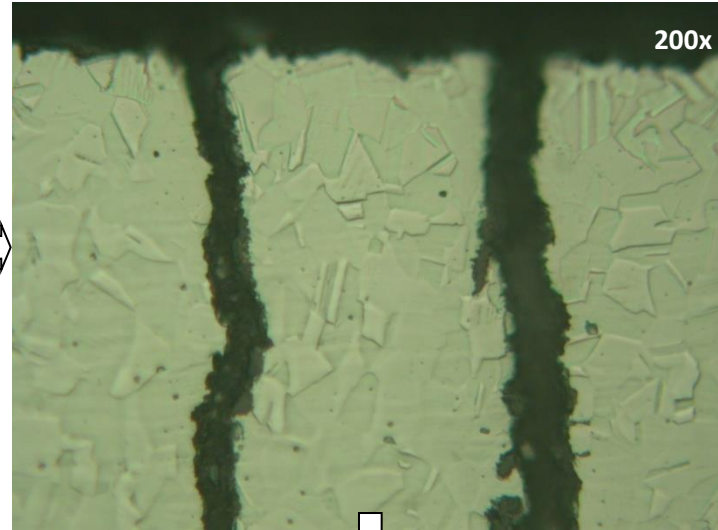
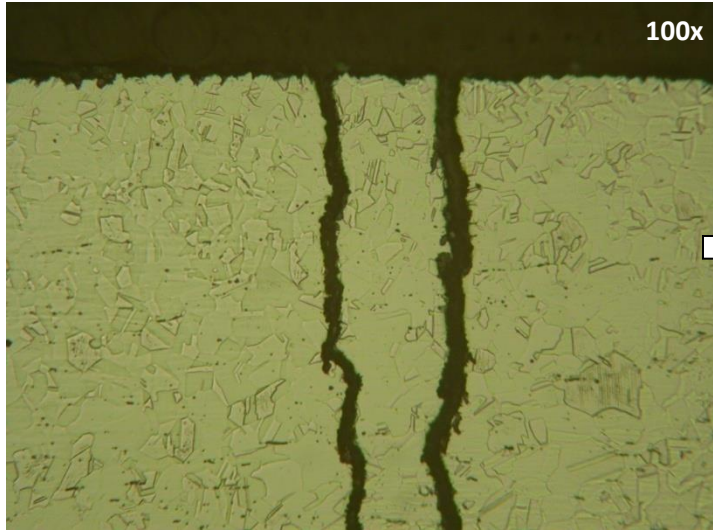


Macrostructures obtained from specimen A2 showing the weld seam and two or three parallel cracks that were originated from the external surface of the tube. In addition there is also likely some weld defect (incomplete fusion) formed in root of the weld.

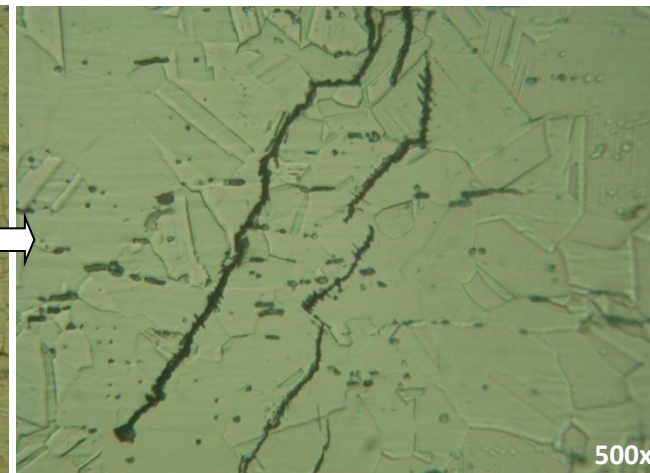
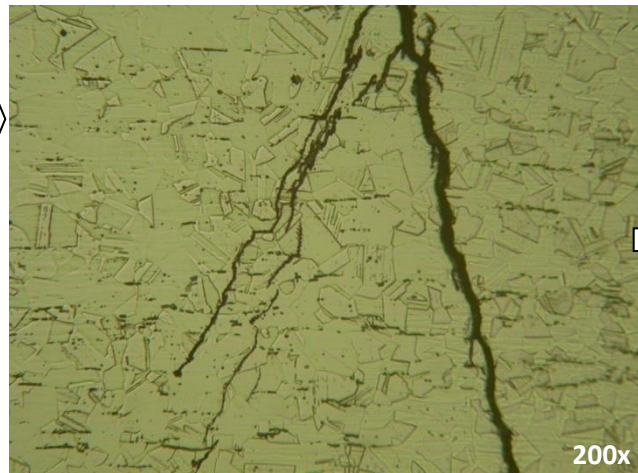
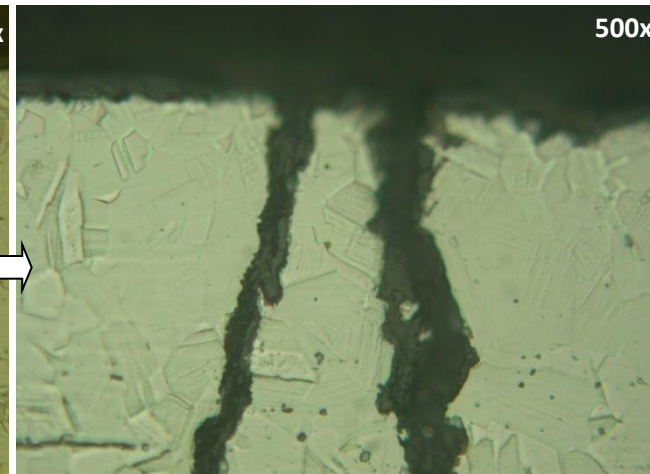
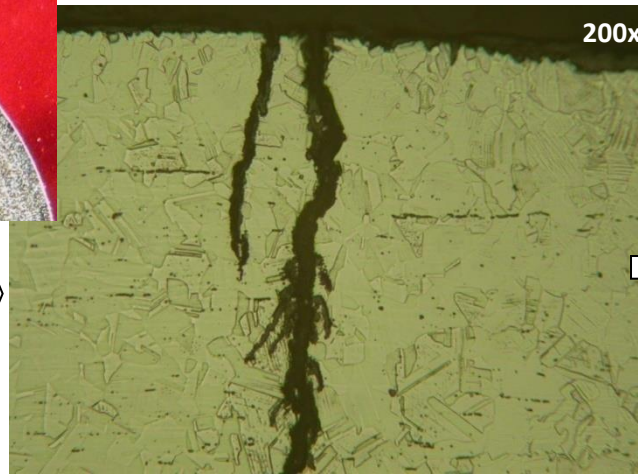
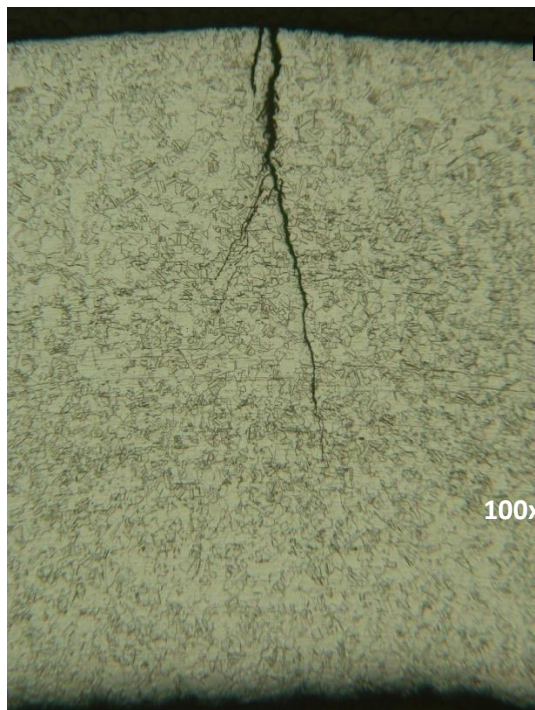
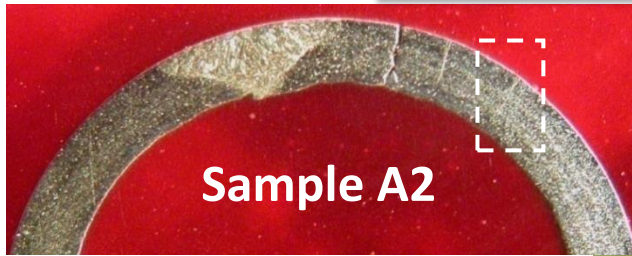


Microstructures obtained from specimen A2 around the crack area showing a large bulbous crack with some lobes typical of corrosion fatigue. This corrosion fatigue was clearly originated from the outside surface and propagated toward the internal wall of the tube by transgranular cracking and filled with oxides and/or corrosion products. On the right side there is also seen other parallel cracking originated from the external surface.

Sample A2

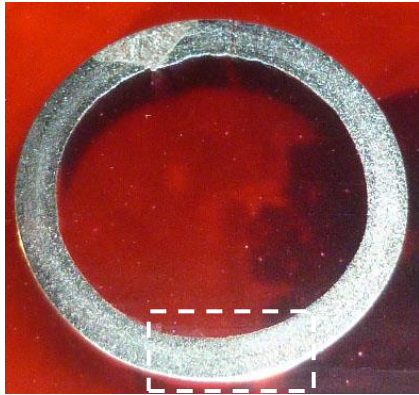


Microstructures obtained from specimen A2 at higher magnification, showing two parallel cracking due to corrosion fatigue that propagated transgranularly through the austenitic grains of the tube material made of 304L stainless steel.

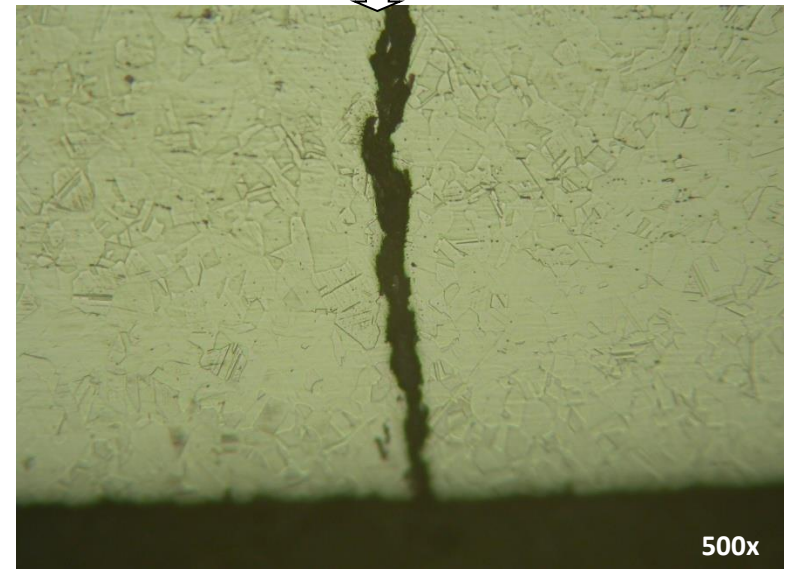
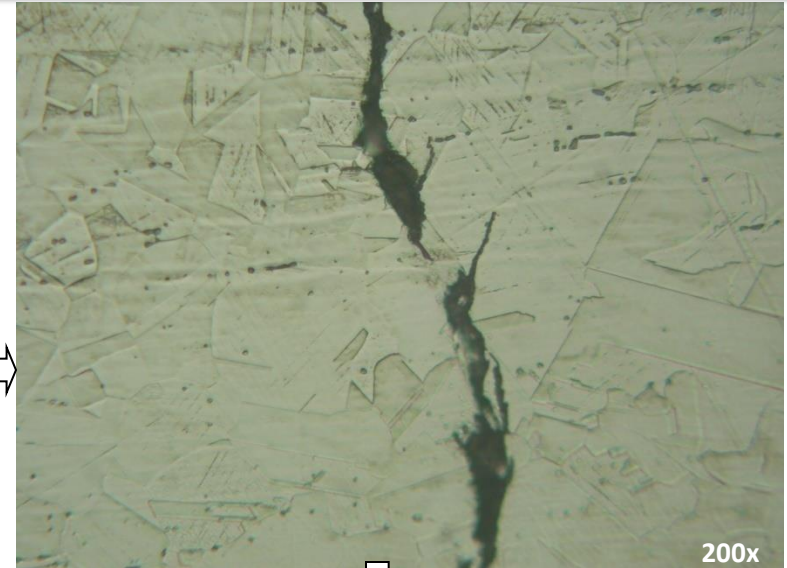


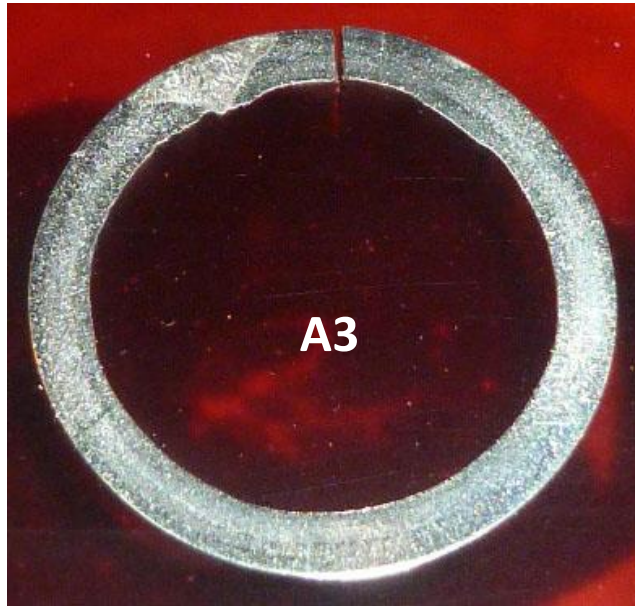
Microstructures obtained from specimen A2 at location around the third parallel cracks showing two other corrosion fatigue cracks which in later stage were continued by SCC with some branching in transgranular manner. It is also seen from the microstructures that some of the propagated cracks of corrosion fatigue and SCC were likely affected by the presence of some defect in the tube material such as oxides/inclusions and/or carbides.

Sample A2



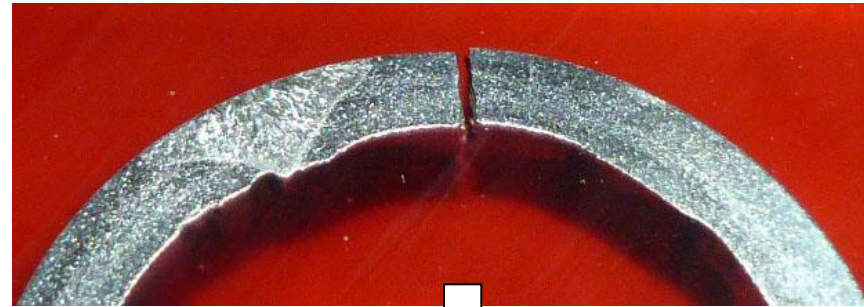
Microstructures obtained from specimen A2 at location approximately 180° from the multiple parallel cracks/weld seam area showing only single corrosion fatigue crack initiated from the external surface of the tube.



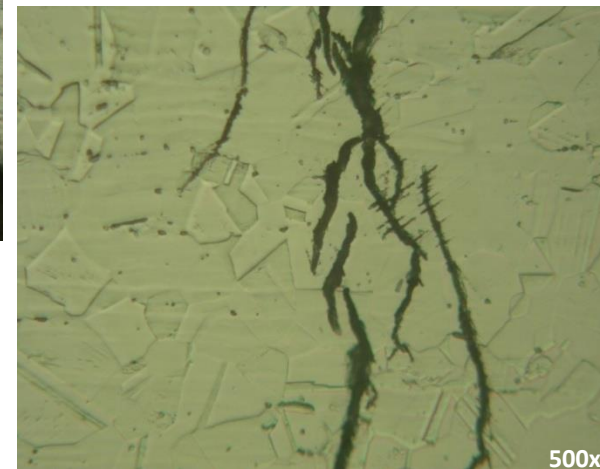
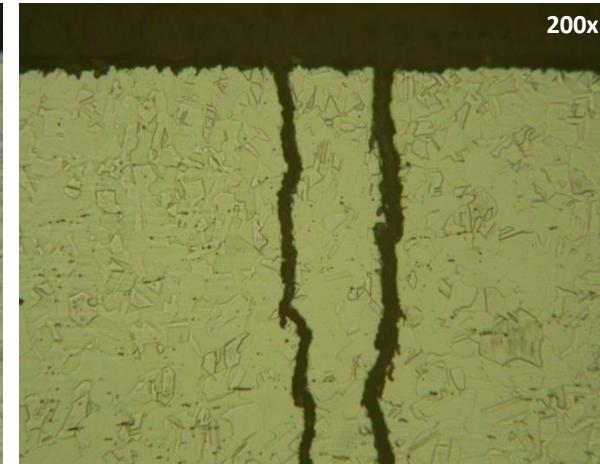
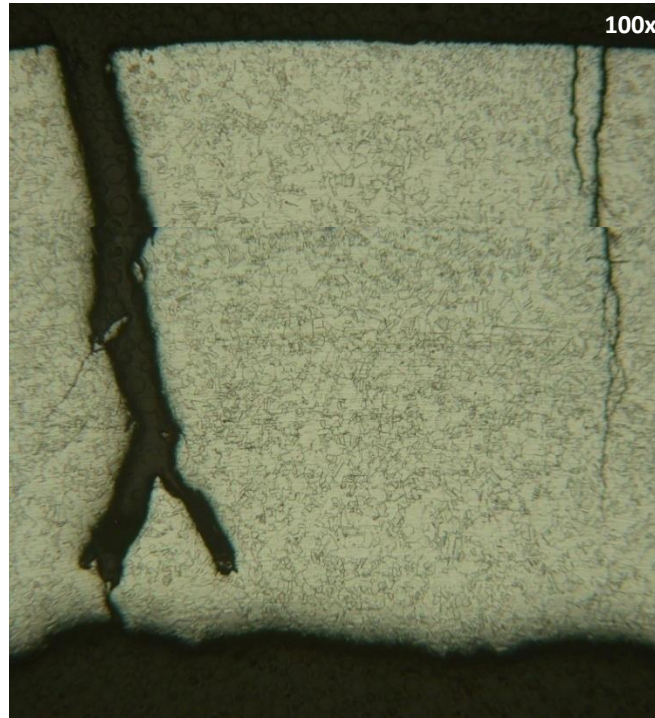
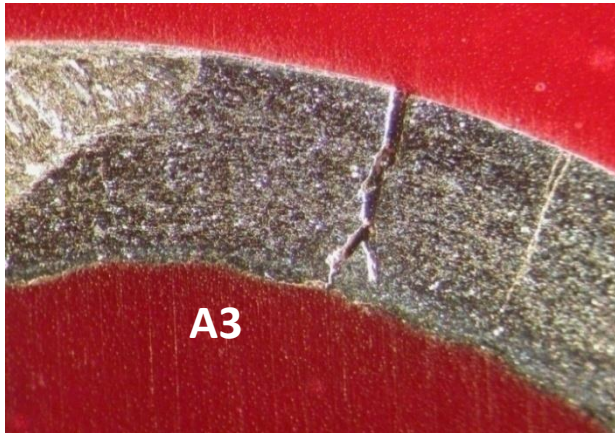


Sample A3

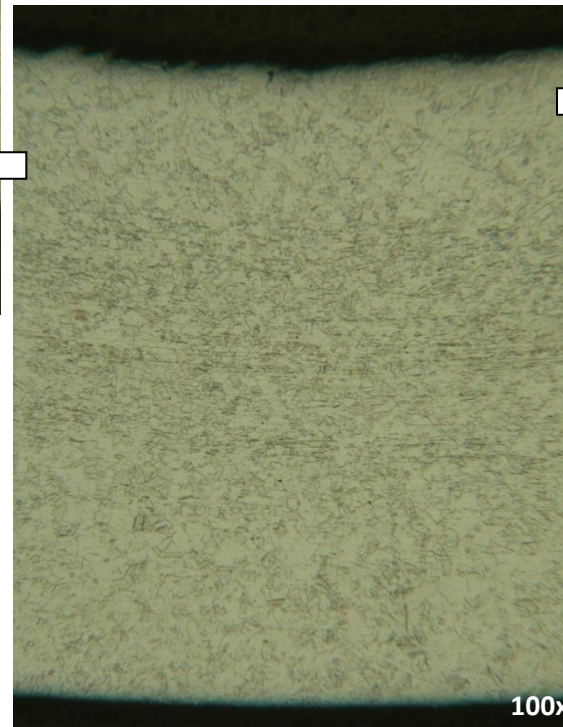
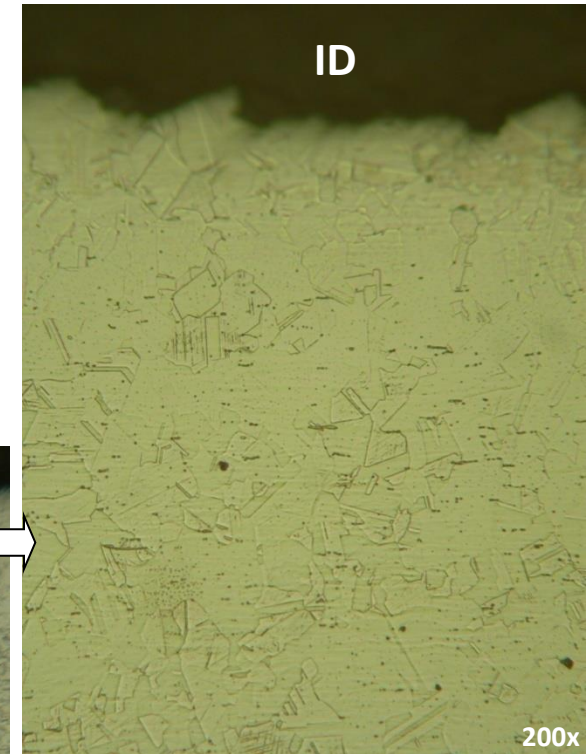
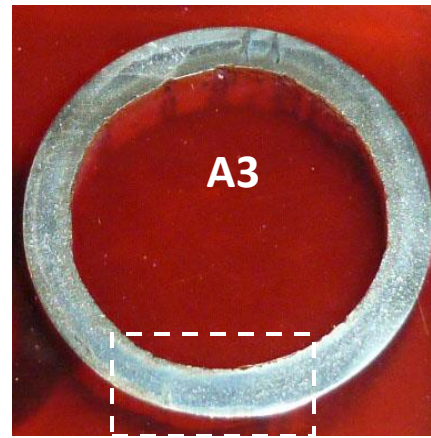
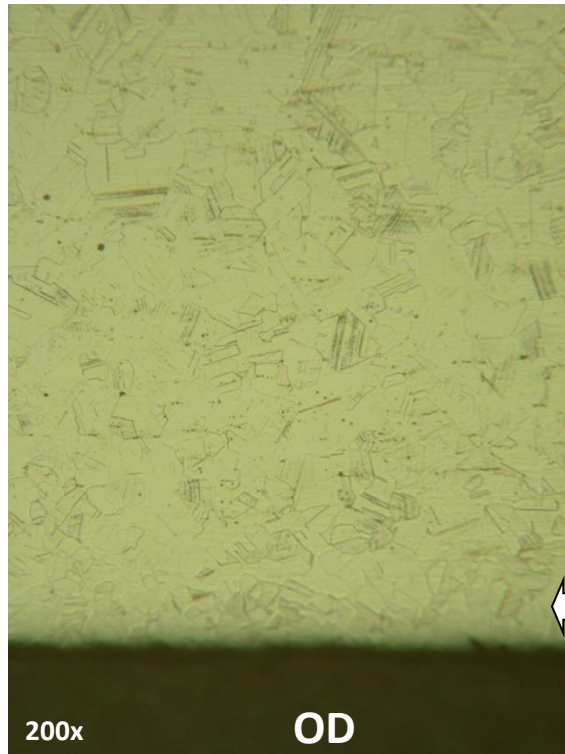
Macrostructures obtained from specimen A3 located around the weld seam and the adjacent multiple parallel cracks showing some weld defect (incomplete fusion in root of the weld) and a number of damaged area due to erosion corrosion in the tube internal wall.



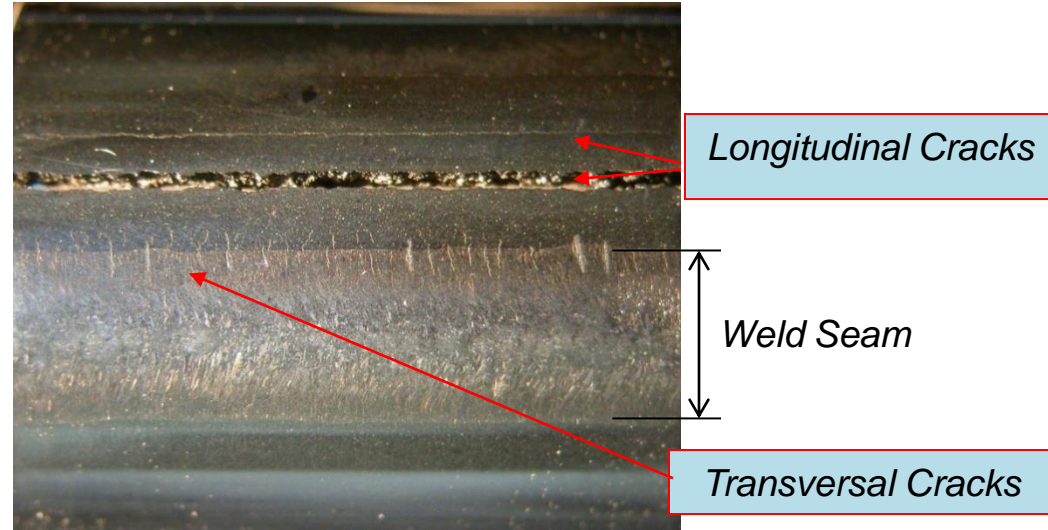
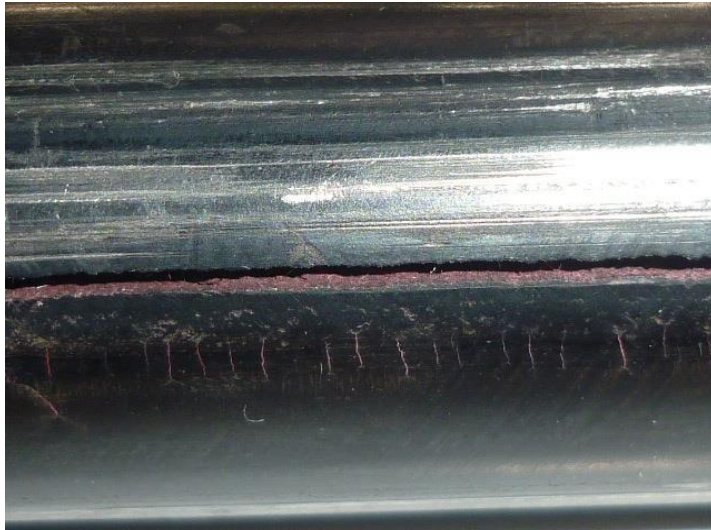
Sample A3



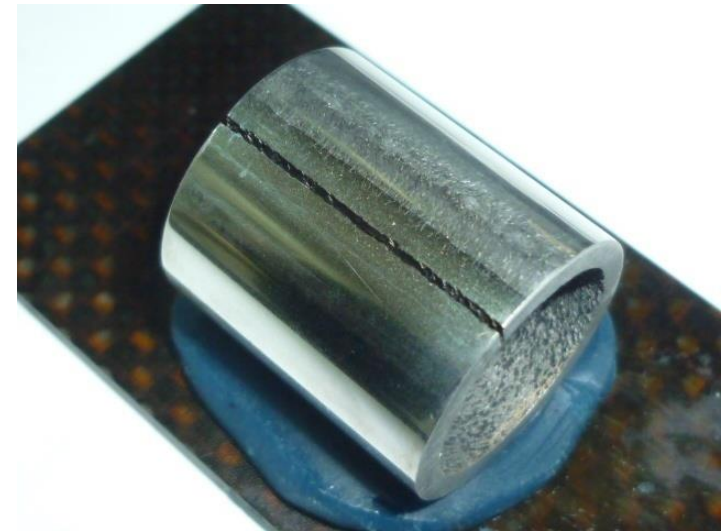
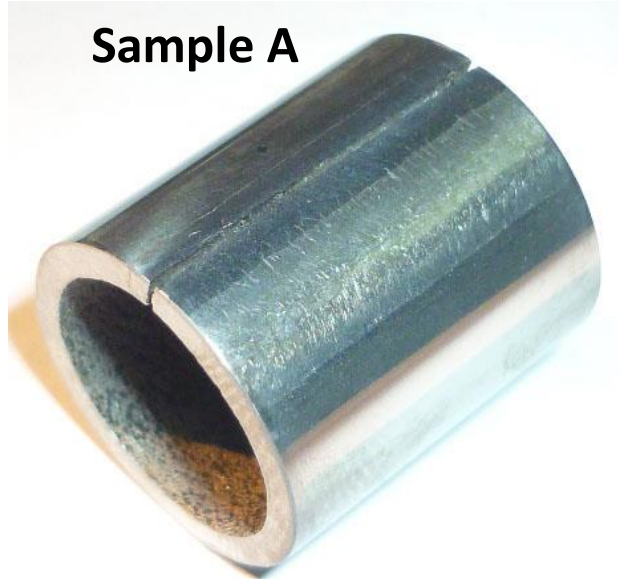
Microstructures obtained from specimen A3 located around the weld seam and the adjacent multiple parallel cracks showing two parallel corrosion fatigue cracks originated from the external surface of the tube and filled with oxides and/or corrosion products. As clearly seen, these two corrosion fatigue cracks were subsequently followed by SCC with branching in transgranular manner.



Microstructures obtained from specimen A3 at location approximately around 180° or at the opposite side of the multiple parallel cracks of the tube showing no any corrosion fatigue crack or SCC. This indicated that the tensile bending stress that may have formed on this external tube surface was not sufficient to promote any fatigue cracking.



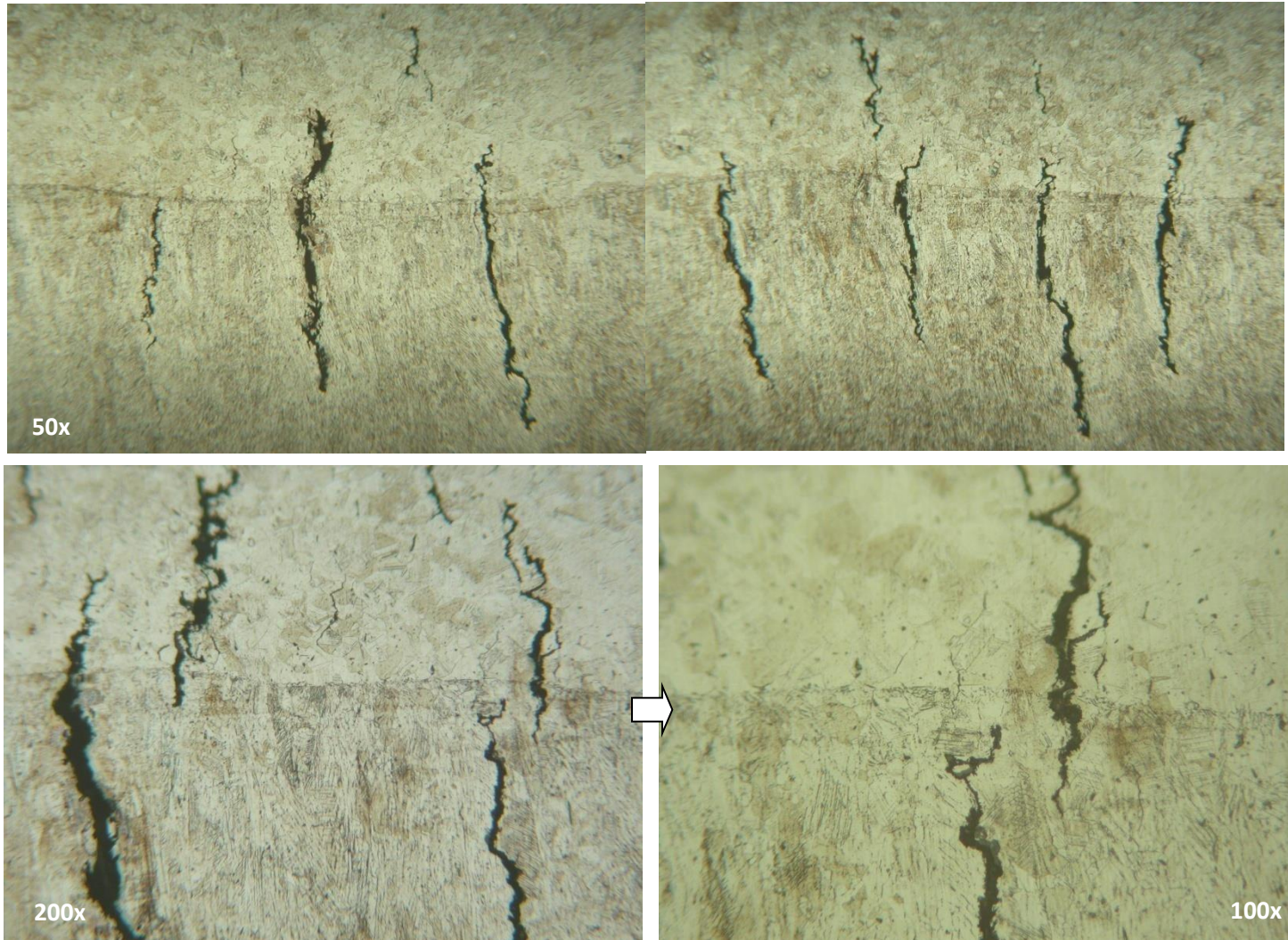
Sample A

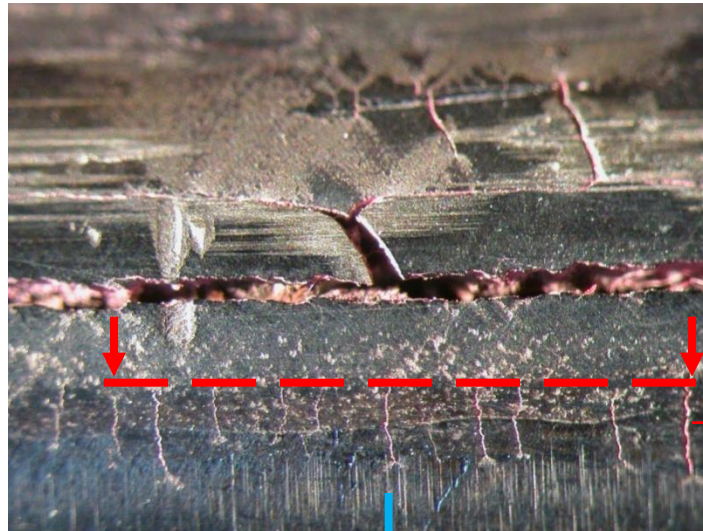


Macrostructures obtained from some area in the tube piece A at its external surface around the primary longitudinal crack. The aim was to reveal multiple parallel cracks in the circular or transverse direction around the tube circumference.

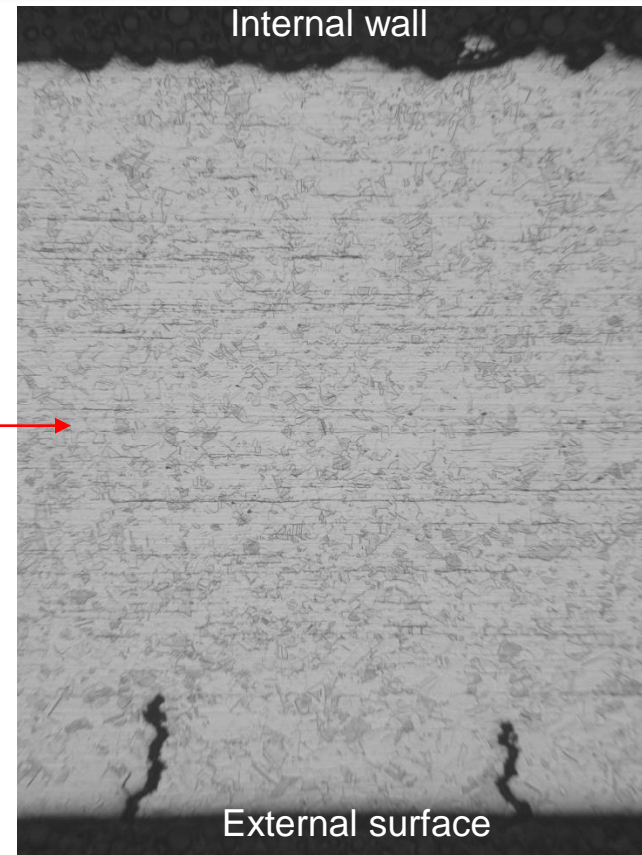
(continued)**Sample A**

Microstructures obtained from some area shown before showing multiple parallel cracks in the circular or transverse direction around the tube circumference. These parallel cracks were formed across the weld seam/HAZ of the tube typical of corrosion fatigue cracking. In addition to several surface cracking, there are also a number of fine cracks formed on the tube surface due to some possible dispersed oxides and/or carbides formation in the tube material.

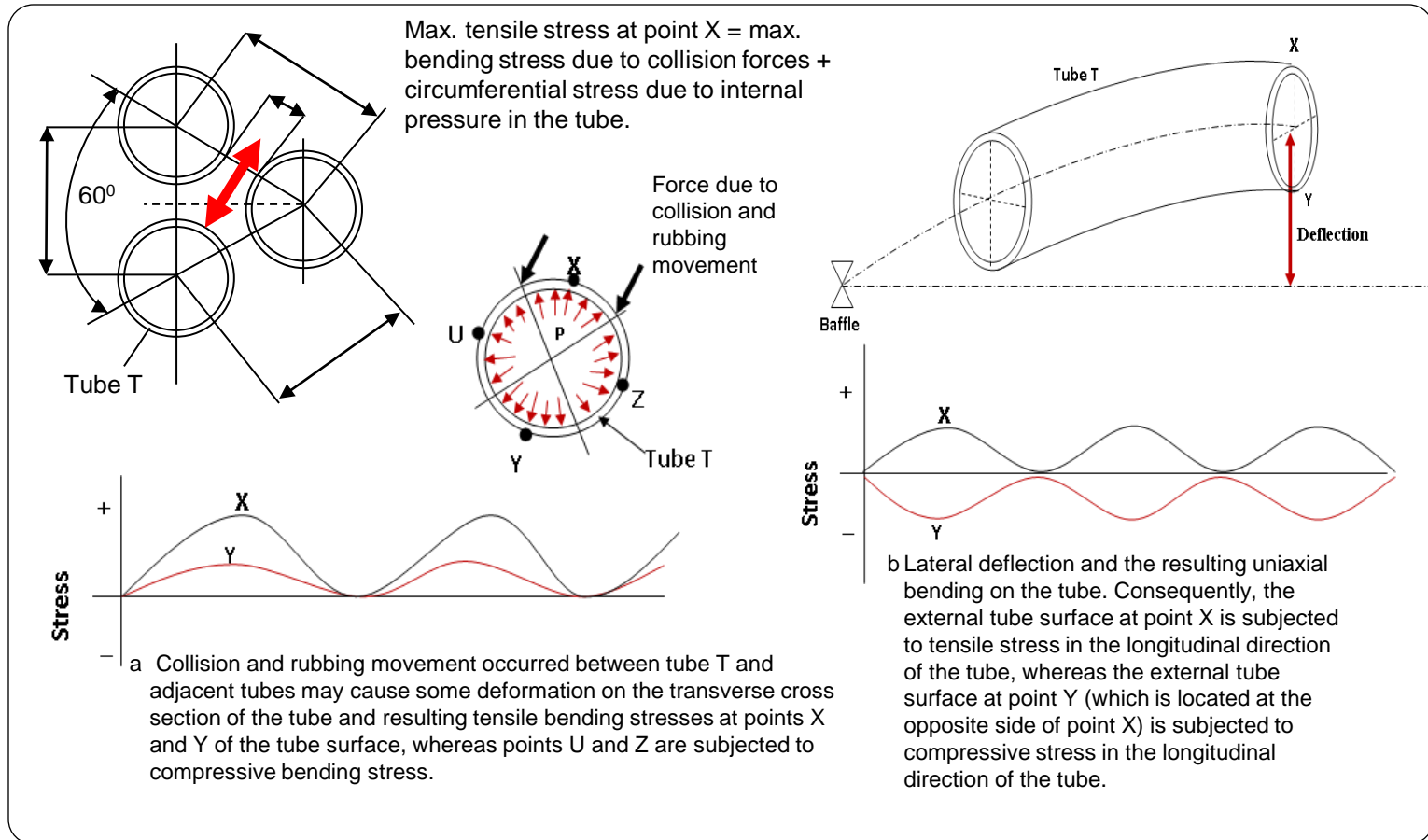




Sample A

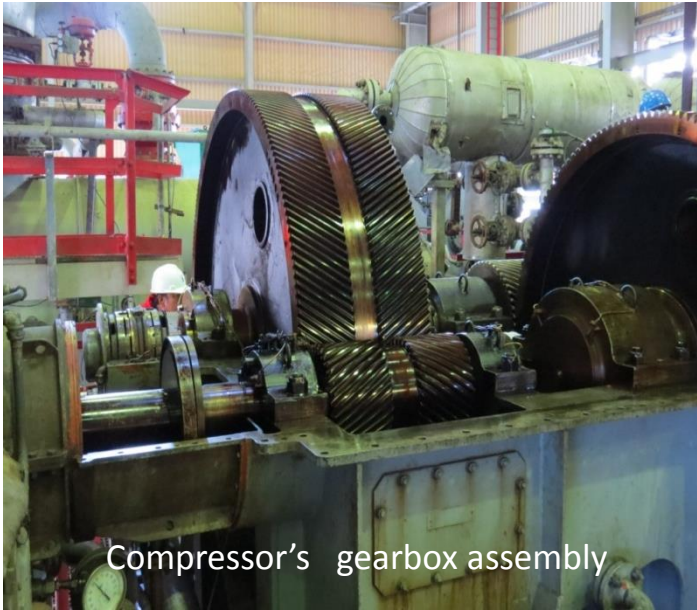


Transverse section in the longitudinal direction of tube piece A in area located close to the primary crack and across the multiple circular parallel cracks showing the corrosion fatigue cracks initiated from the external surface of the tube. In this particular area, no any SCC was formed following the corrosion fatigue cracks. This indicated that in this area only corrosion fatigue occurred, and the cracks path tended to be bulbous with a number of lobes. The crack tips themselves were appeared somewhat blunted and filled with oxides and/or corrosion products.

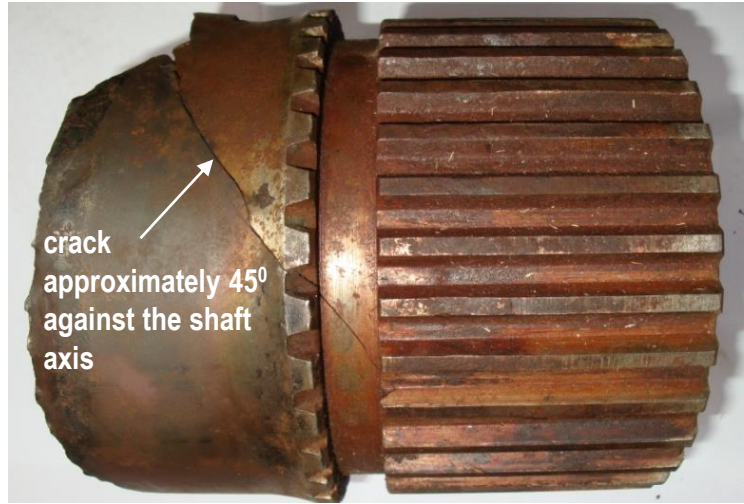


Schematic illustration of dynamic loadings that may occur on tubes due to steam flow-induced vibration.

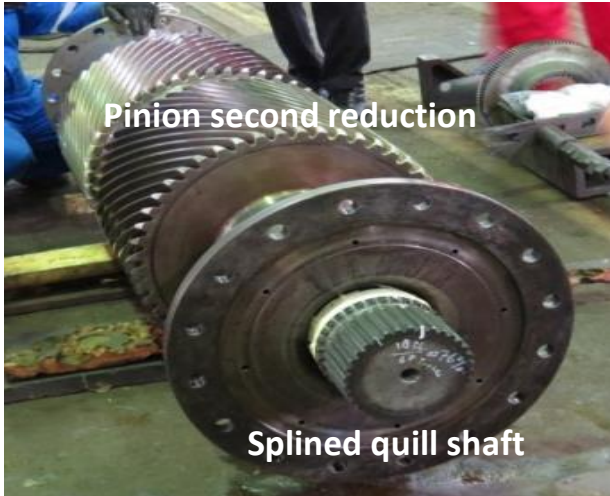
ROOT CAUSE FAILURE ANALYSIS ON FATIGUE CRACK INTERMEDIATE QUILL SHAFT OF A HYDROGEN MAKE-UP COMPRESSOR



Compressor's gearbox assembly



crack approximately 45° against the shaft axis



Pinion second reduction

Splined quill shaft



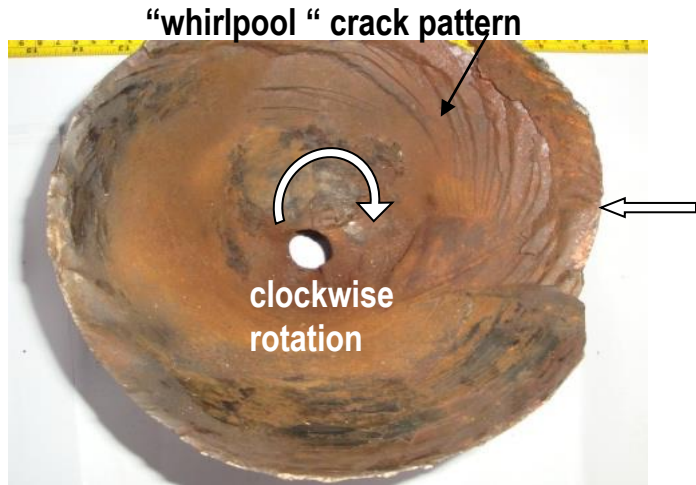
cone like fracture

dark/black temper color

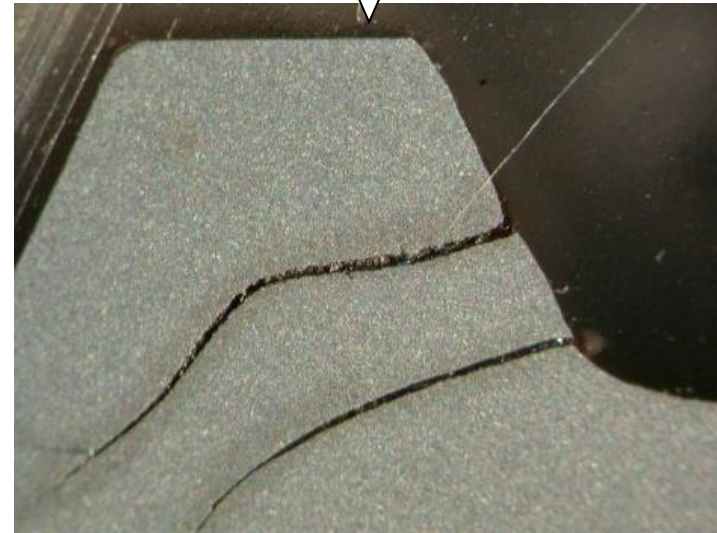
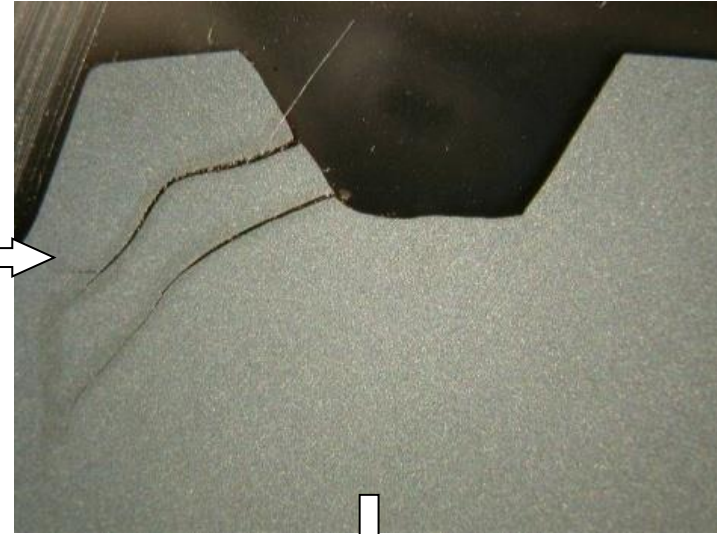
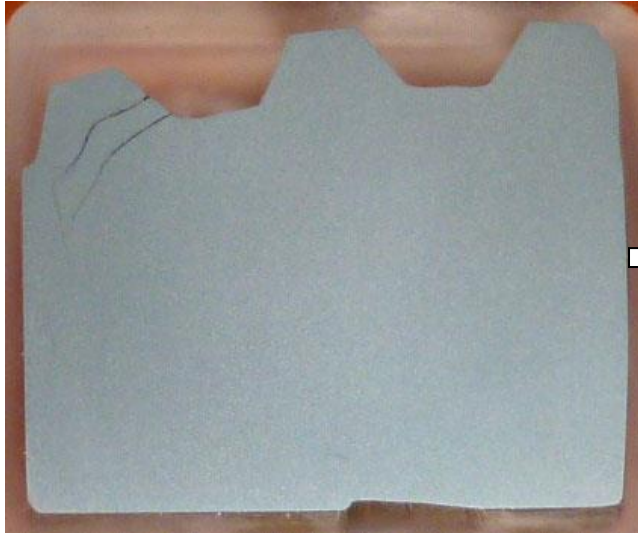


cup like fracture

**ROOT CAUSE FAILURE ANALYSIS ON
FATIGUE CRACK INTERMEDIATE QUILL SHAFT
OF A HYDROGEN MAKE-UP COMPRESSOR (continued)**

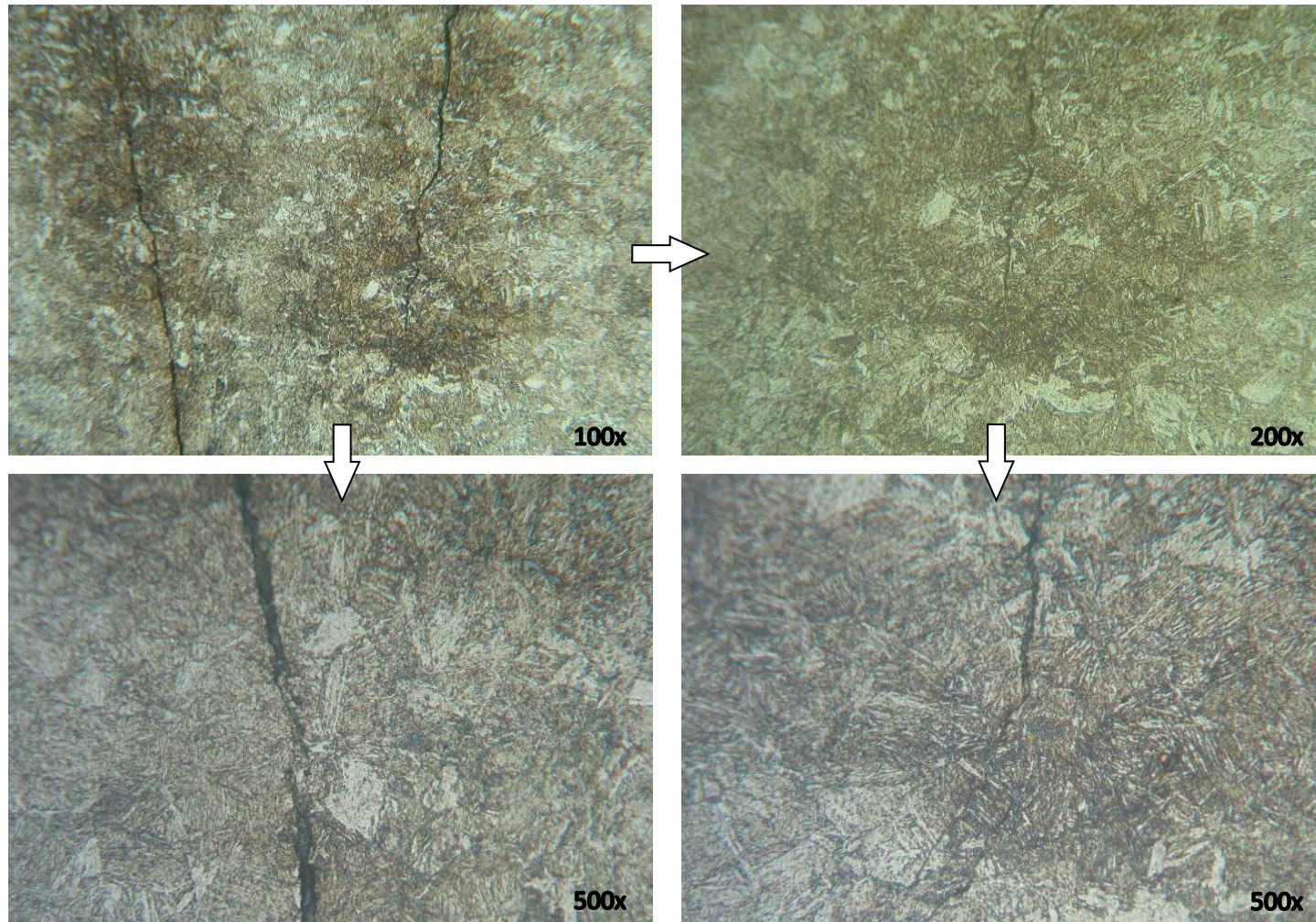


**ROOT CAUSE FAILURE ANALYSIS ON
FATIGUE CRACK INTERMEDIATE QUILT SHAFT
OF A HYDROGEN MAKE-UP COMPRESSOR (continued)**



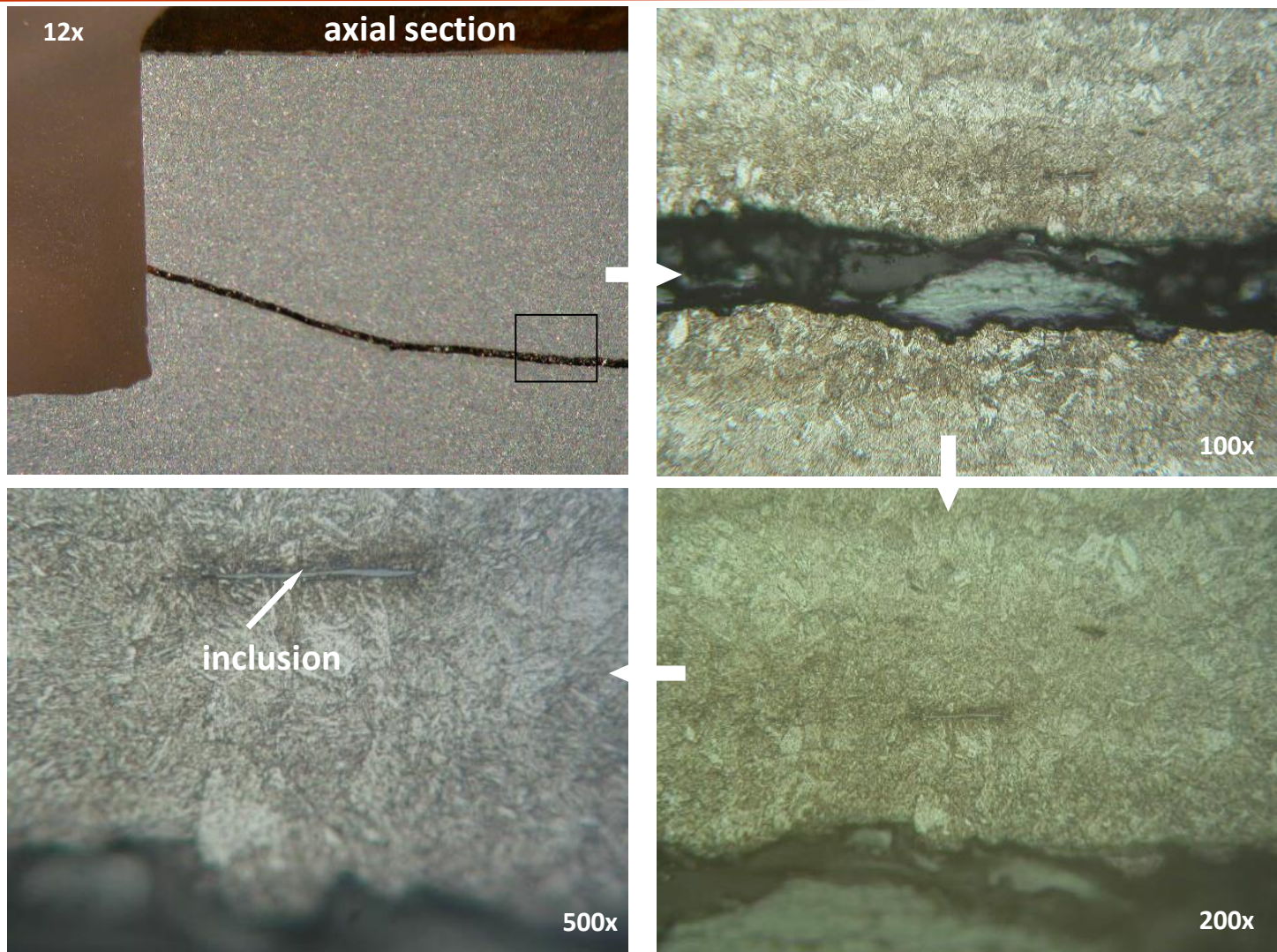
Polished and etched specimen showing two secondary fatigue cracks formed on a spline tooth. Formation of the second cracking was due probably to a bad contact engagement between the shaft splines and the splines of the mating coupling hub. This was probably caused by some misalignment and/or geometric clearance problem.

**ROOT CAUSE FAILURE ANALYSIS ON
FATIGUE CRACK INTERMEDIATE QUILL SHAFT
OF A HYDROGEN MAKE-UP COMPRESSOR (continued)**



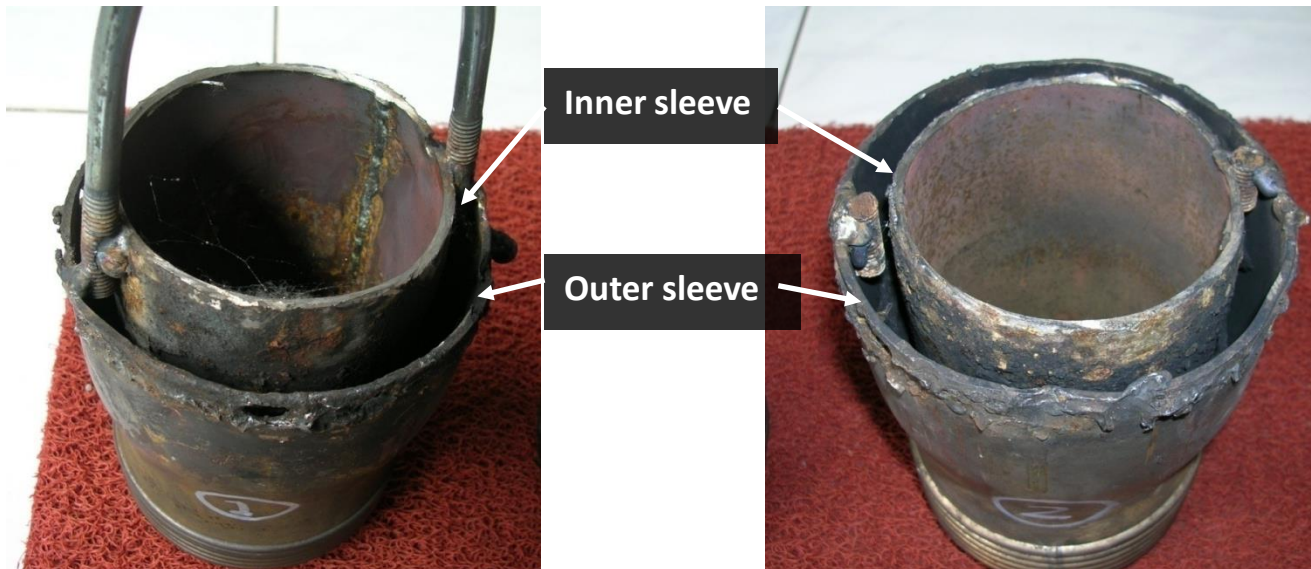
Microstructures obtained at location around the crack tips

**ROOT CAUSE FAILURE ANALYSIS ON
FATIGUE CRACK INTERMEDIATE QUILL SHAFT
OF A HYDROGEN MAKE-UP COMPRESSOR (continued)**

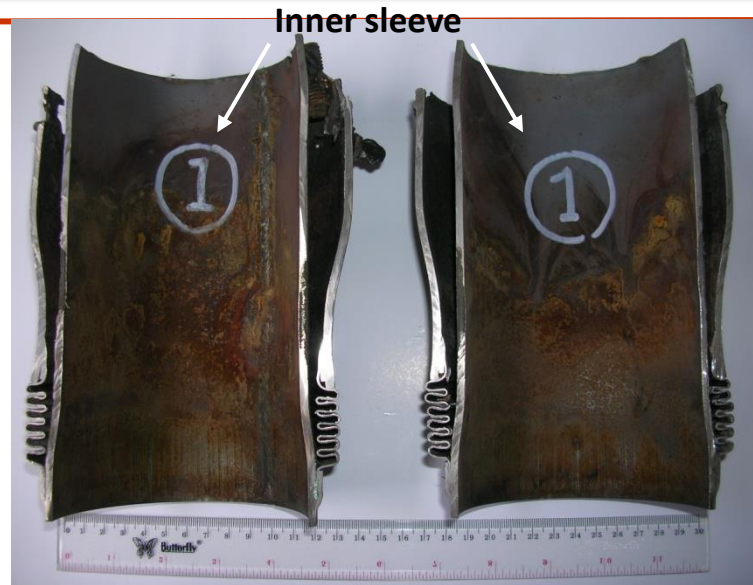


Microstructures obtained at a cracked spline tooth indicated by rectangular grid.

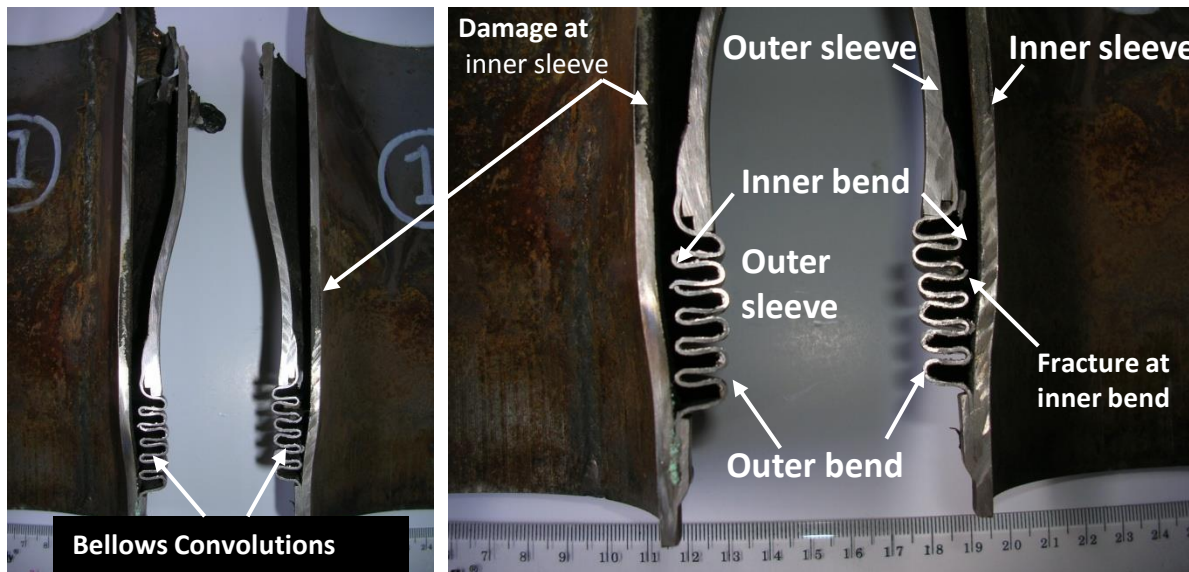
FAILURE ANALYSIS OF AIR PREHEATER TUBE COMPENSATORS



FAILURE ANALYSIS OF AIR PREHEATER TUBE COMPENSATORS (continued)



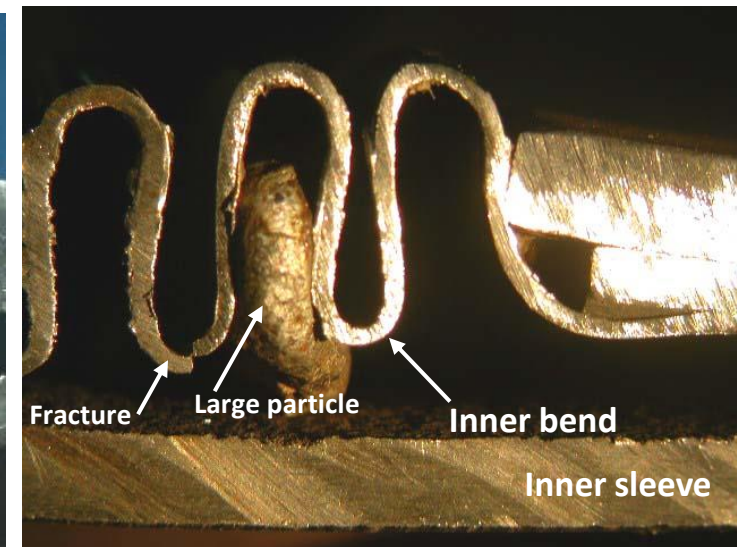
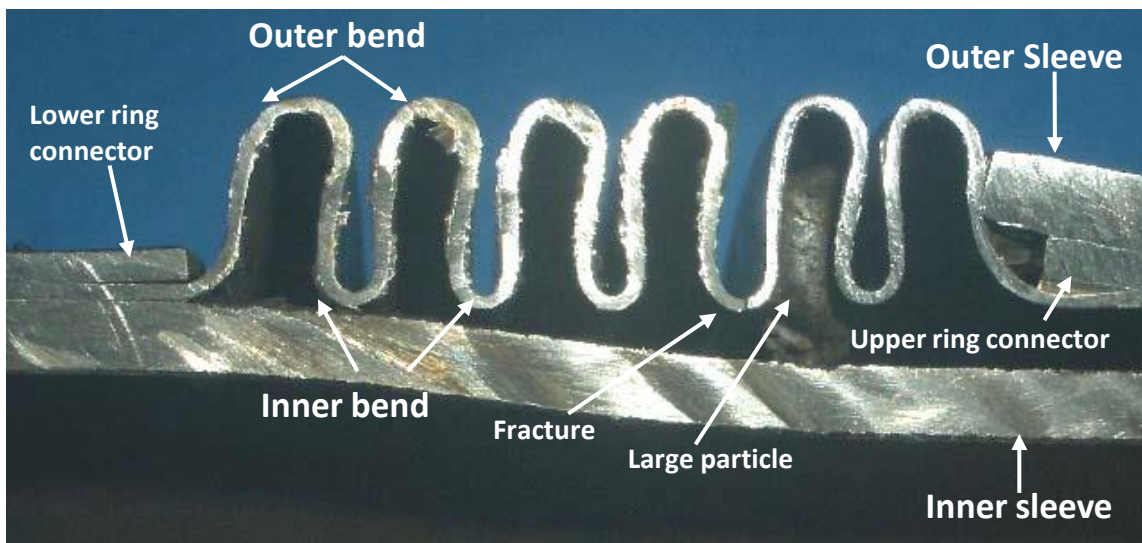
The APH Tube Compensator-1 was split in half showing the inner sleeve, the outer sleeve and the bellows assembly. The bellows assembly consisted of 6 (six) bellows convolutions, the upper ring connector (welded to the outer sleeve), and the lower ring connector (welded to the inner sleeve).

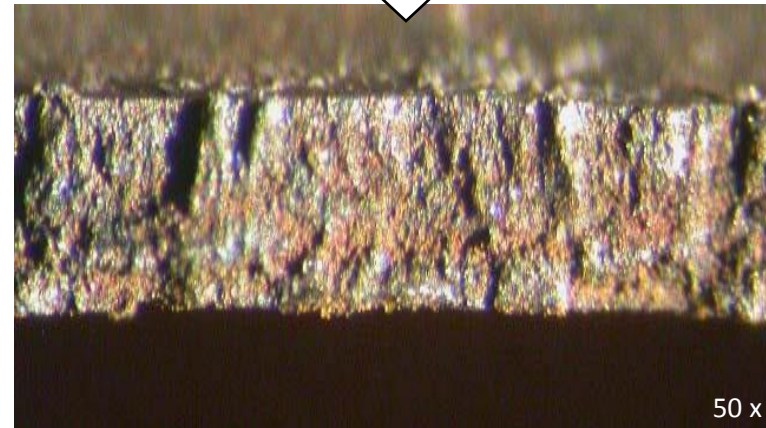
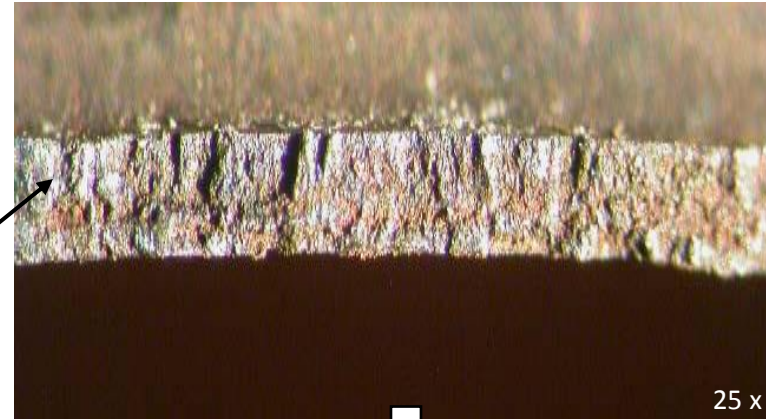
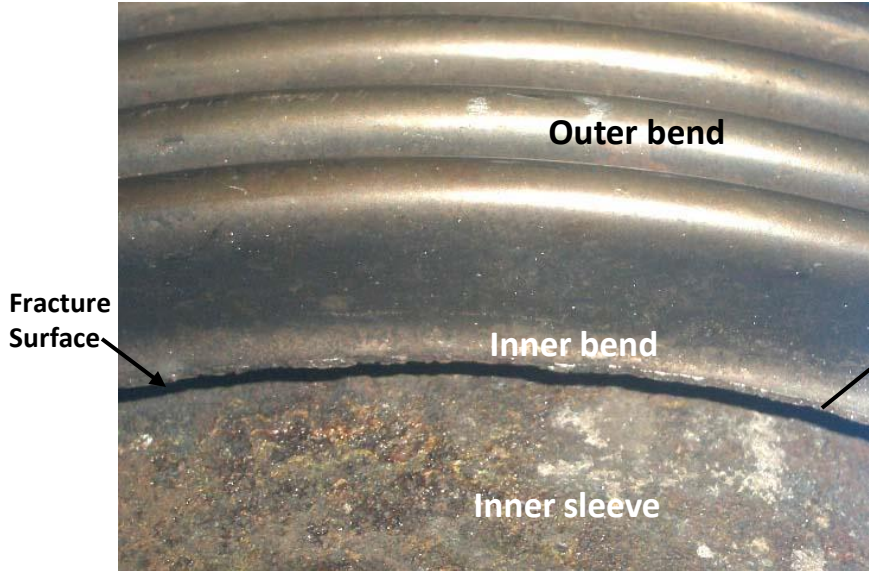


FAILURE ANALYSIS OF AIR PREHEATER TUBE COMPENSATORS (continued)

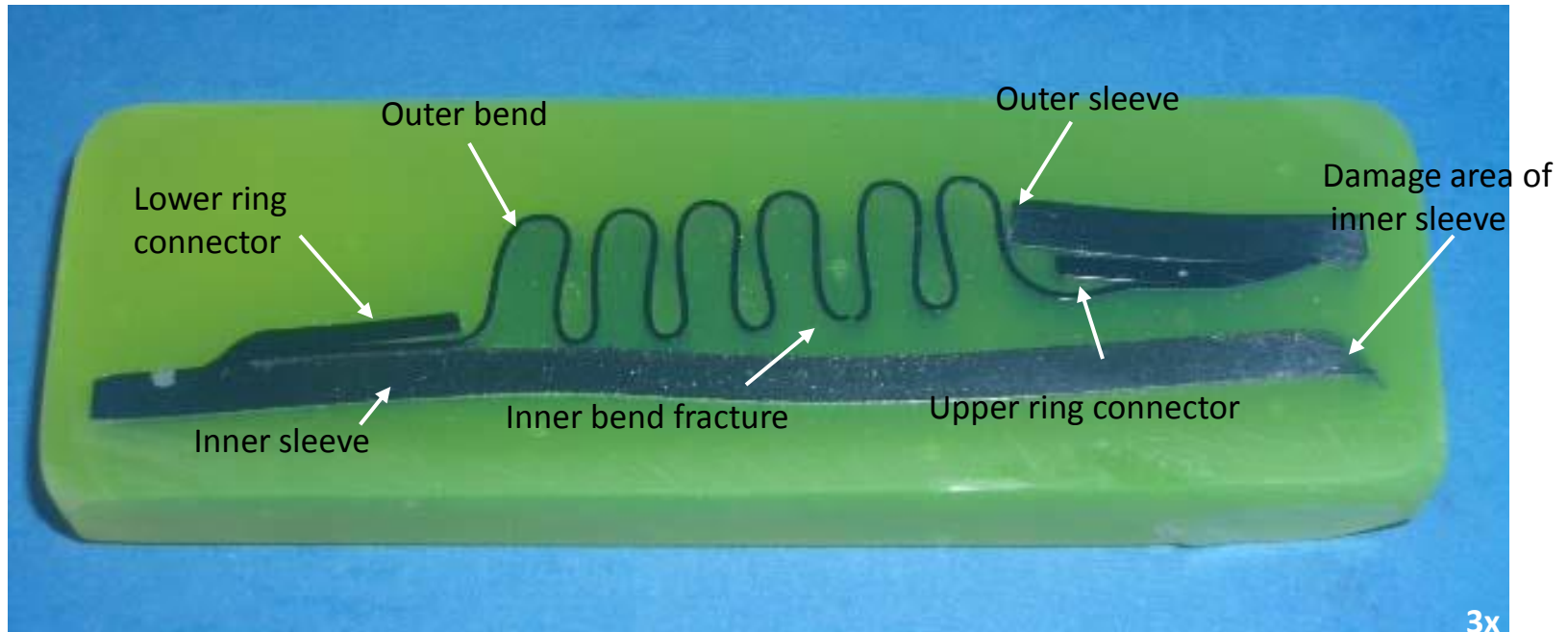


Cross section of the bellows assembly of the APH Tube Compensator-1, showing the 6 (six) bellows convolutions and some portion of the inner and the outer sleeve. It was also apparently seen that a large particle was stuck inside the second bellows convolution and some fracture was formed on the bellows second inner bend convolution.



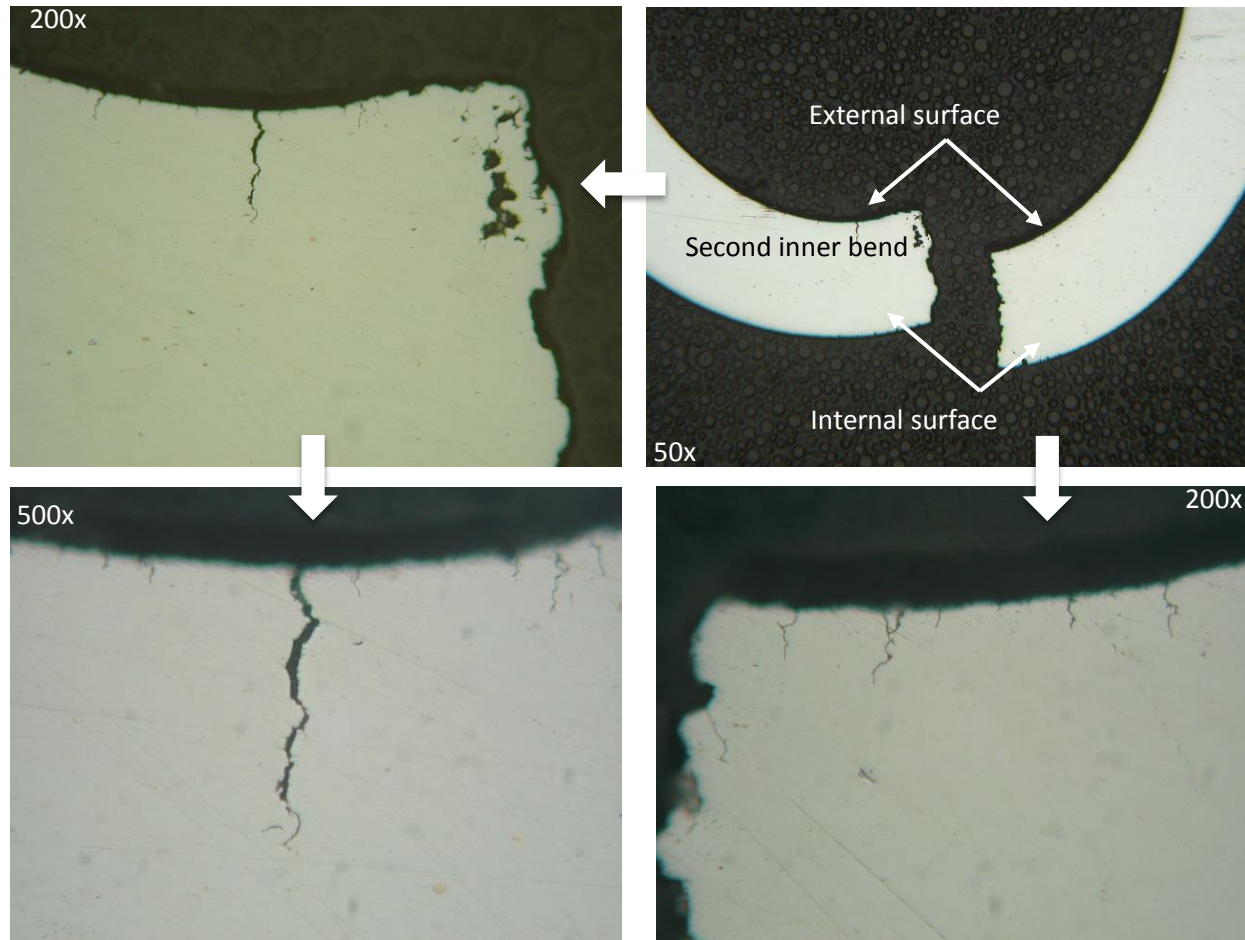


Fracture surface of the bellows inner bend convolution of the failed APH Tube Compensator-1.

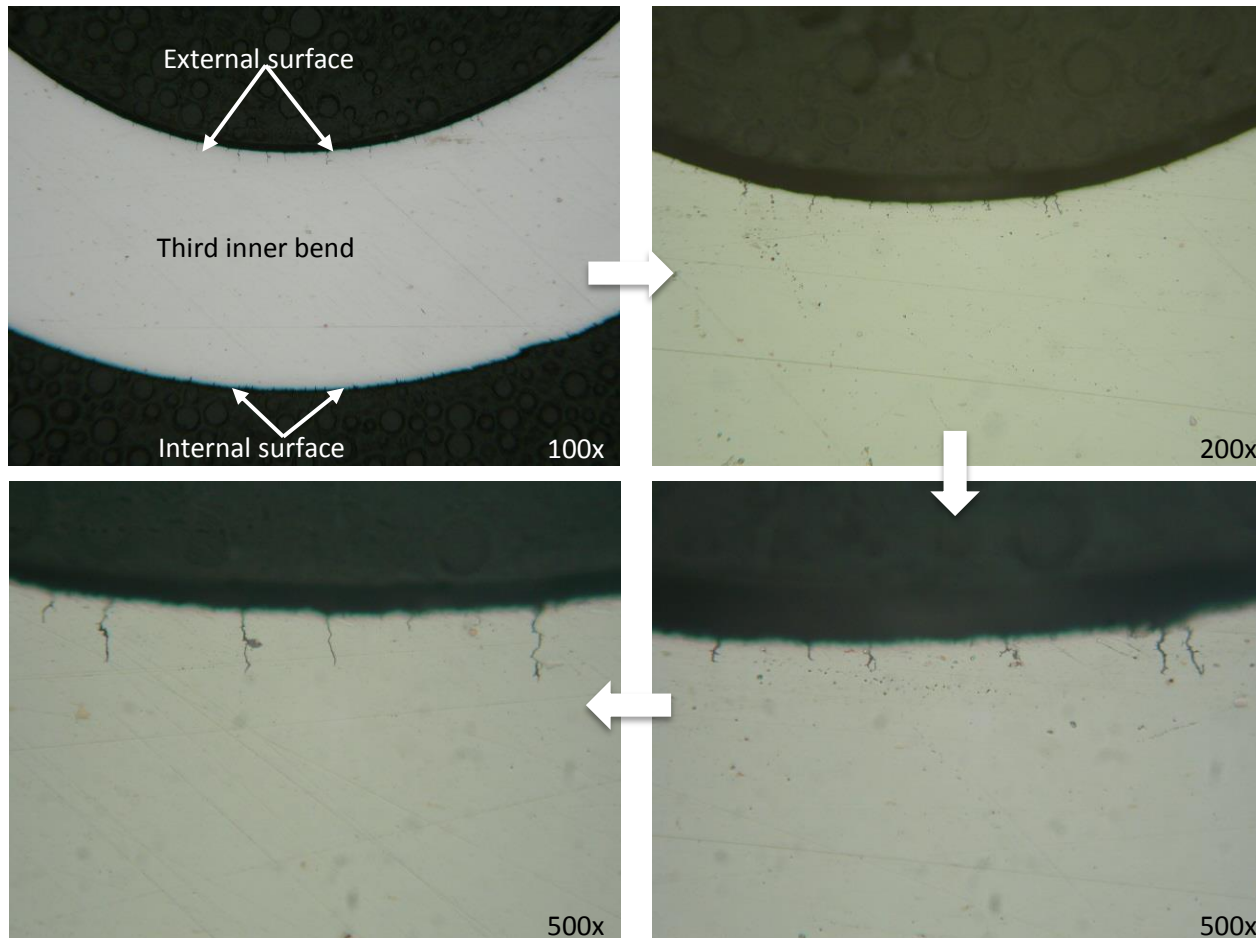


As polished and etched specimen that was sectioned from the failed APH Tube Compensator-1

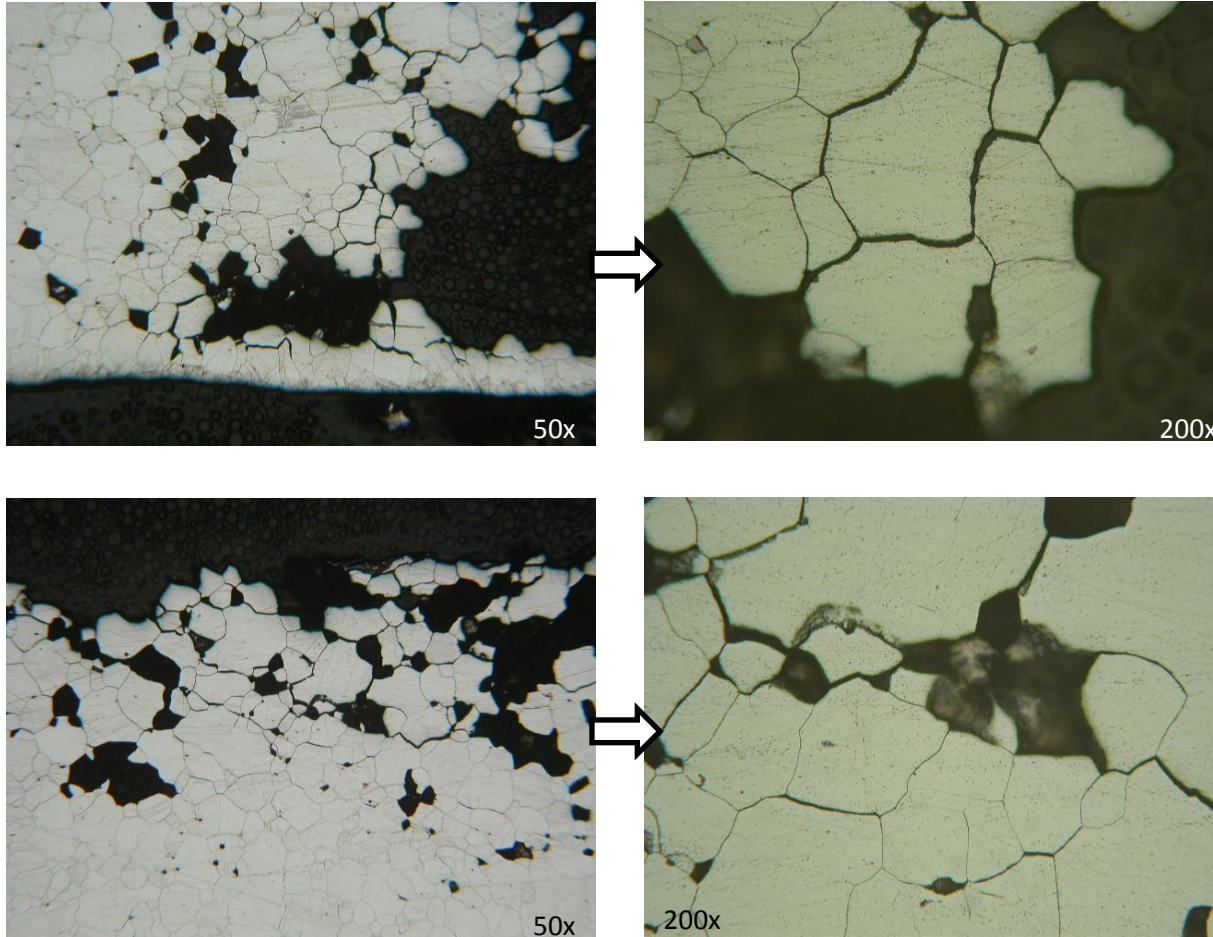
FAILURE ANALYSIS OF AIR PREHEATER TUBE COMPENSATORS (continued)



Microscopic examination on the un-etched specimen performed around the fracture area of the bellows second inner bend convolution of the APH Tube Compensator-1, showing multiple cracks that were originated from the external surface of the inner bend.

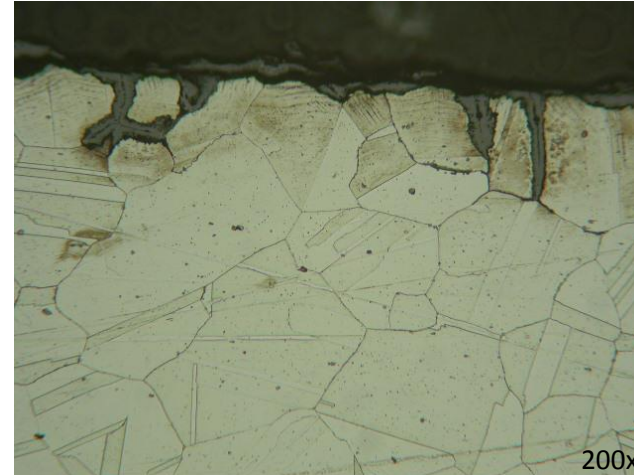
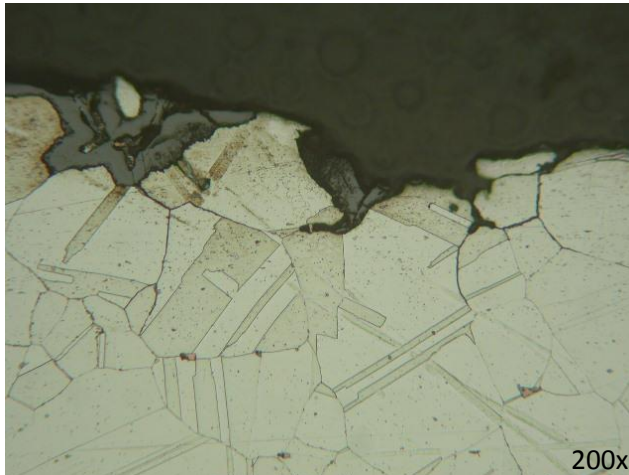
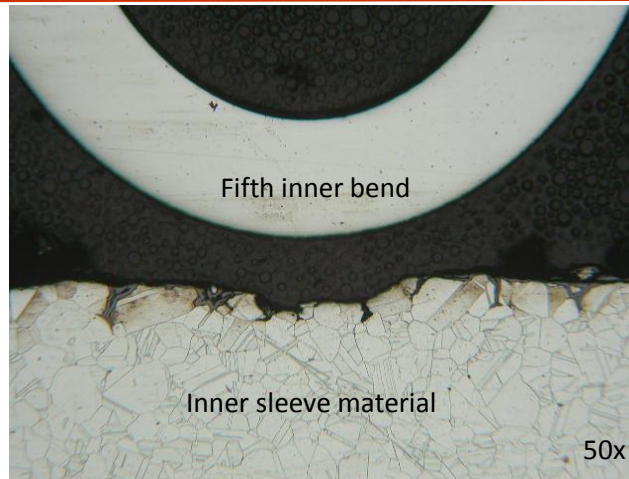


Microscopic examination on the un-etched specimen performed on the bellows third inner bend convolution of the APH Tube Compensator-1, showing multiple cracks that were originated from the external surface of the inner bend.



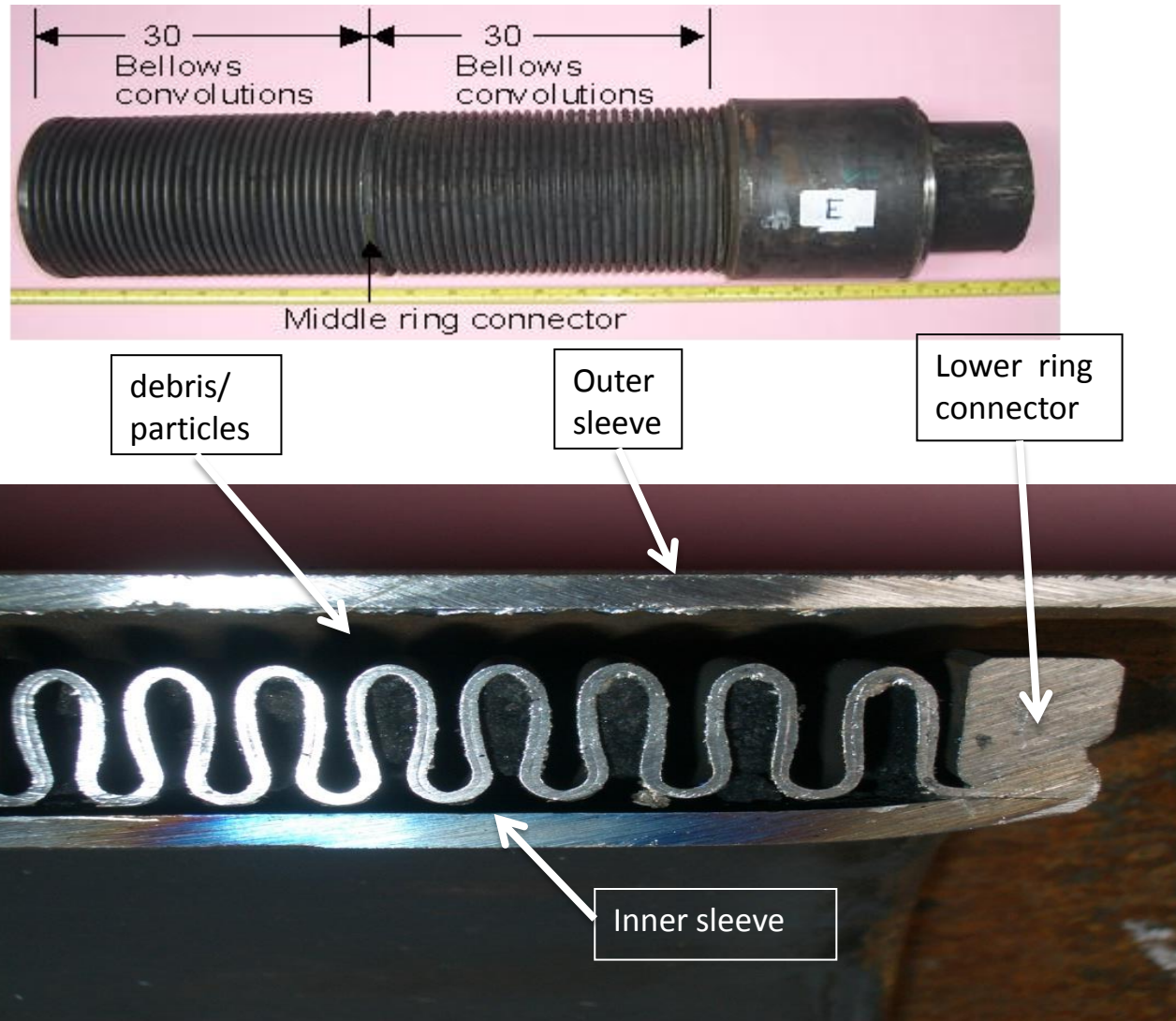
Microstructures obtained from etched specimen of the inner sleeve material of the APH Tube Compensator-1 at location where the damage was observed. The inner sleeve at this particular area was heavily damaged by intergranular attack due probably to a combination effect of corrosion, oxidation and/or carburization.

FAILURE ANALYSIS OF AIR PREHEATER TUBE COMPENSATORS (continued)



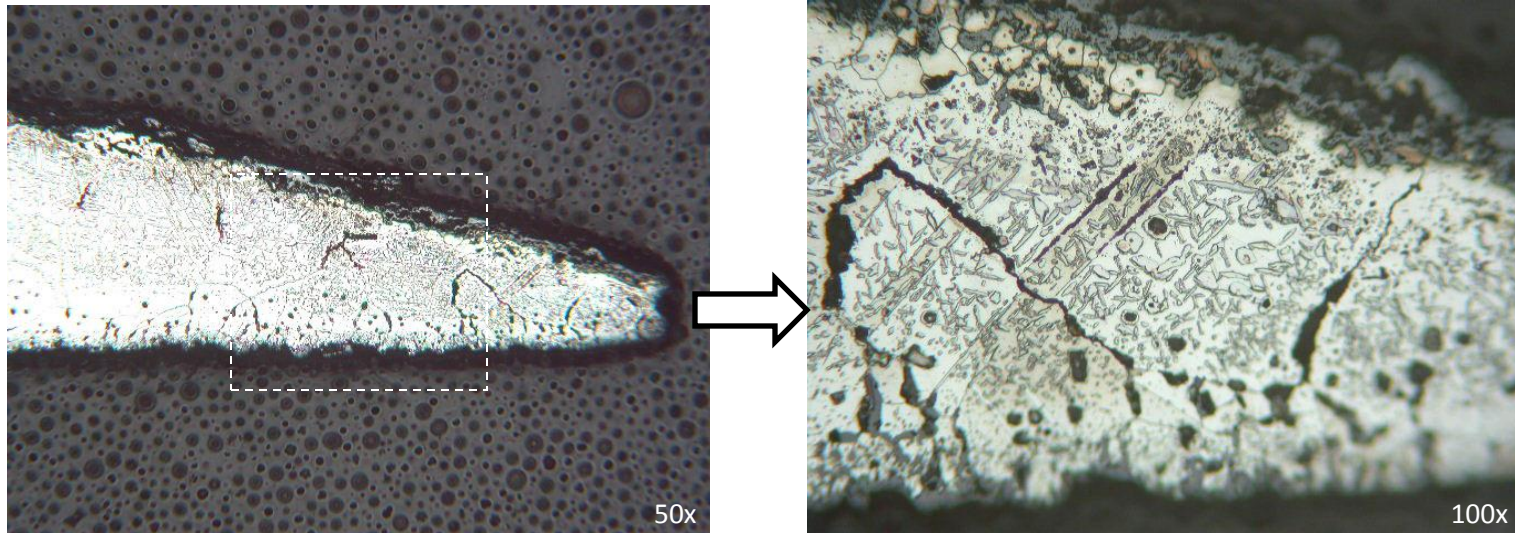
Similar microstructures as seen before was also observed in other location of the inner sleeve (the area that facing to the bellows fifth inner bend convolution) of the APH Tube Compensator-1, but with a lesser degree of damage

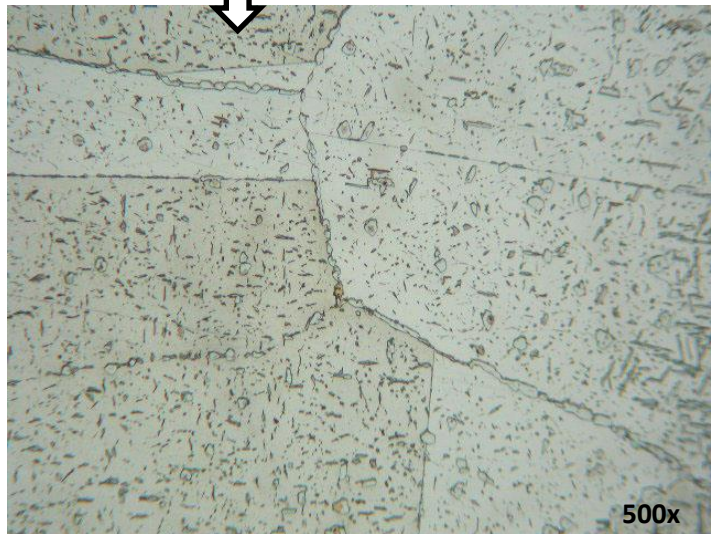
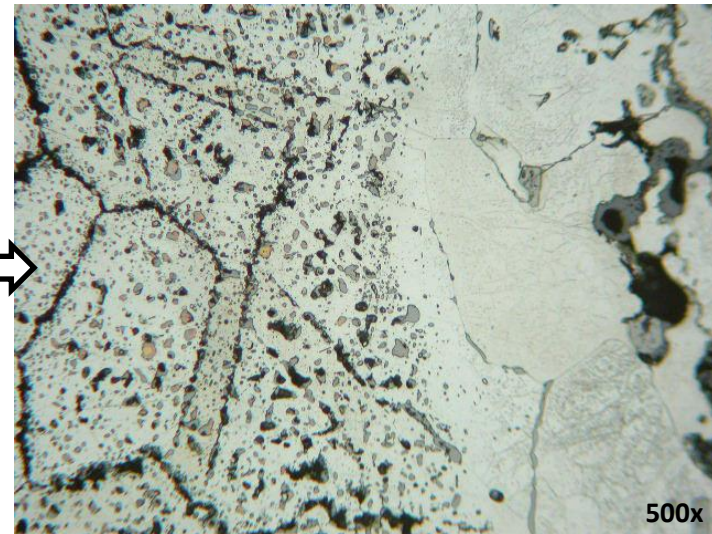
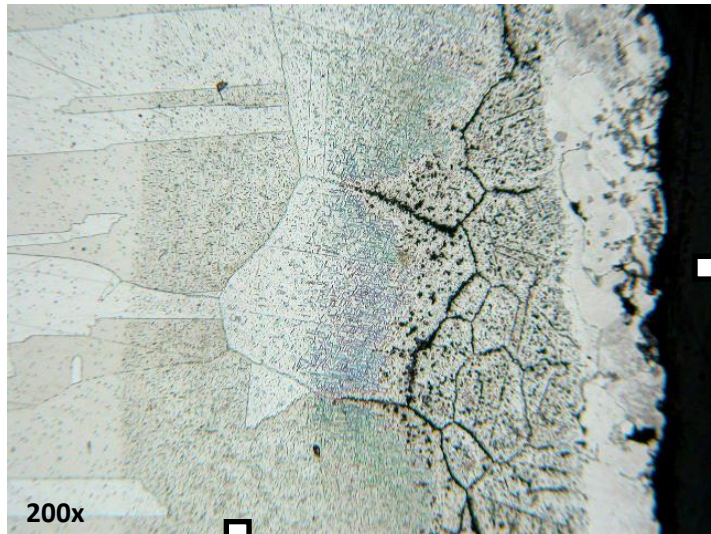
FAILURE INVESTIGATION AND ANALYSIS OF HE TUBE COMPENSATORS DUE TO HIGH TEMPERATURE RELATED CORROSION



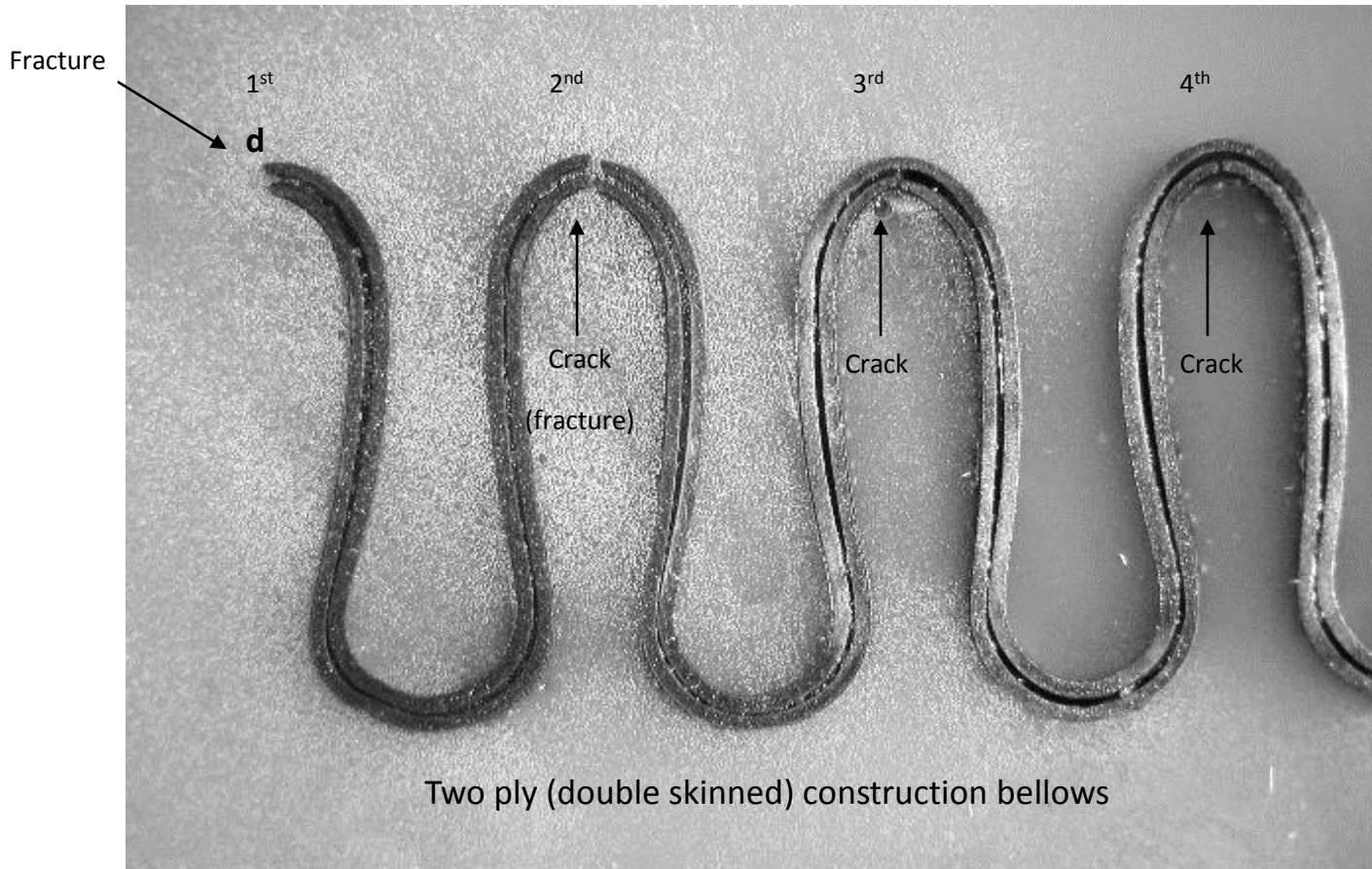


Specimen preparation for metallographic examination on the damaged area of the upper inner and outer sleeves of HE tube compensator

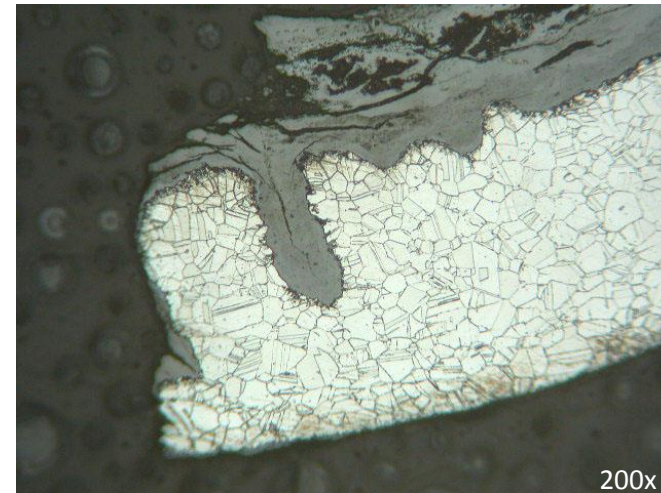
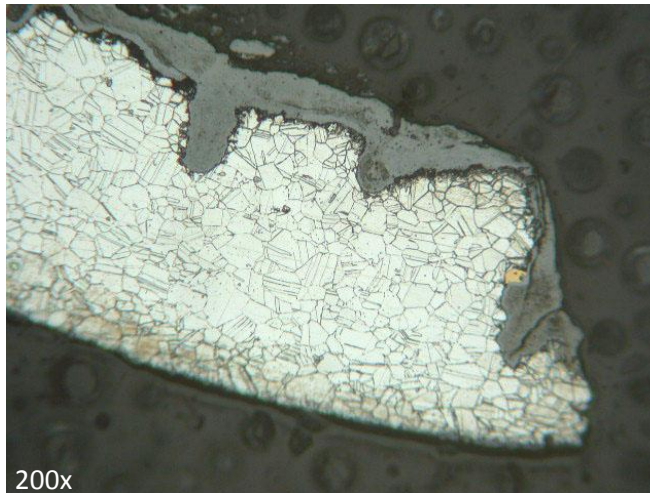
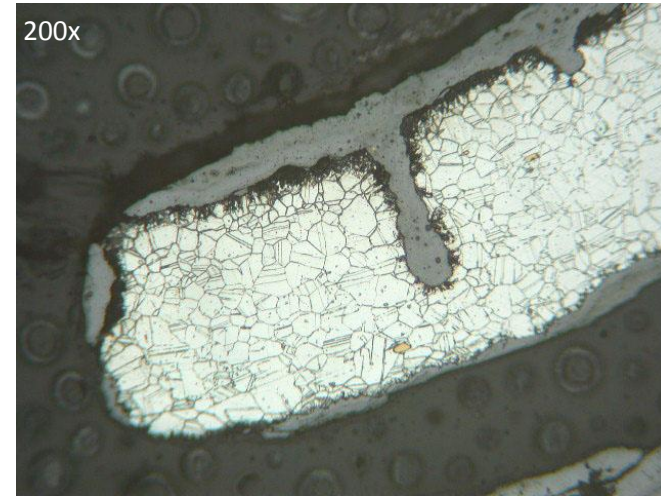
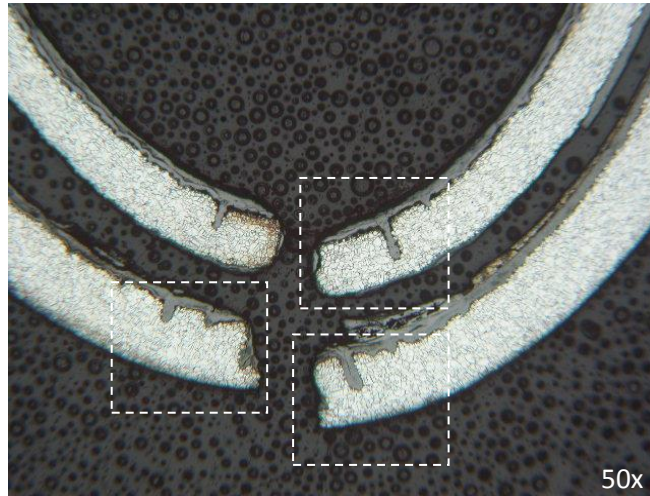




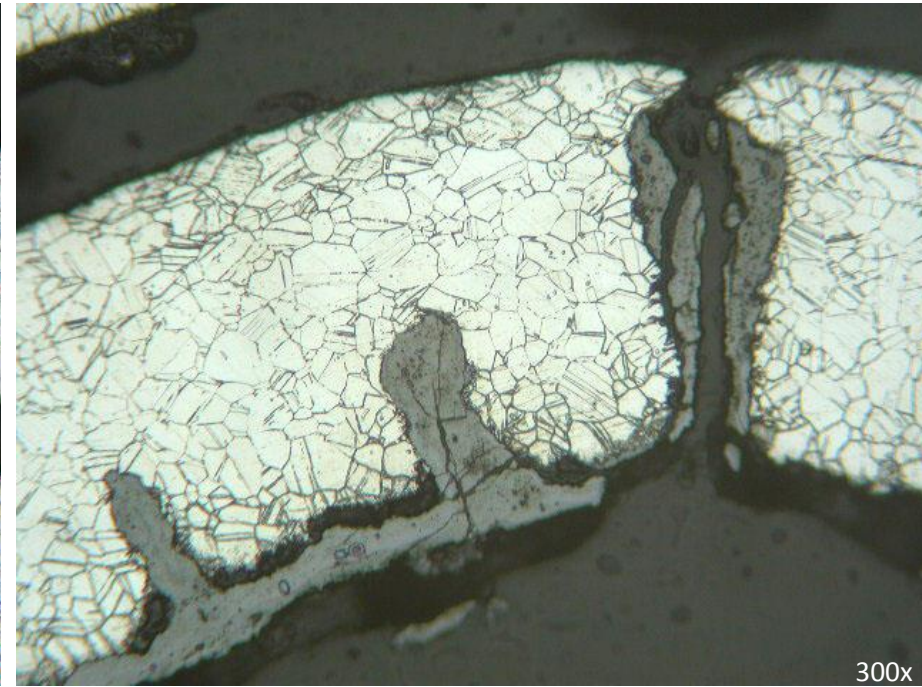
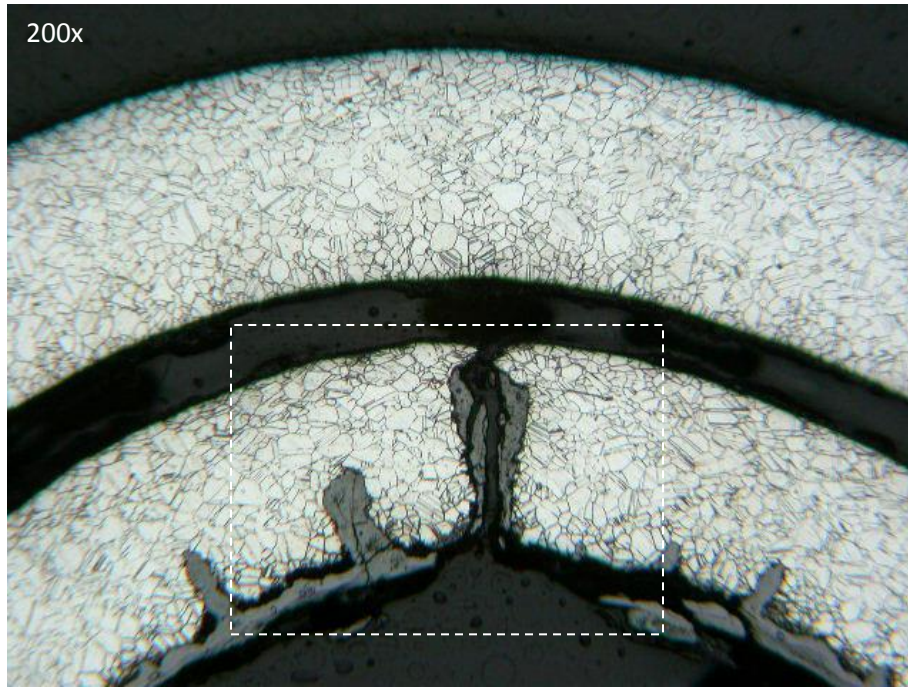
Microstructures obtained on the specimen of the damaged upper inner sleeve of HE tube compensator A.



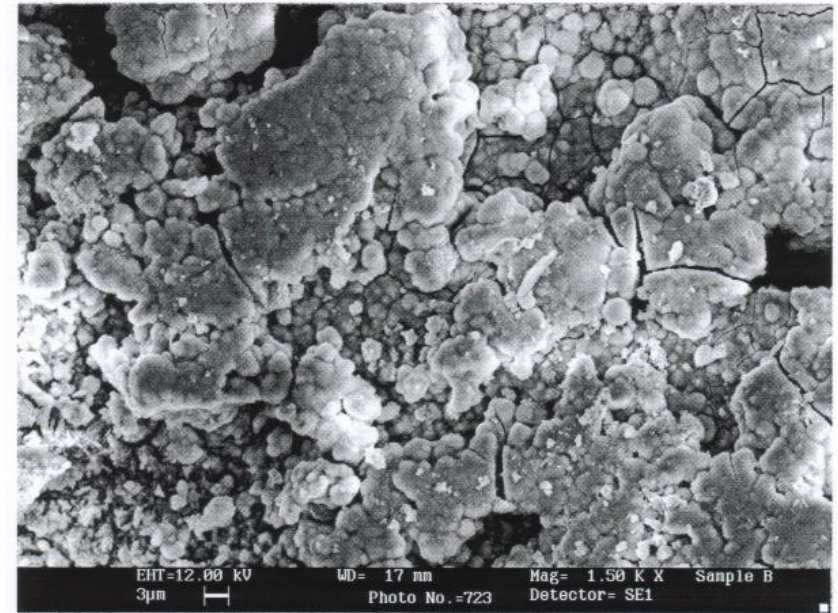
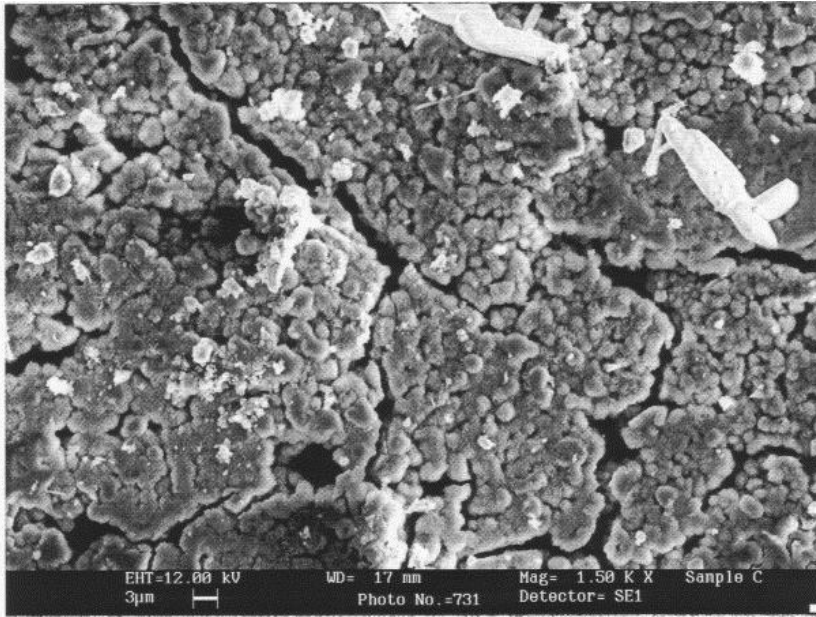
Specimen preparation for metallographic examination on the bellows cross section of the failed HE tube compensator B.



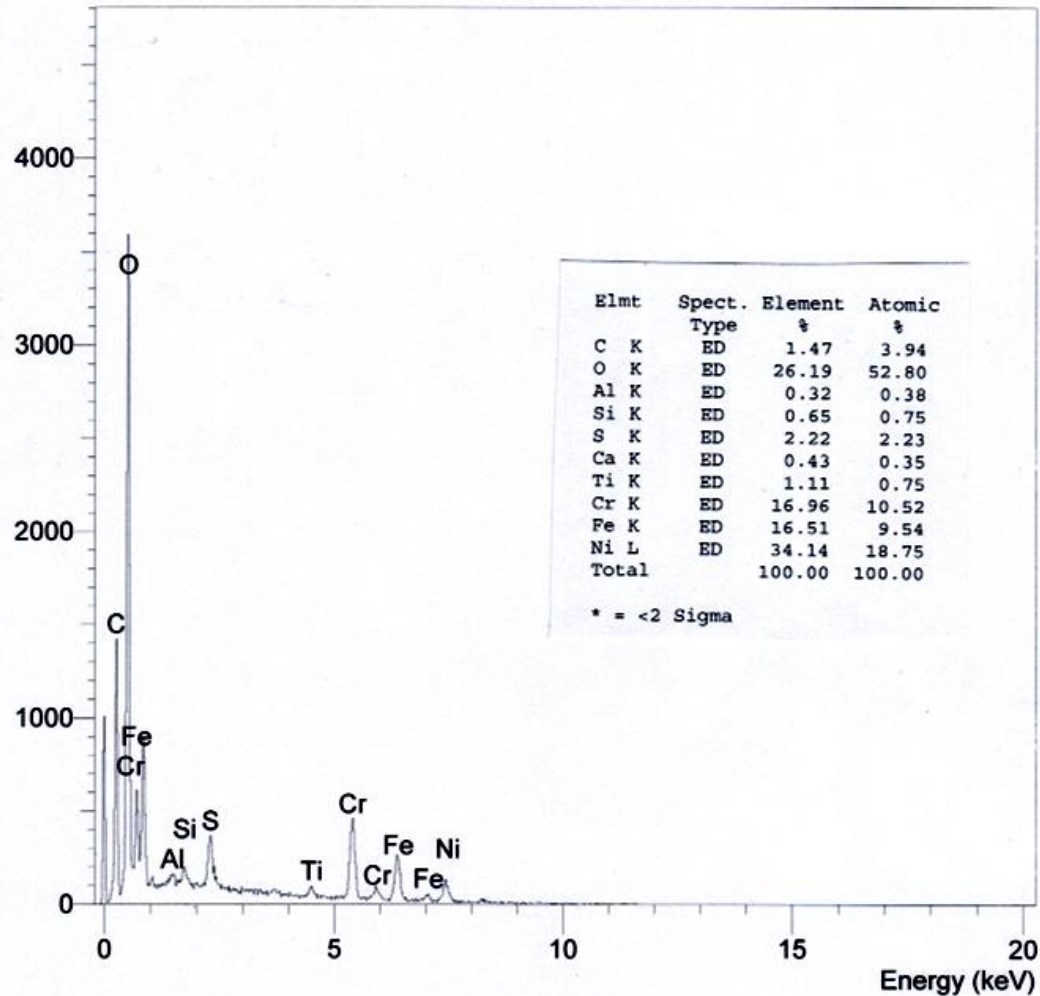
Microstructures obtained on the bend surface (peak) of the bellows first convolution at location d shown in the previous figure (HE tube compensator B).



Microstructures obtained on the bend surface (peak) of the bellows fourth convolution of the failed HE tube compensator D.

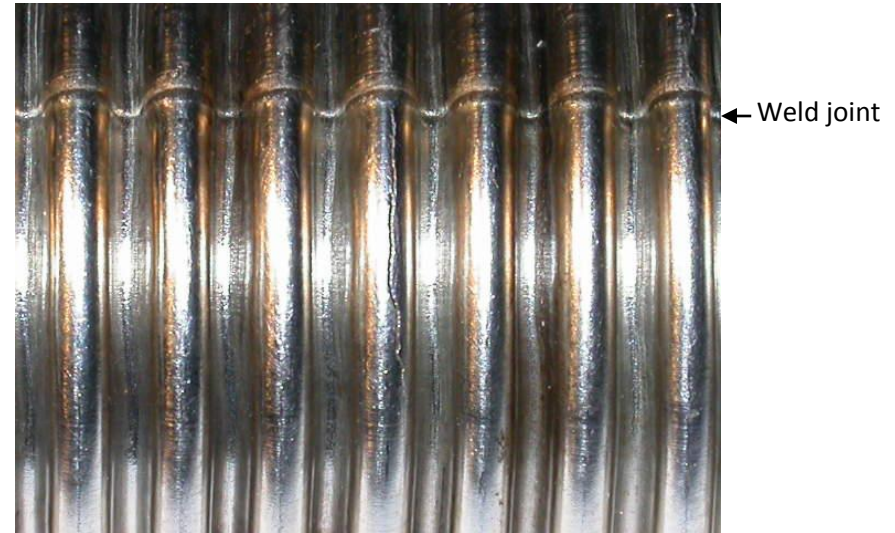


SEM micrographs of some surface fracture of the failed bellows (HE tube compensator B) at different magnifications



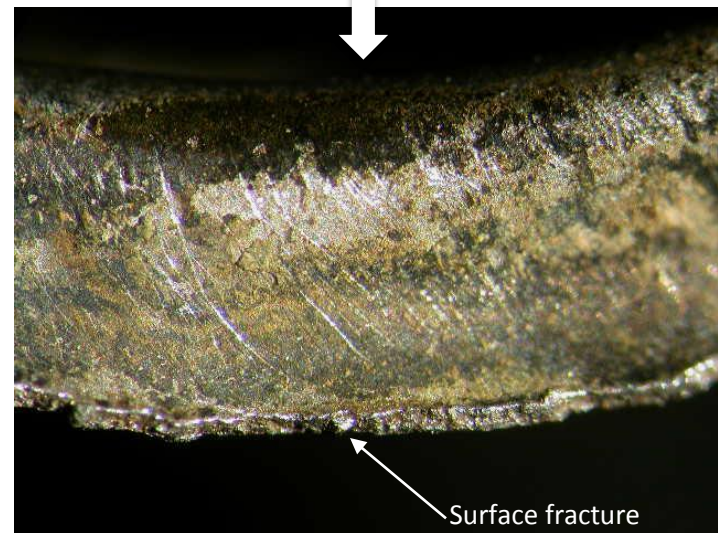
EDS spectrum of elements representing the corresponding location taken from some surface fracture of the failed bellows (HE tube compensator B)

FAILURE INVESTIGATION AND ANALYSIS OF CRACKED HOSE BELLOWS DUE TO STRESS-CORROSION

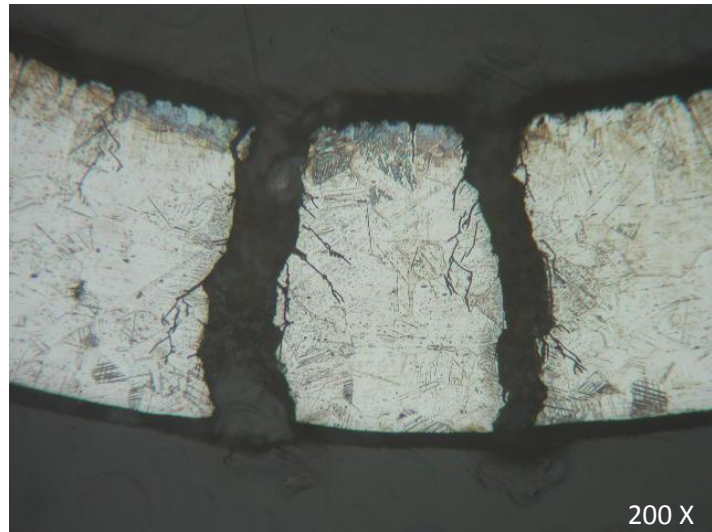
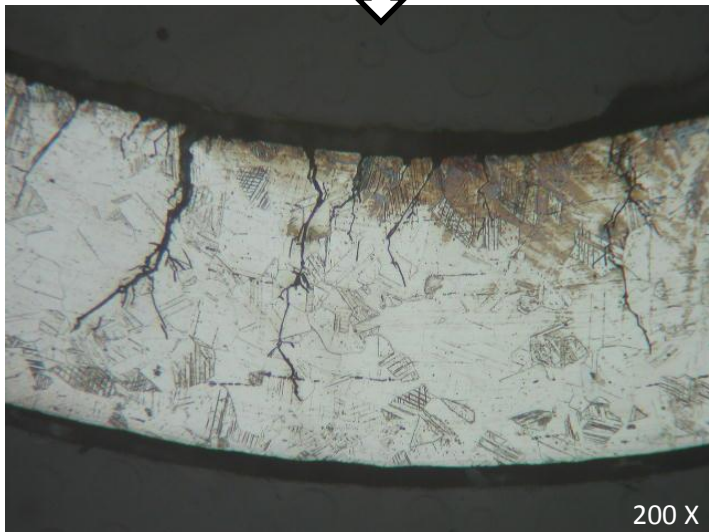
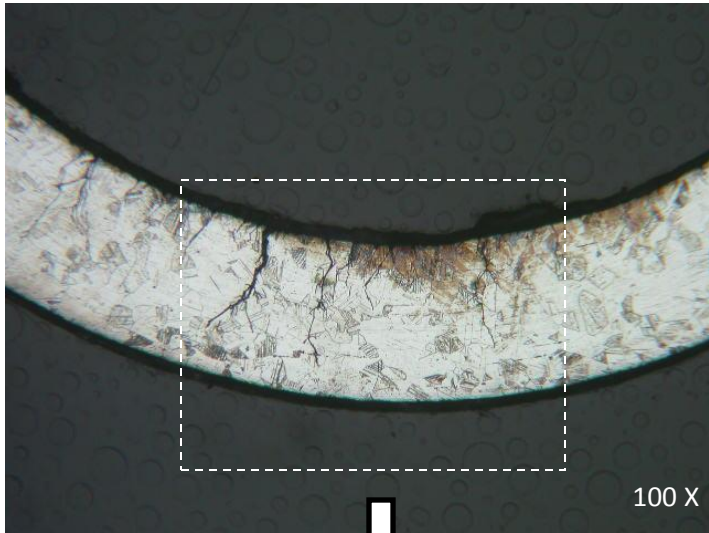




Other crack was also observed at different location of the failed hose bellows. Most of the cracks were found to form at the outside bend of the bellows convolution.

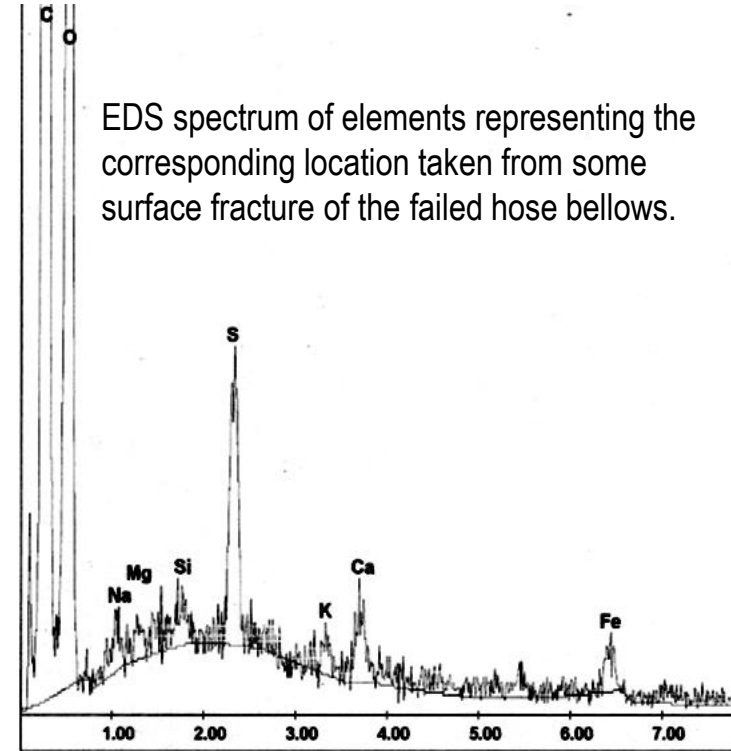
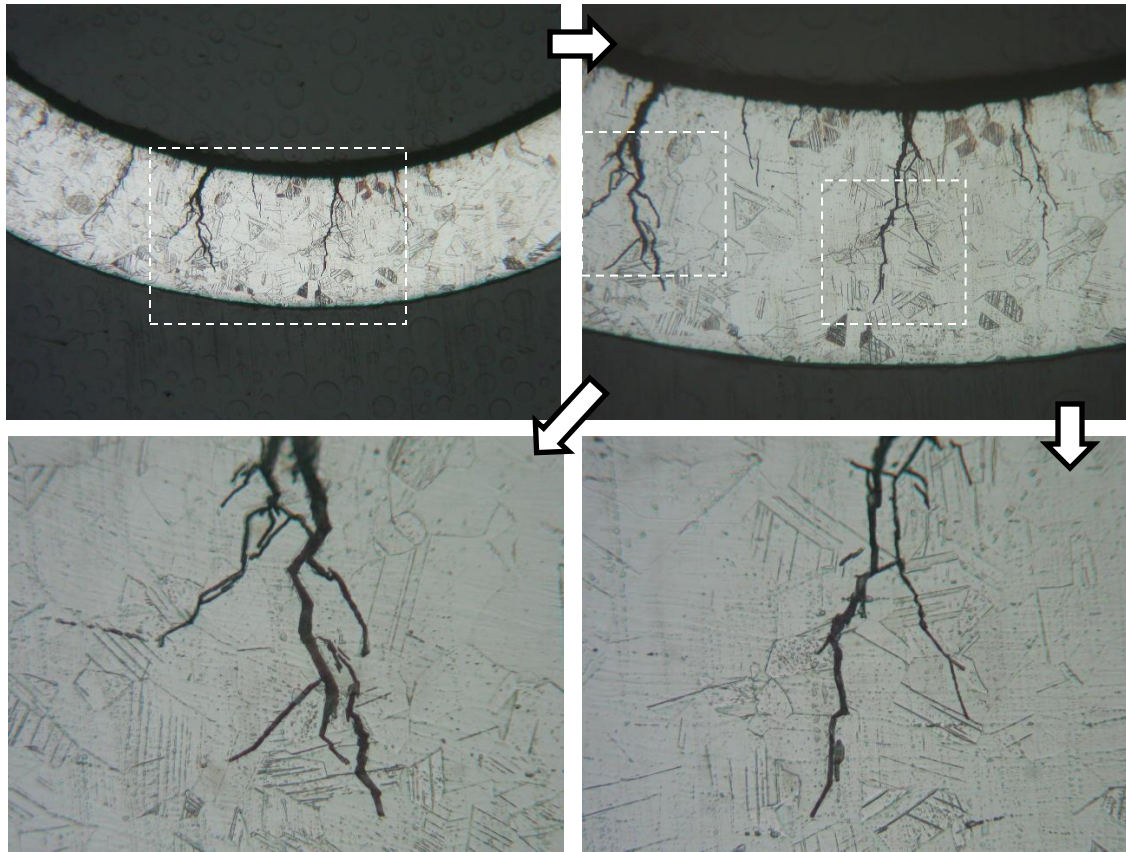


Surface fracture of the failed hose bellows obtained from the large crack .



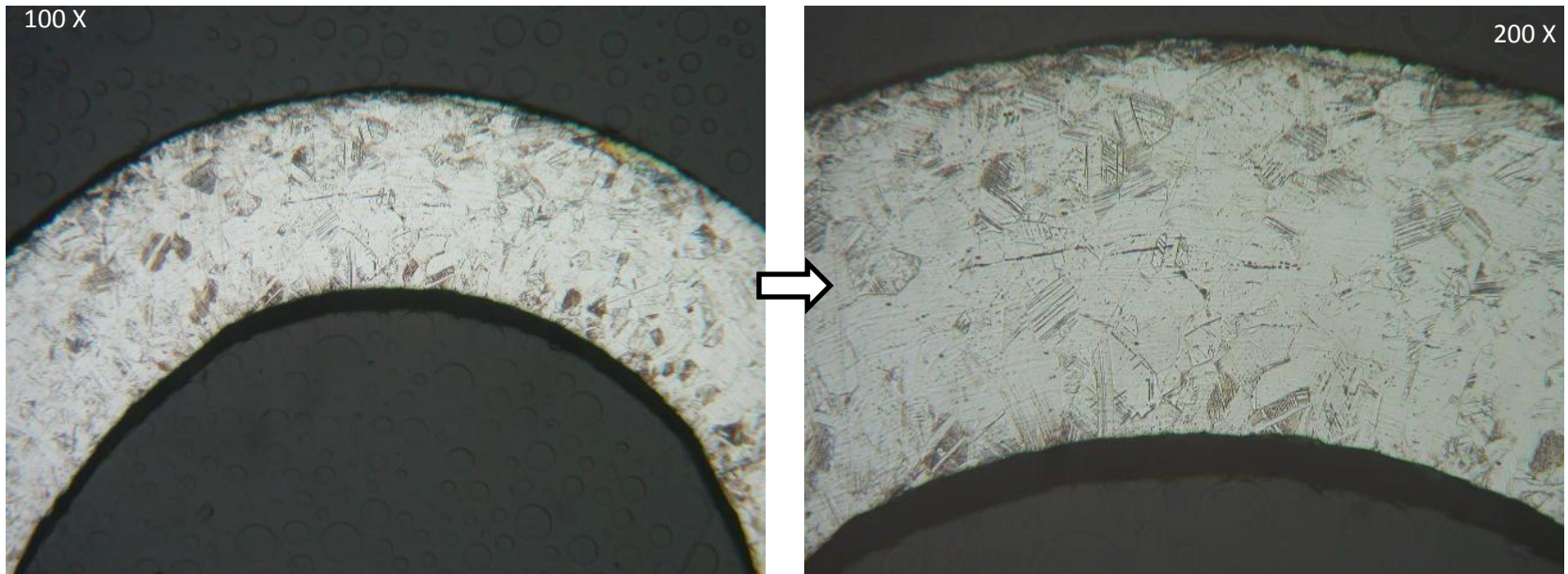
Microstructures having large and small cracks obtained at different external bend of the bellows convolution. Several cracks branching were observed.

FAILURE INVESTIGATION AND ANALYSIS OF CRACKED HOSE BELLOWS DUE TO STRESS-CORROSION (continued)



Element	Wt %	At %
C K	53.83	61.40
O K	43.90	37.59
NaK	0.58	0.35
MgK	0.19	0.11
SiK	0.15	0.07
S K	0.70	0.30
K K	0.10	0.03
CaK	0.22	0.07
FeK	0.34	0.08
Total	100.00	100.00

Several transgranular stress-corrosion cracks were also observed to form at other external bend of the bellows convolutions due to applied bending tensile stress



Microstructures obtained at the internal bend of the bellows convolution, showing no cracks formation due to the absence of applied tensile stress. Instead, in this area the applied compressive stress may be present.

ROOT CAUSE FAILURE ANALYSIS ON BOILER TUBE DUE TO SHORT-TERM LOCALIZED OVERHEATING

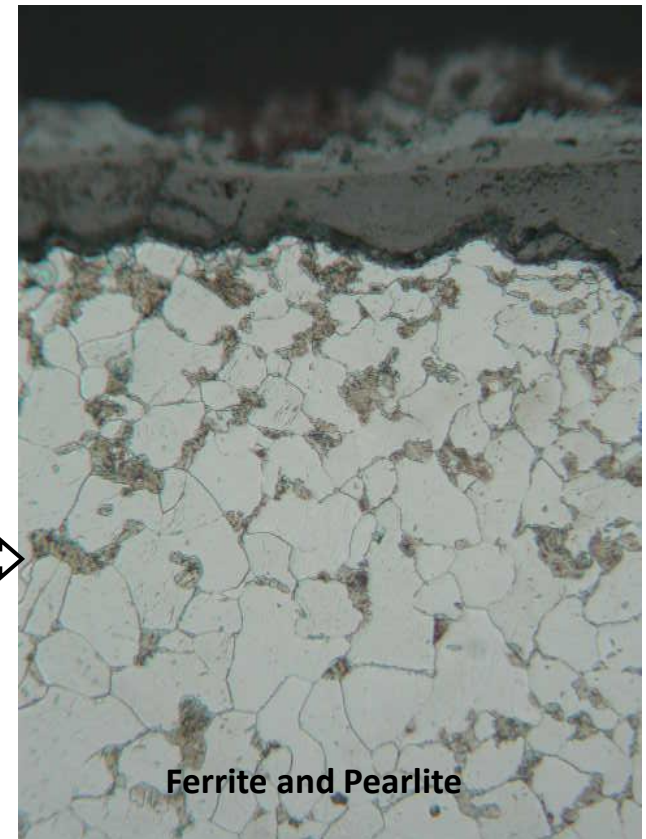
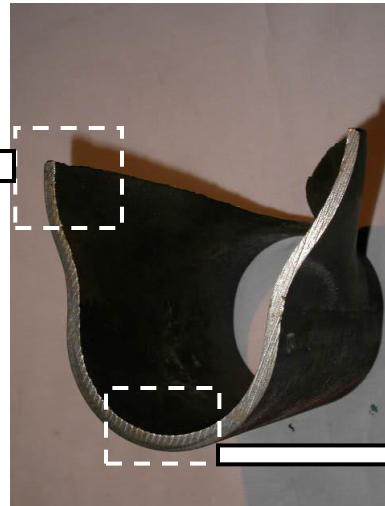
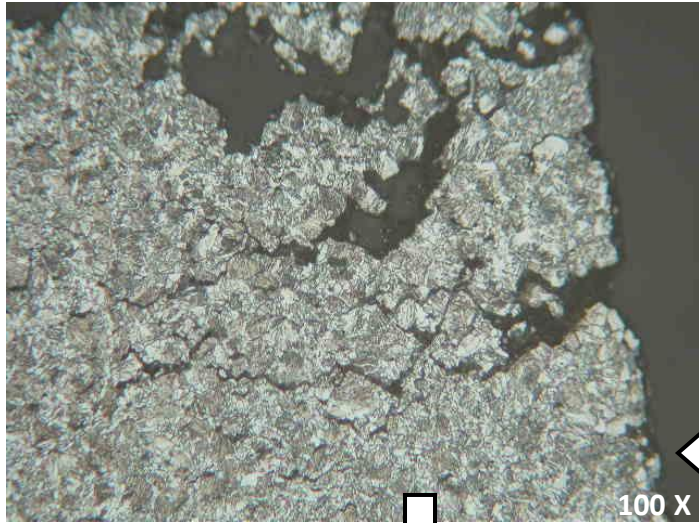


Tube burst due to short-term
localized overheating



ROOT CAUSE FAILURE ANALYSIS ON BOILER TUBE DUE TO SHORT-TERM LOCALIZED OVERHEATING (continued)

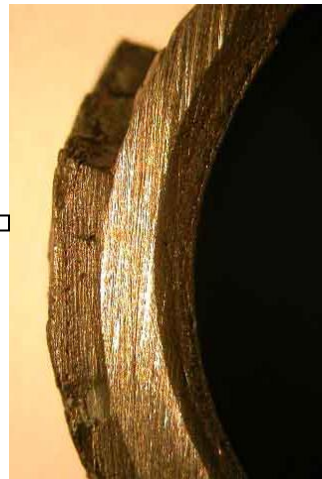
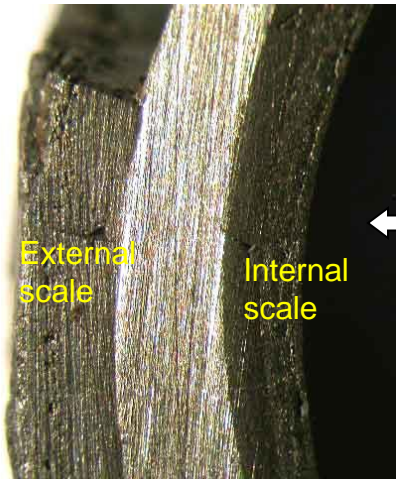
Tube burst due to short-term localized overheating



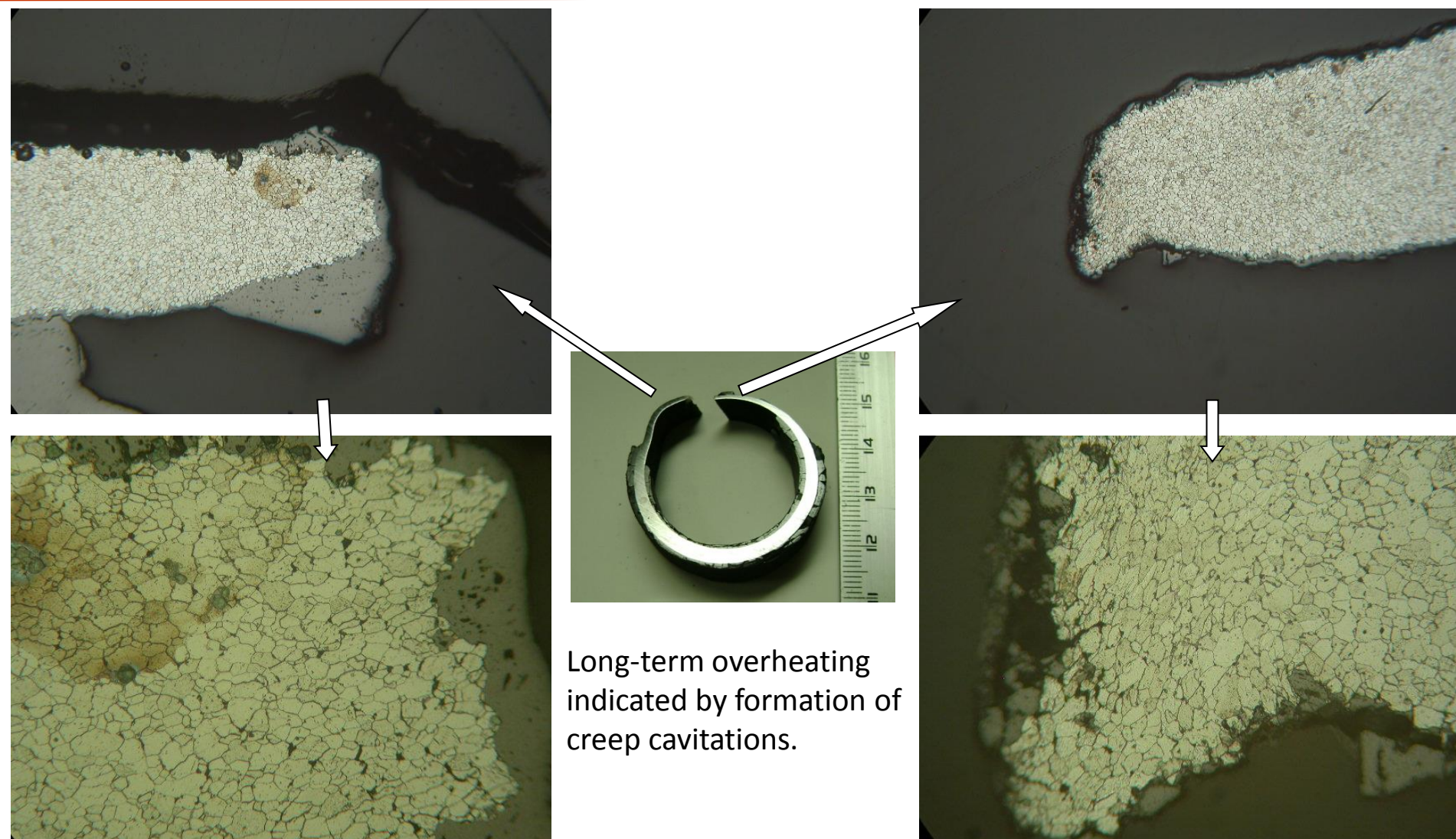
FAILURE ANALYSIS ON LONG-TERM OVERHEATED SUPERHEATER STEAM BOILER TUBE



Tube burst due to long-term overheating

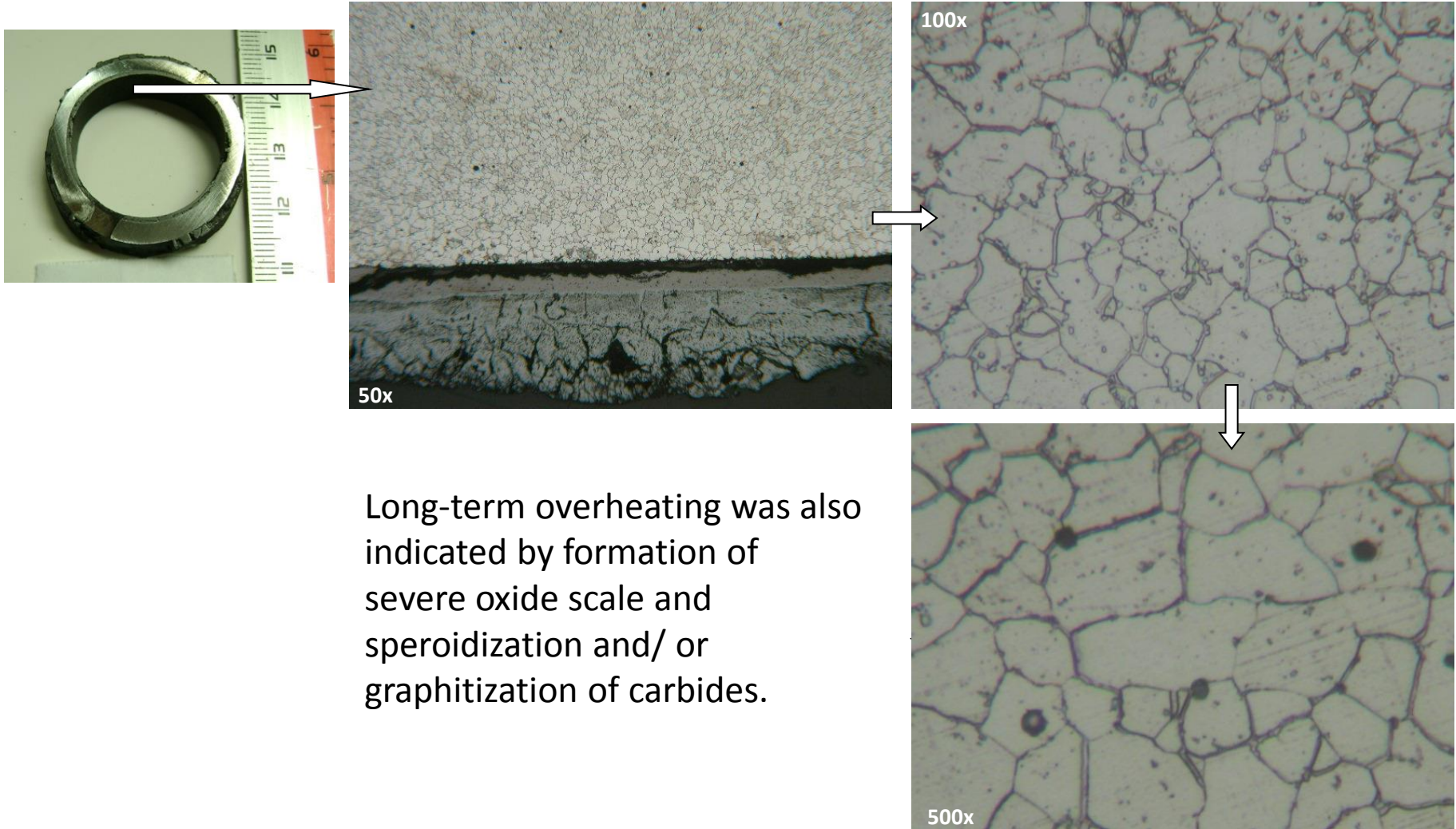


FAILURE ANALYSIS ON LONG-TERM OVERHEATED SUPERHEATER STEAM BOILER TUBE (continued)



Long-term overheating indicated by formation of creep cavitations.

FAILURE ANALYSIS ON LONG-TERM OVERHEATED SUPERHEATER STEAM BOILER TUBE (continued)

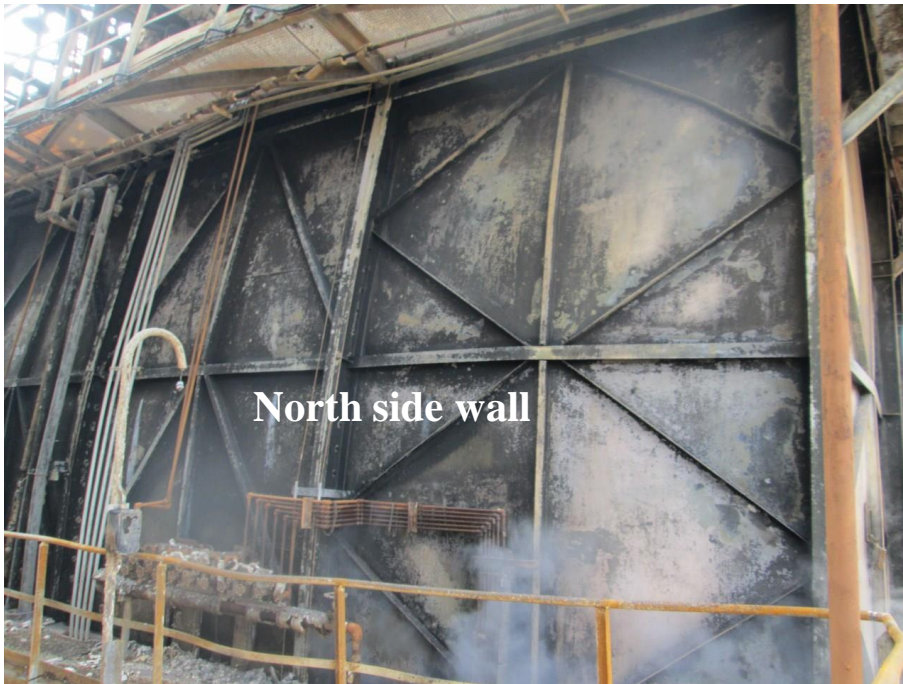


Long-term overheating was also indicated by formation of severe oxide scale and spheroidization and/ or graphitization of carbides.

TUBE BURST OF HCU HEATER DUE TO SHORT-TERM LOCALIZED OVERHEATING



TUBE BURST OF HCU HEATER DUE TO SHORT-TERM LOCALIZED OVERHEATING (continued)

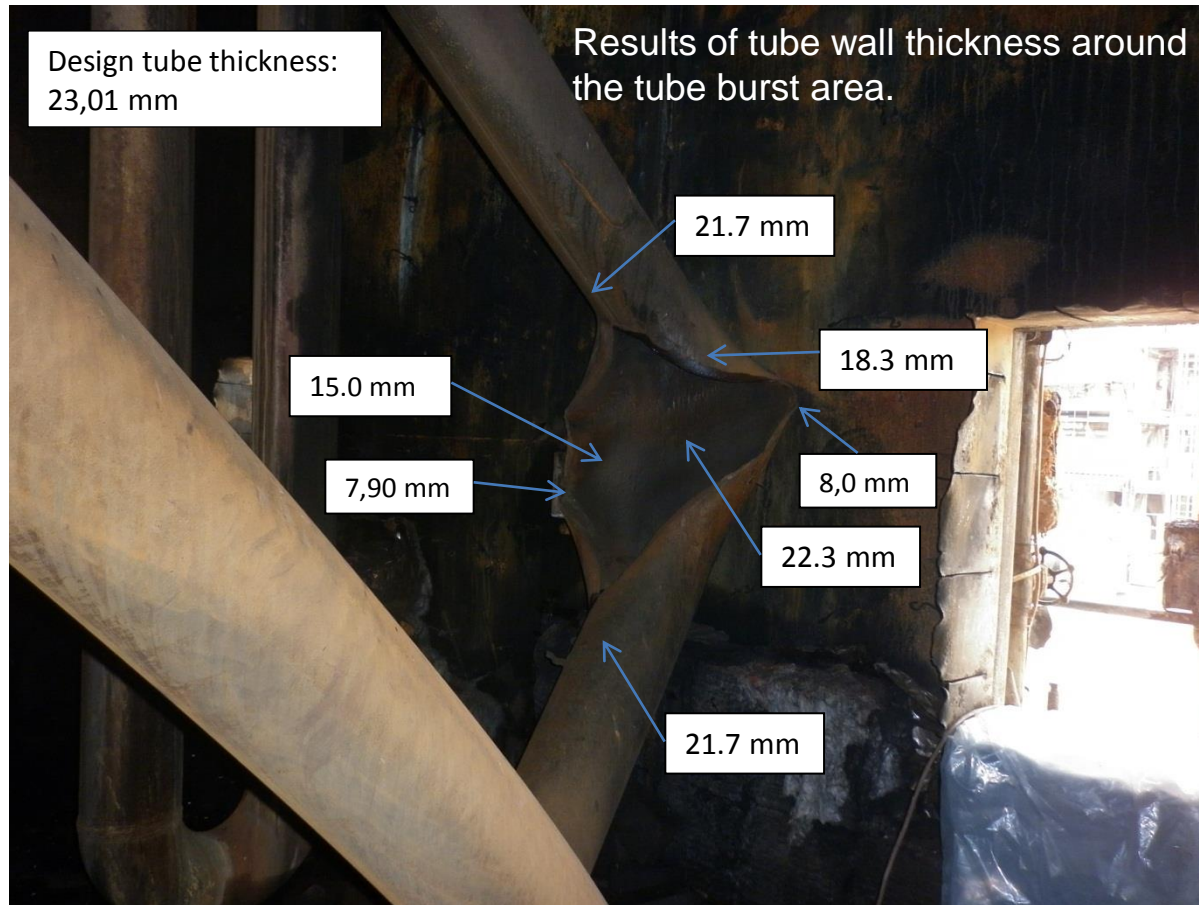


Heavy deformation occurred on the HCU wall furnace due to tube burst related incident



Due to the effect of ***“jet-reaction”*** in the event of incident, the burst tube had been forced to move from its initial position.

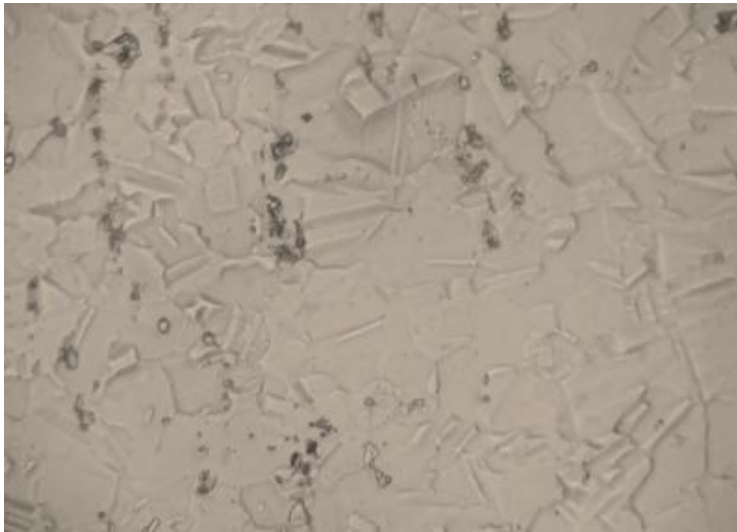
TUBE BURST OF HCU HEATER DUE TO SHORT-TERM LOCALIZED OVERHEATING (continued)



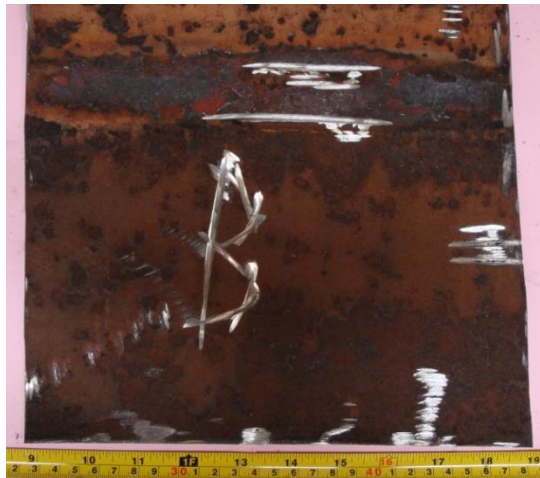
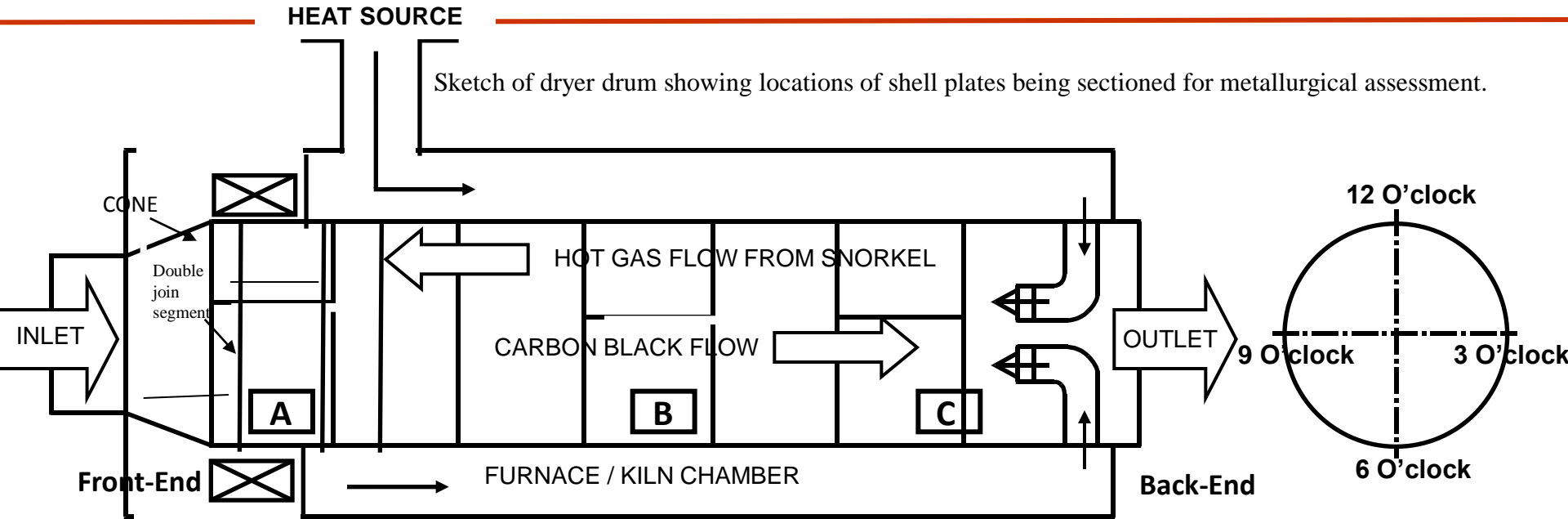
TUBE BURST OF HCU HEATER DUE TO SHORT-TERM LOCALIZED OVERHEATING (continued)



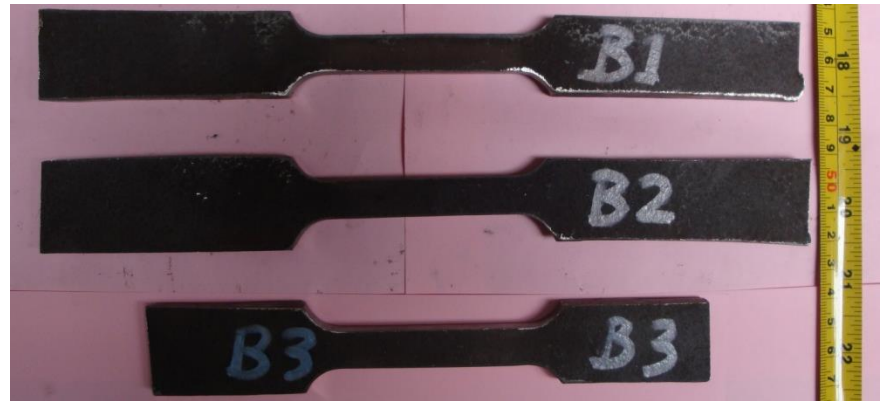
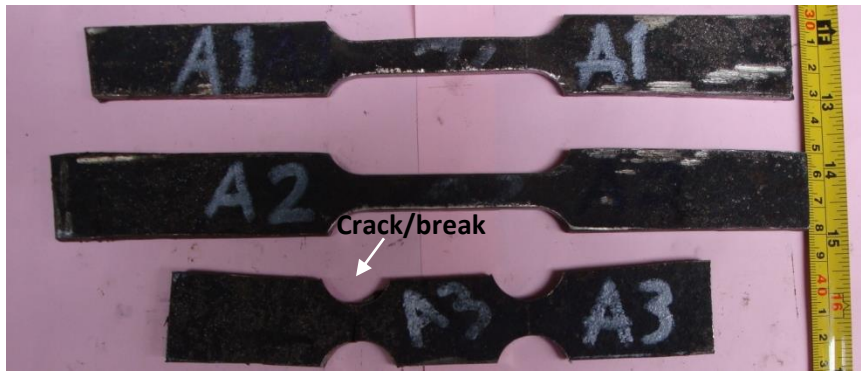
TUBE BURST OF HCU HEATER DUE TO SHORT-TERM LOCALIZED OVERHEATING (continued)



ROOT CAUSE FAILURE ANALYSIS ON SHELL PLATES OF CARBON BLACK DRYER DRUM



ROOT CAUSE FAILURE ANALYSIS ON SHELL PLATES OF CARBON BLACK DRYER DRUM (continued)



Tensile test specimens obtained from the shell plate sections A, B and C. Note that specimen A3 was crack and broken during machining.

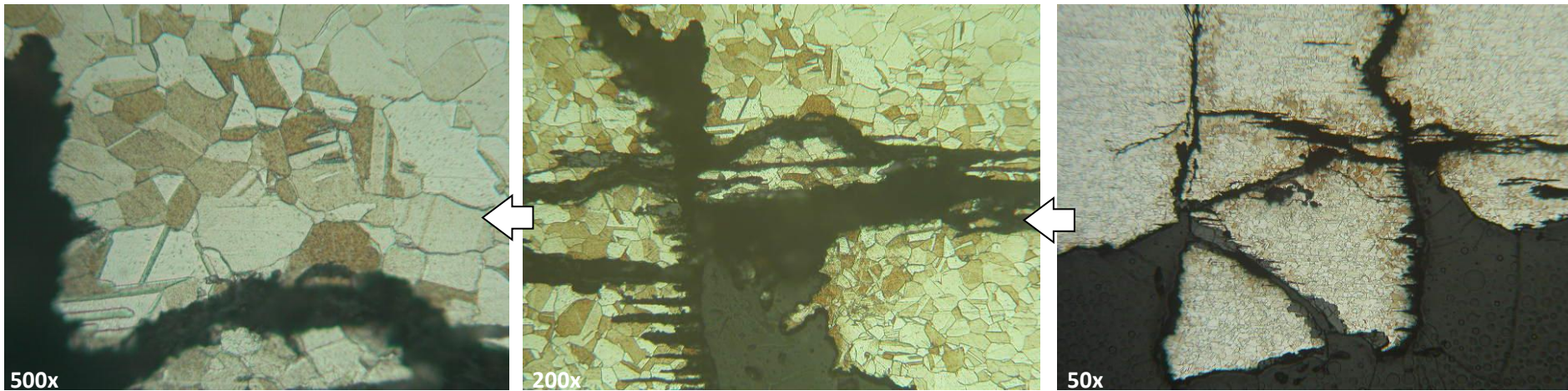
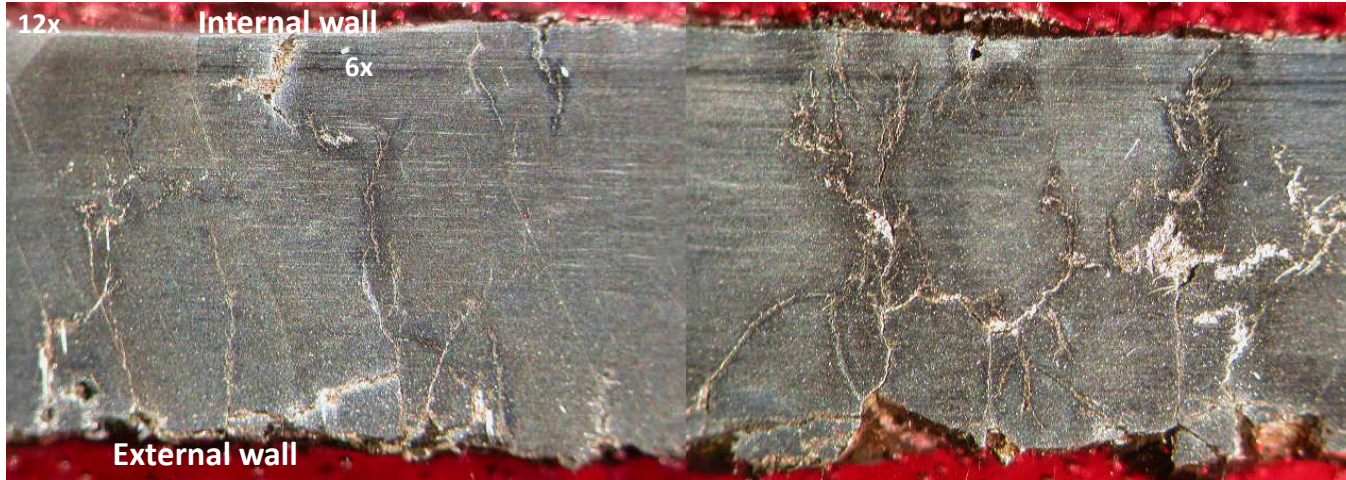
Note:

A1 and A2; B1 and B2; C1 and C2:

parallel to the Dryer Drum inlet direction.

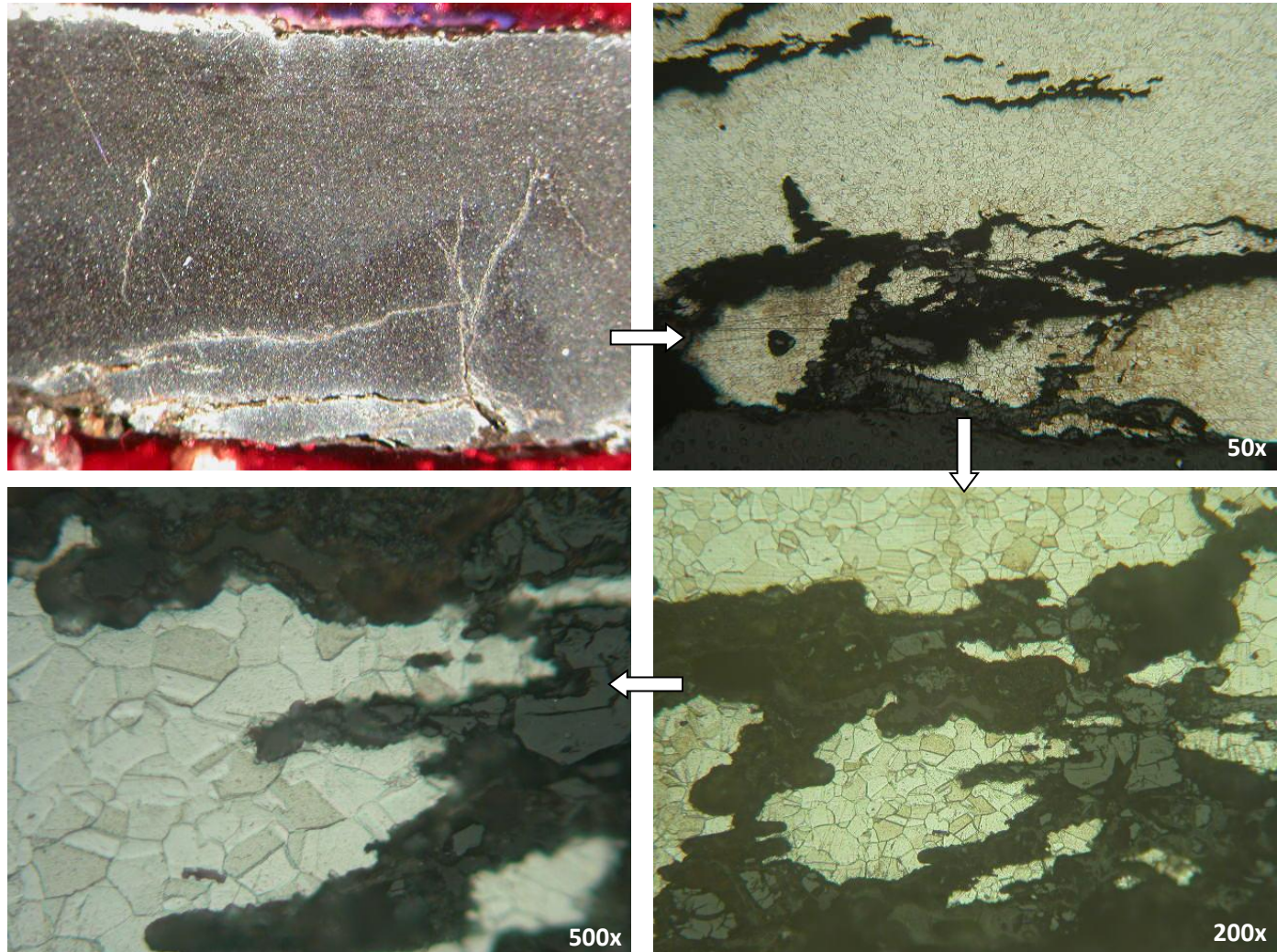
A3; B3 and C3: perpendicular to the Dryer Drum inlet direction.

ROOT CAUSE FAILURE ANALYSIS ON SHELL PLATES OF CARBON BLACK DRYER DRUM (continued)



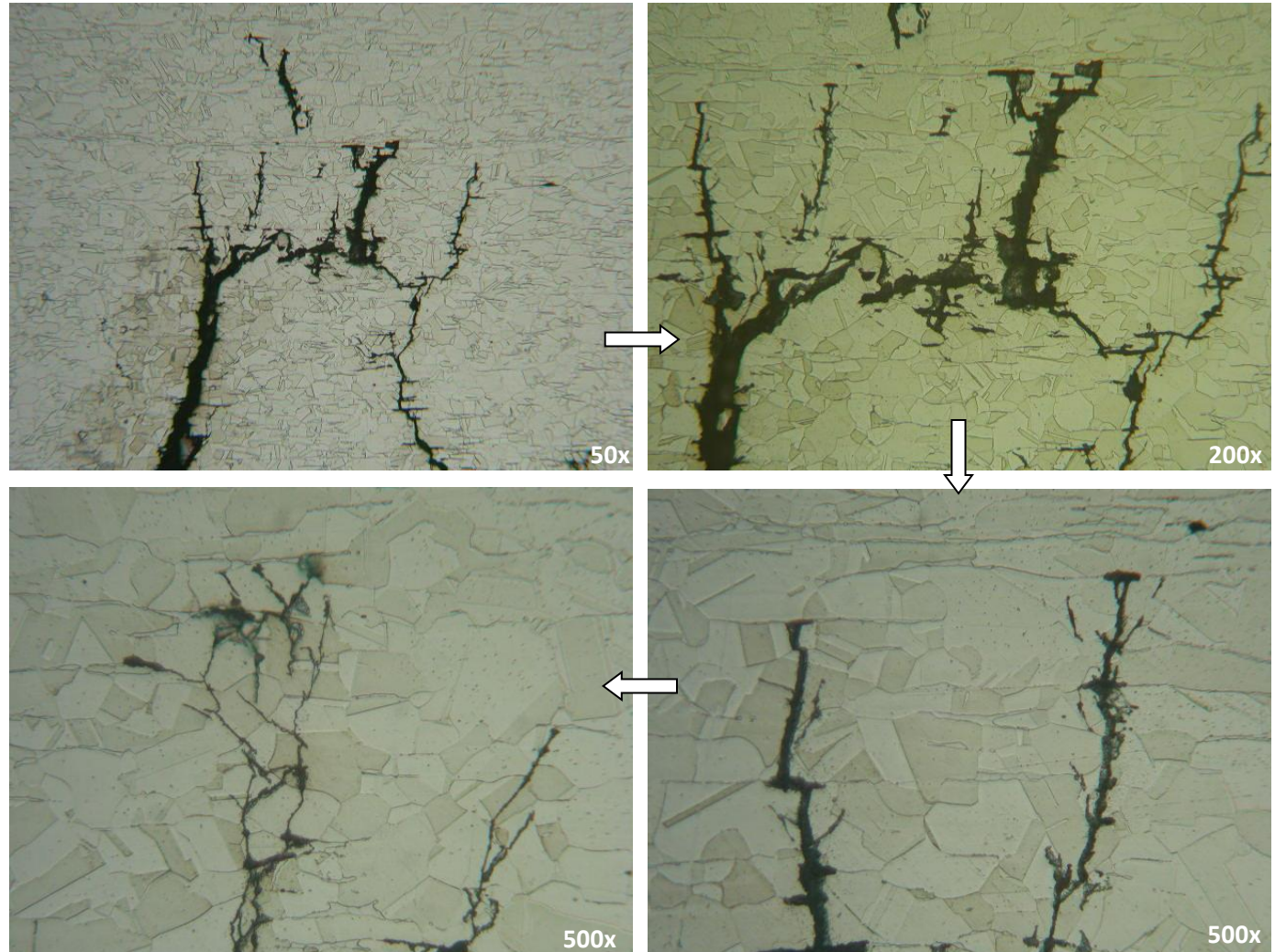
As polished and etched specimen A1 obtained from the shell plate A (A1 was sectioned parallel to the dryer drum inlet direction).

ROOT CAUSE FAILURE ANALYSIS ON SHELL PLATES OF CARBON BLACK DRYER DRUM (continued)



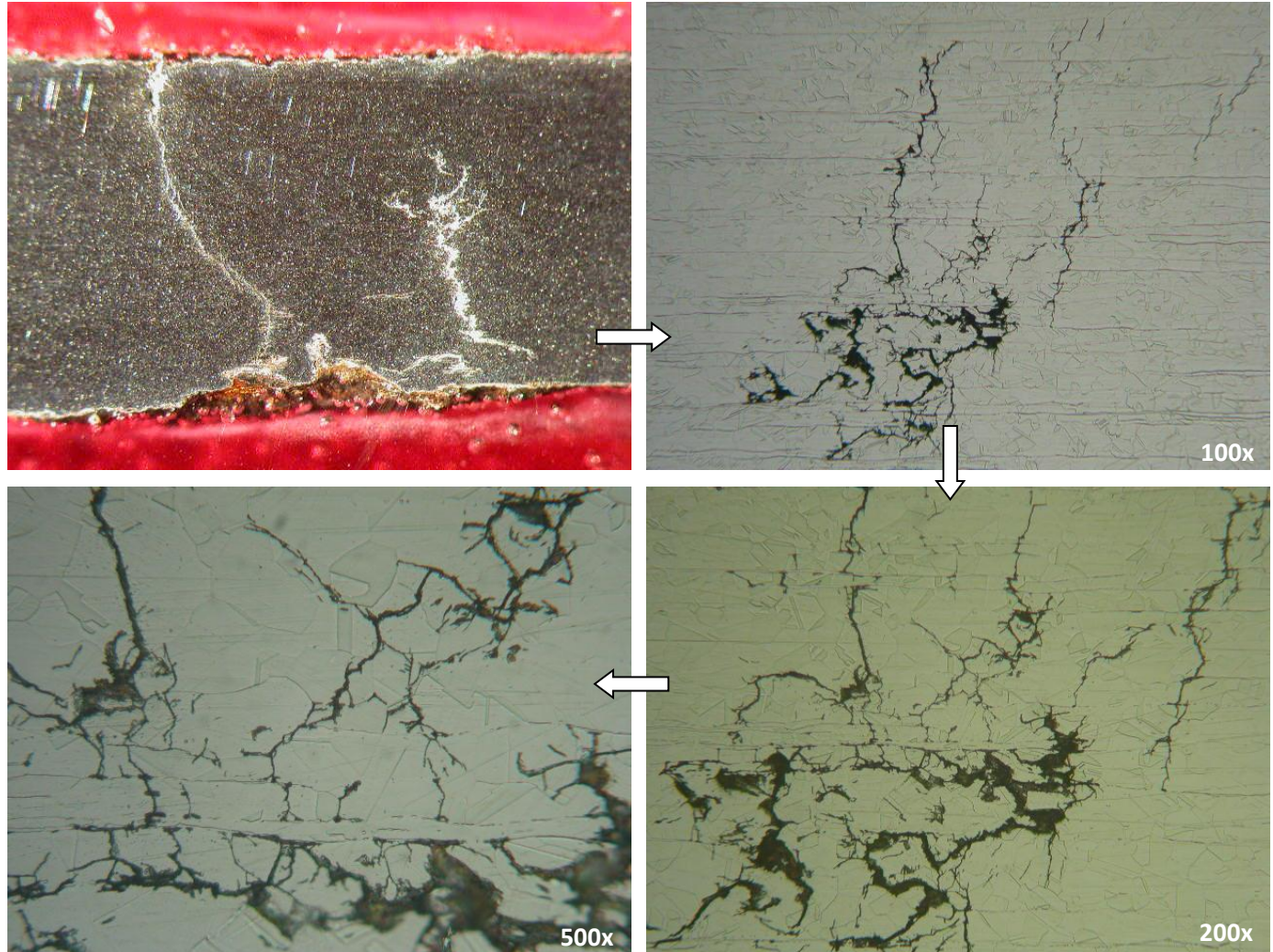
Microstructures obtained from specimen A2 at location as indicated.

ROOT CAUSE FAILURE ANALYSIS ON SHELL PLATES OF CARBON BLACK DRYER DRUM (continued)



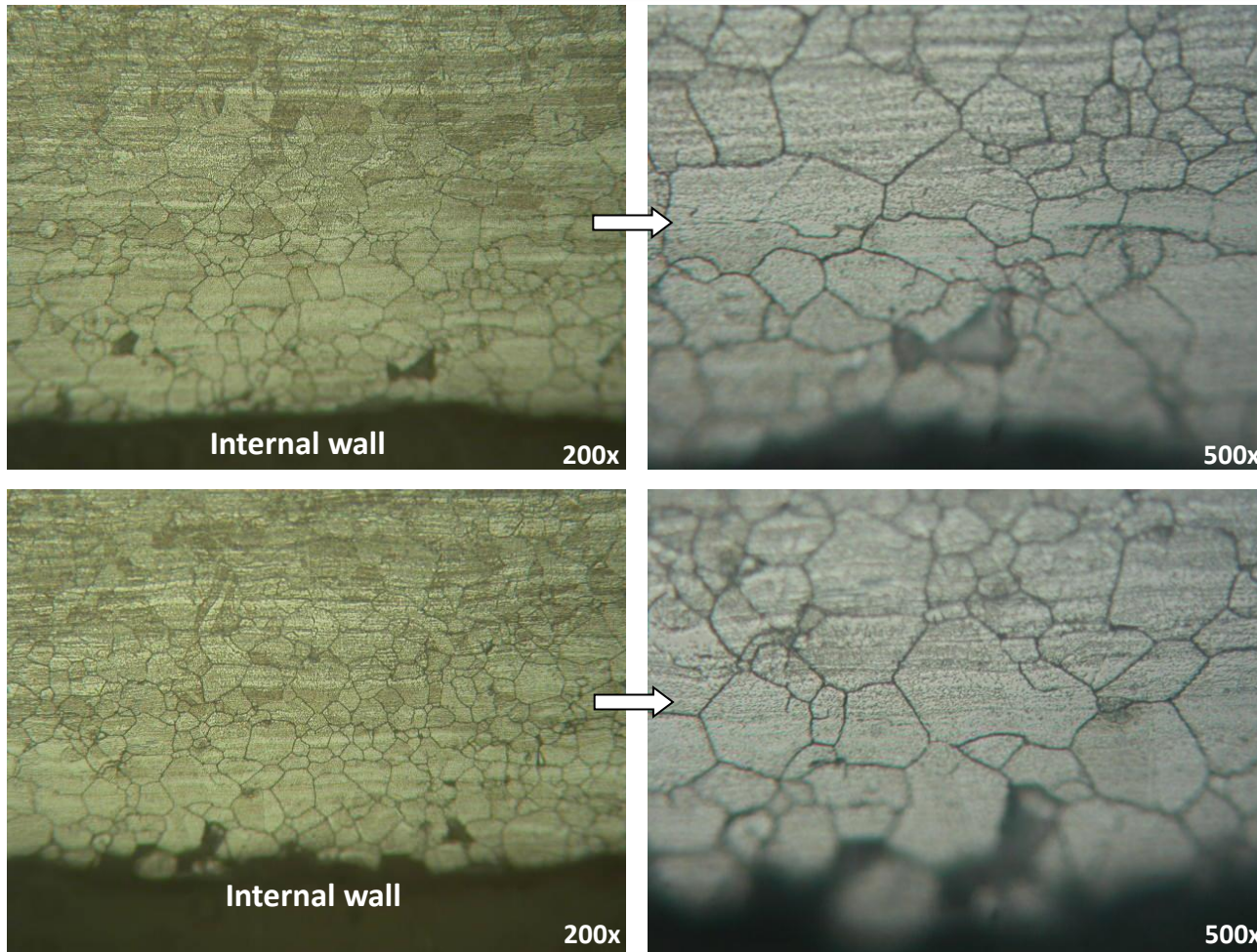
Microstructures obtained from specimen A2 at location as indicated.

ROOT CAUSE FAILURE ANALYSIS ON SHELL PLATES OF CARBON BLACK DRYER DRUM (continued)



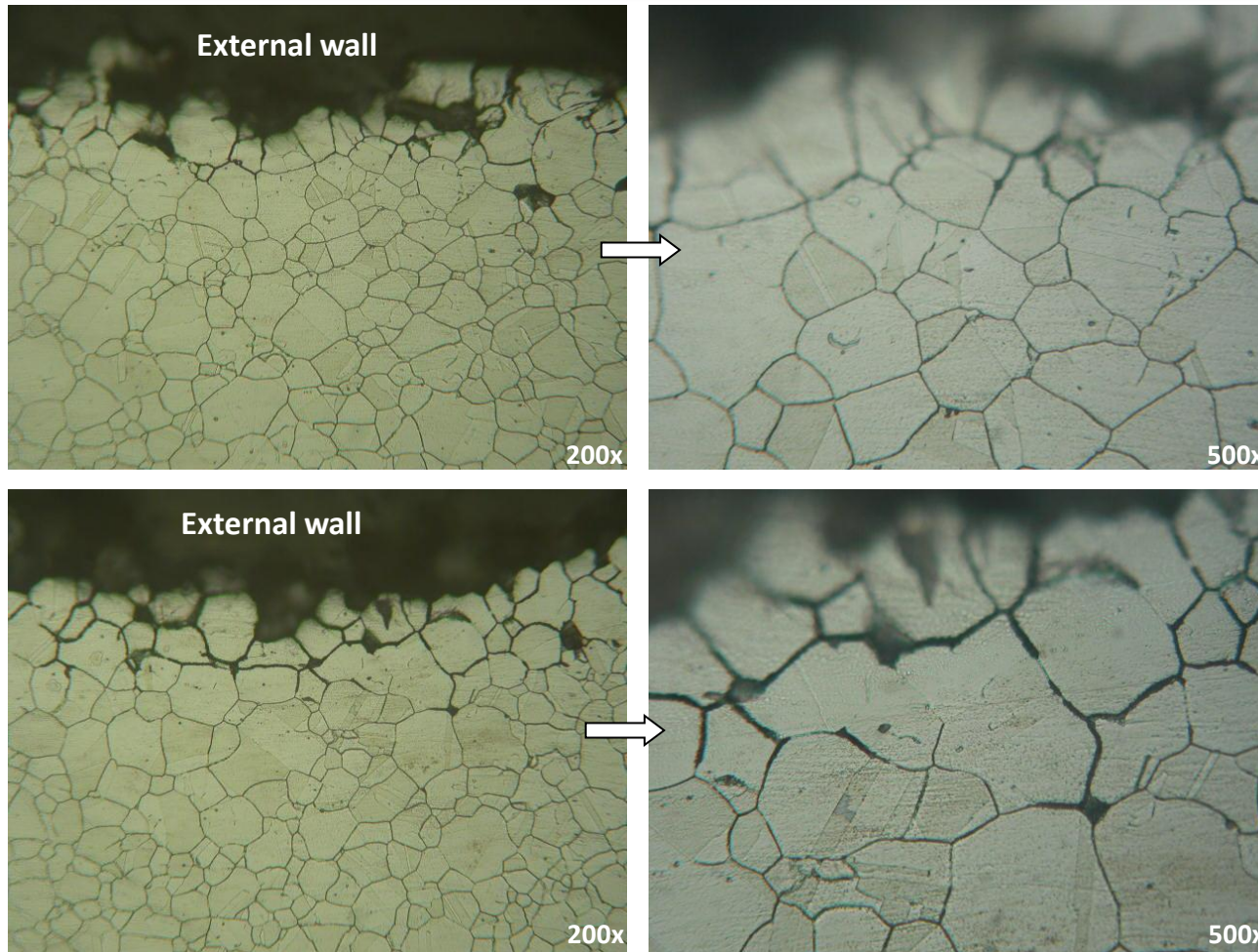
Microstructures obtained from specimen A3 at location as indicated.

ROOT CAUSE FAILURE ANALYSIS ON SHELL PLATES OF CARBON BLACK DRYER DRUM (continued)



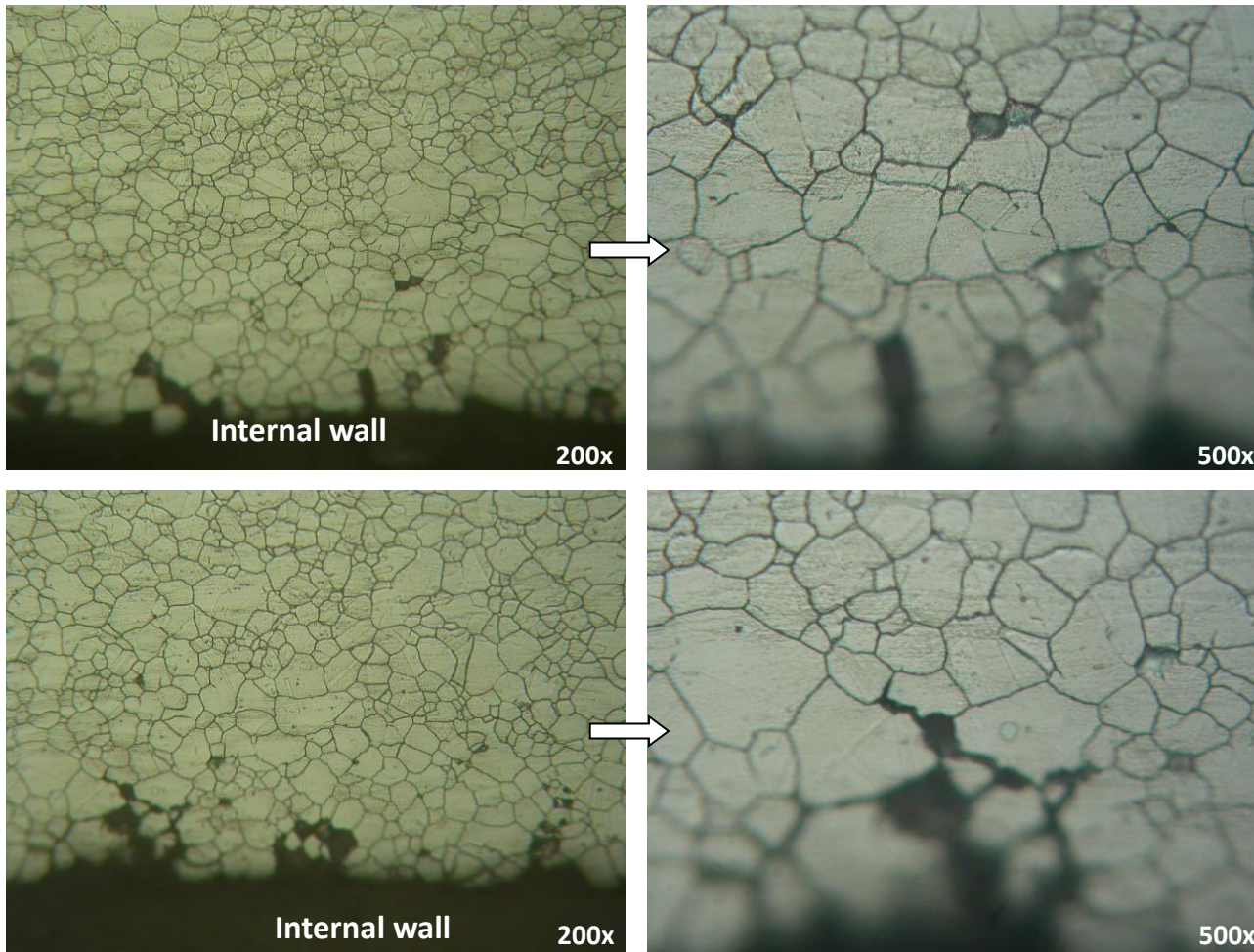
Microstructures obtained from specimen B4 of the shell plate B at location different from specimen B2 (B4 was sectioned perpendicular to the dryer drum inlet direction).

ROOT CAUSE FAILURE ANALYSIS ON SHELL PLATES OF CARBON BLACK DRYER DRUM (continued)



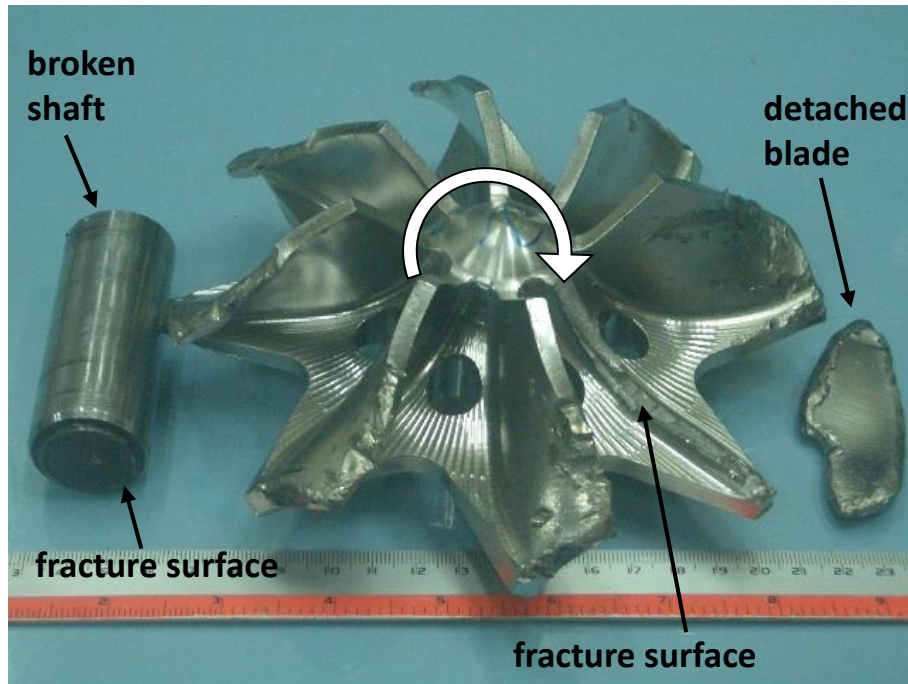
Microstructures obtained from specimen C1 of the shell plate C at location as indicated (specimen C1 was sectioned parallel to the dryer drum inlet direction).

ROOT CAUSE FAILURE ANALYSIS ON SHELL PLATES OF CARBON BLACK DRYER DRUM (continued)

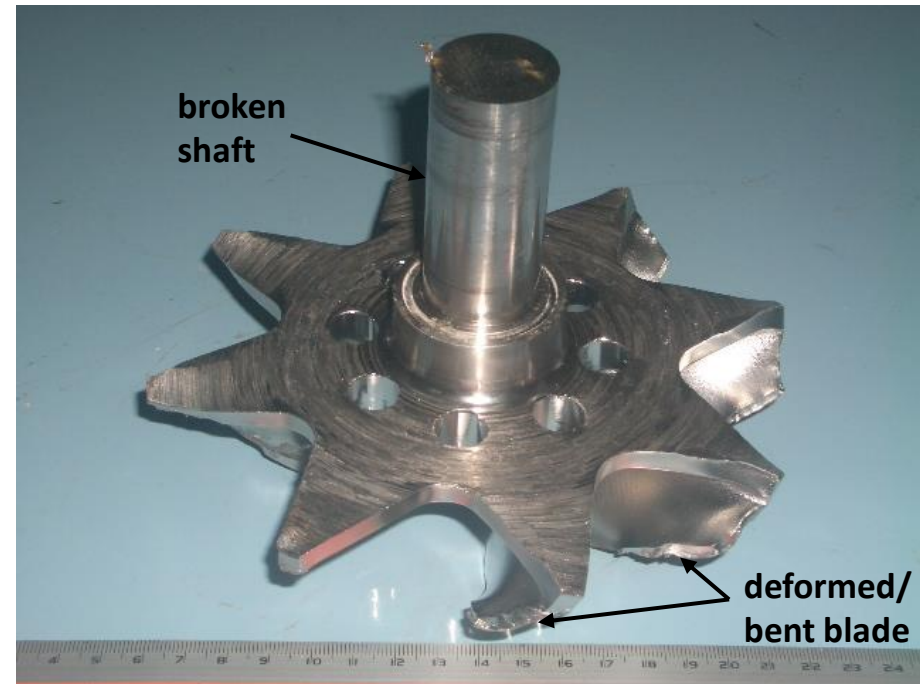


Microstructures obtained from specimen C1 of the shell plate C at location as indicated (specimen C1 was sectioned parallel to the dryer drum inlet direction).

FAILURE ANALYSIS OF FIRST AND SECOND STAGE IMPELLERS OF A REACTOR FEED PUMP



Top (front) view

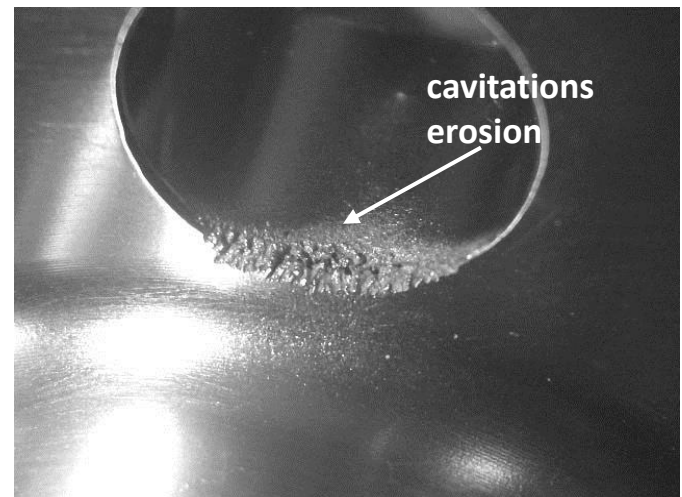
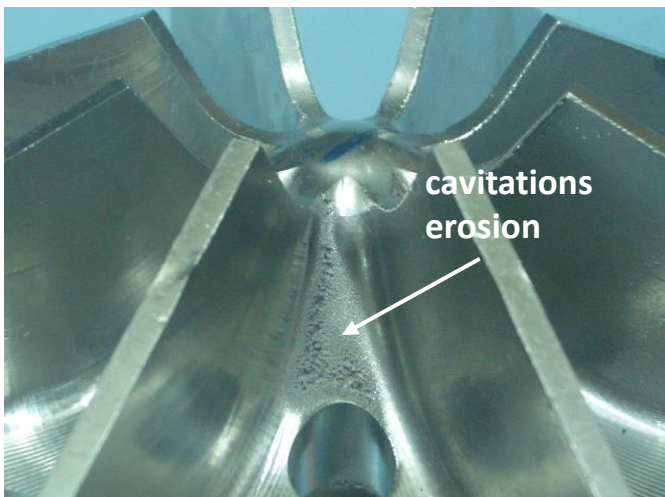
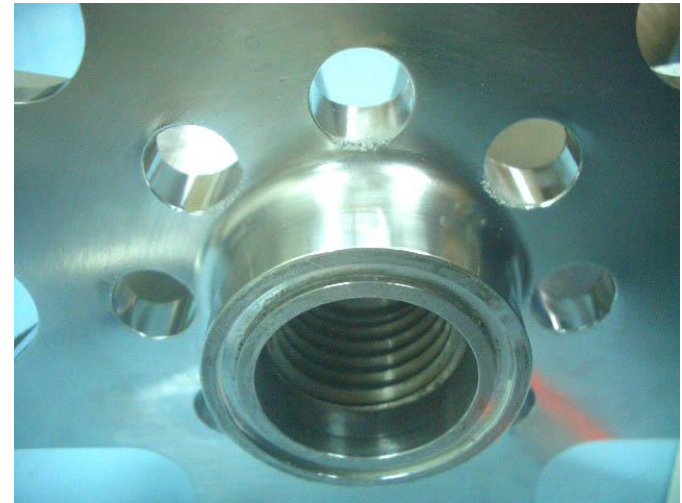
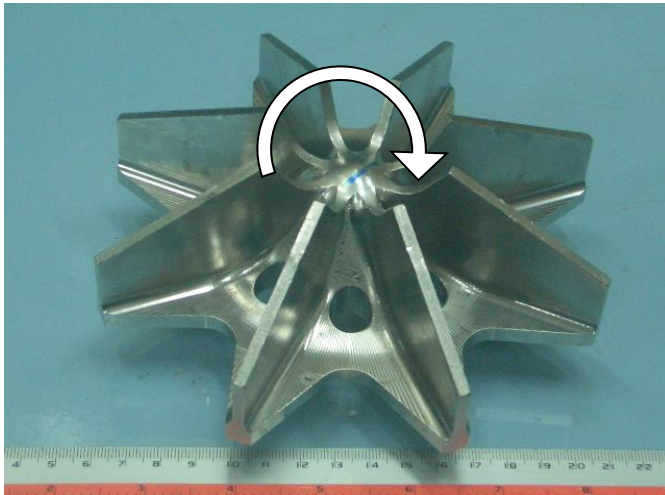


Bottom (back) view: Placing the broken shaft back together

As-received fractured pump impeller and shaft (second stage) showing the fractured (detached) blade and the broken impeller shaft.

Note : clockwise arrow indicates direction of rotation

FAILURE ANALYSIS OF FIRST AND SECOND STAGE IMPELLERS OF A REACTOR FEED PUMP (continued)



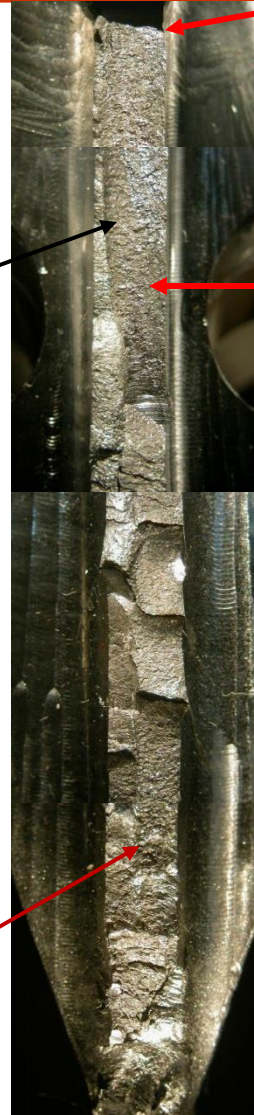
As-received pump impeller (first stage), showing cavitations erosion damage in the vicinity of the section change at the hub/blade interface and at the balance hole of the impelle. Note: clockwise arrow indicates direction of rotation

FAILURE ANALYSIS OF FIRST AND SECOND STAGE IMPELLERS OF A REACTOR FEED PUMP (continued)

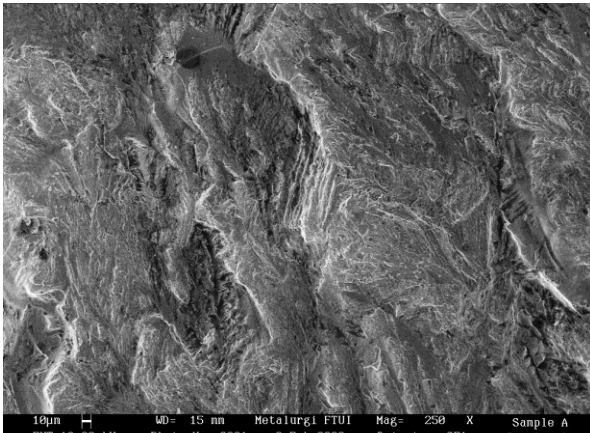
Initial fatigue fracture



Beach marks

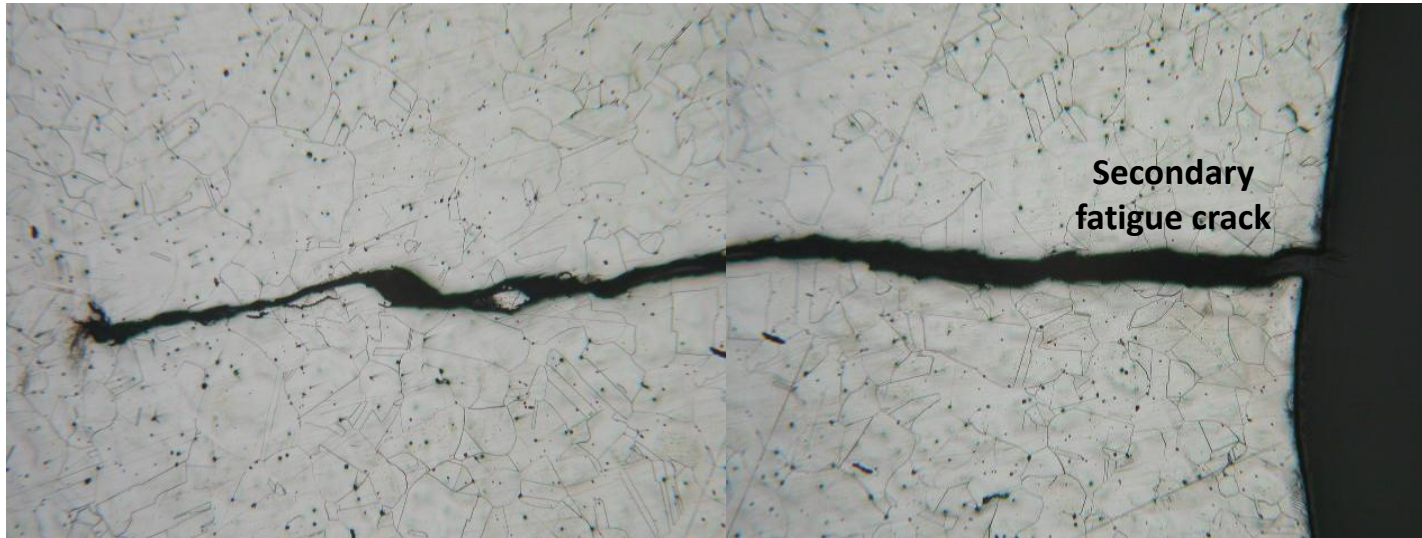
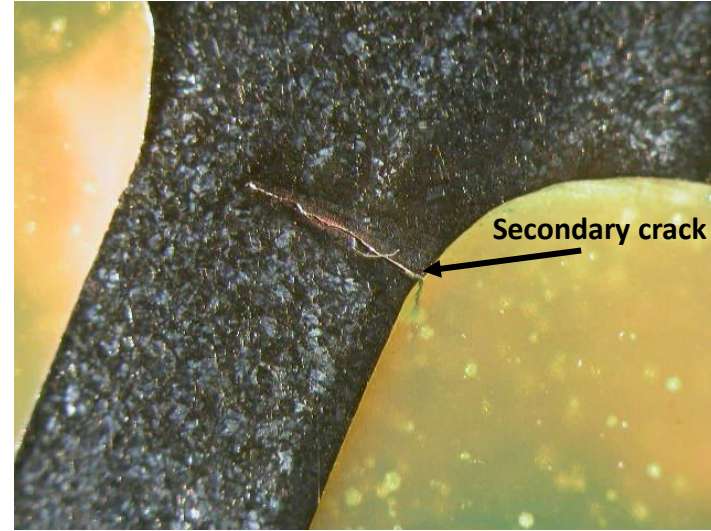
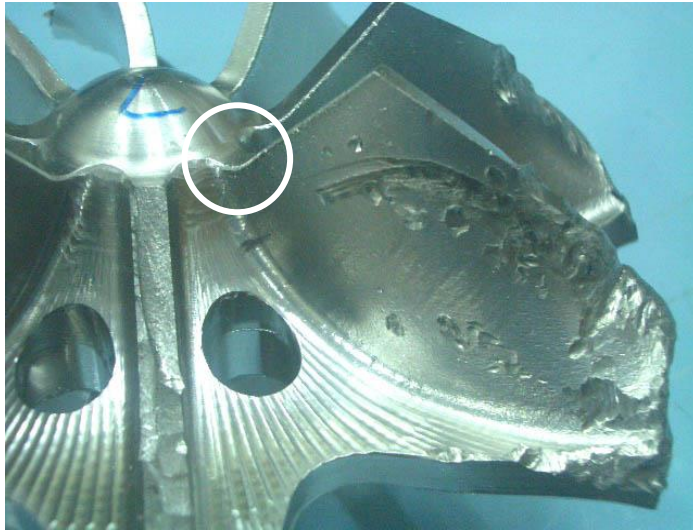


SEM fractograph

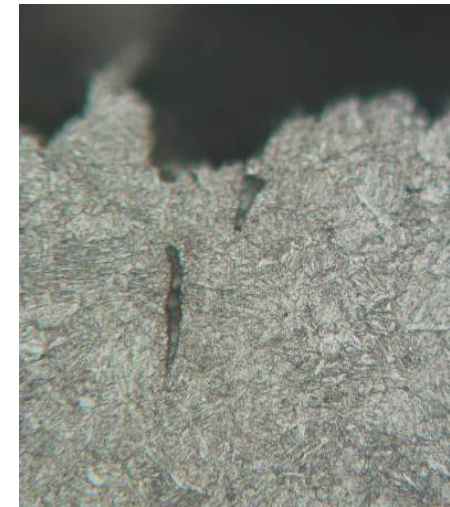
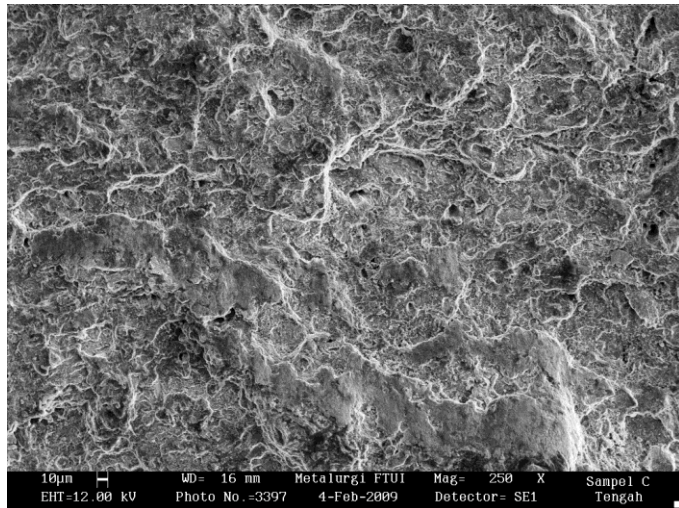
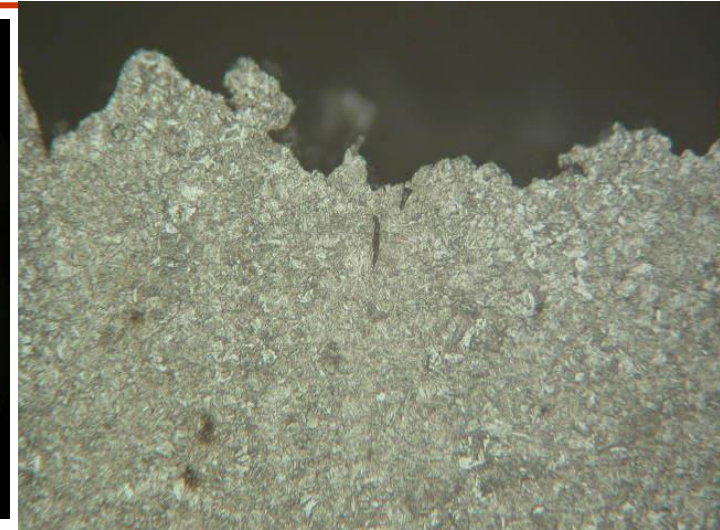


Final Fracture

FAILURE ANALYSIS OF FIRST AND SECOND STAGE IMPELLERS OF A REACTOR FEED PUMP (continued)

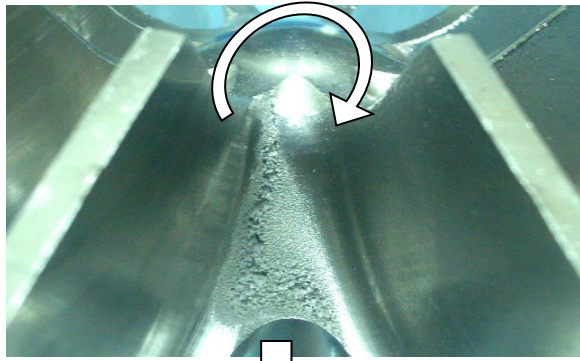


FAILURE ANALYSIS OF FIRST AND SECOND STAGE IMPELLERS OF A REACTOR FEED PUMP (continued)

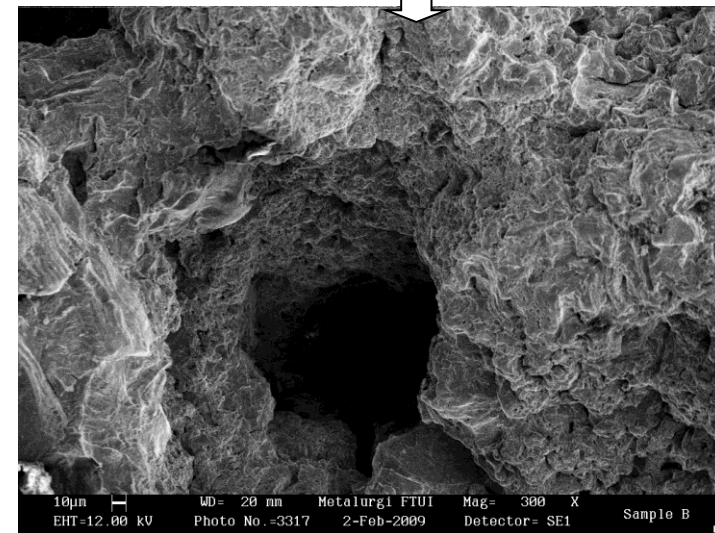
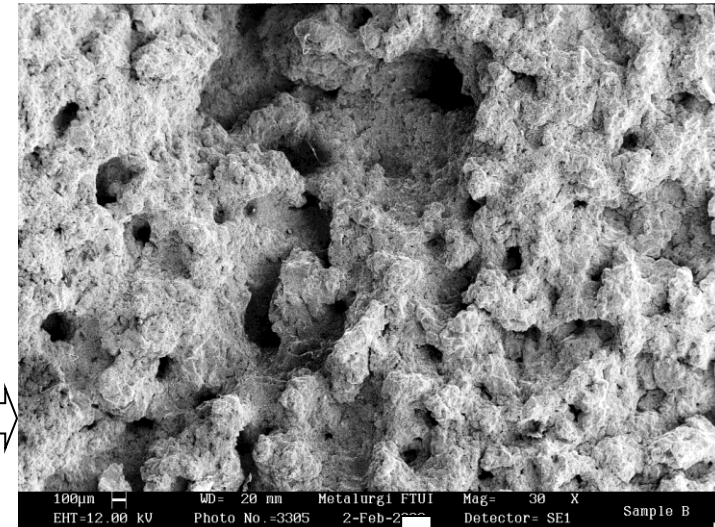


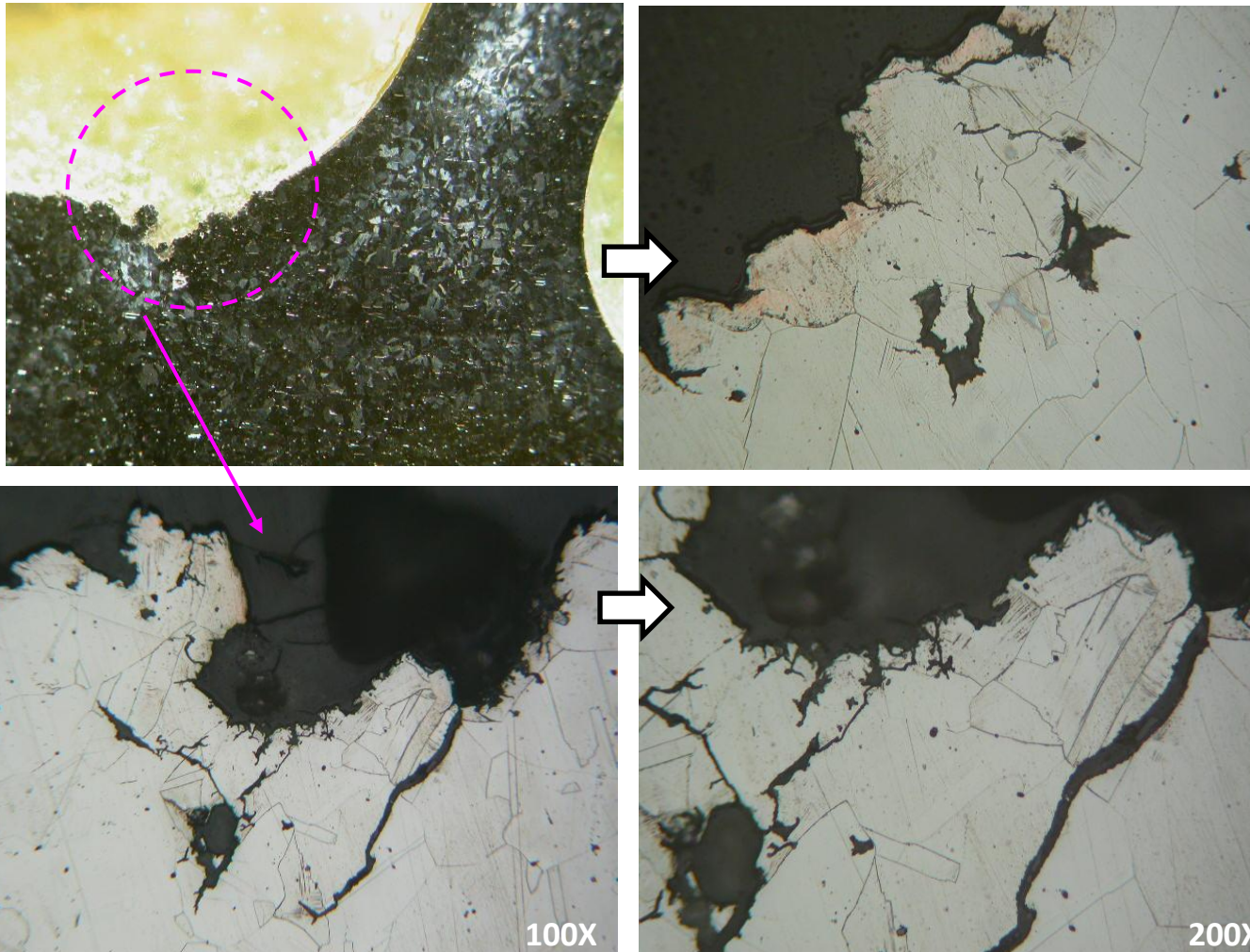
SEM micrographs obtained from fracture surface of the broken impeller shaft (second stage) showing typical brittle fracture morphology

FAILURE ANALYSIS OF FIRST AND SECOND STAGE IMPELLERS OF A REACTOR FEED PUMP (continued)



SEM micrographs obtained from region that damaged by cavitations erosion of the first stage impeller



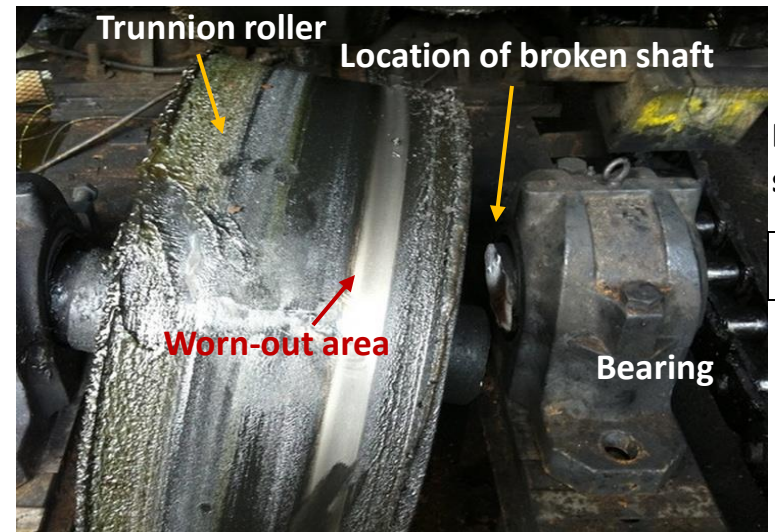


Microstructures obtained from cross section around the hub/blade interface of the first stage impeller which was damaged by cavitations erosion

ROOT CAUSE FAILURE ANALYSIS OF A BROKEN TRUNNION SHAFT OF A DRYER DRUM DUE TO MECHANICAL FATIGUE

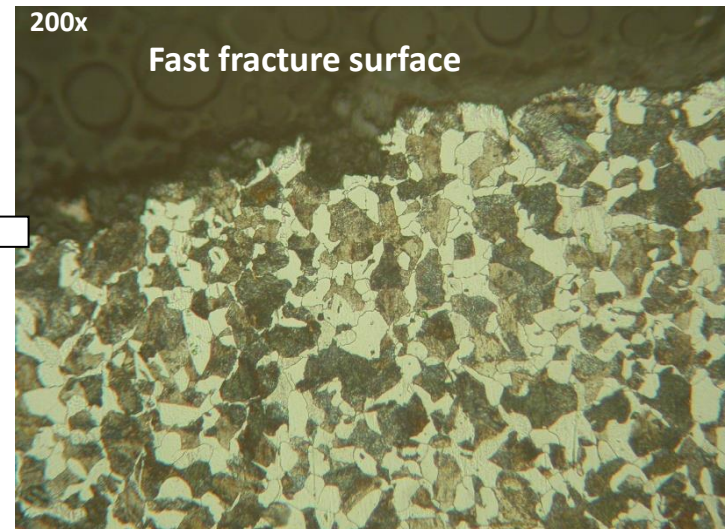
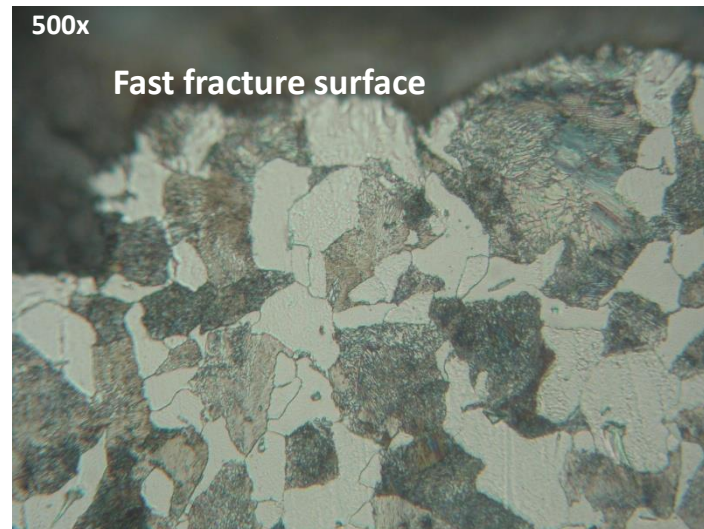
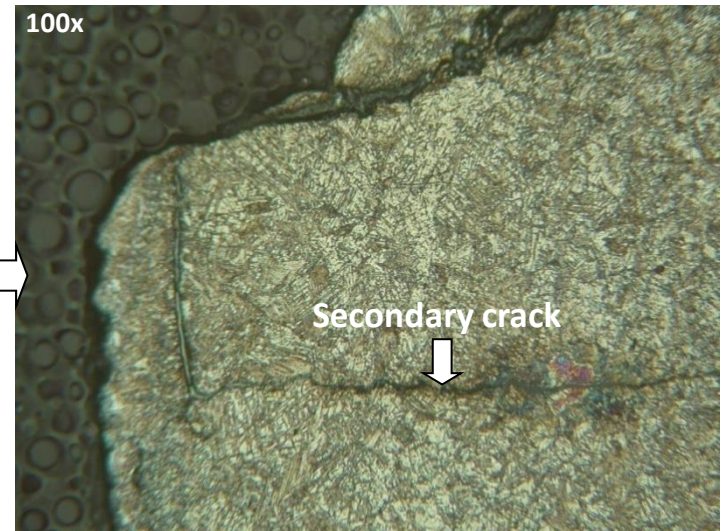
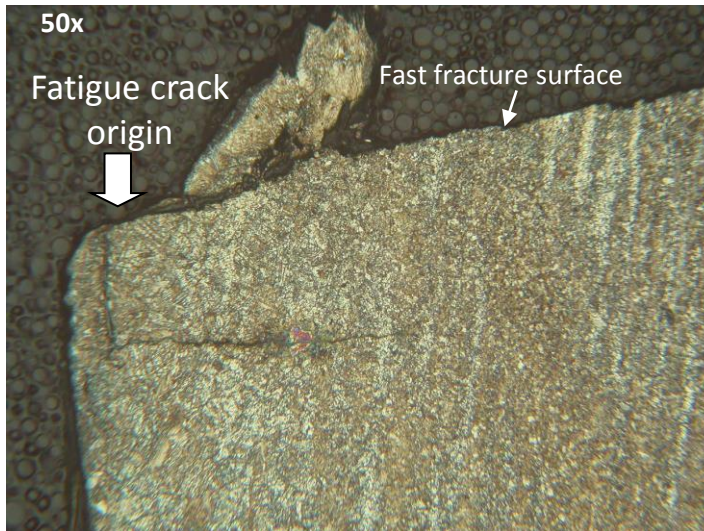


Fatigue fracture surface of the trunnion shaft.

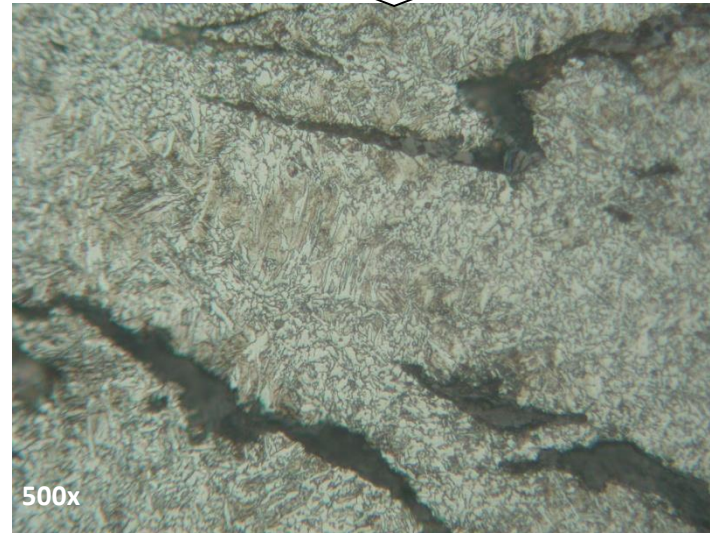
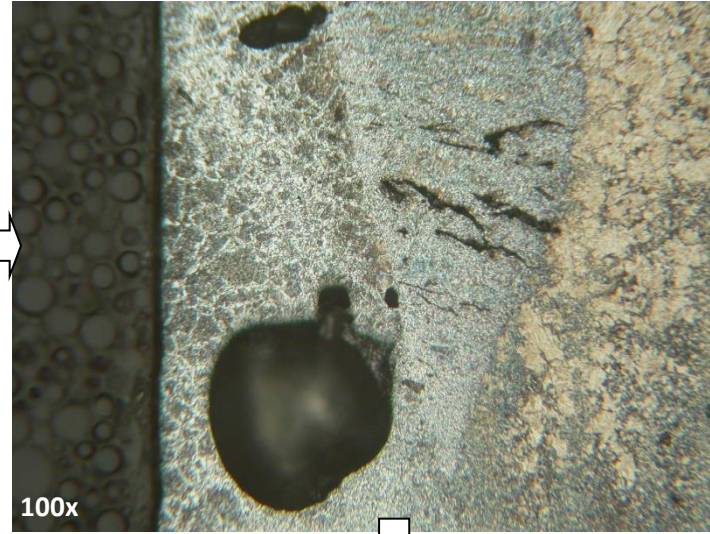
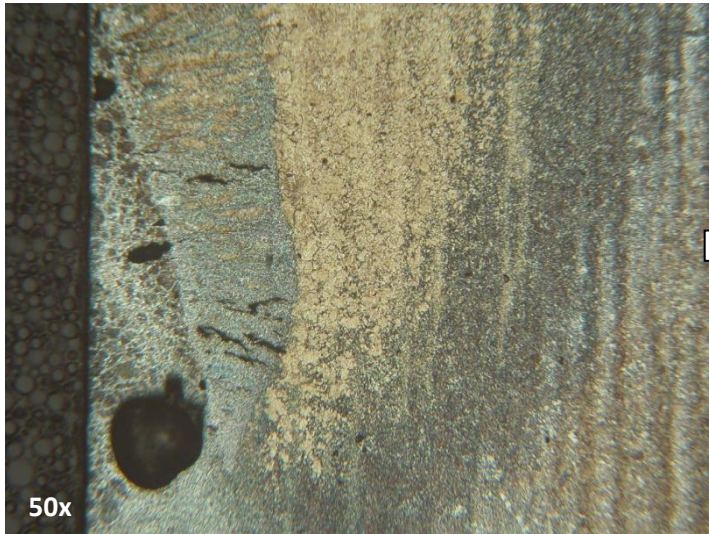


ROOT CAUSE FAILURE ANALYSIS OF A BROKEN TRUNNION SHAFT OF A DRYER DRUM DUE TO MECHANICAL FATIGUE (continued)

Microstructures obtained from the specimen, showing the microstructures located around the fatigue crack origin area and around the fast fracture area, respectively. The microstructures in the fatigue crack origin area consist of Widmanstatten structure typical of weld metal of carbon/low-alloy steel, whereas the microstructures in the fast fracture area consist of large ferrite and pearlite. In addition, there is also seen a secondary crack formed in the area close to the fatigue crack origin.

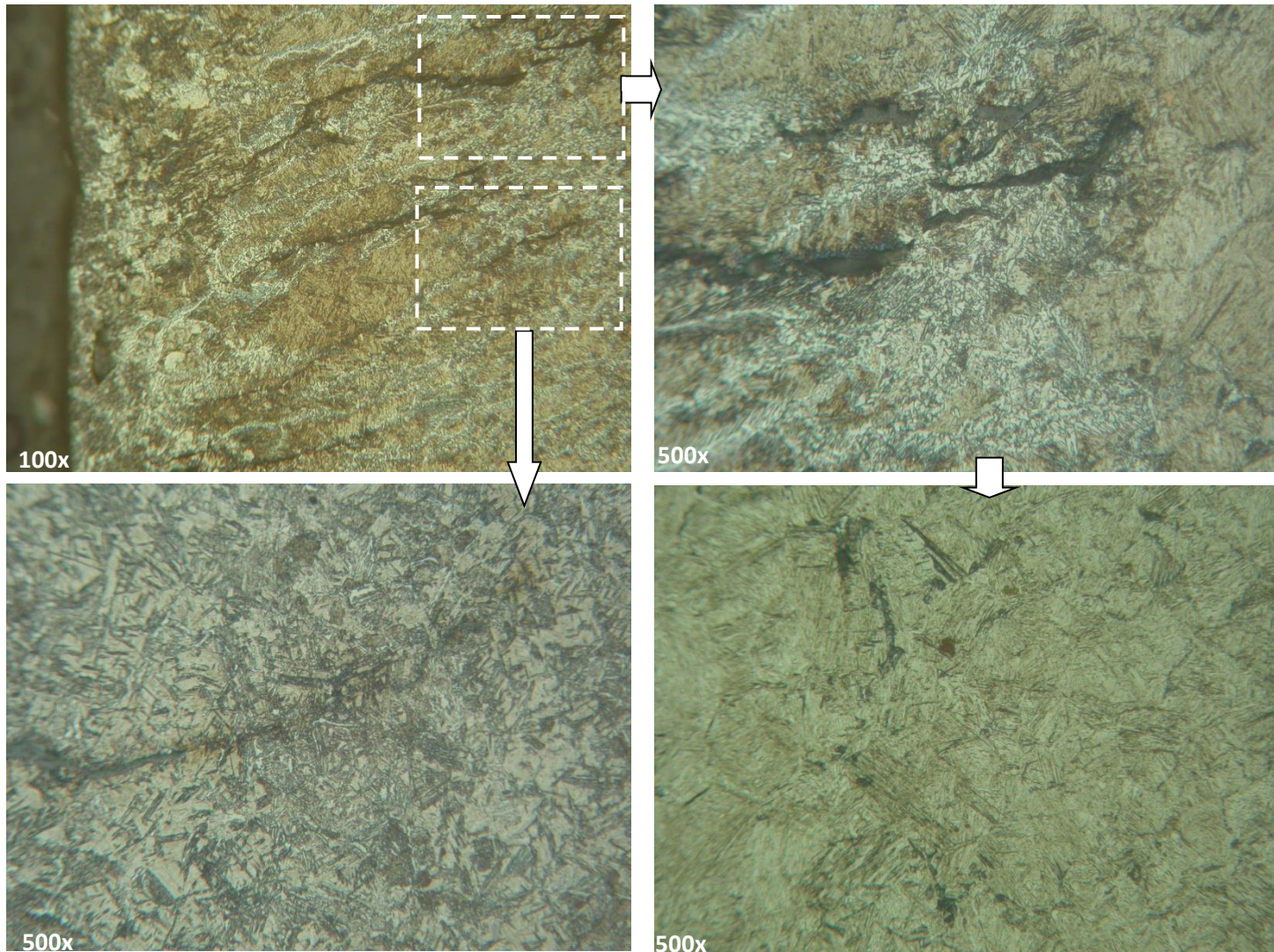


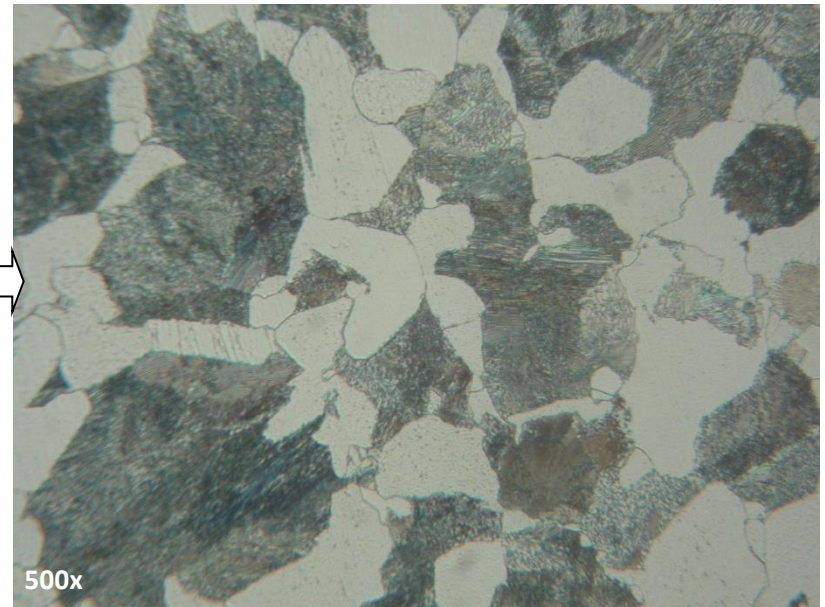
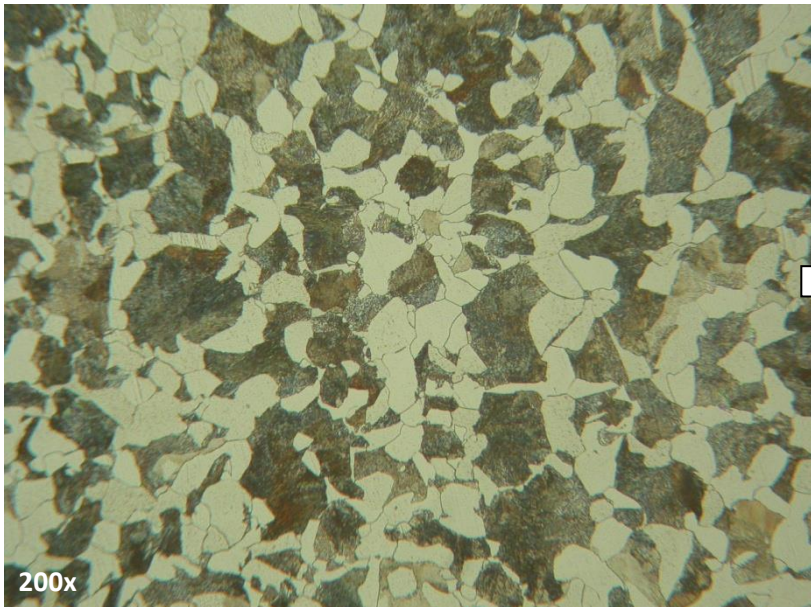
ROOT CAUSE FAILURE ANALYSIS OF A BROKEN TRUNNION SHAFT OF A DRYER DRUM DUE TO MECHANICAL FATIGUE (continued)



Microstructures obtained from the specimen at a distance away of the fatigue crack origin, showing several weld defects such as gas porosity and inclusions formed within the weld metal. This indicated that the broken shaft has been given some weld repair on its outer surface diameter previously.

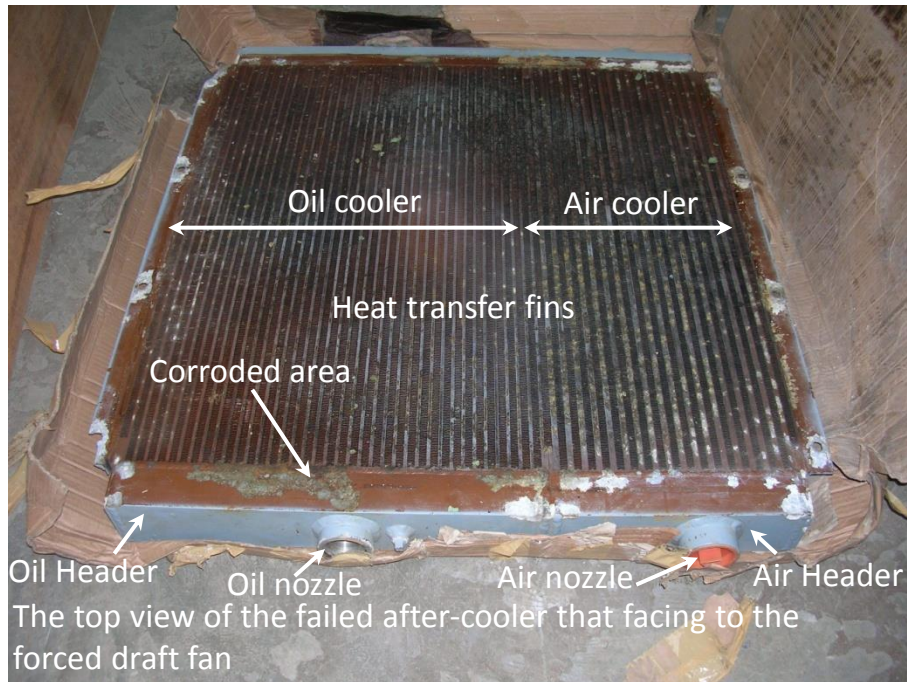
Microstructures obtained from the specimen at a distance away from the fatigue crack origin, showing weld metal microstructures with several inclusions and/or secondary cracks. This further indicated that the broken shaft has been given some weld repair on its outer surface diameter previously.



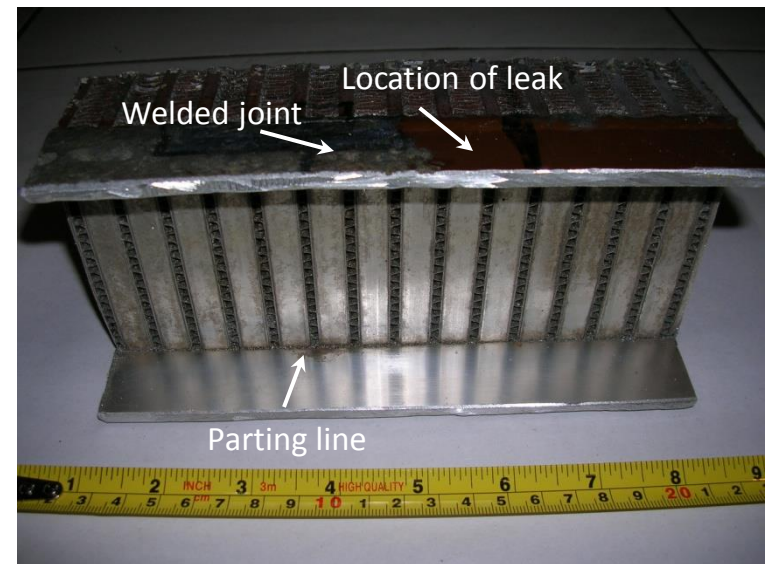


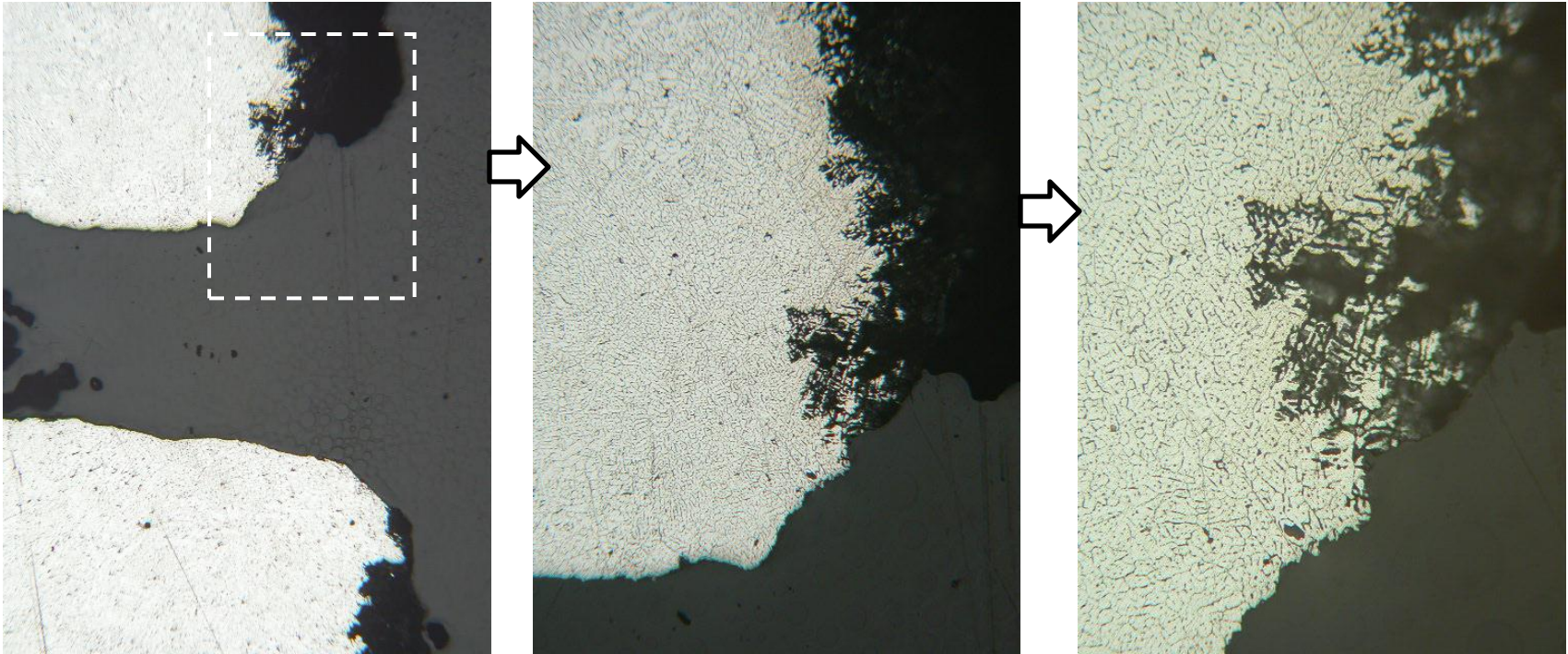
Microstructures obtained from the specimen located around the base metal of the broken shaft, showing large grains of ferrite and pearlite, typical of medium carbon steel in the as annealed condition. These microstructures are in accordance with the chemical composition of the broken shaft material obtained, which is made of AISI 1045. According to the standard requirement, for the AISI 1050 (which is close to the AISI 1045) in the as annealed condition, its minimum tensile strength is of 635MPa, and its hardness value is of 187 HB or 197 HV.

FAILURE ANALYSIS OF LEAKED AIR COMPRESSOR AFTERCOOLER / OIL COOLER DUE TO CORROSION

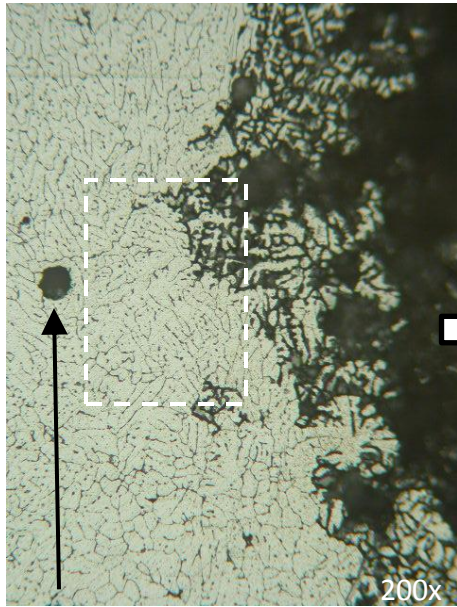


Close up view of the inside header port, showing a number of oil passages containing distributor fins and parting line of the weld joint between header and side bars/parting sheets.

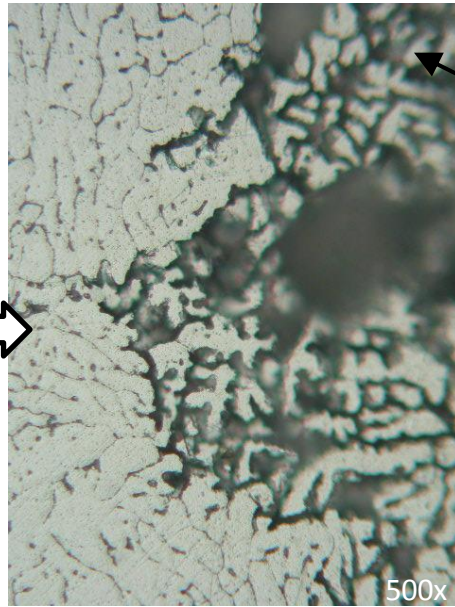




Some microstructures obtained from the damaged area showing inter-dendrite corrosion

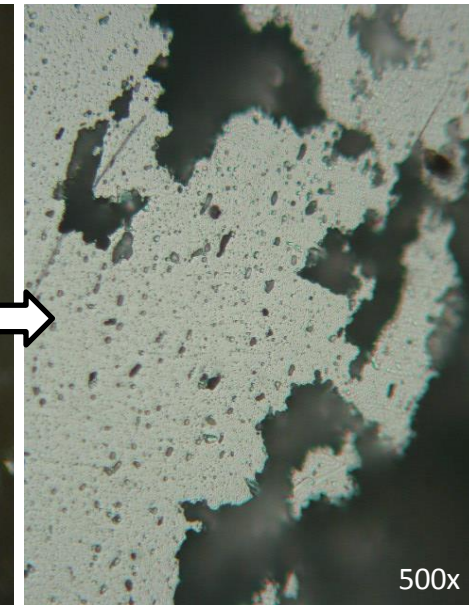
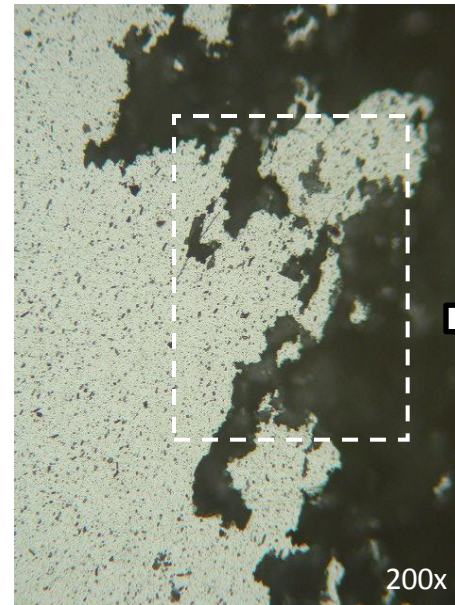


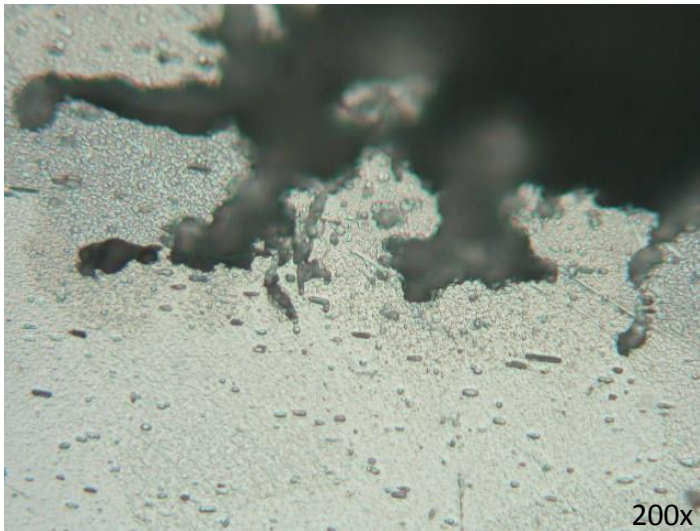
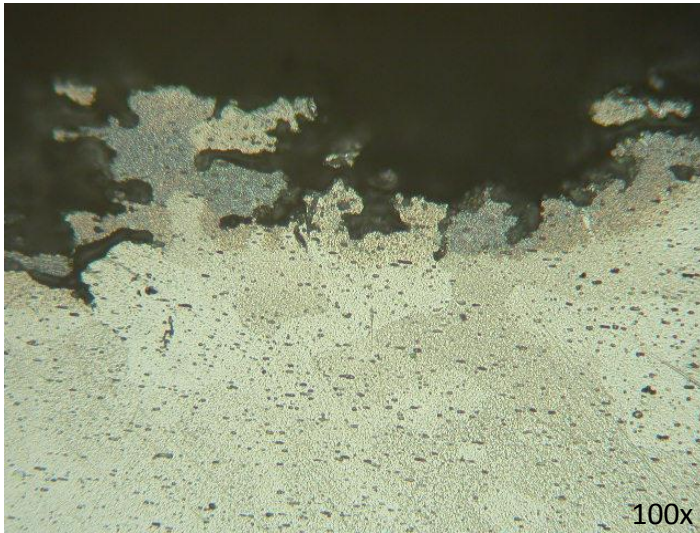
Pinhole (gas porosity)



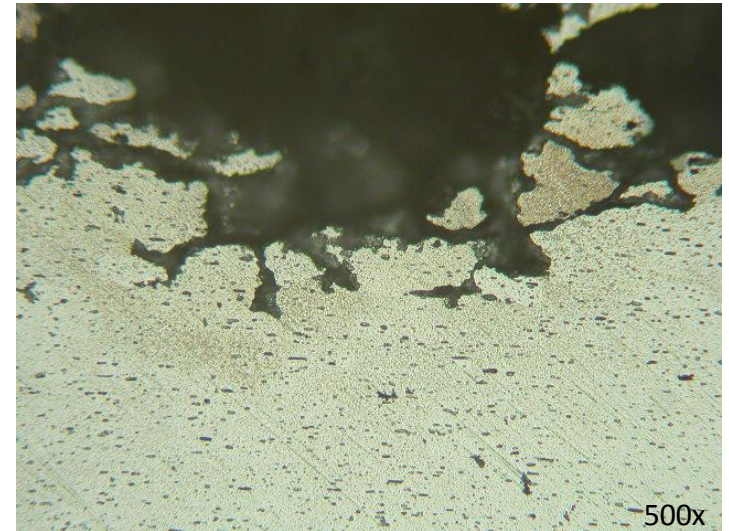
Inter-dendrite
corrosion

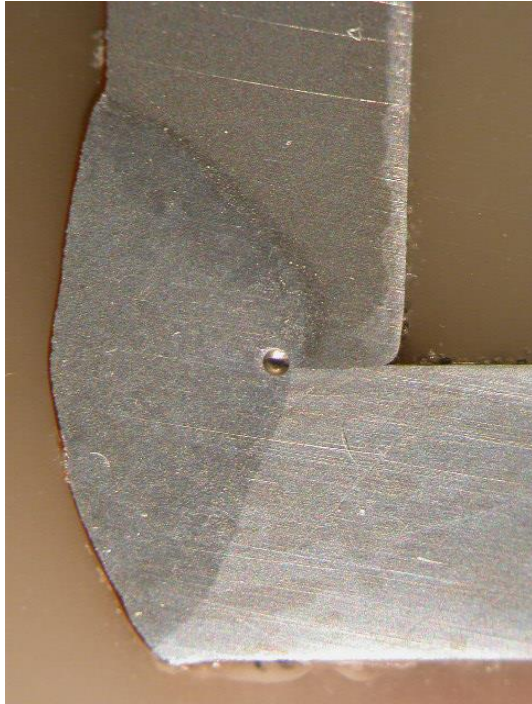
Microstructures obtained from some location of header surface, showing heavily corroded area



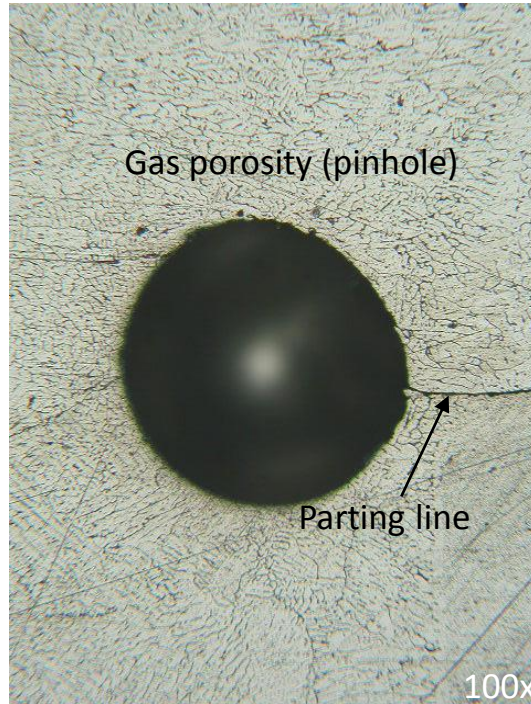


Cross section of a polished and etched specimen obtained from the corroded area of header surface

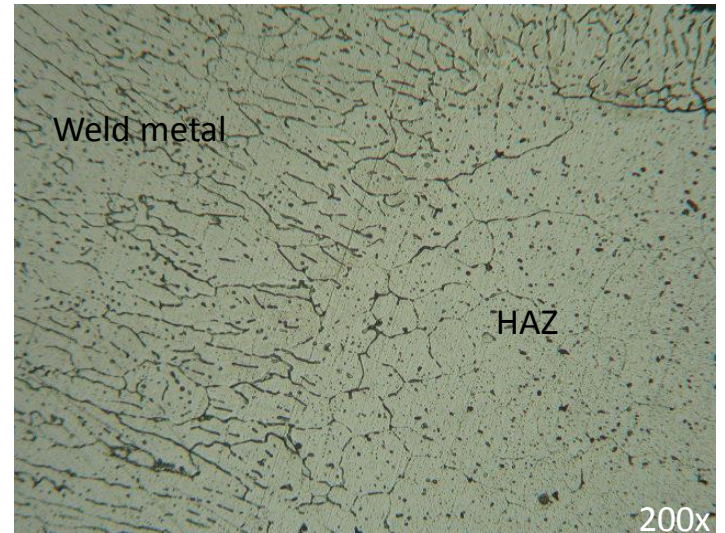




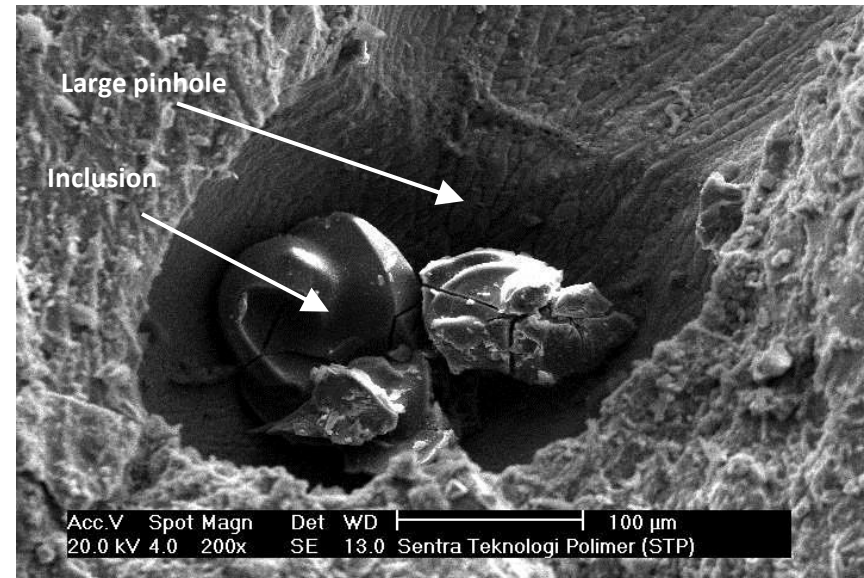
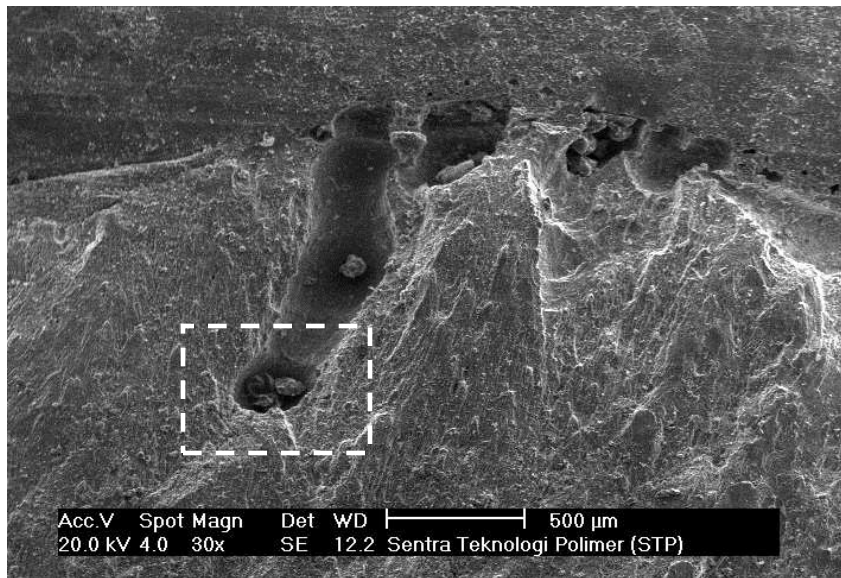
Microstructures obtained from welded area



Location 1

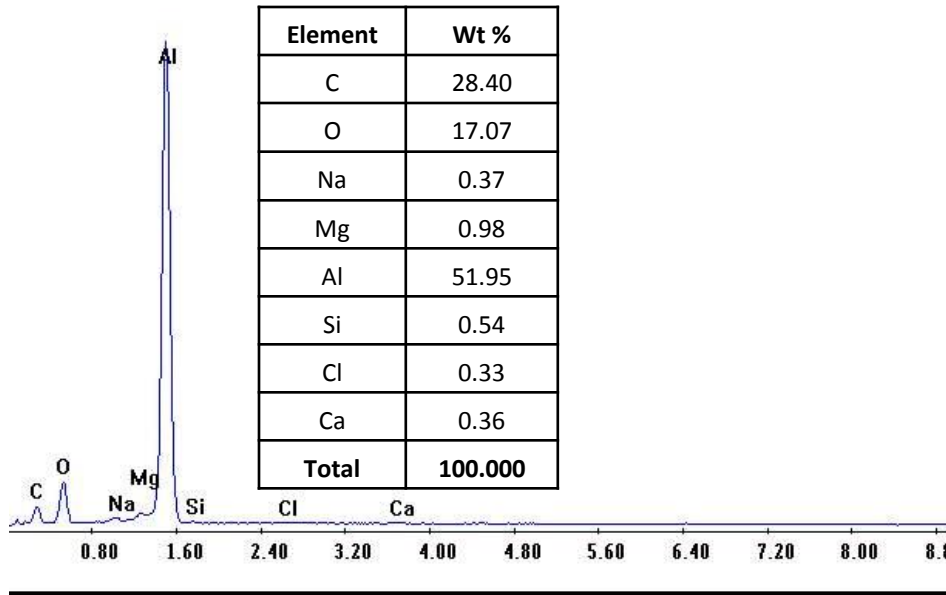


Location 2



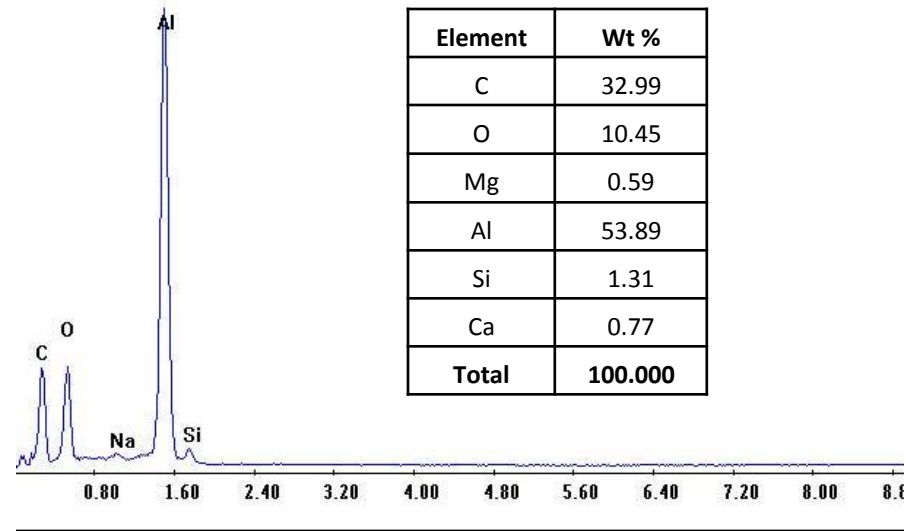
SEM micrographs of some surface fracture obtained from the leak portion of the weld joint between the header and side bar/parting sheet.

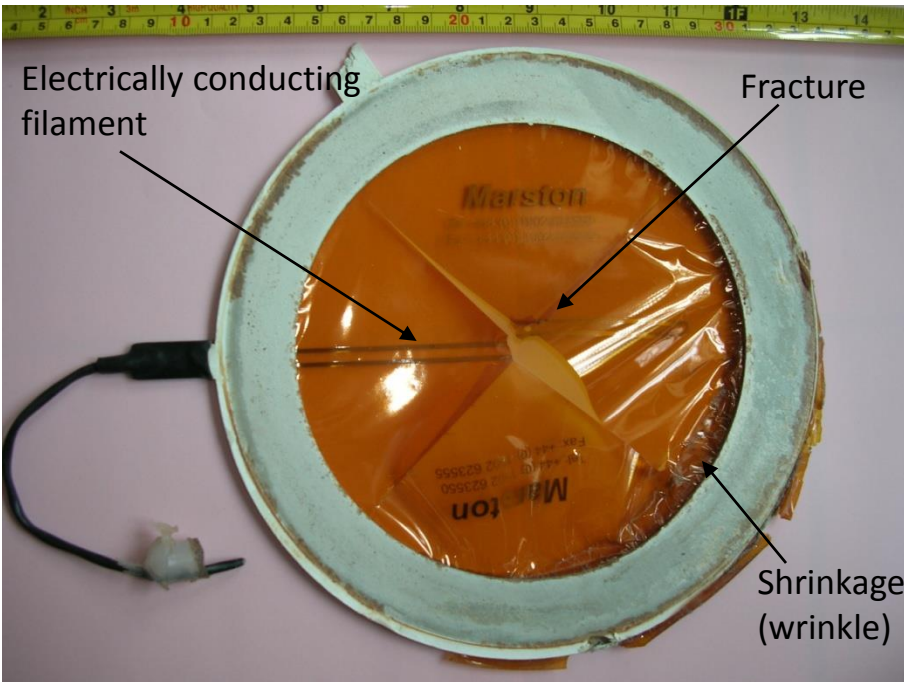
Label A: Sample Al base metal



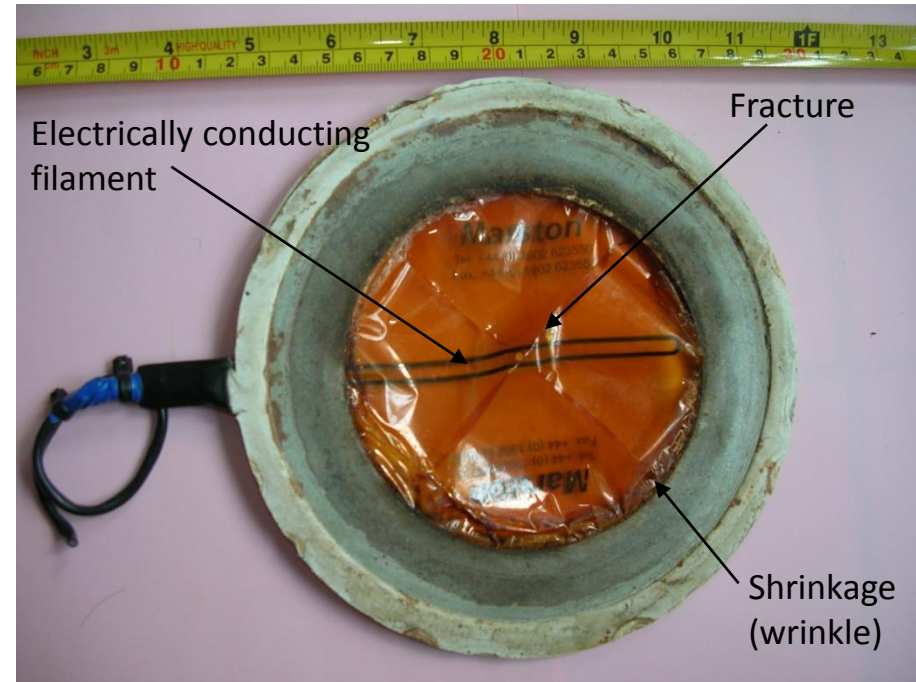
EDS spectrum of elements representing the corresponding composition of header material at some location.

Label A: Sample Al inklusi dalam lubang



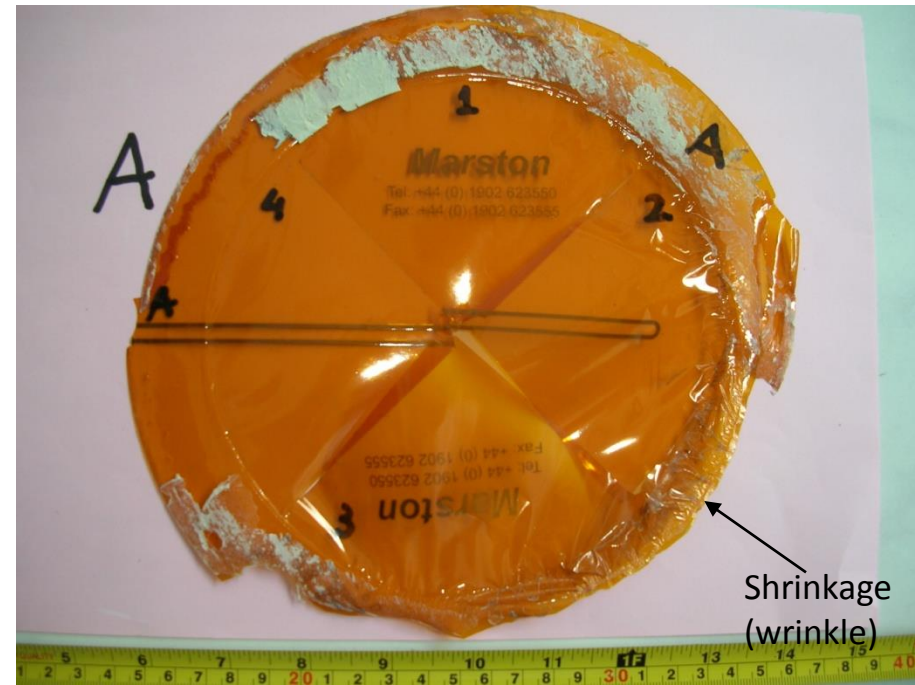


(A)

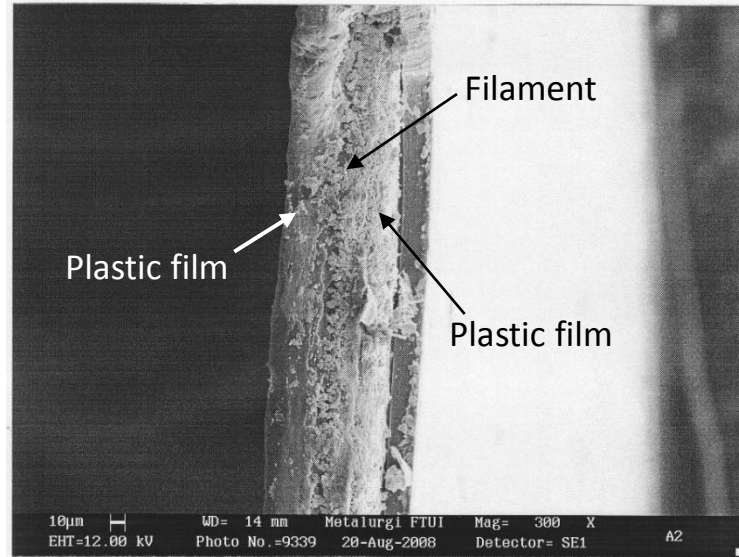
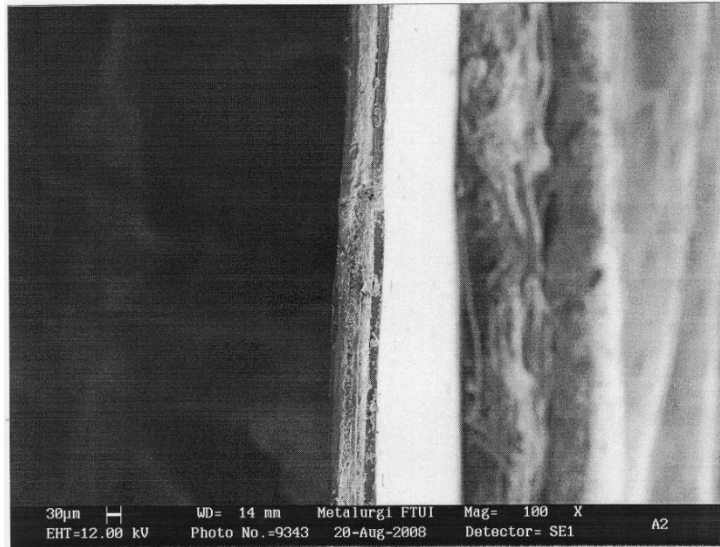


(B)

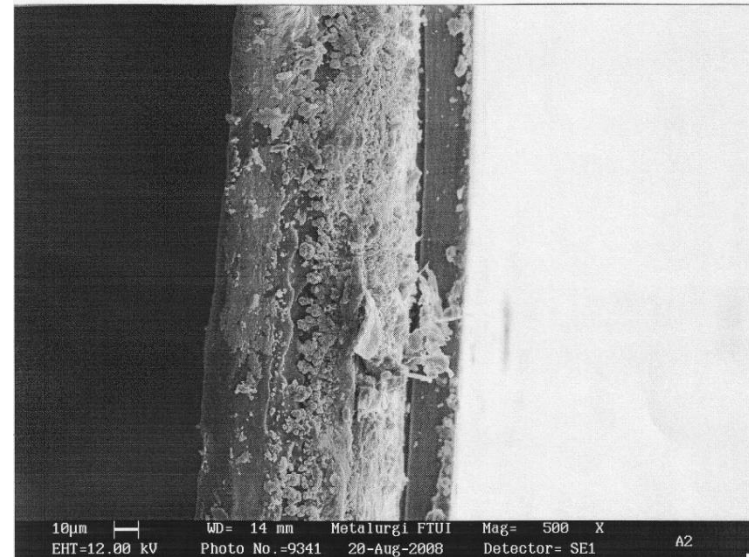
The as received two burst disc indicators (A & B) for failure analysis

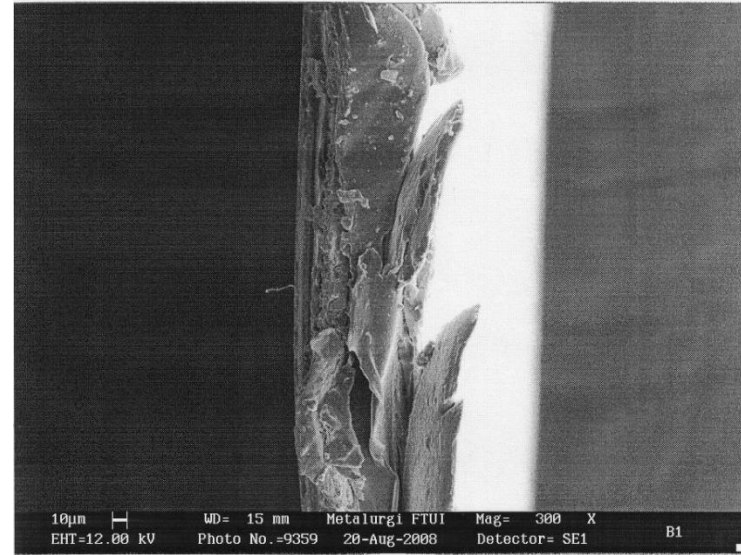
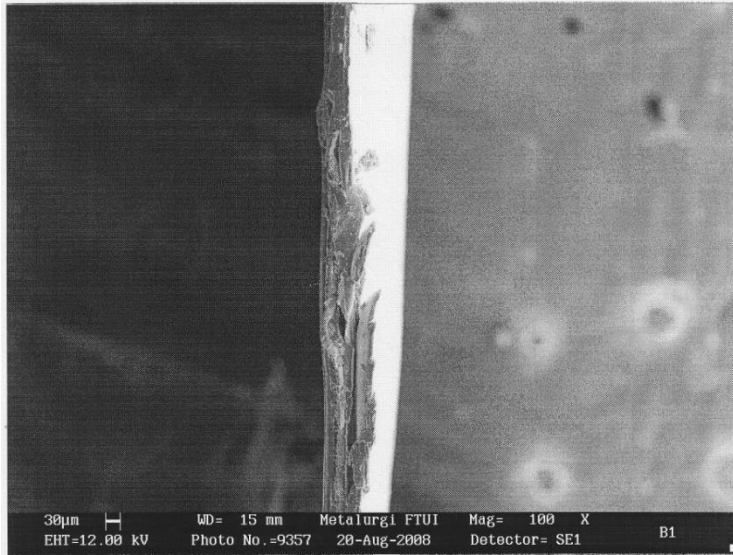


A close-up view of the burst disc indicator (A) showing shrinkage or wrinkle occurred on the plastic film around the disc edge. This shrinkage or wrinkle may have generated a tensile load to pull and break the filament apart and eventually activated the alarm system.

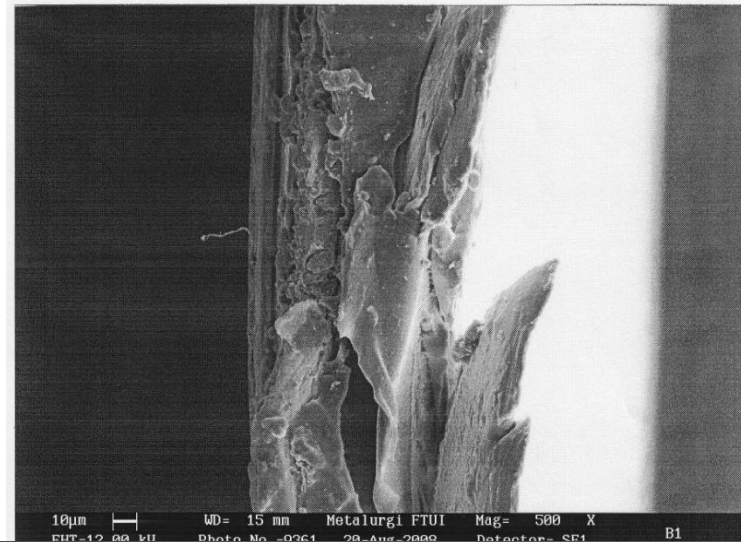


SEM micrographs of some surface fracture obtained from sample A2 (Sample A2 was cut-off from the broken filament at some position of the burst disc indicator A).

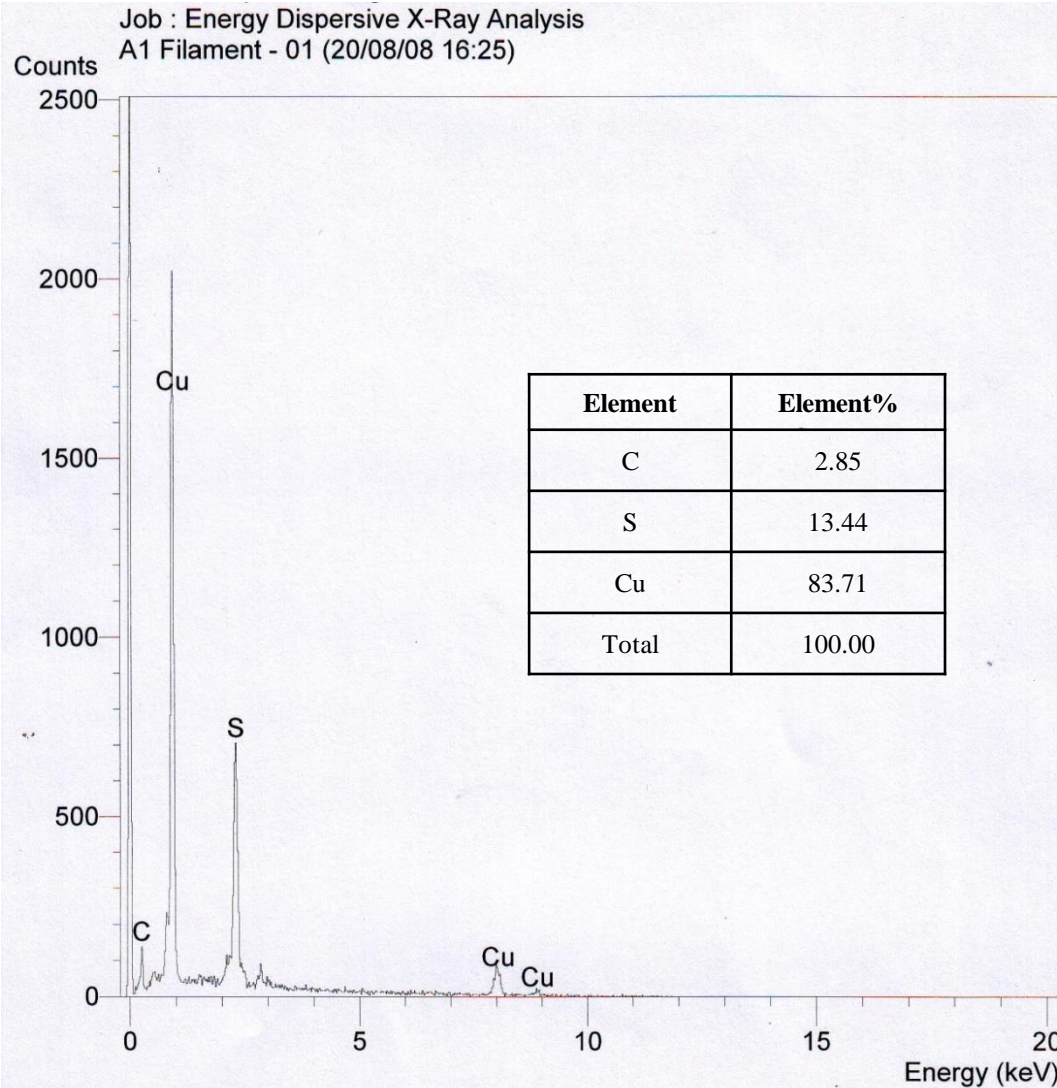




SEM micrographs of some surface fracture obtained from sample B1 at different location

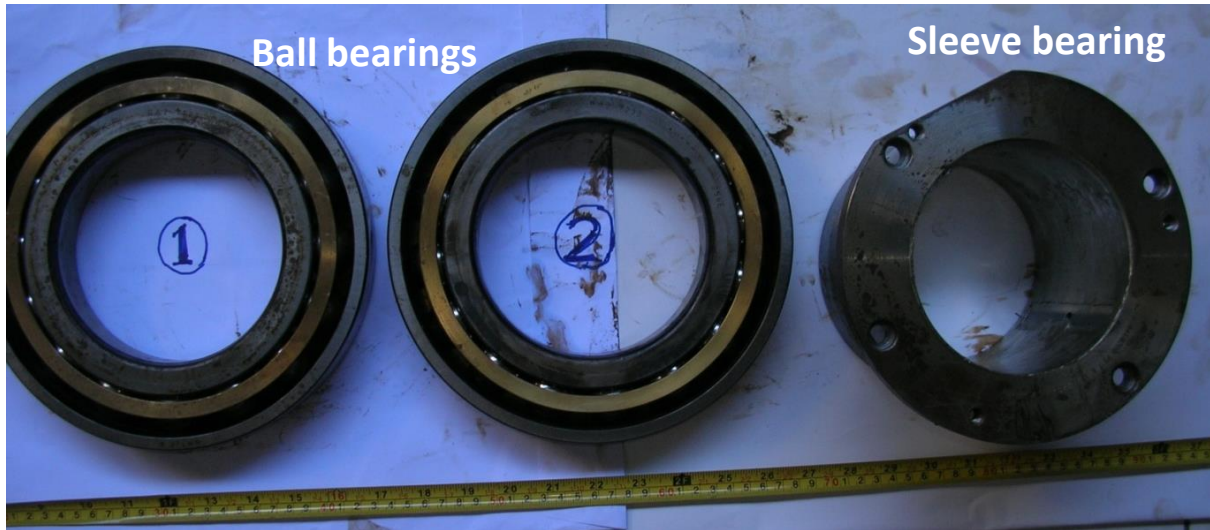


FAILURE ANALYSIS OF RUPTURE DISC INDICATOR (continued)

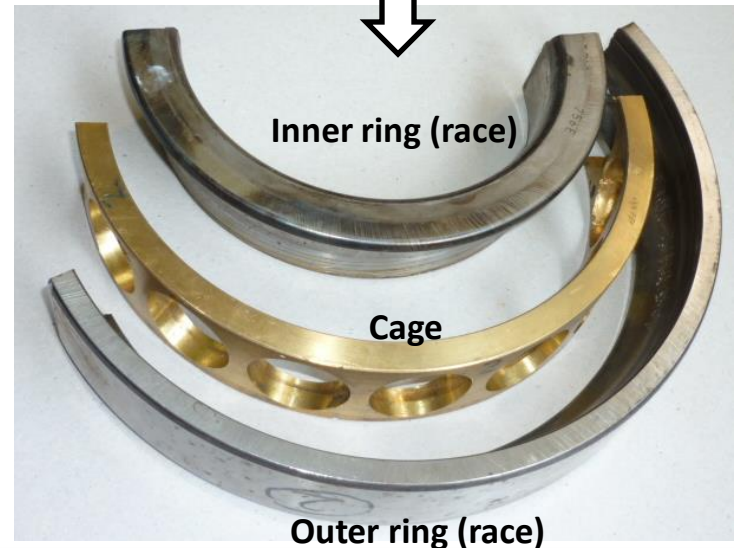


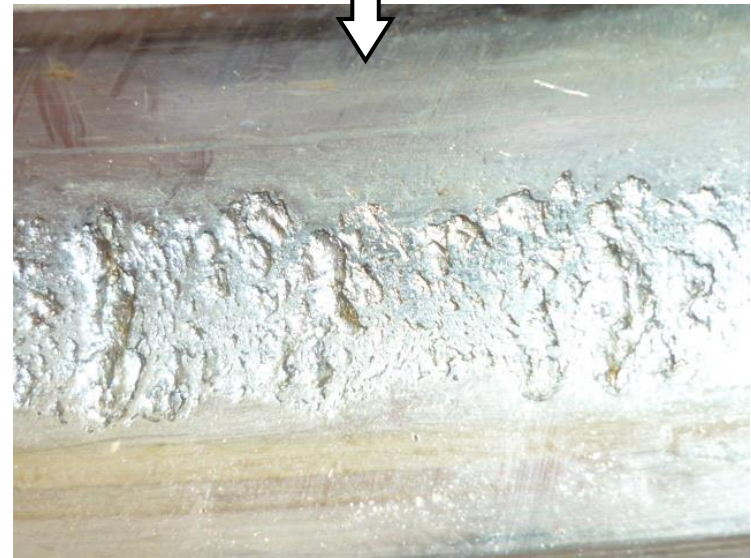
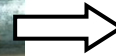
EDS spectrum of elements representing the corresponding composition of the filament material A1 at some test location

FAILURE ANALYSIS OF MOTOR COMPRESSOR BEARINGS OF A CHILLER



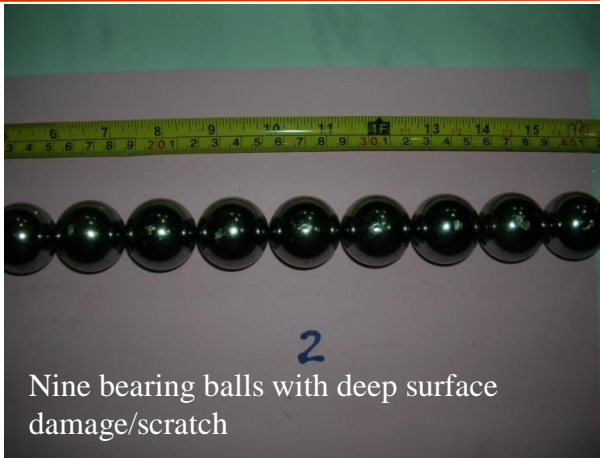
Dismantled parts of ball bearing showing some sections of inner ring (race), cage and outer ring (race).



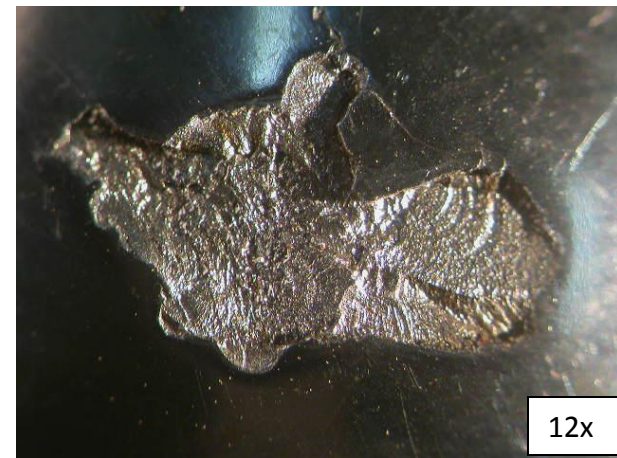


**Damaged area of the outer ring
raceway of ball bearing.**

FAILURE ANALYSIS OF MOTOR COMPRESSOR BEARINGS OF A CHILLER (continued)



Formation of surface damage on a number of bearing balls



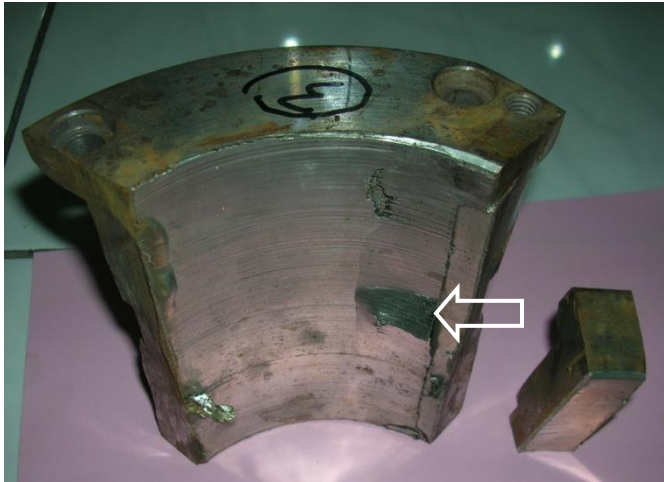
Close up view of surface damage formed on ball no. 1 of the damaged ball bearing

FAILURE ANALYSIS OF MOTOR COMPRESSOR BEARINGS OF A CHILLER (continued)

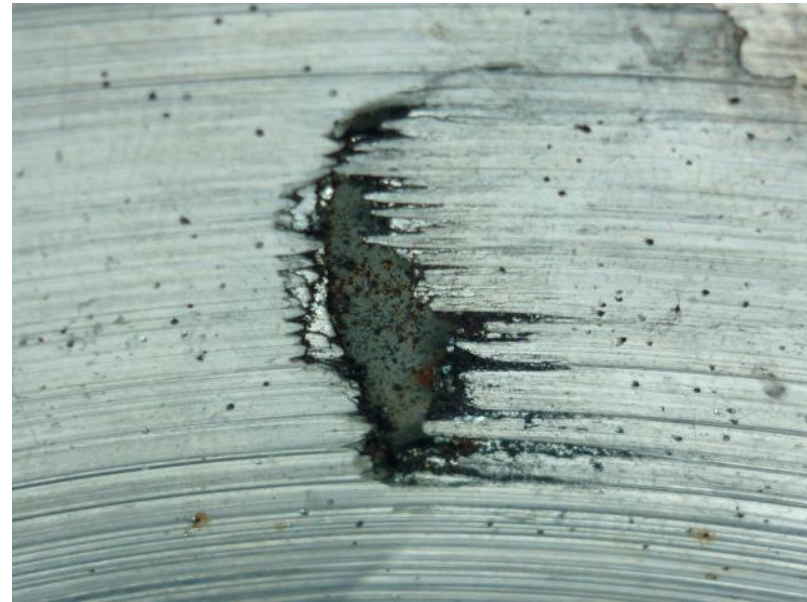
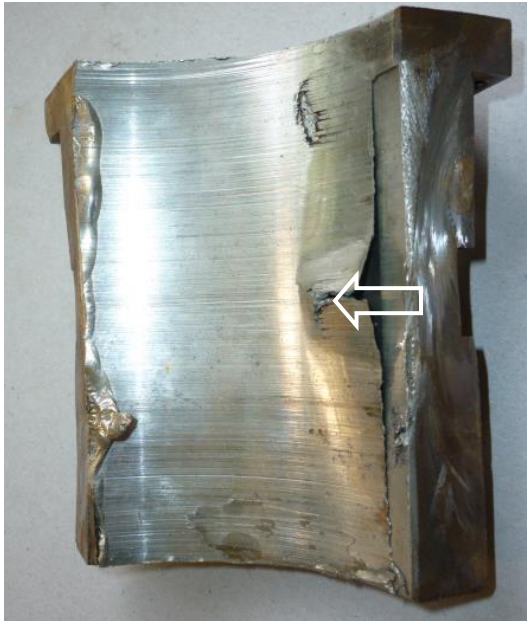


Fracture surfaces obtained from one bearing ball of the damaged ball bearing that was fractured into three fragments. Most of the fracture surfaces exhibit several beach marks indicative of fatigue fracture.



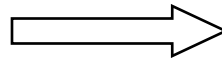
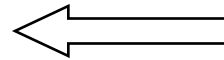
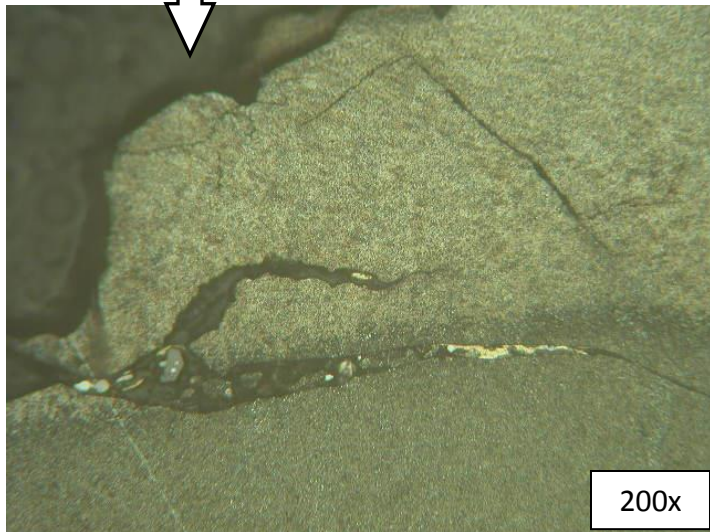
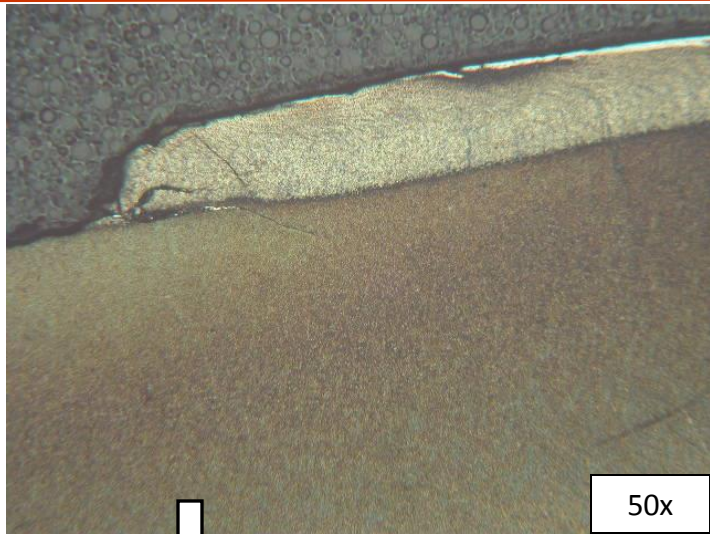


Formation of damage on the internal raceway of sleeve bearing, showing bearing overlay had been severely deformed and worn out causing a lubricating oil hole closed off (see arrow).

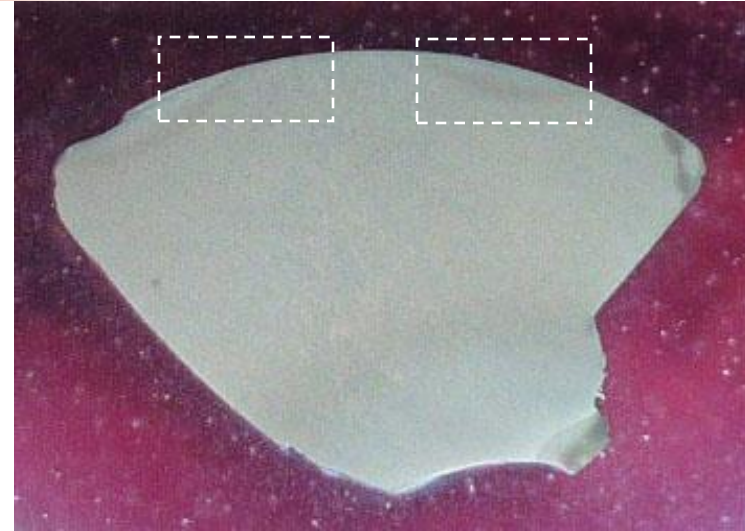


Deep scratch

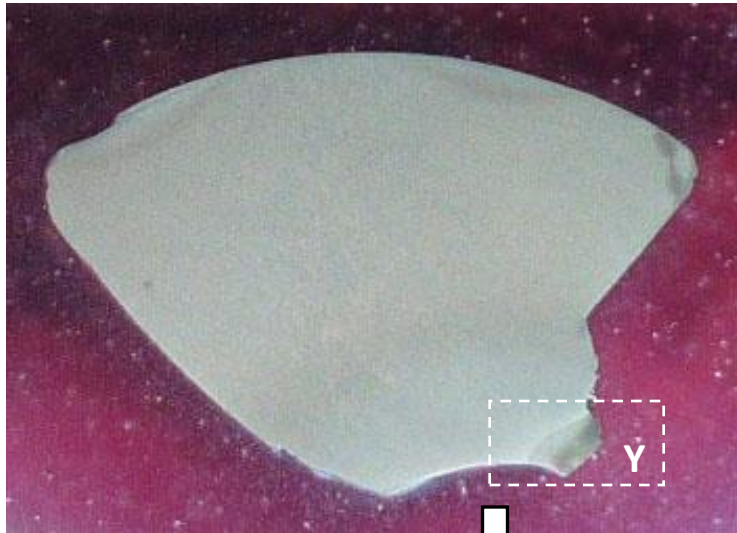
FAILURE ANALYSIS OF MOTOR COMPRESSOR BEARINGS OF A CHILLER (continued)



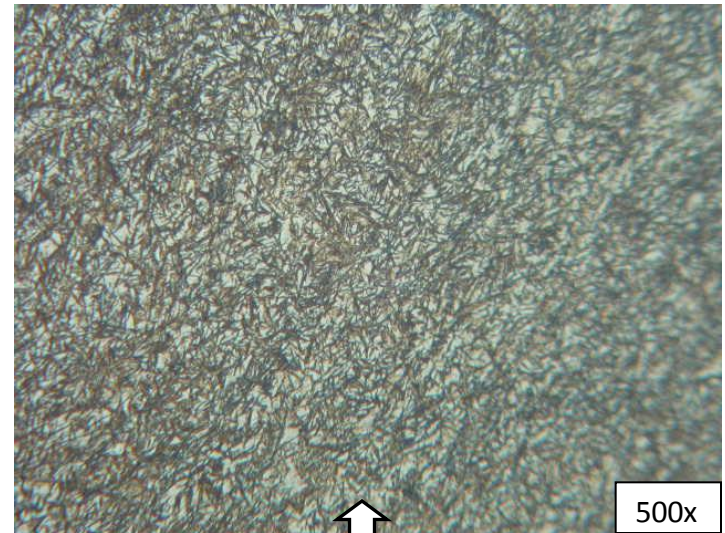
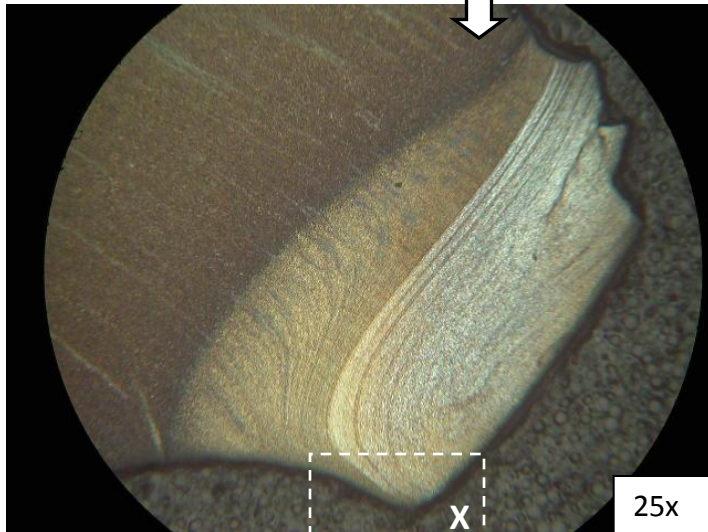
Micrograph of cross section of one of the fractured ball fragments of ball bearing at as indicated location, showing microstructure changes (indicated by white layers) and a number of cracks.



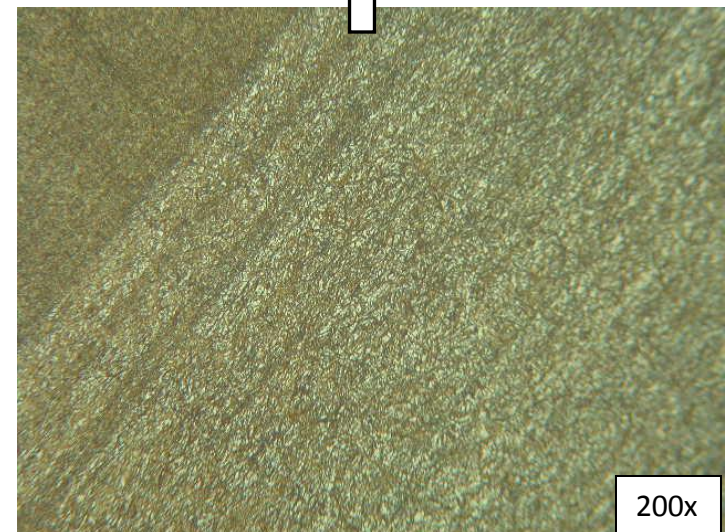
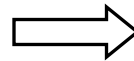
FAILURE ANALYSIS OF MOTOR COMPRESSOR BEARINGS OF A CHILLER (continued)



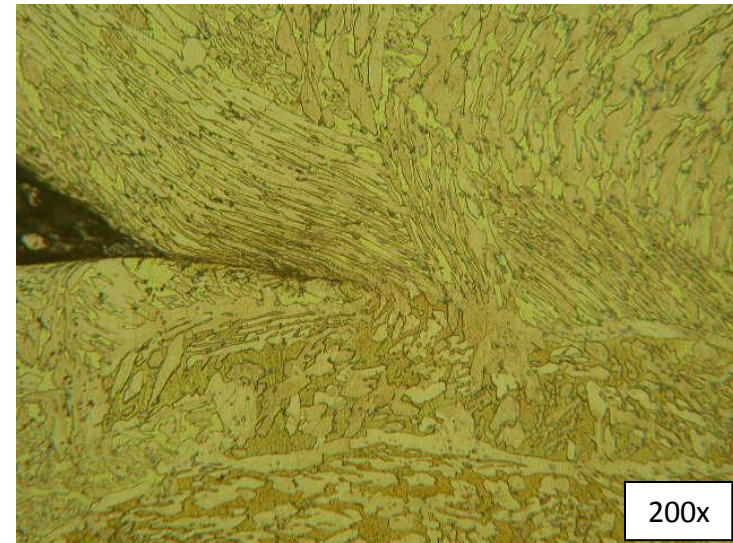
Microstructures obtained from cross section of one of the broken ball bearing fragments of ball bearing at different location as indicated (Y).



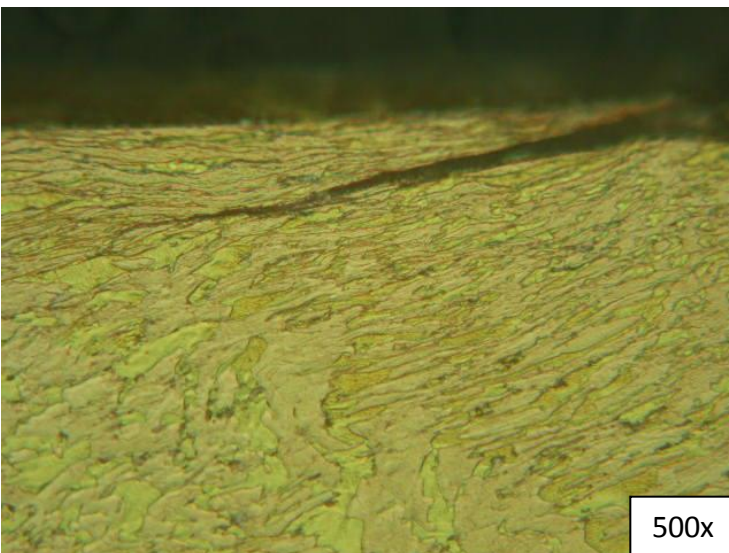
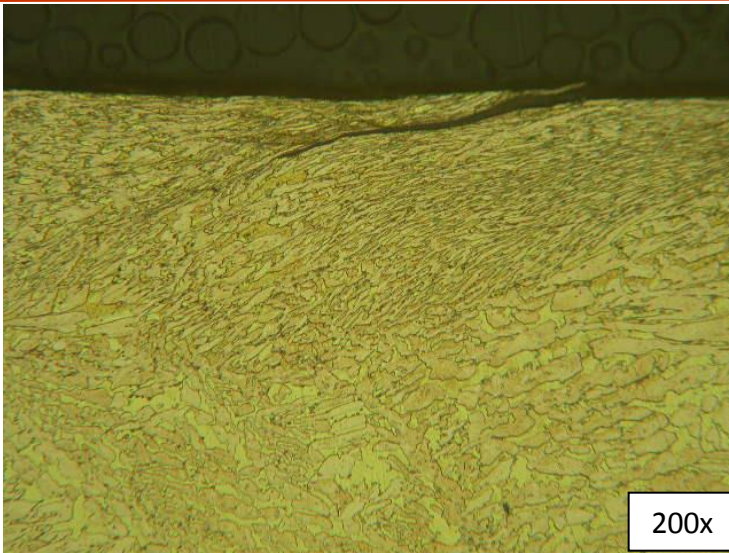
500x



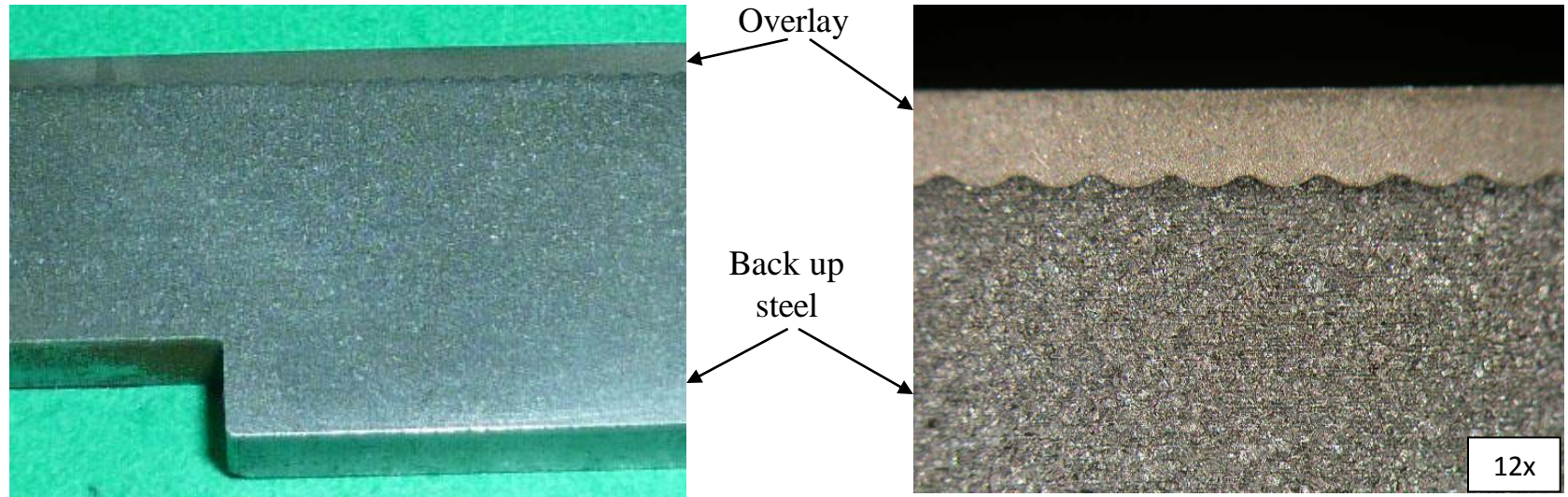
200x



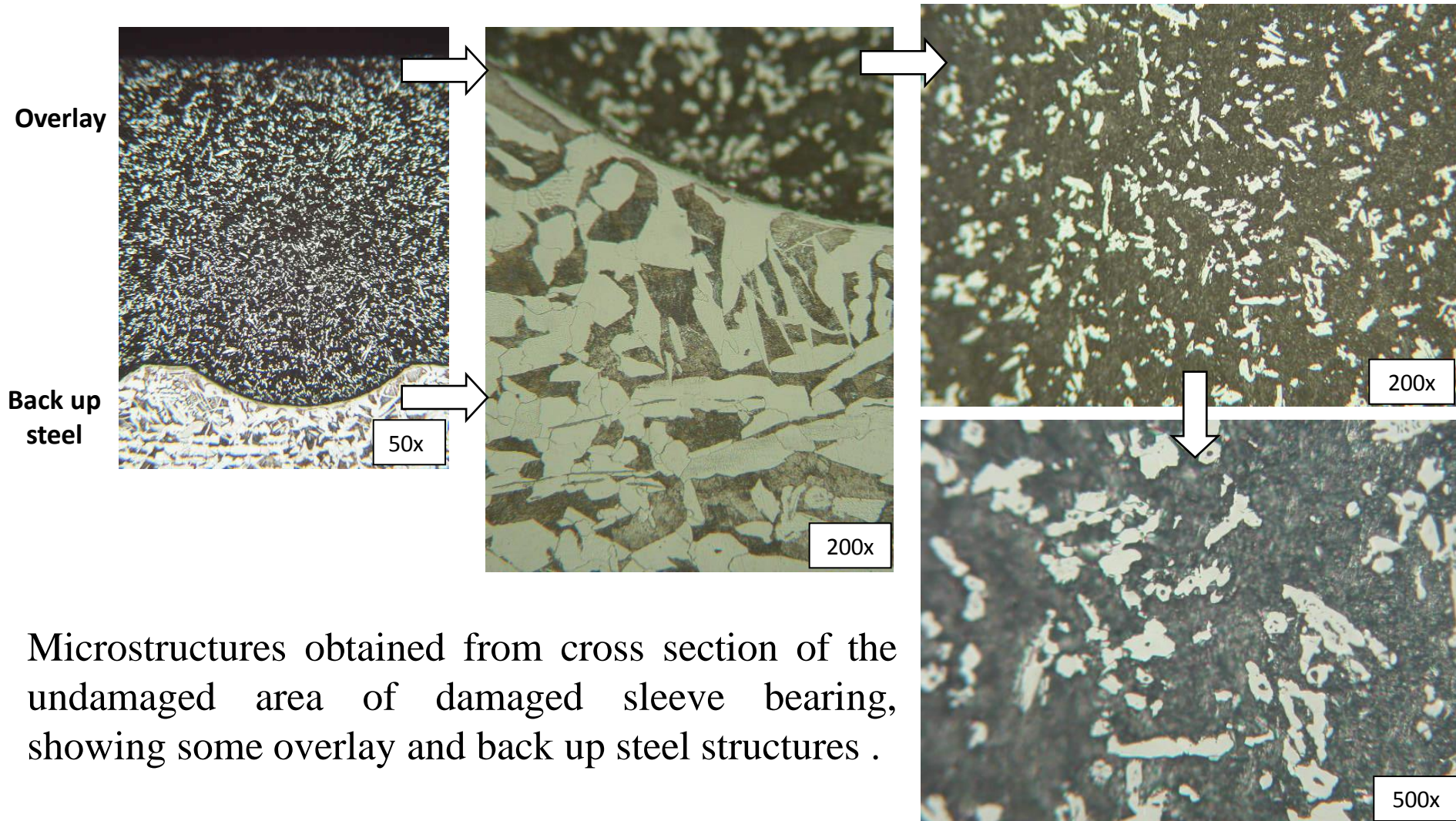
Microstructures obtained from transverse section of the damaged cage of ball bearing.



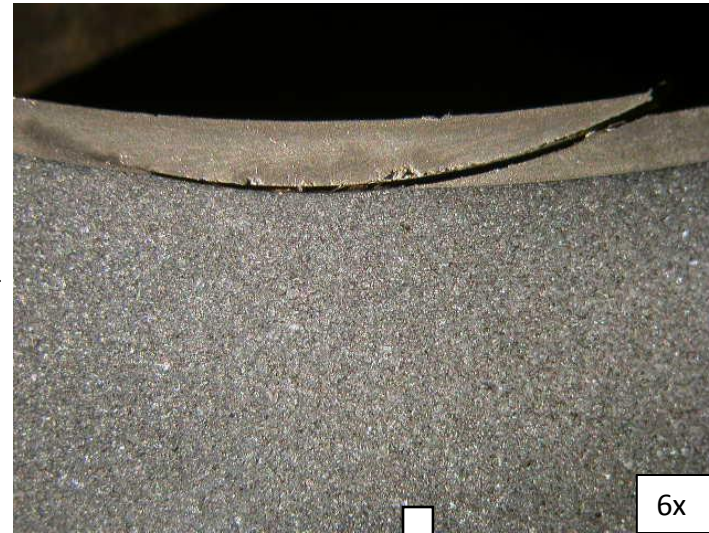
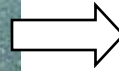
Microstructures obtained from transverse section of the damaged cage of ball bearing.



Microstructures obtained from cross section of the undamaged area of damaged sleeve bearing, showing some overlay and back up steel structures.

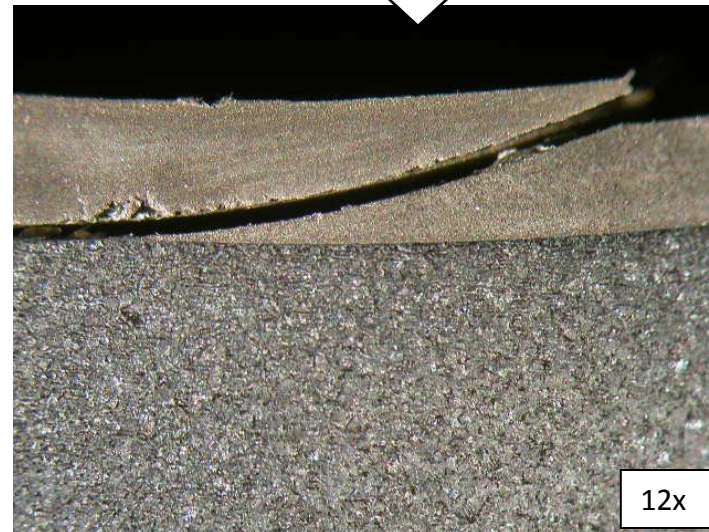


Microstructures obtained from cross section of the undamaged area of damaged sleeve bearing, showing some overlay and back up steel structures .



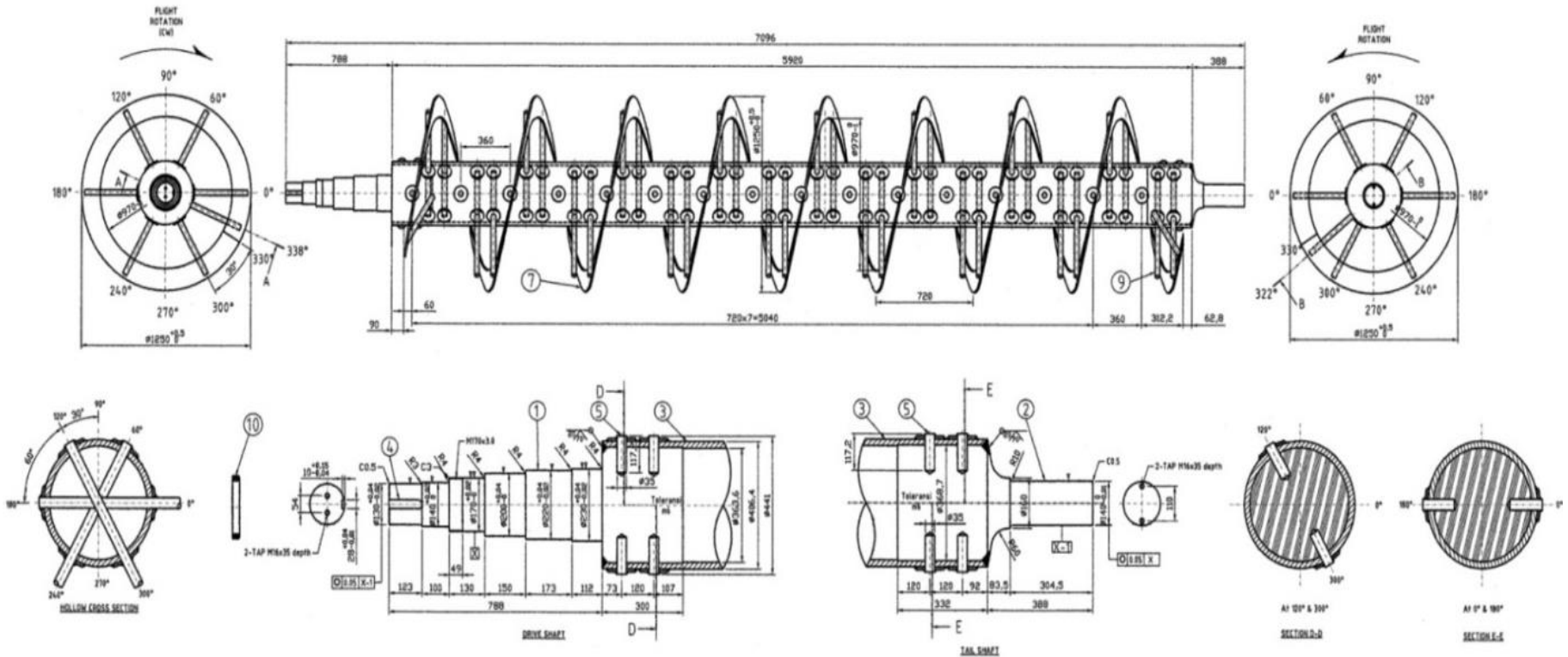
6x

Microstructures obtained from cross section of the damaged area of damaged sleeve bearing.

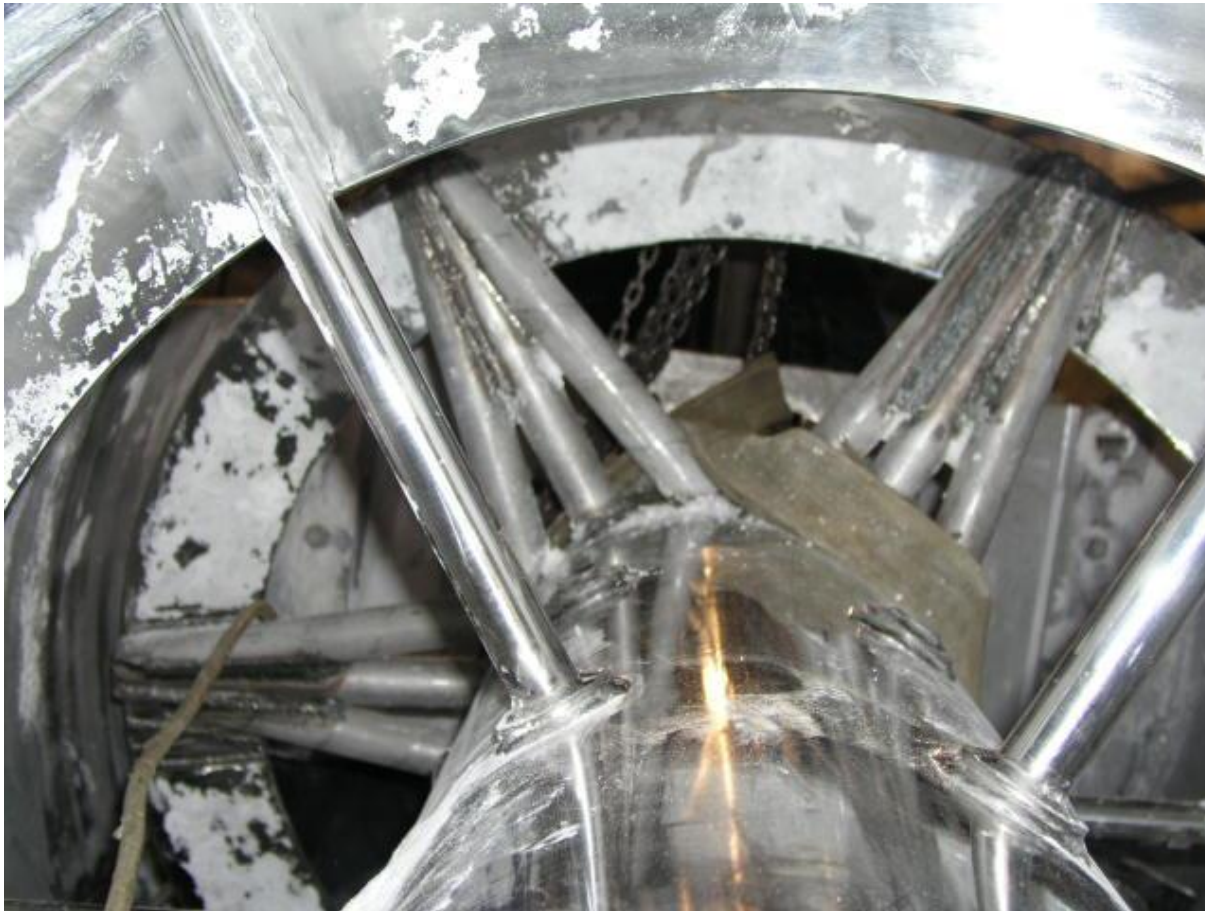


12x

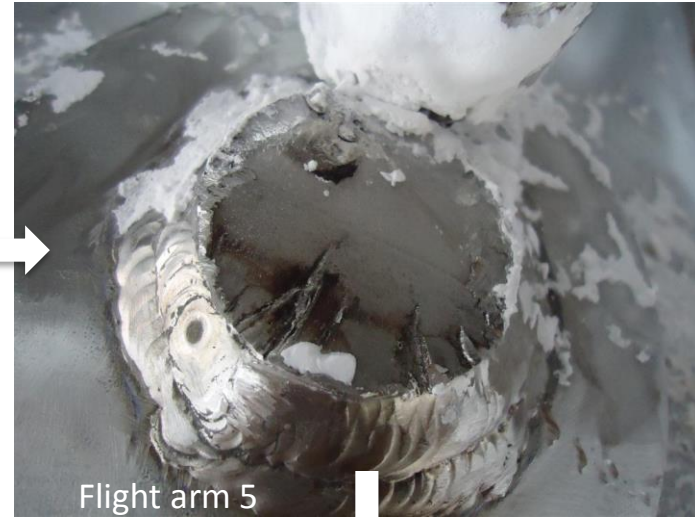
ROOT CAUSE FAILURE ANALYSIS OF BROKEN FLIGHT ARMS OF A SCREW FEEDER DUE TO FATIGUE



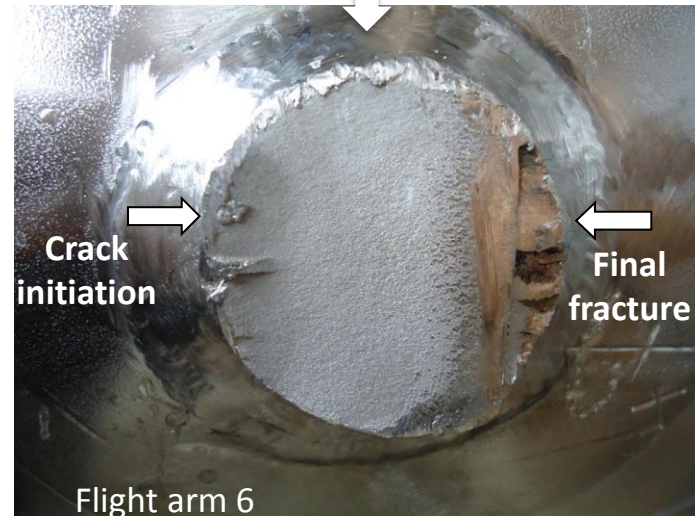
The as built drawing of a screw feeder showing a number of flight arms constructed to the hub shaft/pipe and equipped with ribbon plates.

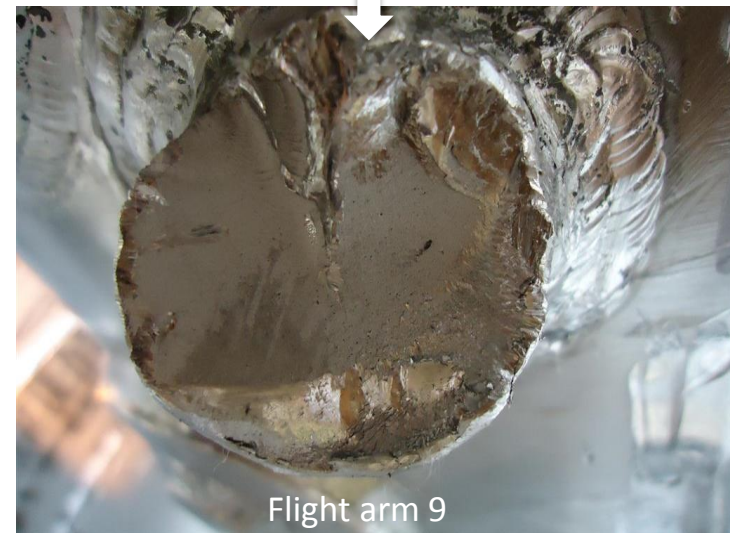
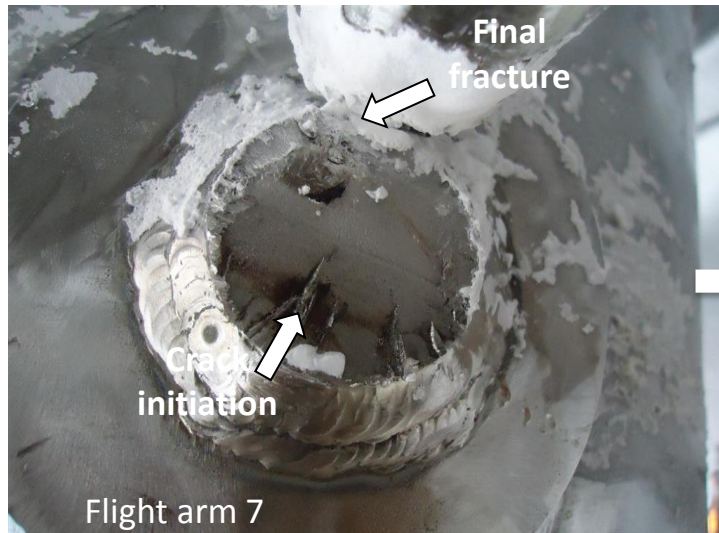


Photograph of some portion of a screw feeder showing some flight arms that were being welded on the hub shaft/pipe, while the other free end of the flight arms were welded to the ribbon plates.



Fracture surfaces of several broken flight arms of a screw feeder. Most of the fracture occurred had been taking place slightly above or within the heat affected zone (HAZ) of the weld joint between the flight arm and the pad plate/hub shaft.





Fracture surfaces of several broken flight arms of a screw feeder. Most of the fracture occurred had been taking place slightly above or within the heat affected zone (HAZ) of the weld joint between the flight arm and the pad plate/hub shaft.



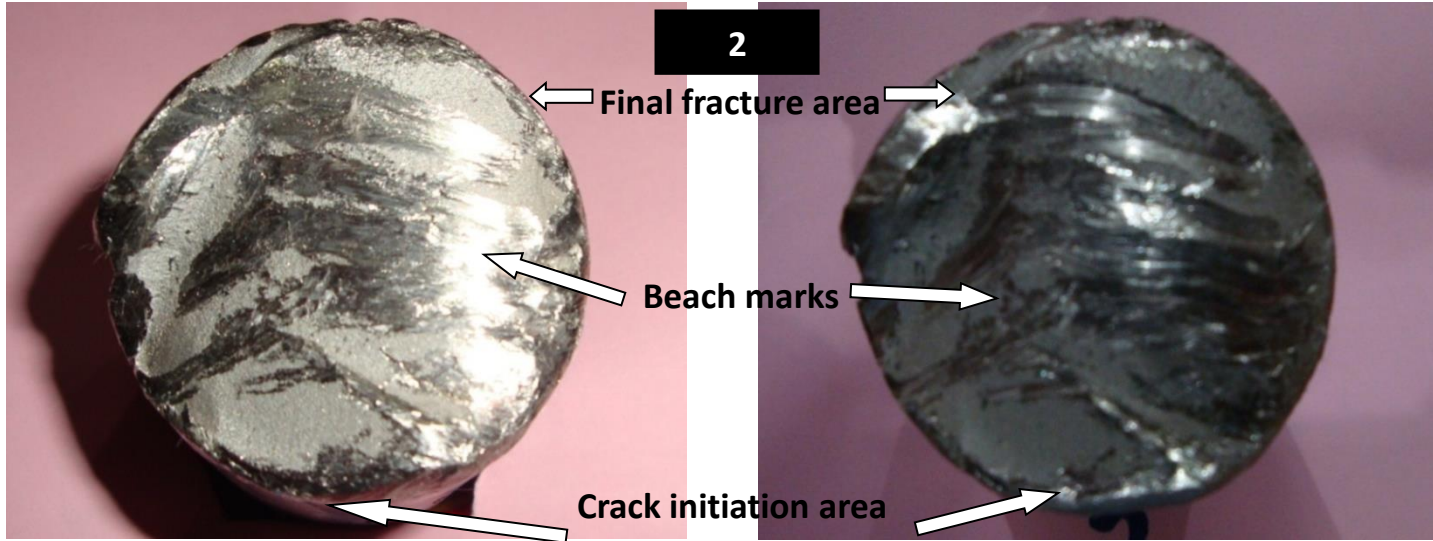
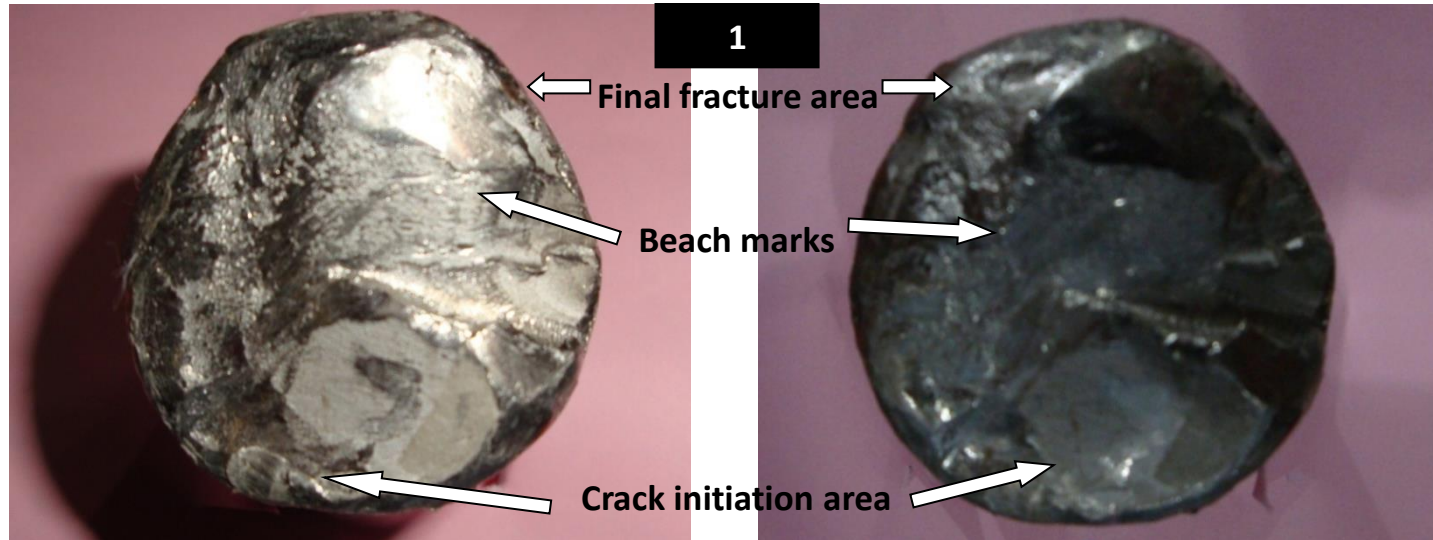
a) Longitudinal view



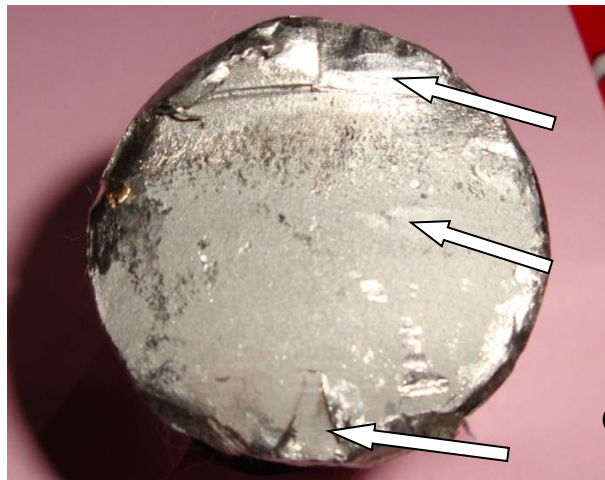
b) View of fracture surfaces

The as received four broken flight arms no. 1 to 4 of a screw feeder for failure analysis. The actual locations of the four broken flight arms being used in this failure analysis were not clearly known.

ROOT CAUSE FAILURE ANALYSIS OF BROKEN FLIGHT ARMS OF A SCREW FEEDER DUE TO FATIGUE (continued)



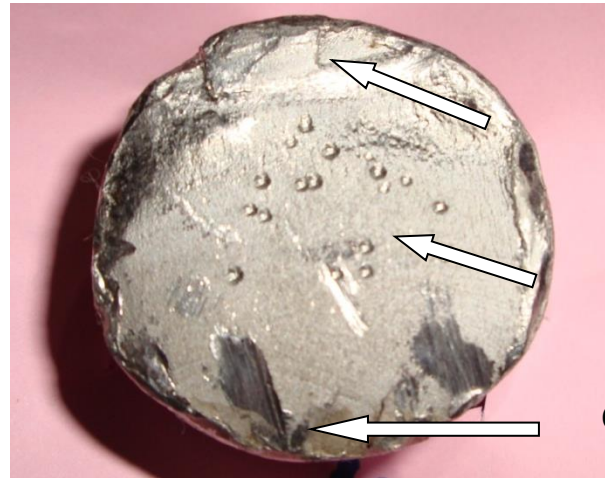
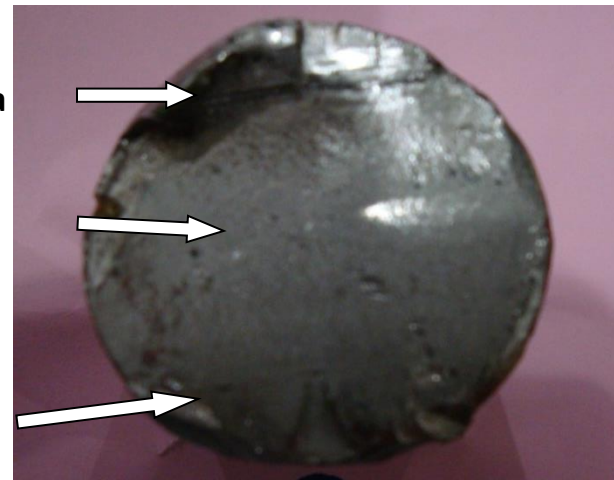
Fracture surfaces of the as received broken flight arms no. 1 to no. 4.



3
Final fracture area

Beach marks

Crack initiation area



4
Final fracture area

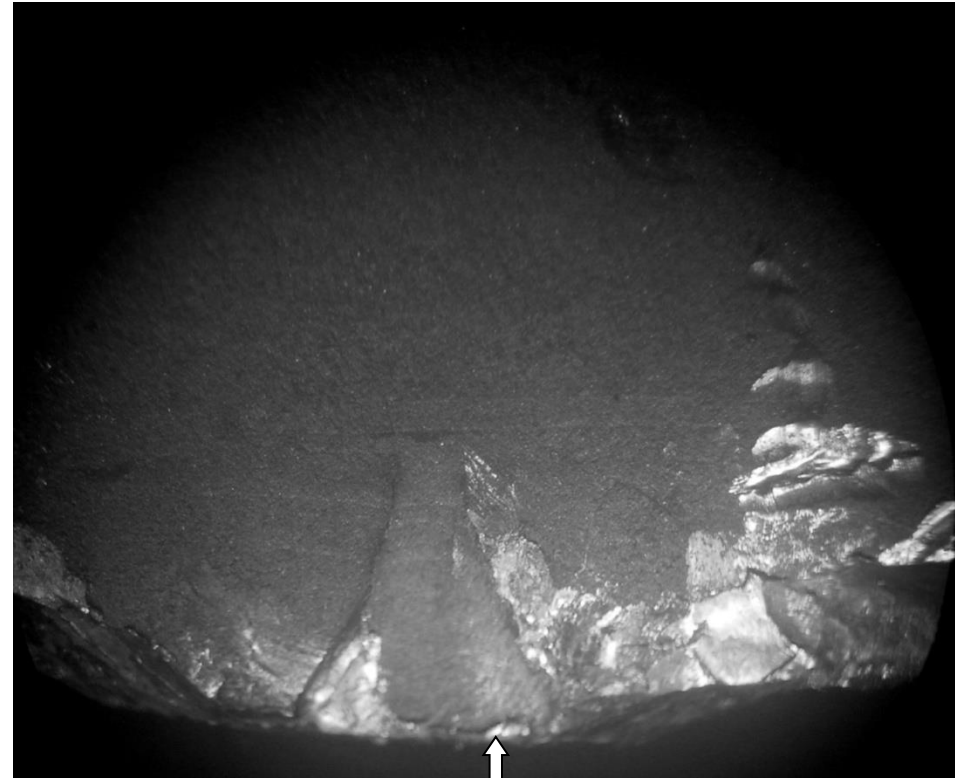
Beach marks

Crack initiation area



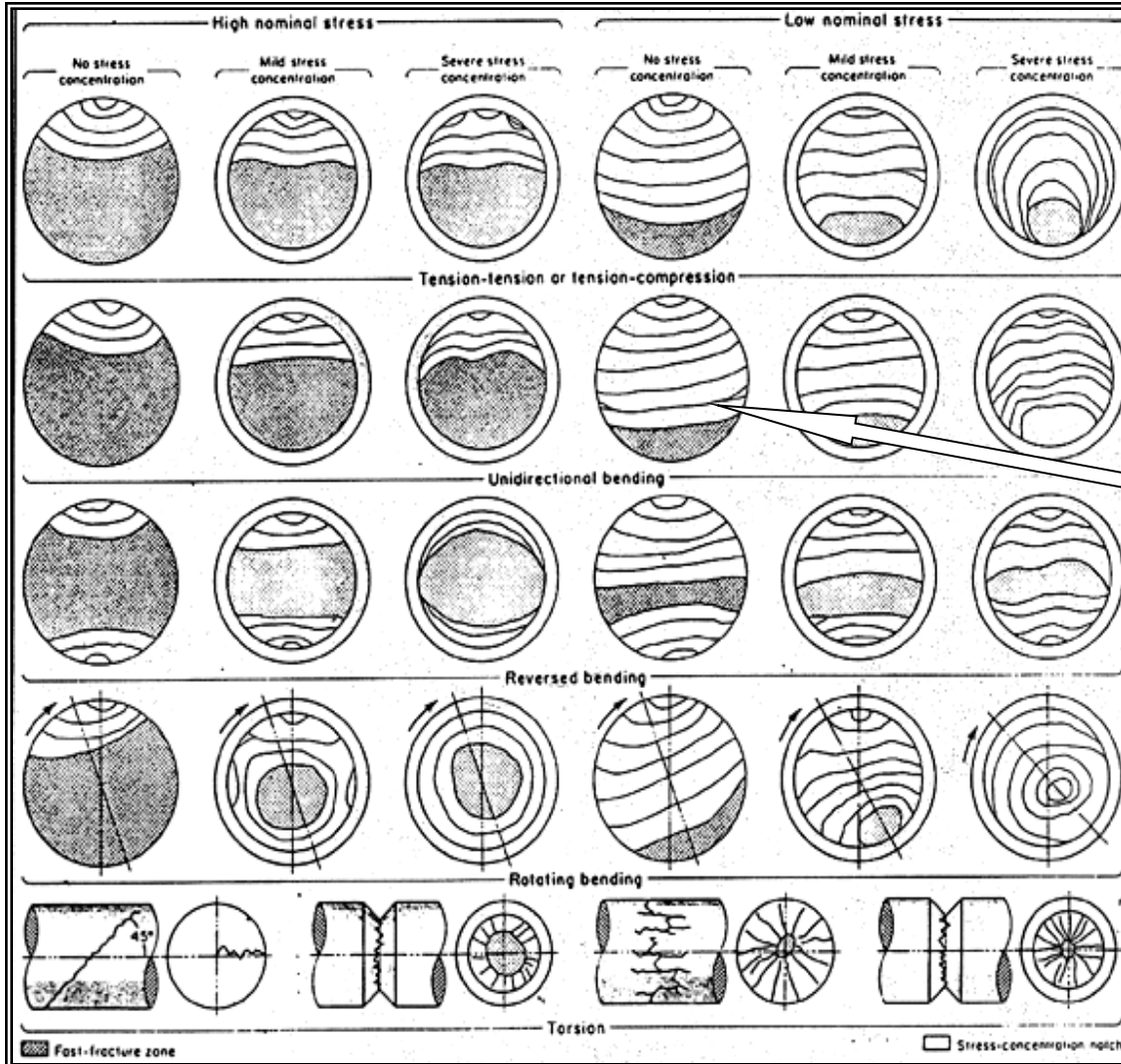
Fracture surfaces of the as received broken flight arms no. 1 to no. 4.

Final fracture area



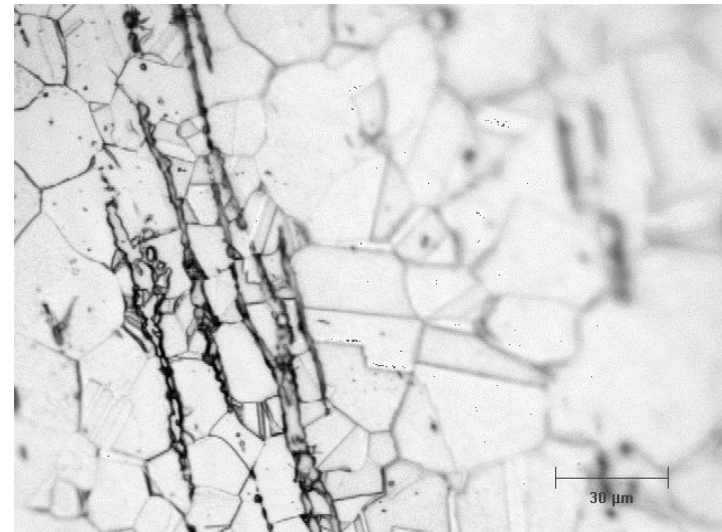
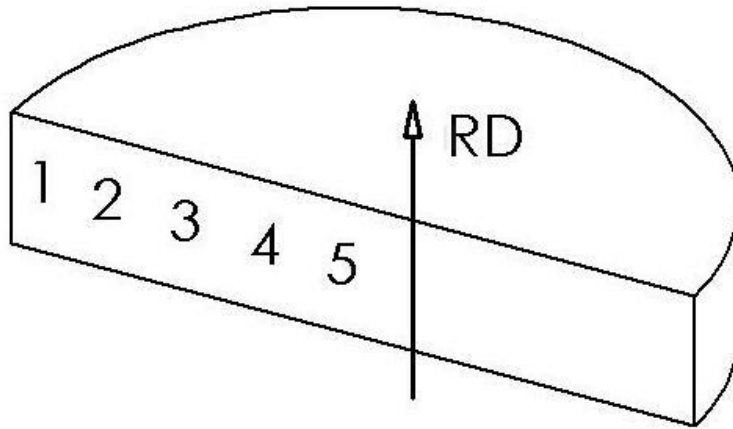
Close up view of fracture surface of the broken flight arm no. 3, showing the fatigue crack initiation, crack propagation and final fracture.

ROOT CAUSE FAILURE ANALYSIS OF BROKEN FLIGHT ARMS OF A SCREW FEEDER DUE TO FATIGUE (continued)



Similar fracture surface as observed from the broken flight arms.

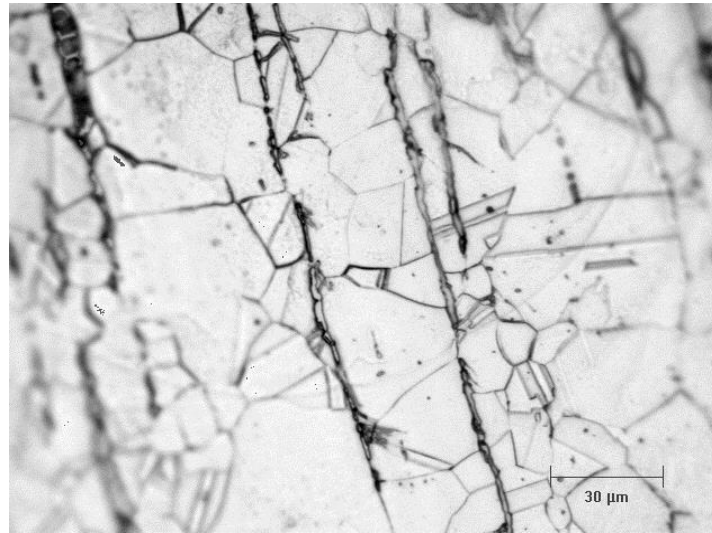
Schematic of marks on surfaces of fatigue fractures produced in smooth and notched components with round cross section under various loading conditions at high and low nominal stress.



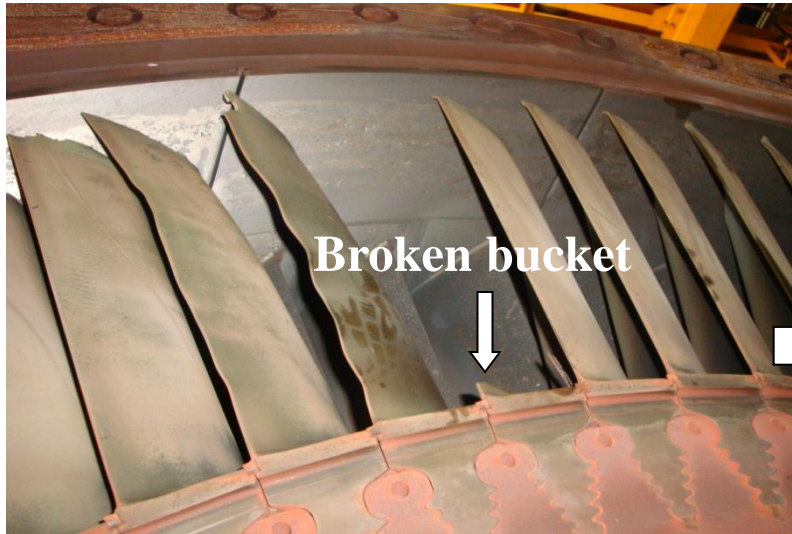
Microstructures obtained from a radial longitudinal section located nearby the fracture surface of broken flight arm no. 1 at location 1.



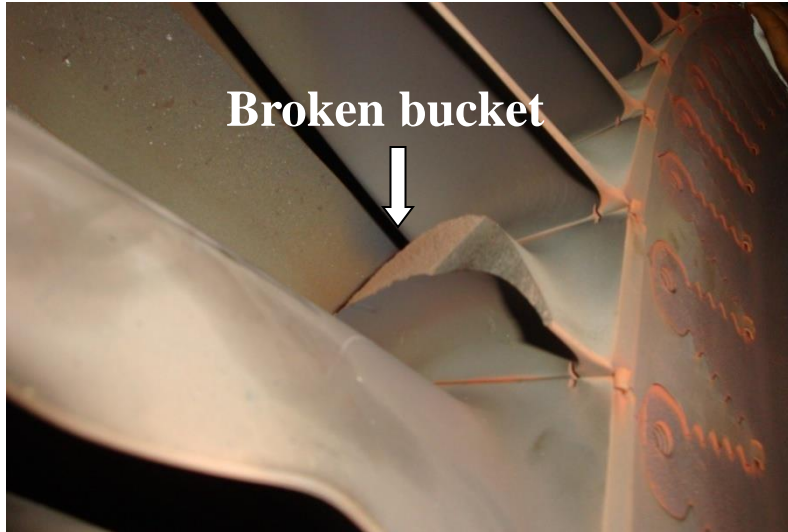
Microstructures obtained from a radial longitudinal section located nearby the fracture surface of broken flight arm no. 1 at location 4.



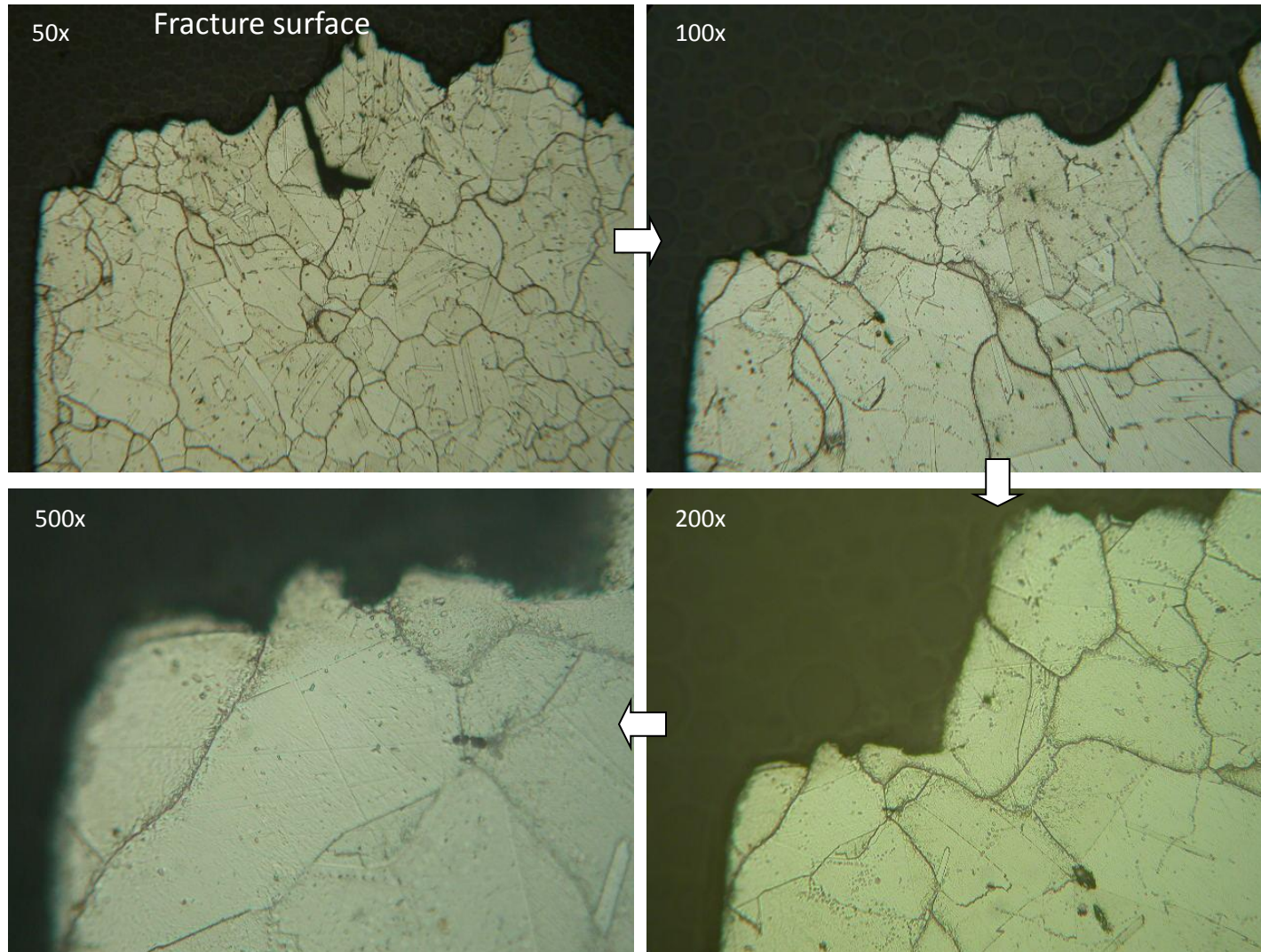
ROOT CAUSE FAILURE ANALYSIS ON BROKEN AND DAMAGE BUCKETS OF A GAS TURBINE POWER PLANT



ROOT CAUSE FAILURE ANALYSIS ON BROKEN AND DAMAGE BUCKETS OF A GAS TURBINE POWER PLANT (continued)



ROOT CAUSE FAILURE ANALYSIS ON BROKEN AND DAMAGE BUCKETS OF A GAS TURBINE POWER PLANT (continued)



Microstructures obtained from some fatigue area at the leading edge of bucket row # 2.

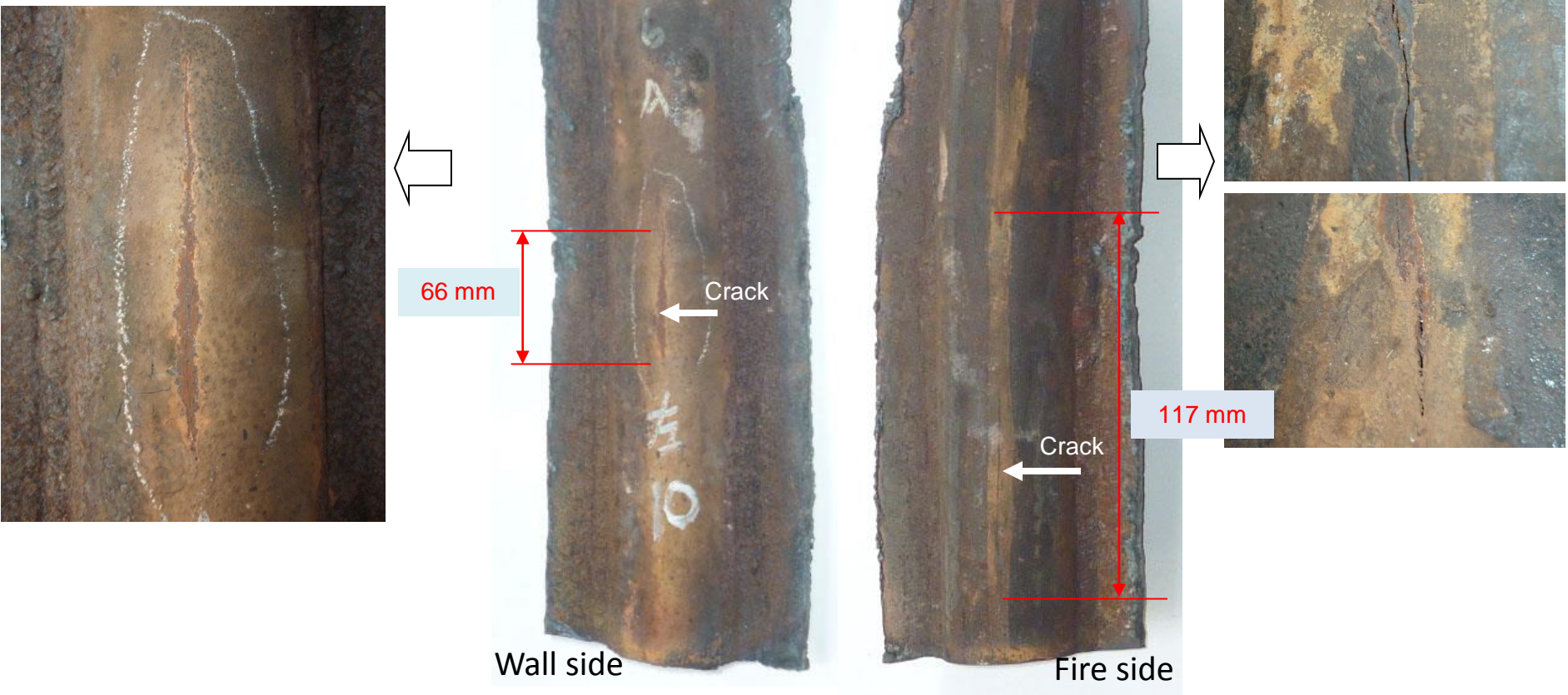
ROOT CAUSE FAILURE ANALYSIS OF CRACKED CAGE SUPERHEATER TUBES DUE TO CAUSTIC STRESS-CORROSION CRACKING



Site Welding
Seam

Leakage Points

ROOT CAUSE FAILURE ANALYSIS OF CRACKED CAGE SUPERHEATER TUBES DUE TO CAUSTIC STRESS-CORROSION CRACKING (continued)



Cracks at the tube surface facing the wall
(wall side cracks)

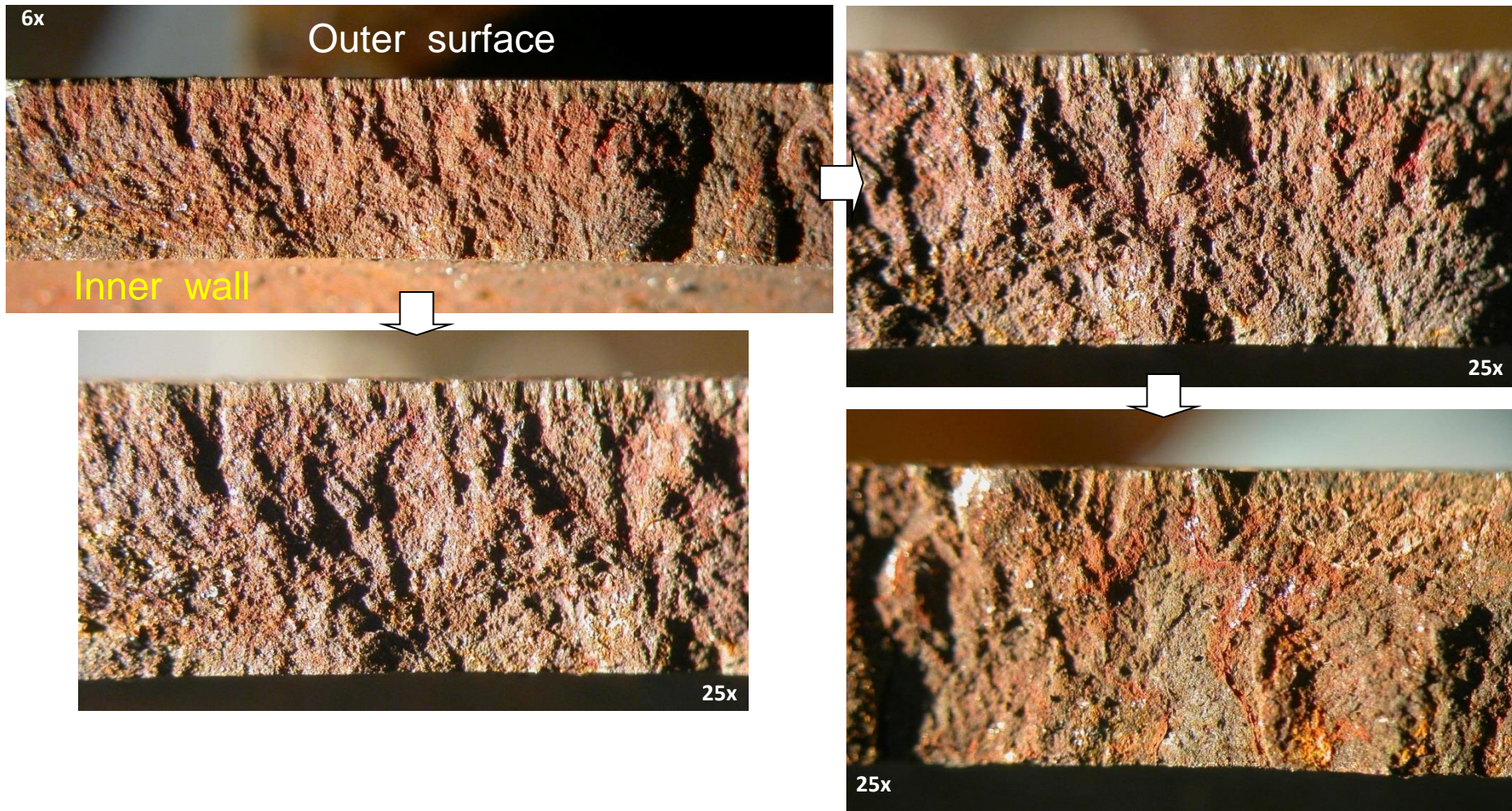
Cracks at the tube surface facing the fire
(fire side cracks)

**ROOT CAUSE FAILURE ANALYSIS
OF CRACKED CAGE SUPERHEATER TUBES
DUE TO CAUSTIC STRESS-CORROSION CRACKING (continued)**



Fire side cracks at the tube internal tube surface

**ROOT CAUSE FAILURE ANALYSIS
OF CRACKED CAGE SUPERHEATER TUBES
DUE TO CAUSTIC STRESS-CORROSION CRACKING (continued)**



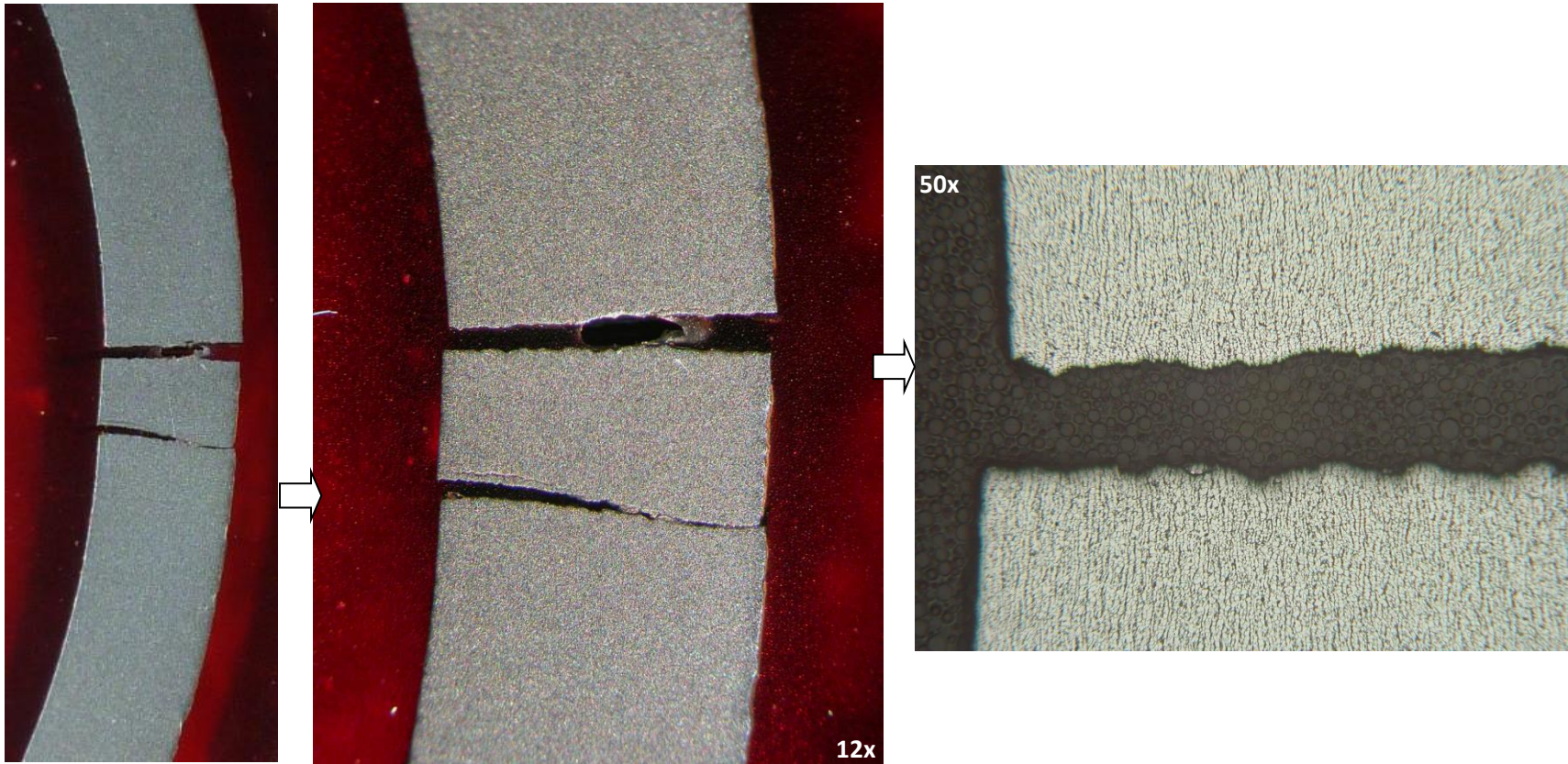
Fracture surface of the fire side cracked tube

**ROOT CAUSE FAILURE ANALYSIS
OF CRACKED CAGE SUPERHEATER TUBES
DUE TO CAUSTIC STRESS-CORROSION CRACKING (continued)**



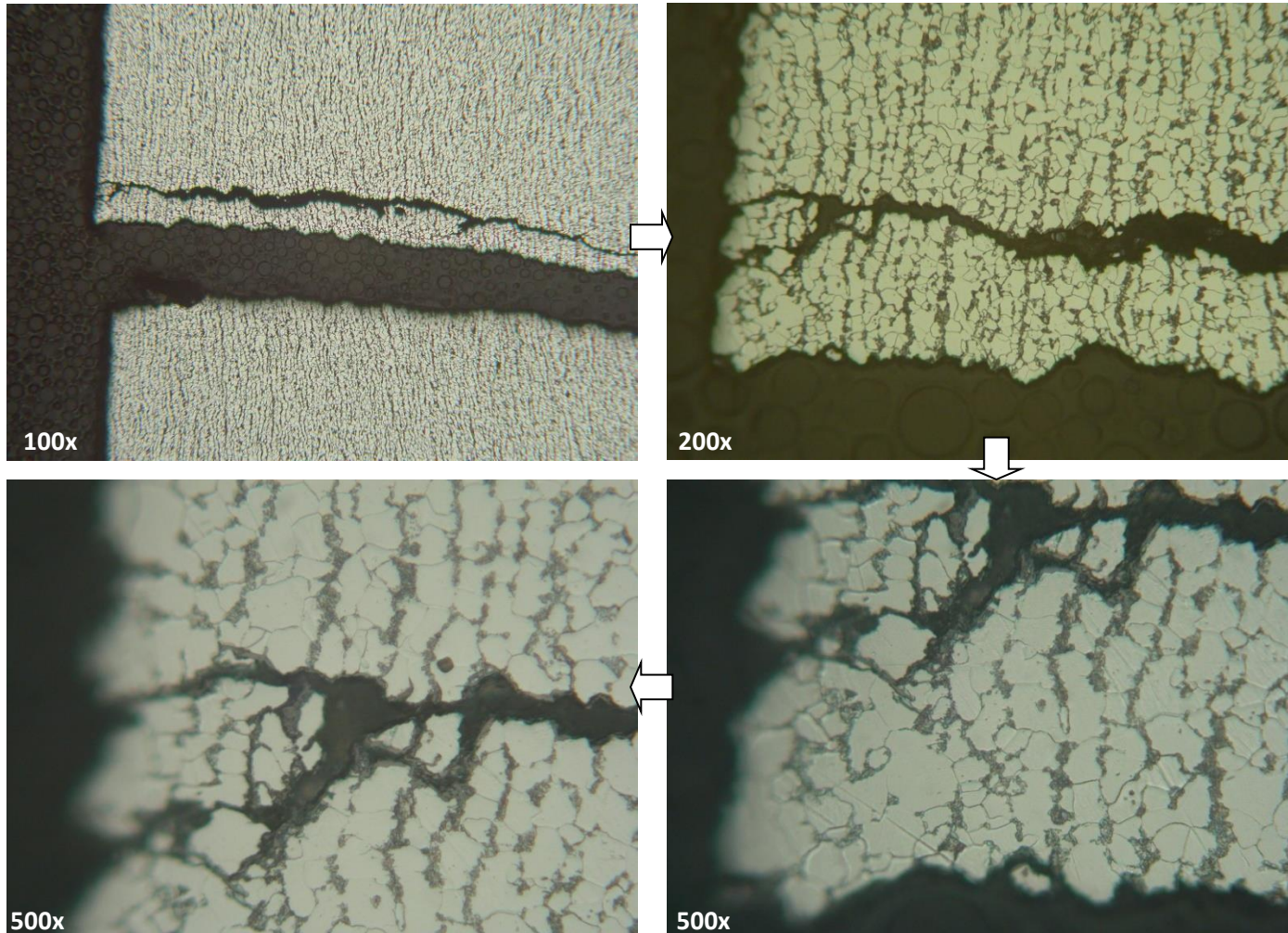
Specimens for metallographic examination of the fire side cracked tube

**ROOT CAUSE FAILURE ANALYSIS
OF CRACKED CAGE SUPERHEATER TUBES
DUE TO CAUSTIC STRESS-CORROSION CRACKING (continued)**



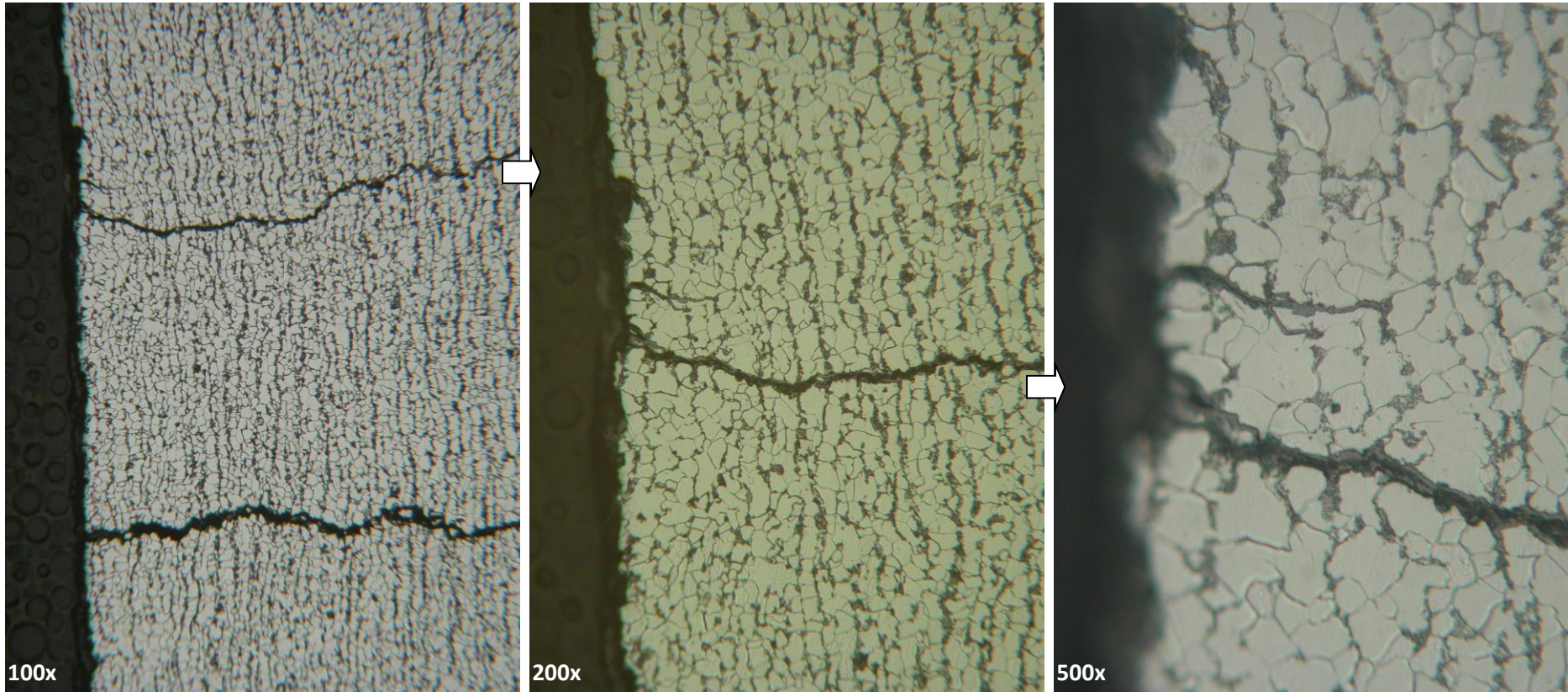
Metallographic examination of the fire side cracked tube

**ROOT CAUSE FAILURE ANALYSIS
OF CRACKED CAGE SUPERHEATER TUBES
DUE TO CAUSTIC STRESS-CORROSION CRACKING (continued)**



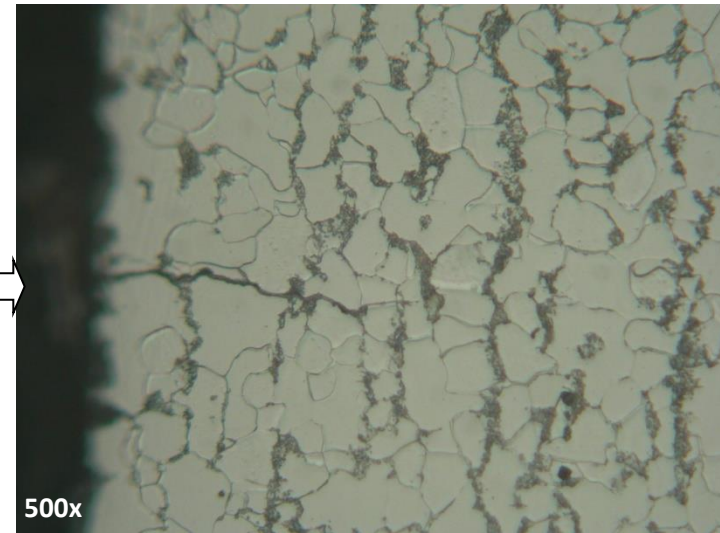
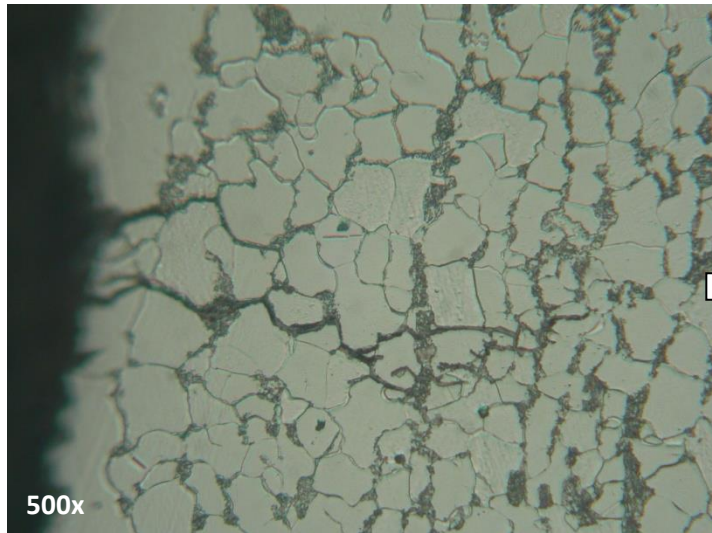
Metallographic examination of the fire side cracked tube

**ROOT CAUSE FAILURE ANALYSIS
OF CRACKED CAGE SUPERHEATER TUBES
DUE TO CAUSTIC STRESS-CORROSION CRACKING (continued)**

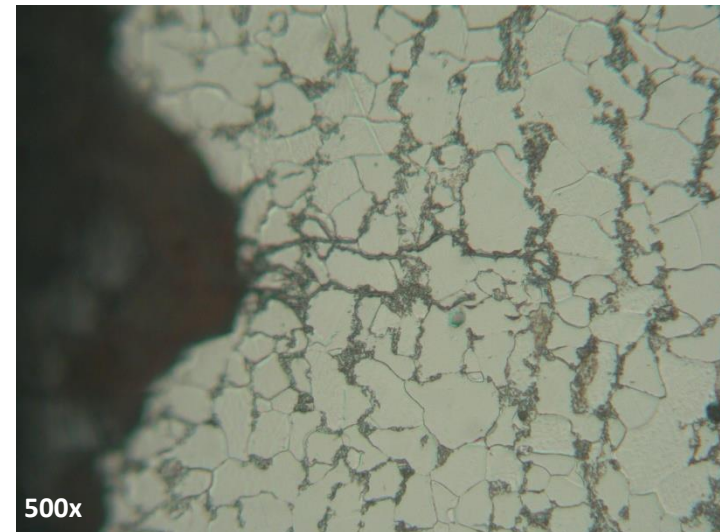


Metallographic examination of the fire side cracked tube

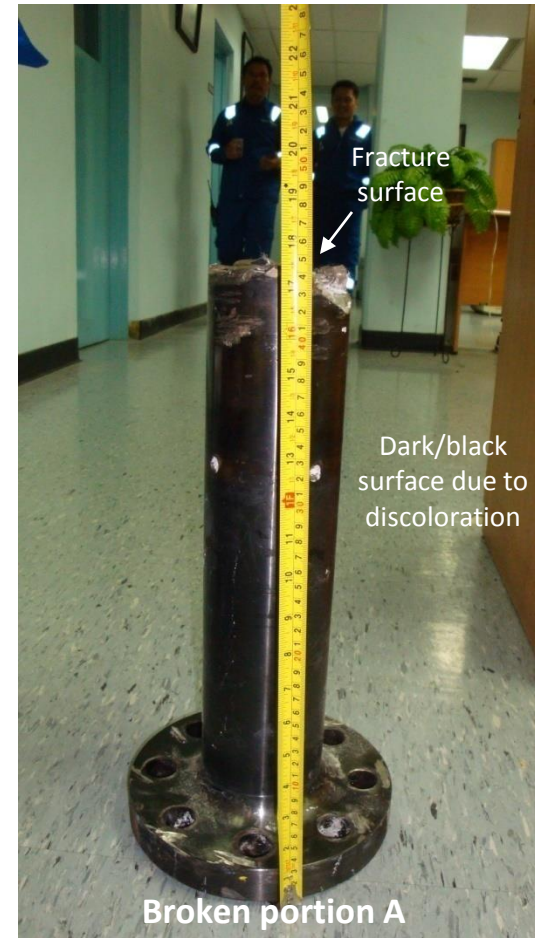
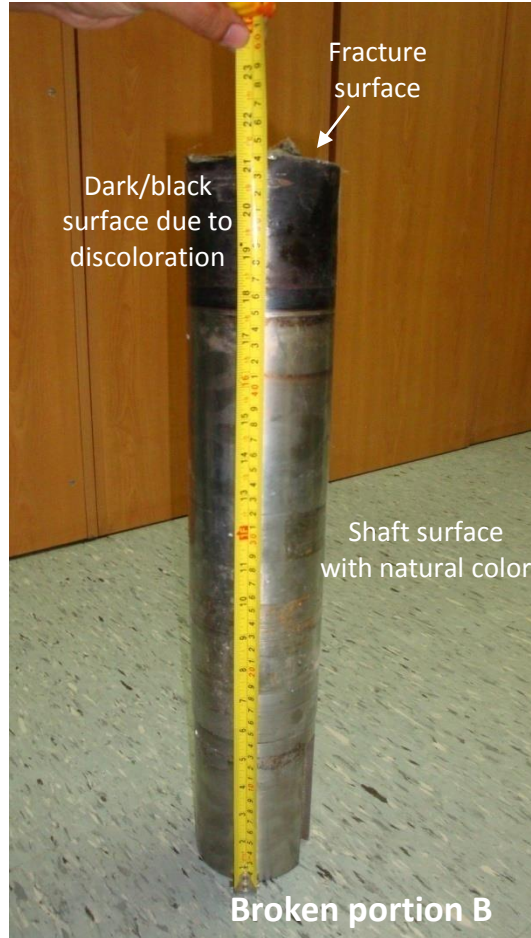
ROOT CAUSE FAILURE ANALYSIS OF CRACKED CAGE SUPERHEATER TUBES DUE TO CAUSTIC STRESS-CORROSION CRACKING (continued)



Metallographic examination
of the fire side cracked tube,
showing intergranular/
interphase SCC



METALLURGICAL FAILURE ANALYSIS OF A BROKEN BEARING SHAFT OF THIRD CRYSTALLIZER DUE TO THERMAL FATIGUE



Photograph of the broken shaft , showing the length of each broken portion A and B of the shaft. Based on these two broken shaft lengths, location of the shaft fracture within the agitator is approximately indicated.

METALLURGICAL FAILURE ANALYSIS OF A BROKEN BEARING SHAFT OF THIRD CRYSTALLIZER DUE TO THERMAL FATIGUE (continued)



Photograph of the section of two broken portions of the bearing shaft at different views. It is clearly seen that most of the shaft outer surface located around the fracture surface were severely damaged due to some rubbing or galling.



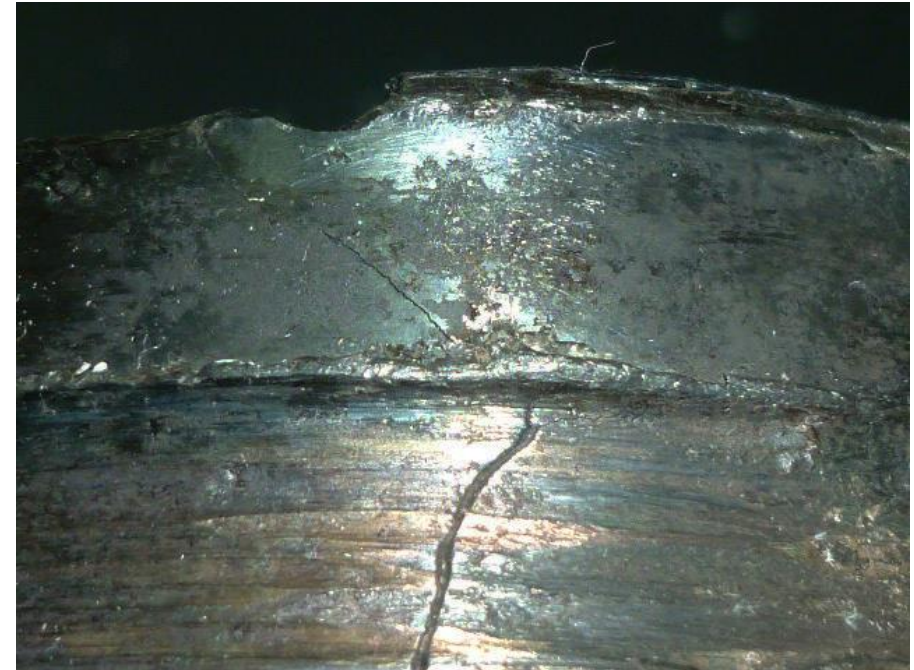
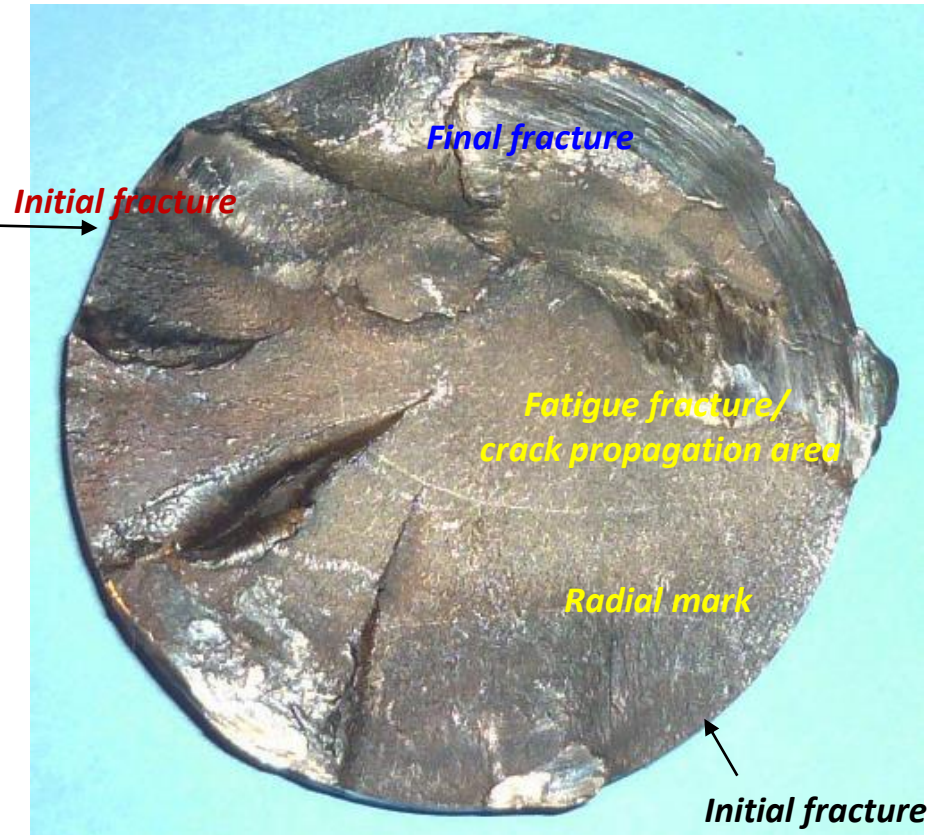
METALLURGICAL FAILURE ANALYSIS OF A BROKEN BEARING SHAFT OF THIRD CRYSTALLIZER DUE TO THERMAL FATIGUE (continued)



Close up views of fracture surface of the broken shaft, showing typical fatigue fracture mode.

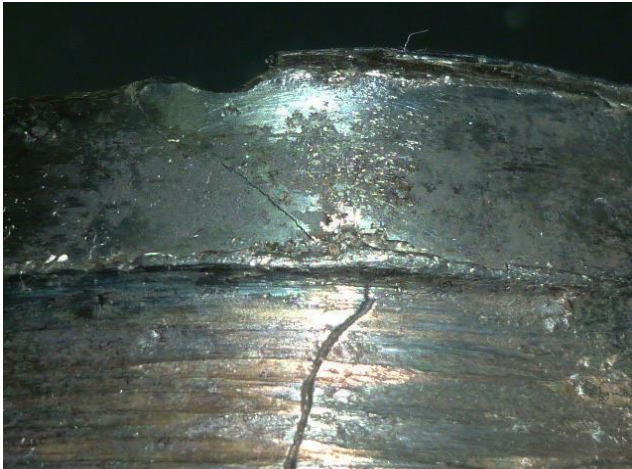
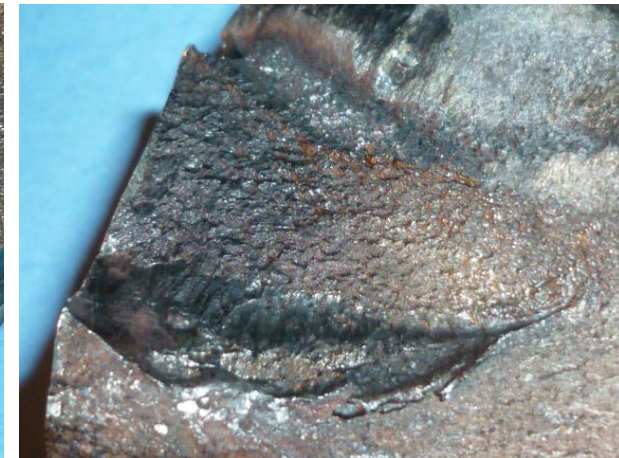
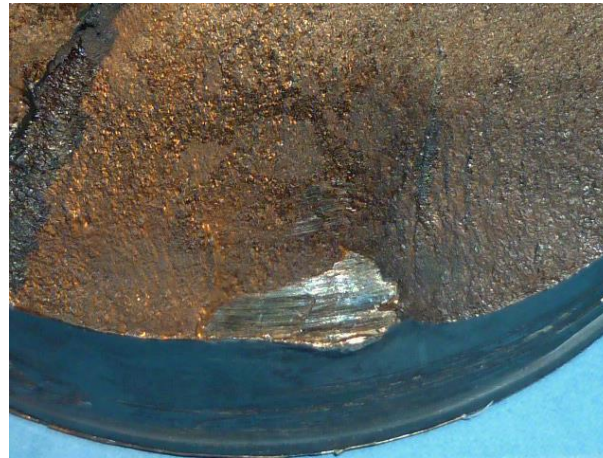


METALLURGICAL FAILURE ANALYSIS OF A BROKEN BEARING SHAFT OF THIRD CRYSTALLIZER DUE TO THERMAL FATIGUE (continued)



Close up view of fatigue fracture surface of the broken shaft, showing the multiple fatigue crack initiation sites, crack propagation area and final fracture area. Also indicated that most the outer surface of the broken shaft located around the fracture surface were severely damaged due to some rubbing or galling in the event of fracture.

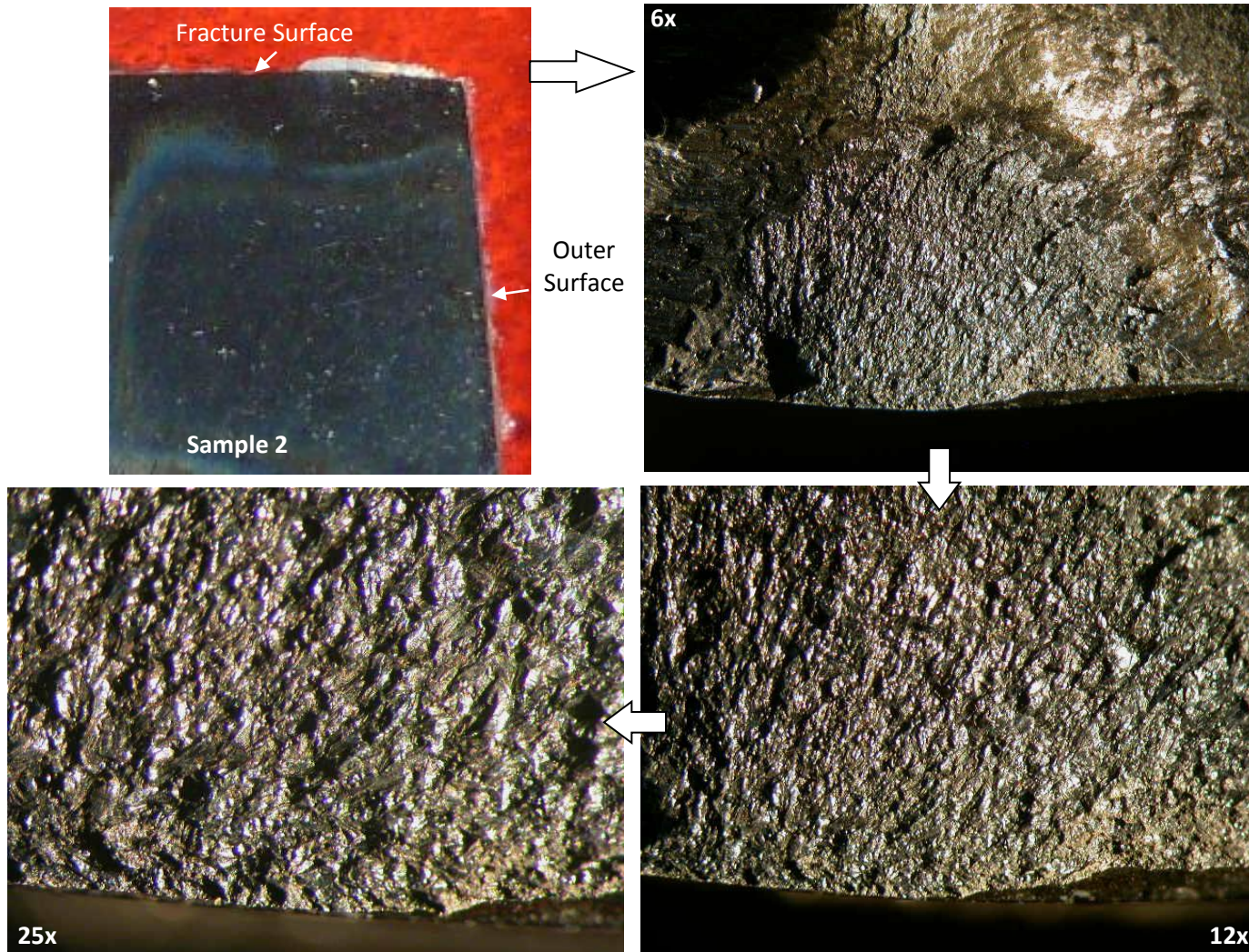
METALLURGICAL FAILURE ANALYSIS OF A BROKEN BEARING SHAFT OF THIRD CRYSTALLIZER DUE TO THERMAL FATIGUE (continued)



Fracture surface of the broken shaft at different locations showing some temper color (dark area).

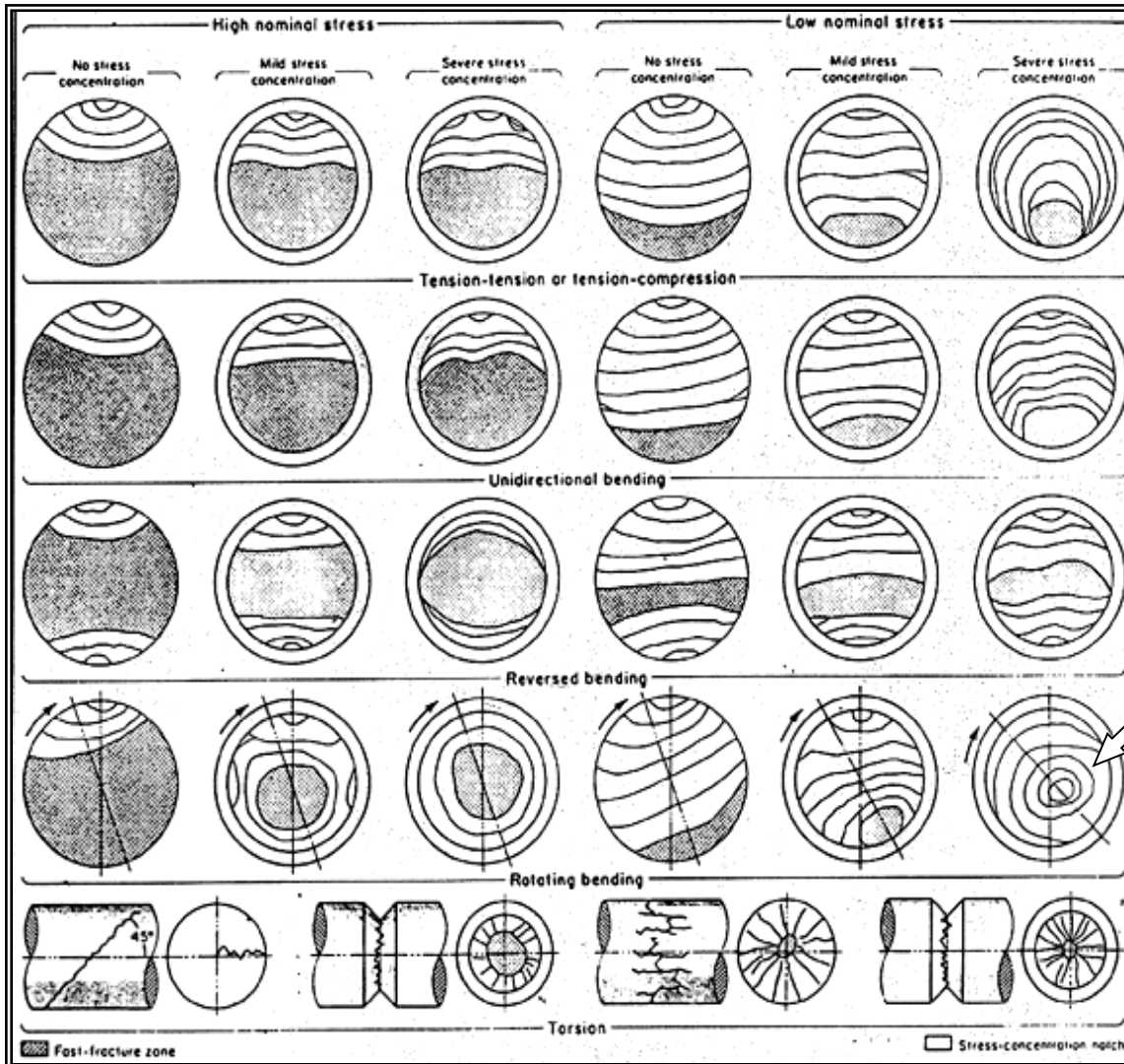


METALLURGICAL FAILURE ANALYSIS OF A BROKEN BEARING SHAFT OF THIRD CRYSTALLIZER DUE TO THERMAL FATIGUE (continued)



Macro-fractograph of fracture surface of sample 2

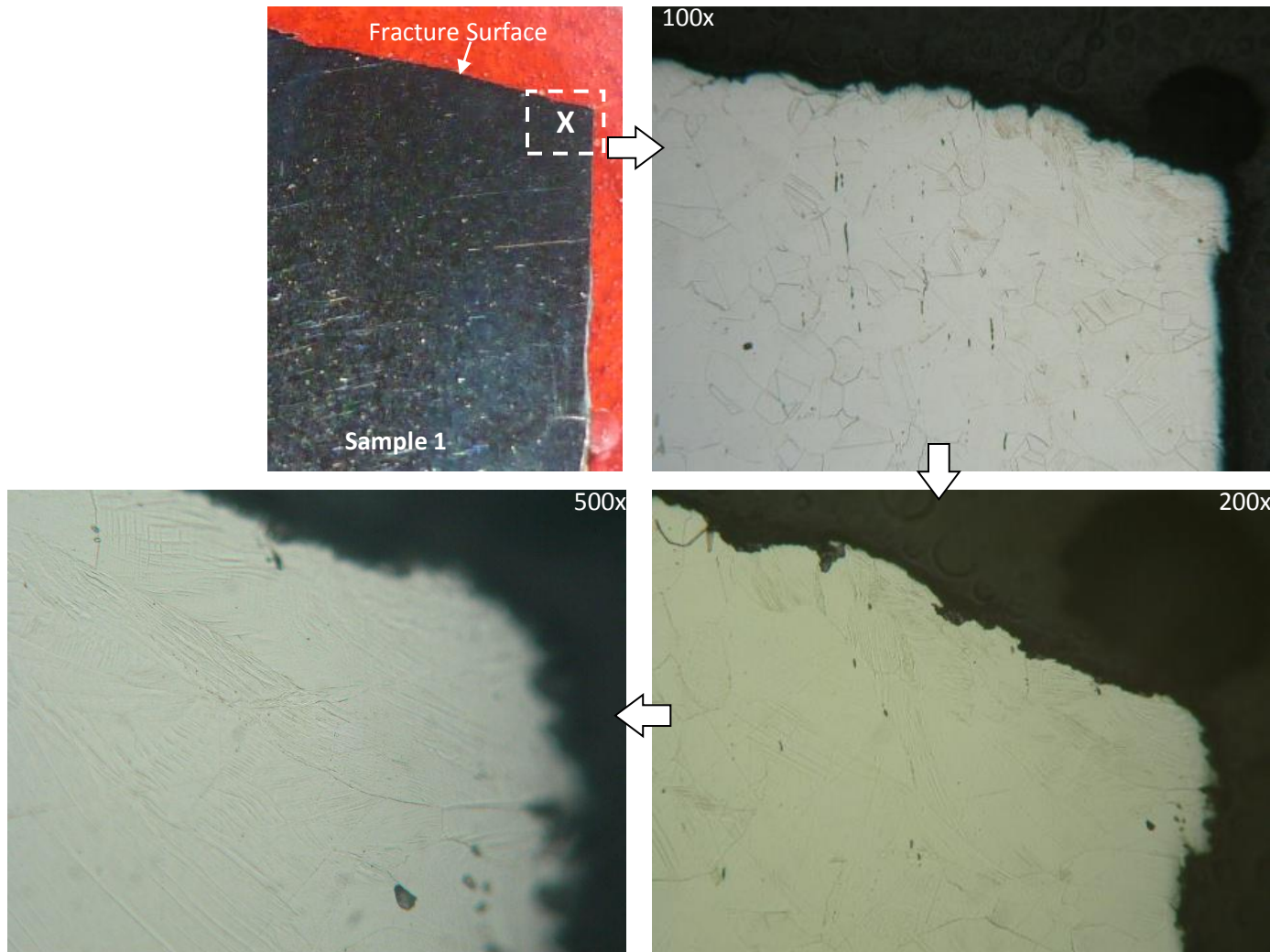
METALLURGICAL FAILURE ANALYSIS OF A BROKEN BEARING SHAFT OF THIRD CRYSTALLIZER DUE TO THERMAL FATIGUE (continued)



Schematic of marks on surfaces of fatigue fractures produced in smooth and notched components with round cross section under various loading conditions at high and low nominal stress.

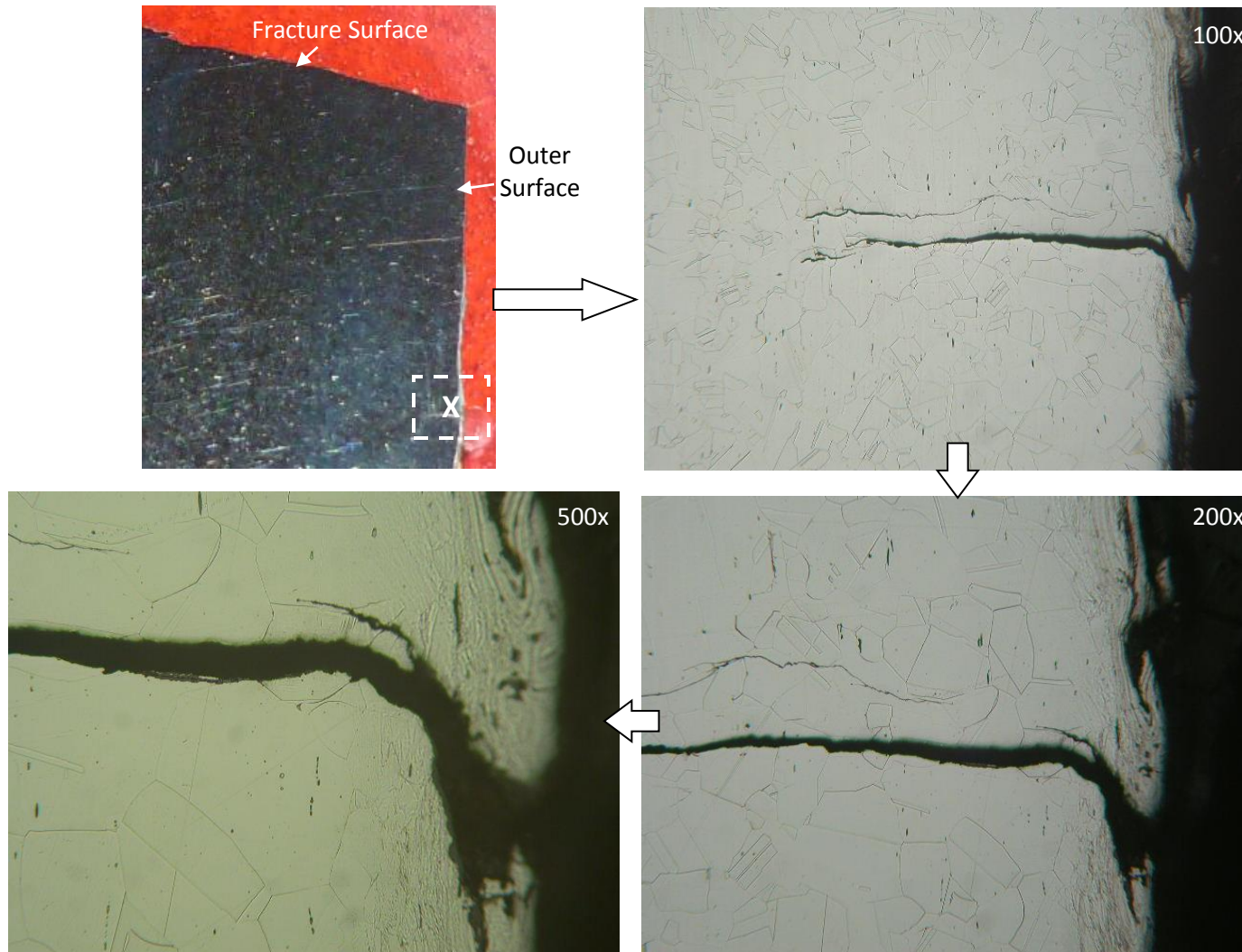
Similar fracture surface as observed from the broken bearing shaft.

METALLURGICAL FAILURE ANALYSIS OF A BROKEN BEARING SHAFT OF THIRD CRYSTALLIZER DUE TO THERMAL FATIGUE (continued)



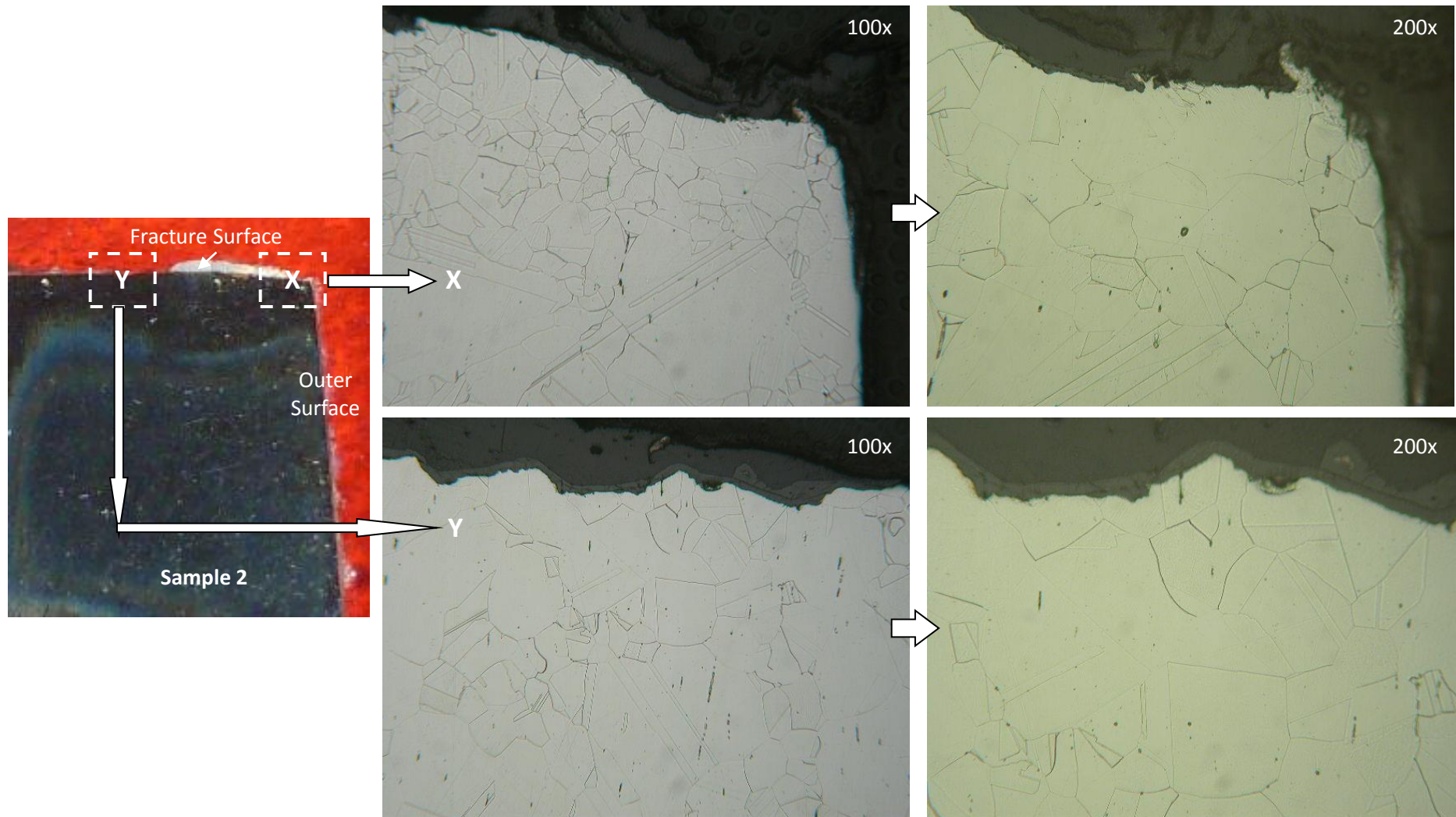
Microstructures obtained from sample 1 at location as indicated by X.

METALLURGICAL FAILURE ANALYSIS OF A BROKEN BEARING SHAFT OF THIRD CRYSTALLIZER DUE TO THERMAL FATIGUE (continued)



Microstructures obtained from sample 1 at location as indicated by X.

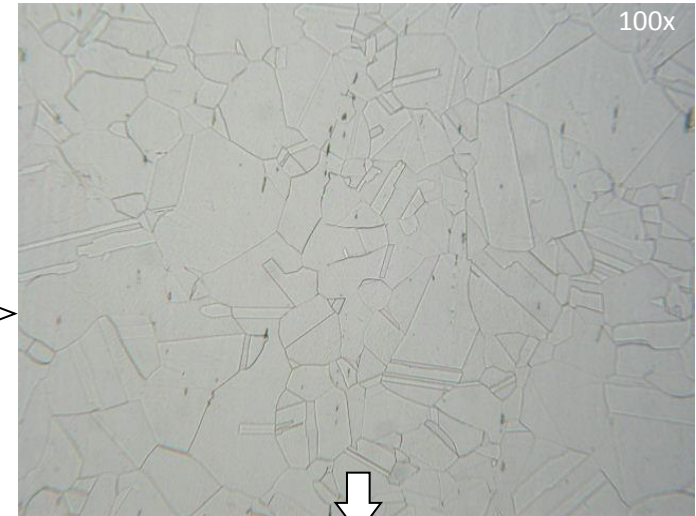
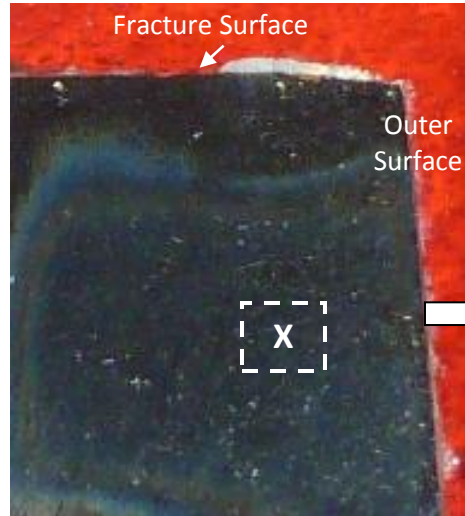
METALLURGICAL FAILURE ANALYSIS OF A BROKEN BEARING SHAFT OF THIRD CRYSTALLIZER DUE TO THERMAL FATIGUE (continued)



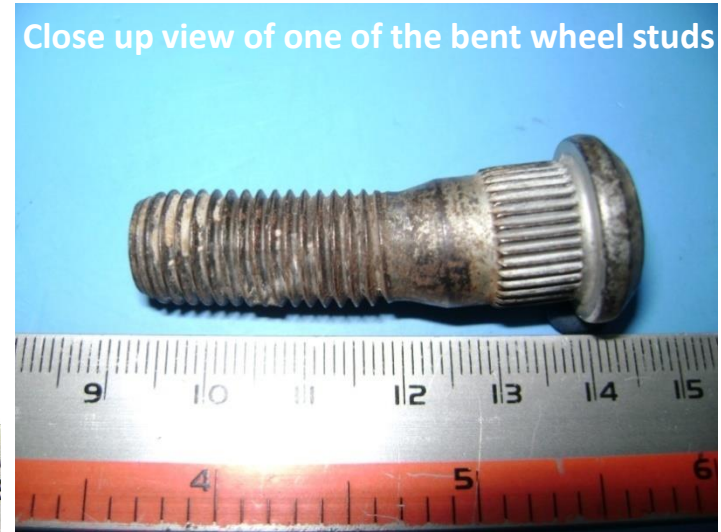
Microstructures obtained from sample 2 at locations as indicated by X and Y.

METALLURGICAL FAILURE ANALYSIS OF A BROKEN BEARING SHAFT OF THIRD CRYSTALLIZER DUE TO THERMAL FATIGUE (continued)

Microstructures obtained from sample 2 at location as indicated by X.



ROOT CAUSE FAILURE ANALYSIS OF DAMAGED WHEEL STUDS AND NUTS OF LIGHT VEHICLES USED IN SUPPORTING A COAL MINE OPERATION



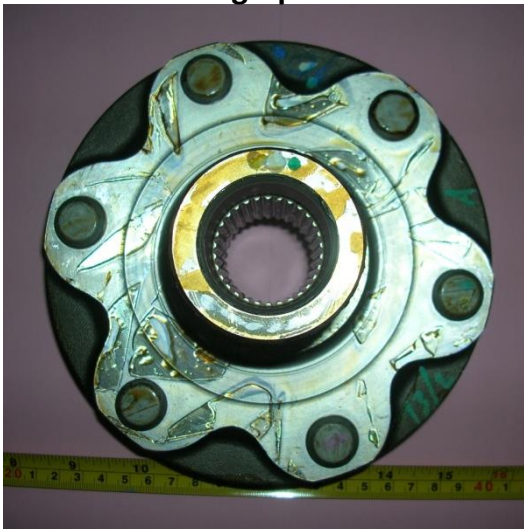
As received samples A which include one broken wheel stud and one undamaged wheel stud recovered from the front left hand wheel position no. 1 of a light vehicle 4x4 after it had been experiencing an incident. This vehicle had traveled 44675 km before the incident occurred.



ROOT CAUSE FAILURE ANALYSIS OF DAMAGED WHEEL STUDS AND NUTS OF LIGHT VEHICLES USED IN SUPPORTING A COAL MINE OPERATION (continued)



Photograph of wheel hub and studs at different view



The OEM front left hand wheel hub of a light vehicle having six wheel studs and three nuts were also used in the present study of failure analysis. They have been purchased from a Car Dealer in Jakarta.

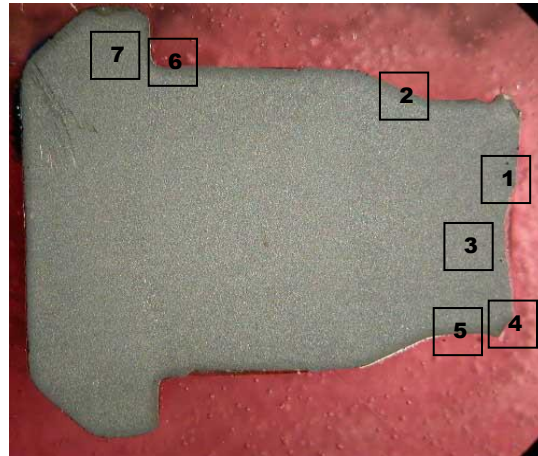
ROOT CAUSE FAILURE ANALYSIS OF DAMAGED WHEEL STUDS AND NUTS OF LIGHT VEHICLES USED IN SUPPORTING A COAL MINE OPERATION (continued)



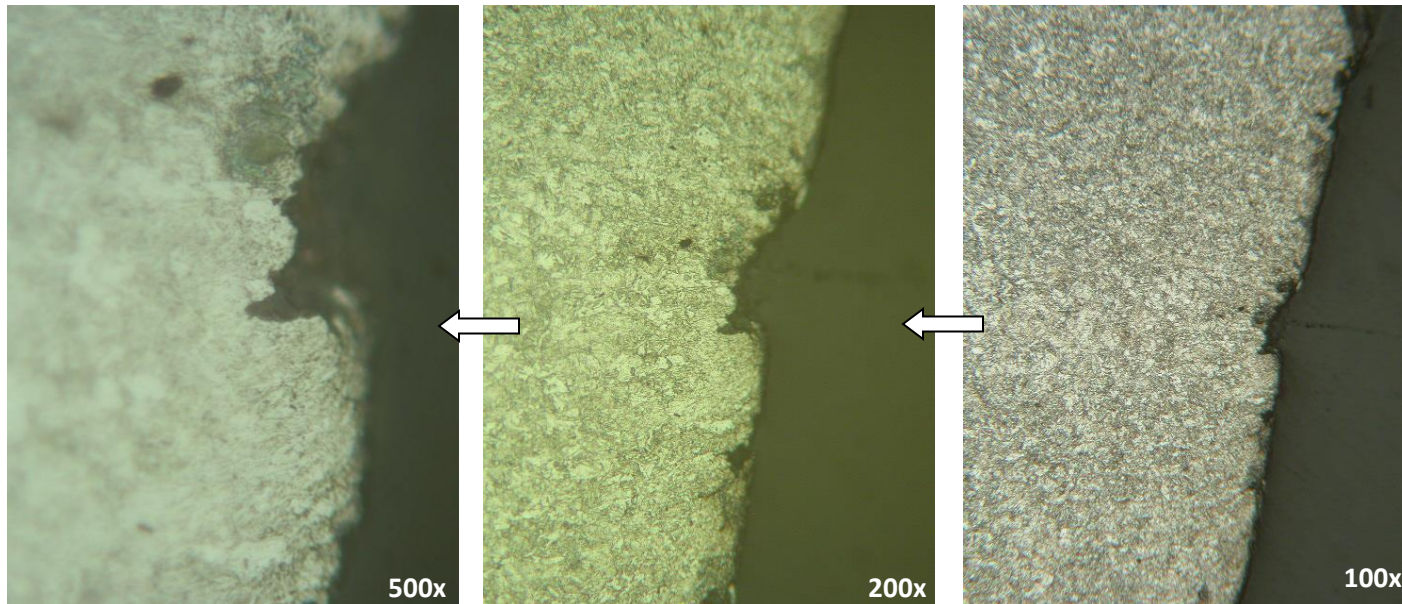
Fracture surface obtained from the broken wheel stud of sample A.



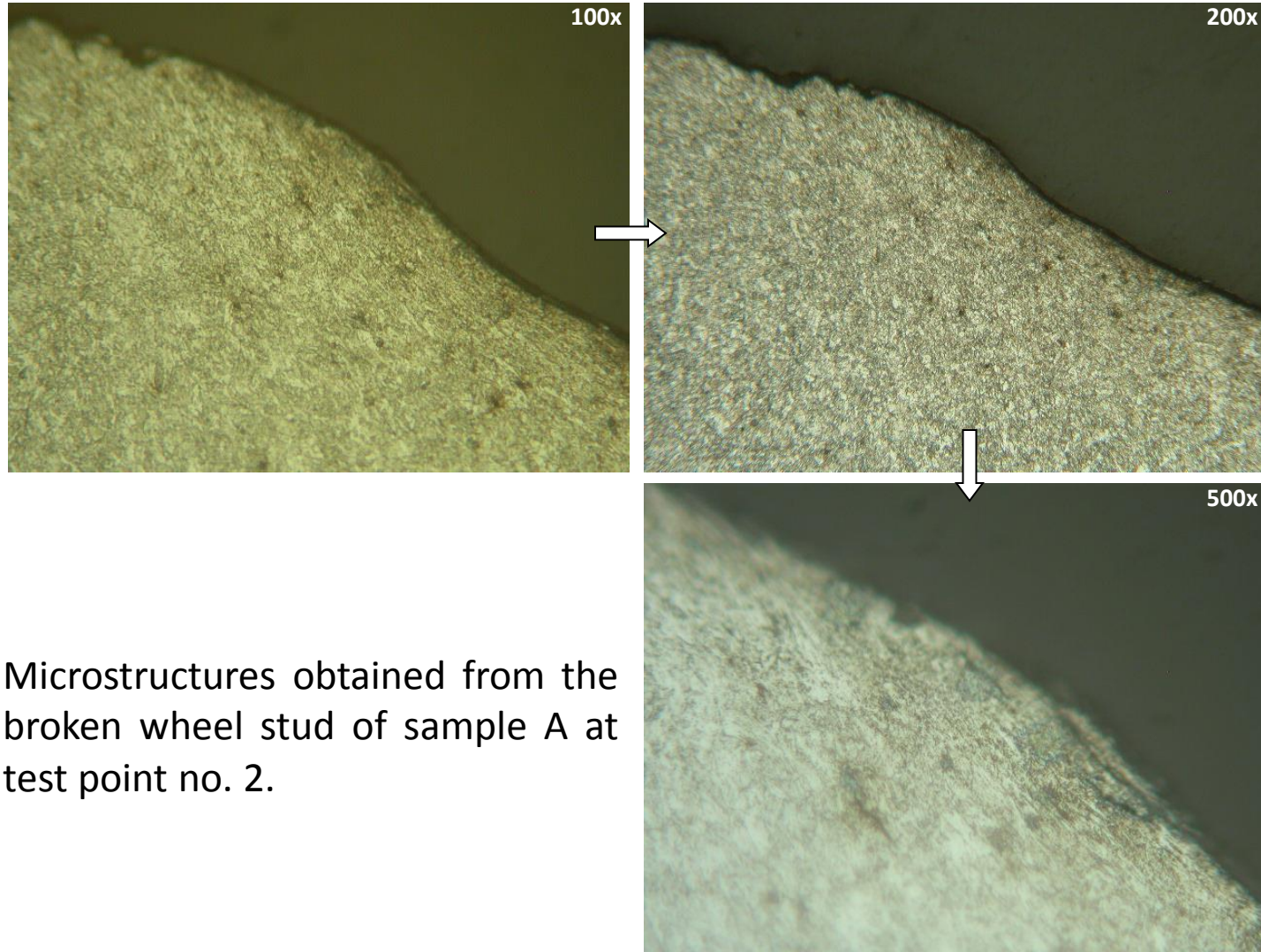
ROOT CAUSE FAILURE ANALYSIS OF DAMAGED WHEEL STUDS AND NUTS OF LIGHT VEHICLES USED IN SUPPORTING A COAL MINE OPERATION (continued)



Microstructures obtained from the broken wheel stud of sample A at test point no. 1.

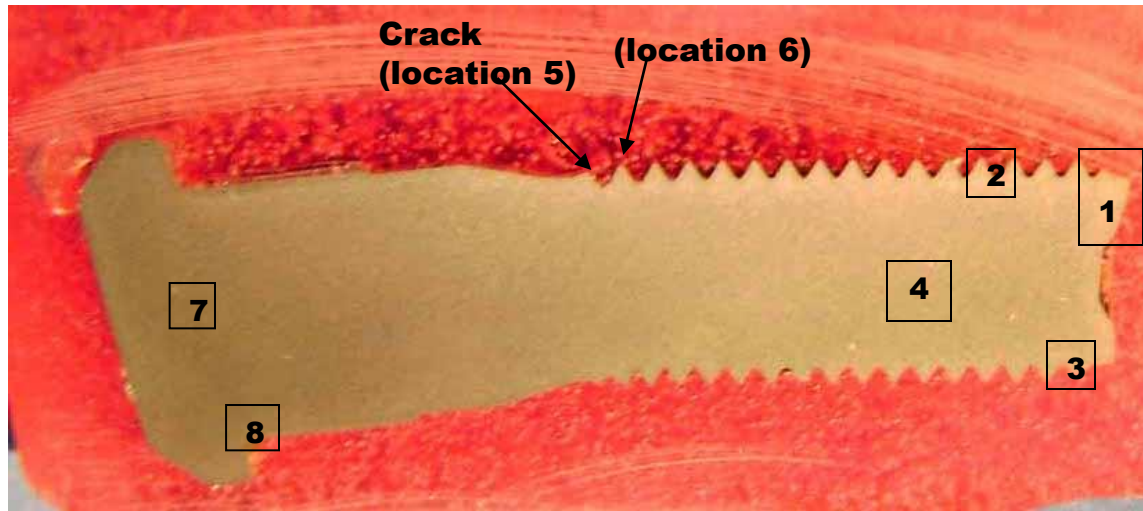


ROOT CAUSE FAILURE ANALYSIS OF DAMAGED WHEEL STUDS AND NUTS OF LIGHT VEHICLES USED IN SUPPORTING A COAL MINE OPERATION (continued)



Microstructures obtained from the broken wheel stud of sample A at test point no. 2.

ROOT CAUSE FAILURE ANALYSIS OF DAMAGED WHEEL STUDS AND NUTS OF LIGHT VEHICLES USED IN SUPPORTING A COAL MINE OPERATION (continued)

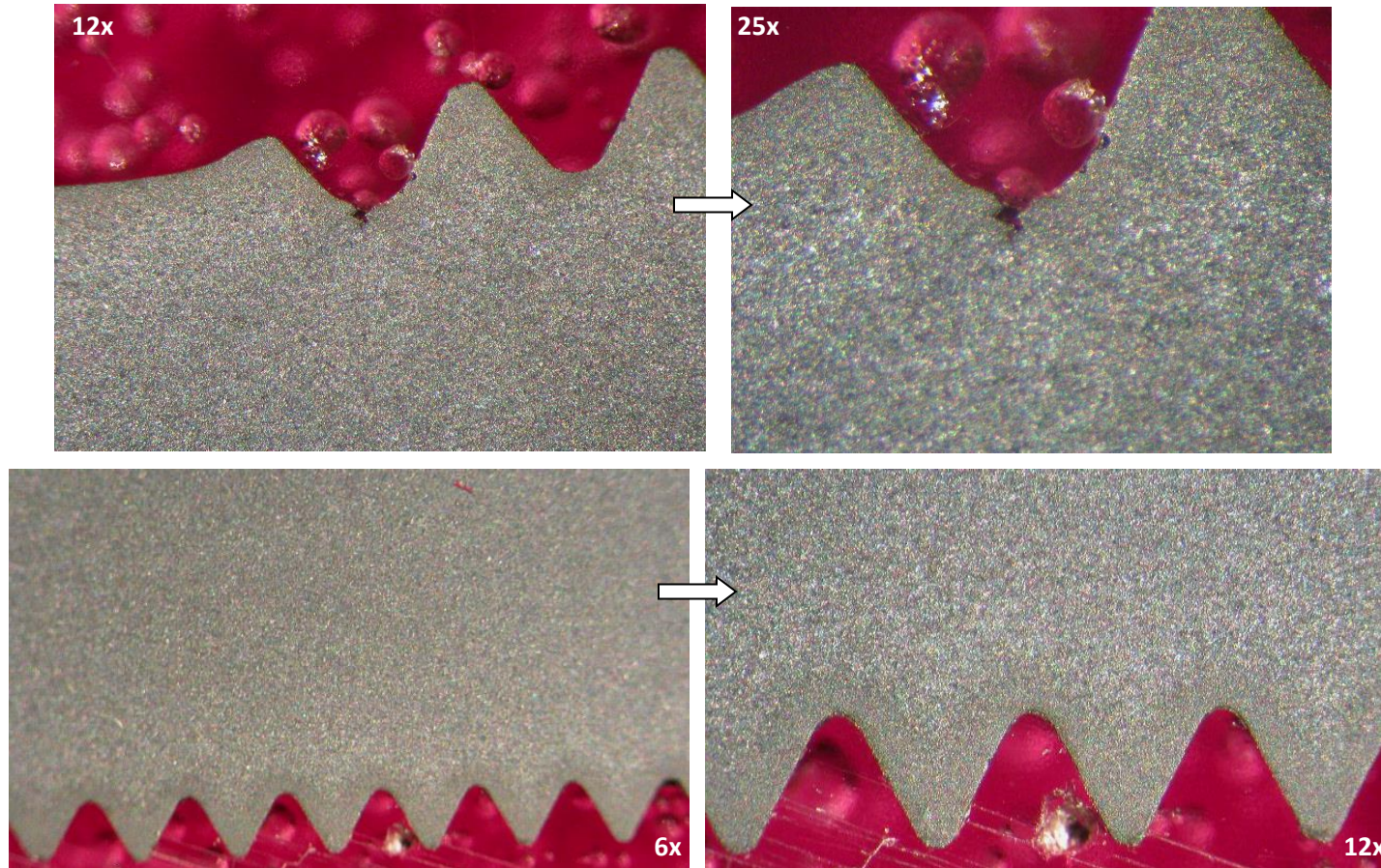


The longitudinal section of the damaged (bent) wheel stud of sample B showing the test points for metallographic examination (test points 1 to 8).

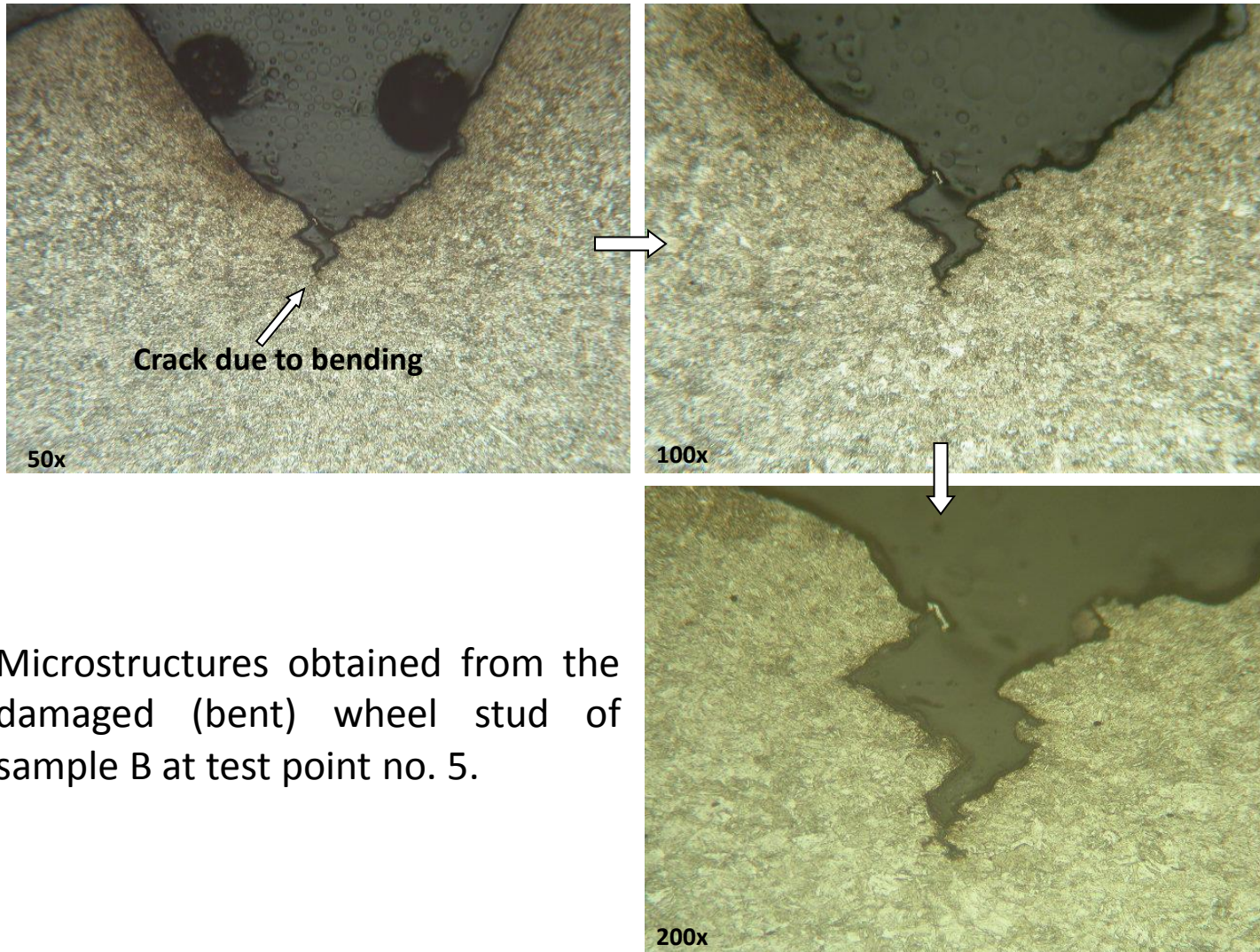


Macrostructures of the longitudinal section of the bent wheel stud of sample B at different locations and magnifications.

ROOT CAUSE FAILURE ANALYSIS OF DAMAGED WHEEL STUDS AND NUTS OF LIGHT VEHICLES USED IN SUPPORTING A COAL MINE OPERATION (continued)



Macrostructures of the longitudinal section of the bent wheel stud of sample B at different locations and magnifications.

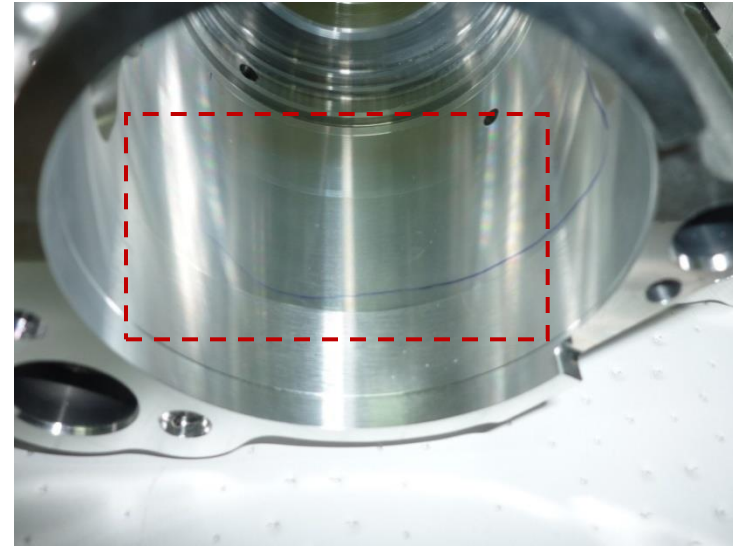
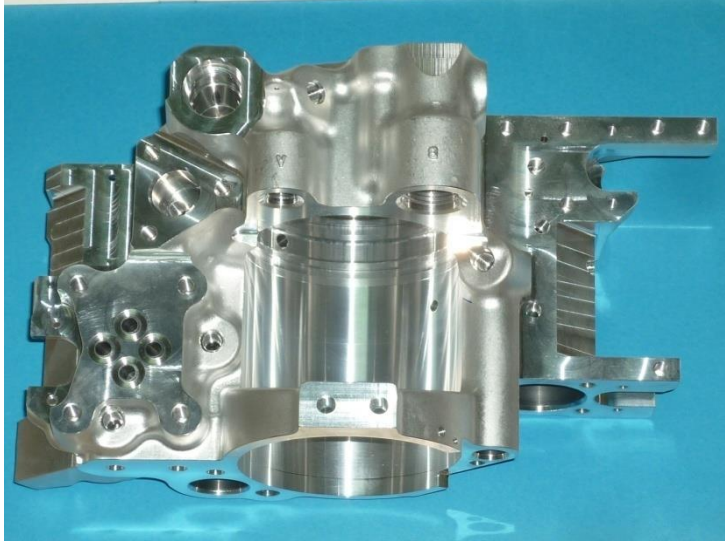


Microstructures obtained from the damaged (bent) wheel stud of sample B at test point no. 5.

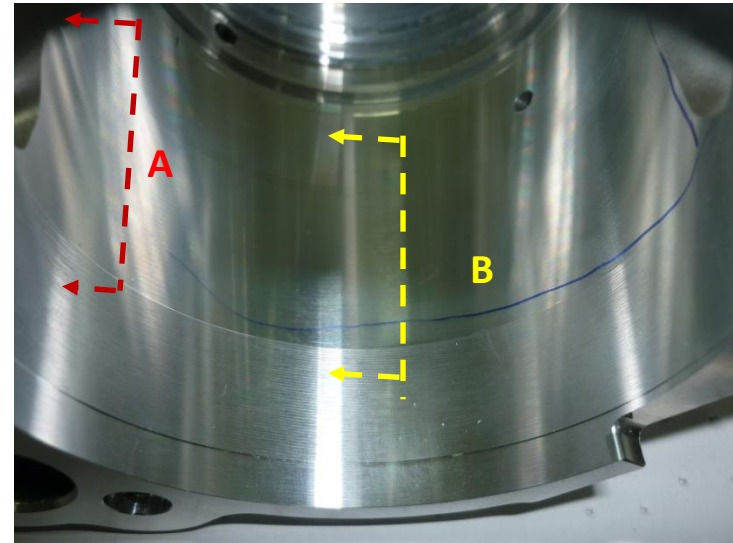
ROOT CAUSE FAILURE ANALYSIS OF A DEFECTIVE MACHINED AL-ALLOY AIRCRAFT AILERON BLOCK



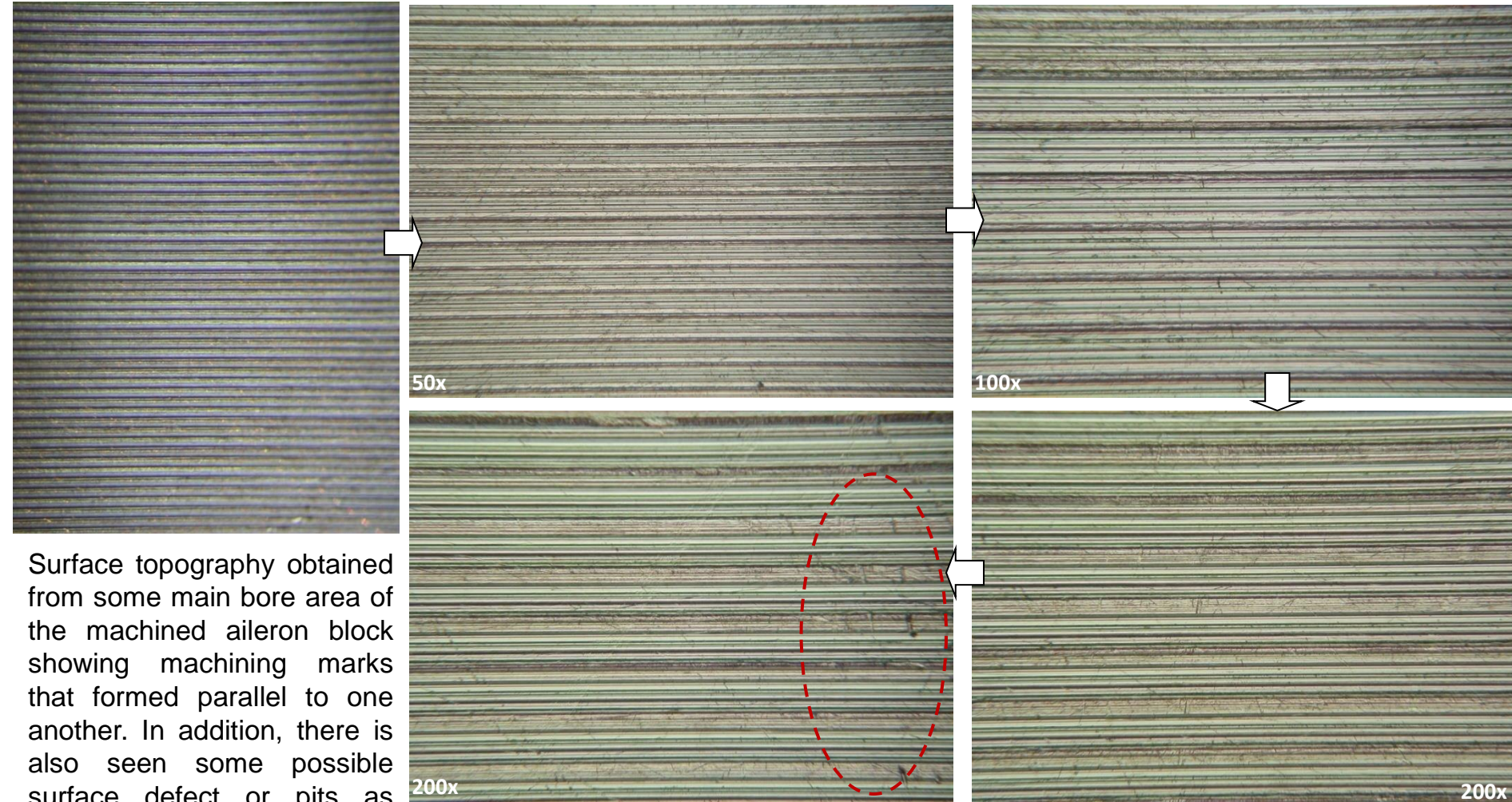
ROOT CAUSE FAILURE ANALYSIS OF A DEFECTIVE MACHINED AL-ALLOY AIRCRAFT AILERON BLOCK (continued)



A number of samples were made from the machined aileron block within its main bore area that had revealed several pits formation for laboratory examination. For metallographic examination, specimens A and B were also cut away in transverse direction.

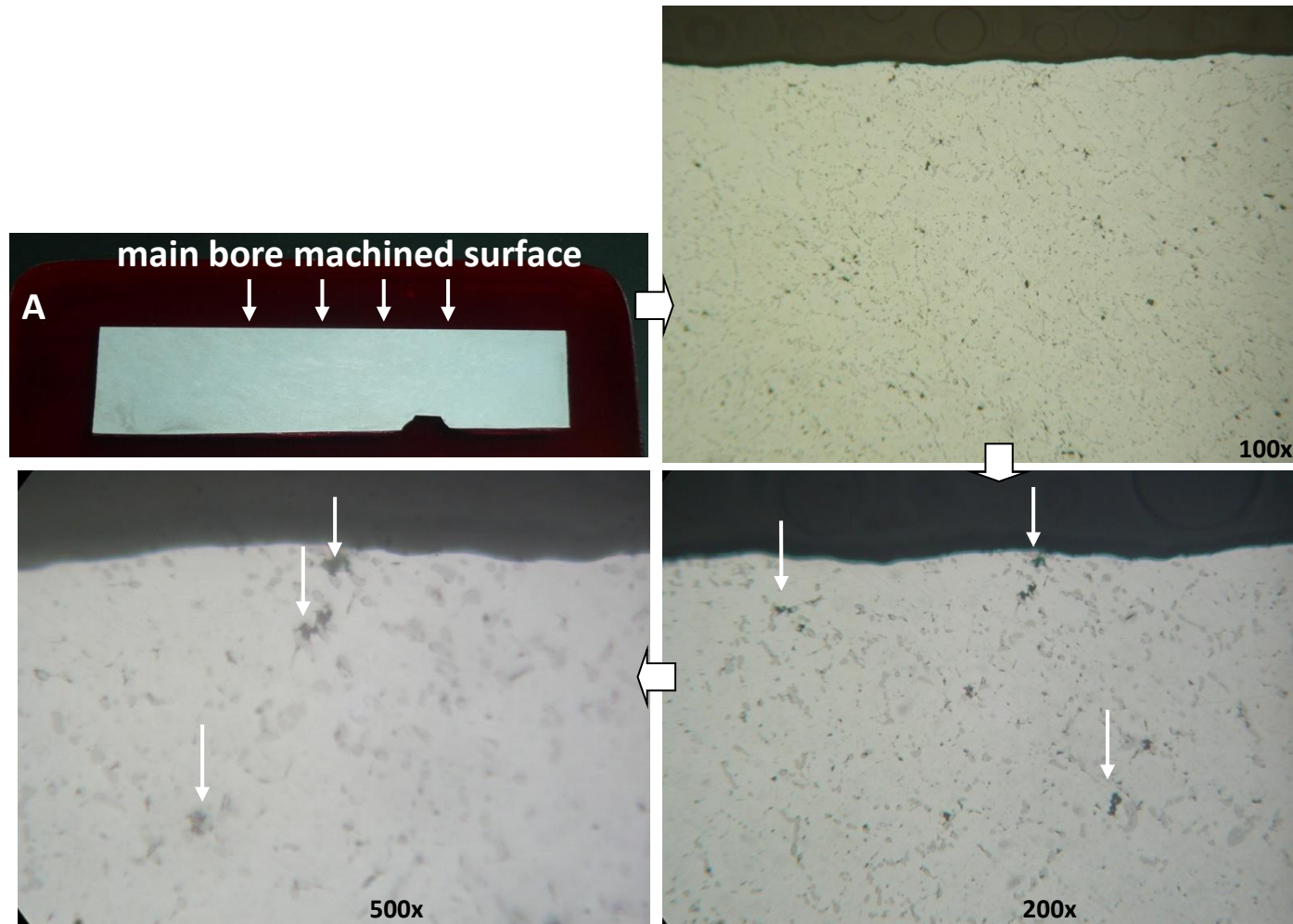


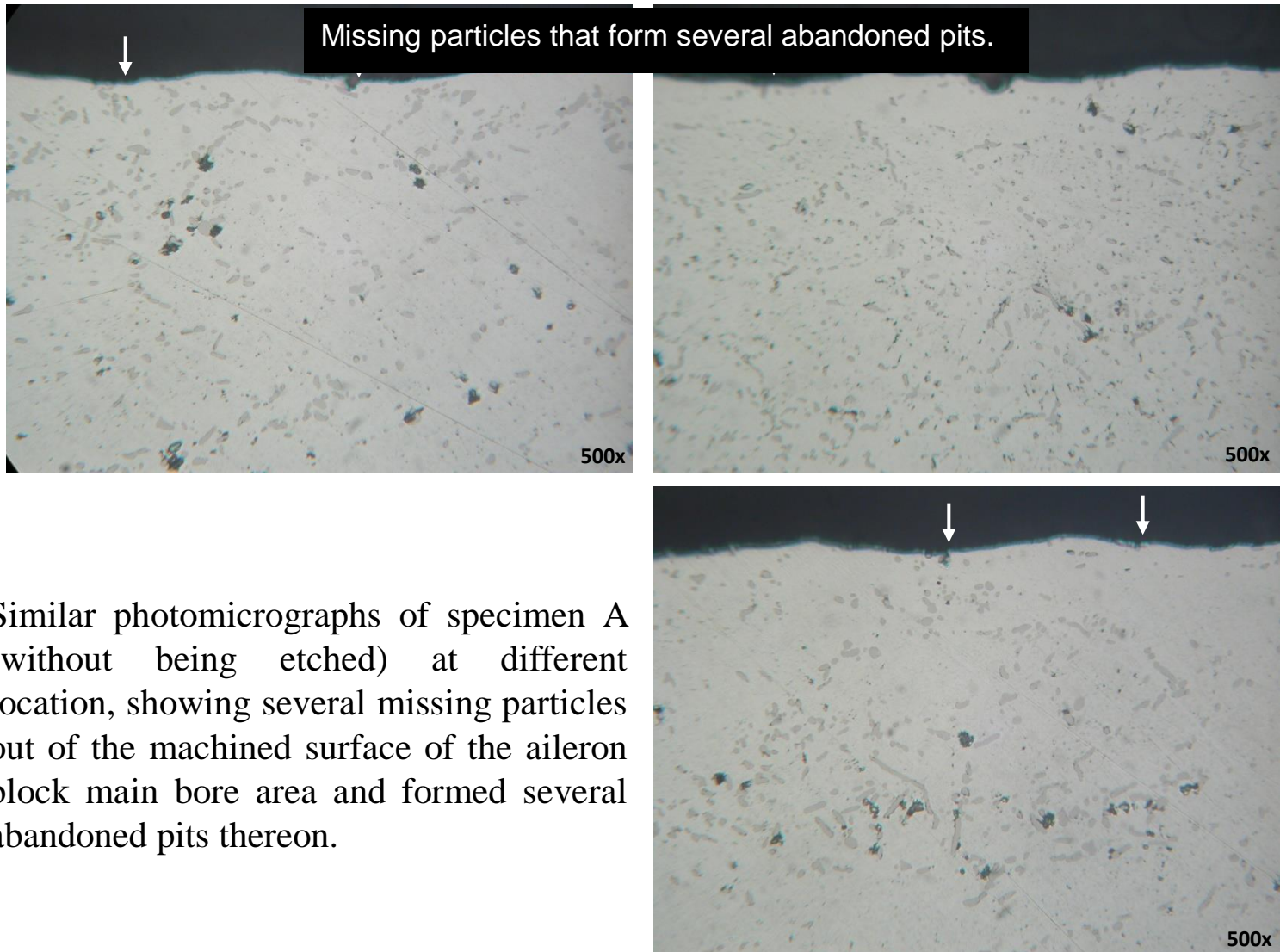
ROOT CAUSE FAILURE ANALYSIS OF A DEFECTIVE MACHINED AL-ALLOY AIRCRAFT AILERON BLOCK (continued)



Surface topography obtained from some main bore area of the machined aileron block showing machining marks that formed parallel to one another. In addition, there is also seen some possible surface defect or pits as indicated.

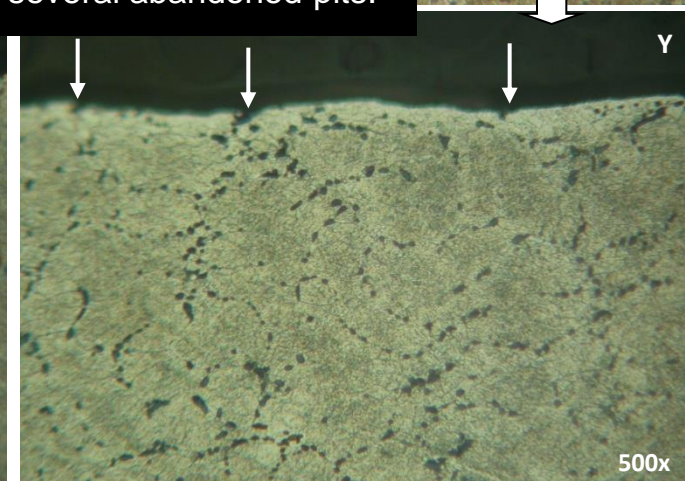
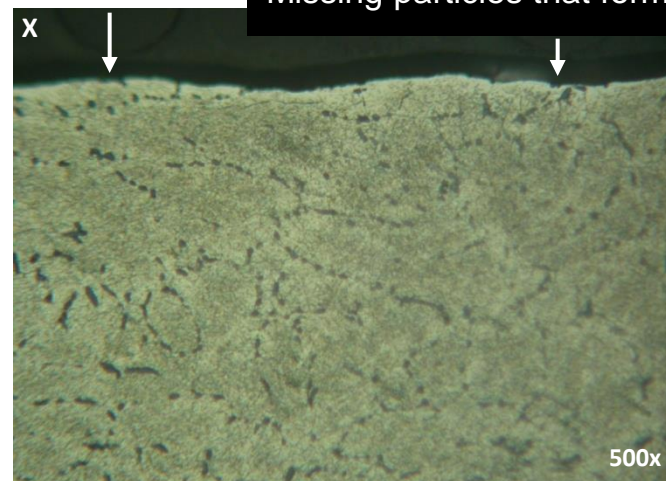
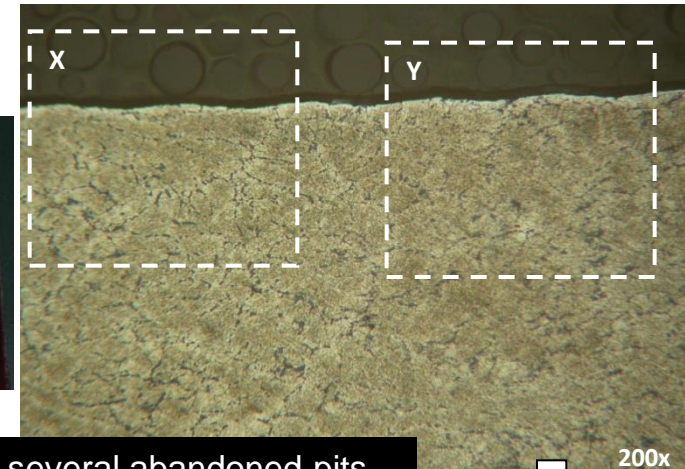
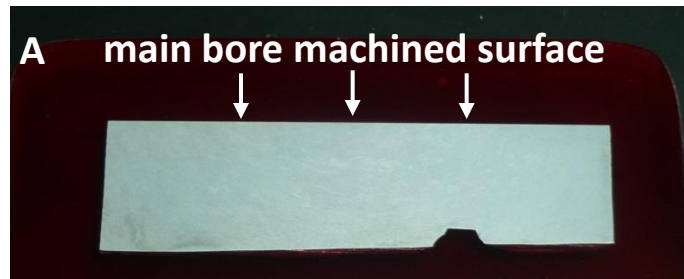
Photomicrographs of unetched specimen A at different magnifications, showing a few black particles and a quite large number of grey particles that formed many islands within the matrix of the aileron block material. In addition, the photomicrographs also exhibit some wavy surface topography which corresponds to the machining marks. Most likely, the black particles as indicated may be associated with some inclusions, while the grey particles are associated with the precipitates that formed on the grain boundaries of the aileron block material.





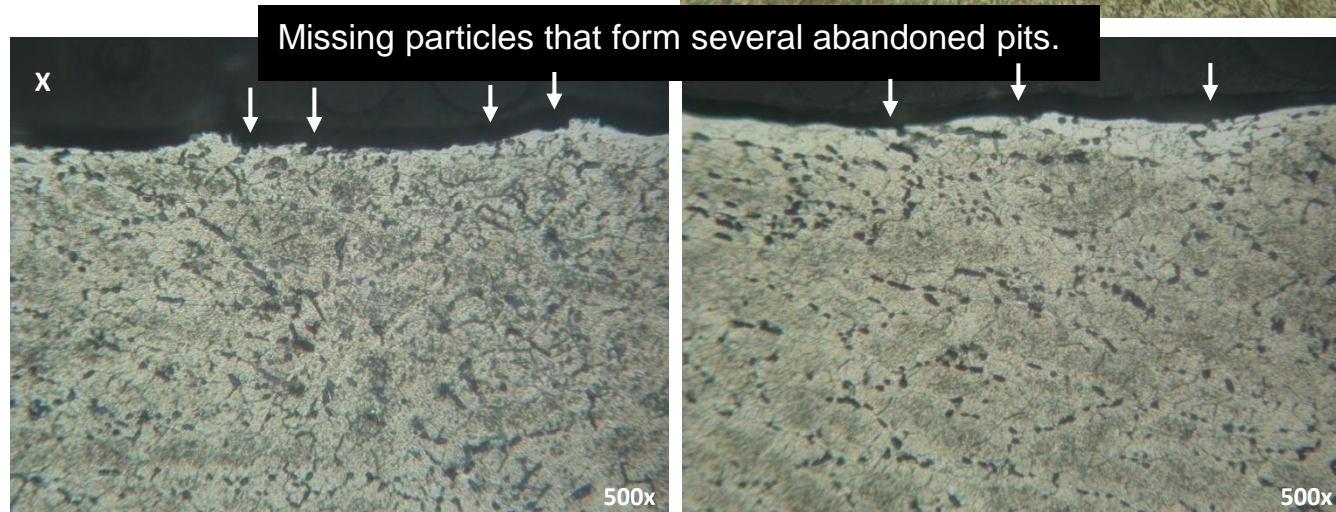
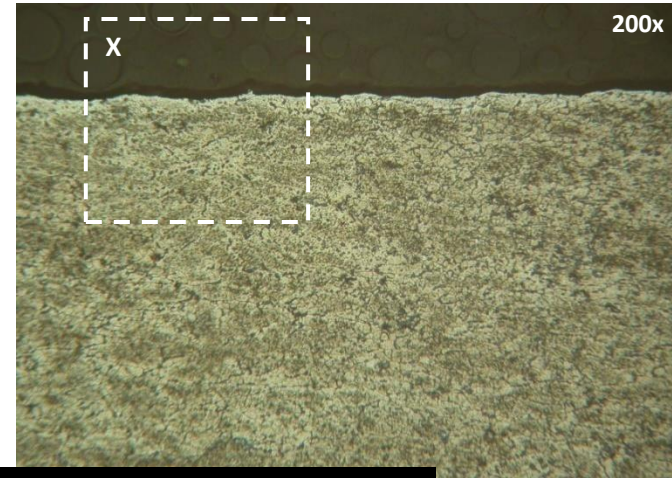
Similar photomicrographs of specimen A (without being etched) at different location, showing several missing particles out of the machined surface of the aileron block main bore area and formed several abandoned pits thereon.

Microstructures obtained from specimen A after being etched at different magnifications, showing typical microstructures of aluminum alloy 2618 containing with several second phase particles or precipitates that formed along the grain boundaries of the aluminum matrix phase. All of these precipitates which were previously appeared in the form of grey color islands in unetched specimen, now they appear black in color after being etched. It is also seen that some precipitates that formed on the machined surface of the aileron block main bore area had left the machined surface and formed some pits.



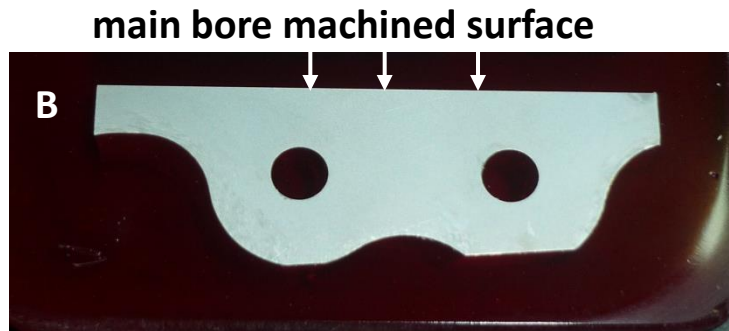
ROOT CAUSE FAILURE ANALYSIS OF A DEFECTIVE MACHINED AL-ALLOY AIRCRAFT AILERON BLOCK (continued)

Microstructures obtained from specimen A after being etched at different magnifications, showing typical of aluminum alloy 2618 containing with several second phase particles or precipitates that formed along the grain boundaries of the aluminum matrix phase. All of these precipitates which were previously appeared in the form of grey color islands in unetched specimen, now they appear black in color after being etched. It is also seen that some precipitates that formed on the machined surface of the aileron block main bore area had left the machined surface and formed several pits.

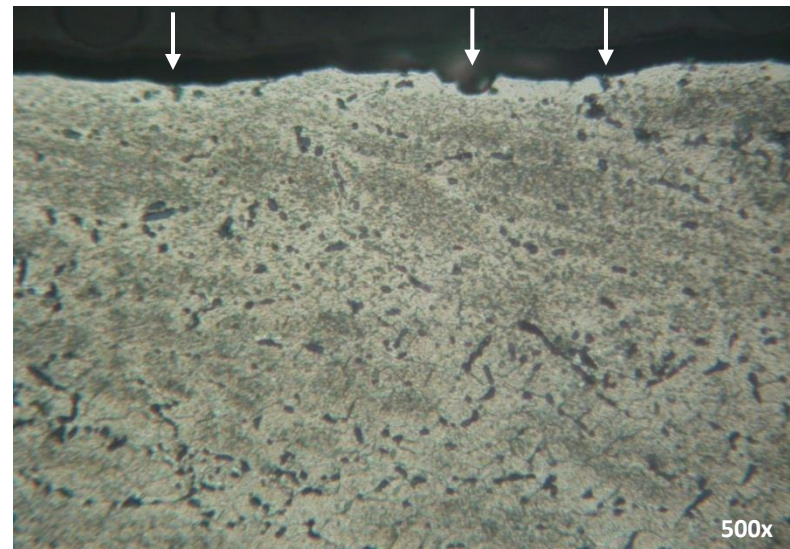
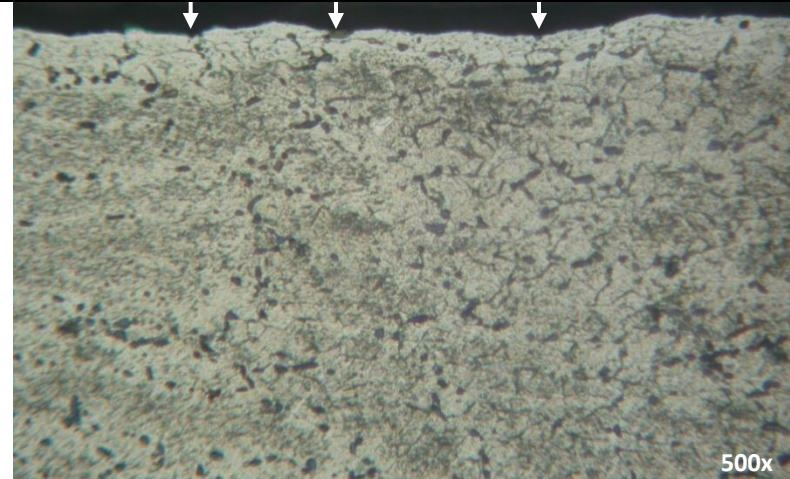


ROOT CAUSE FAILURE ANALYSIS OF A DEFECTIVE MACHINED AL-ALLOY AIRCRAFT AILERON BLOCK (continued)

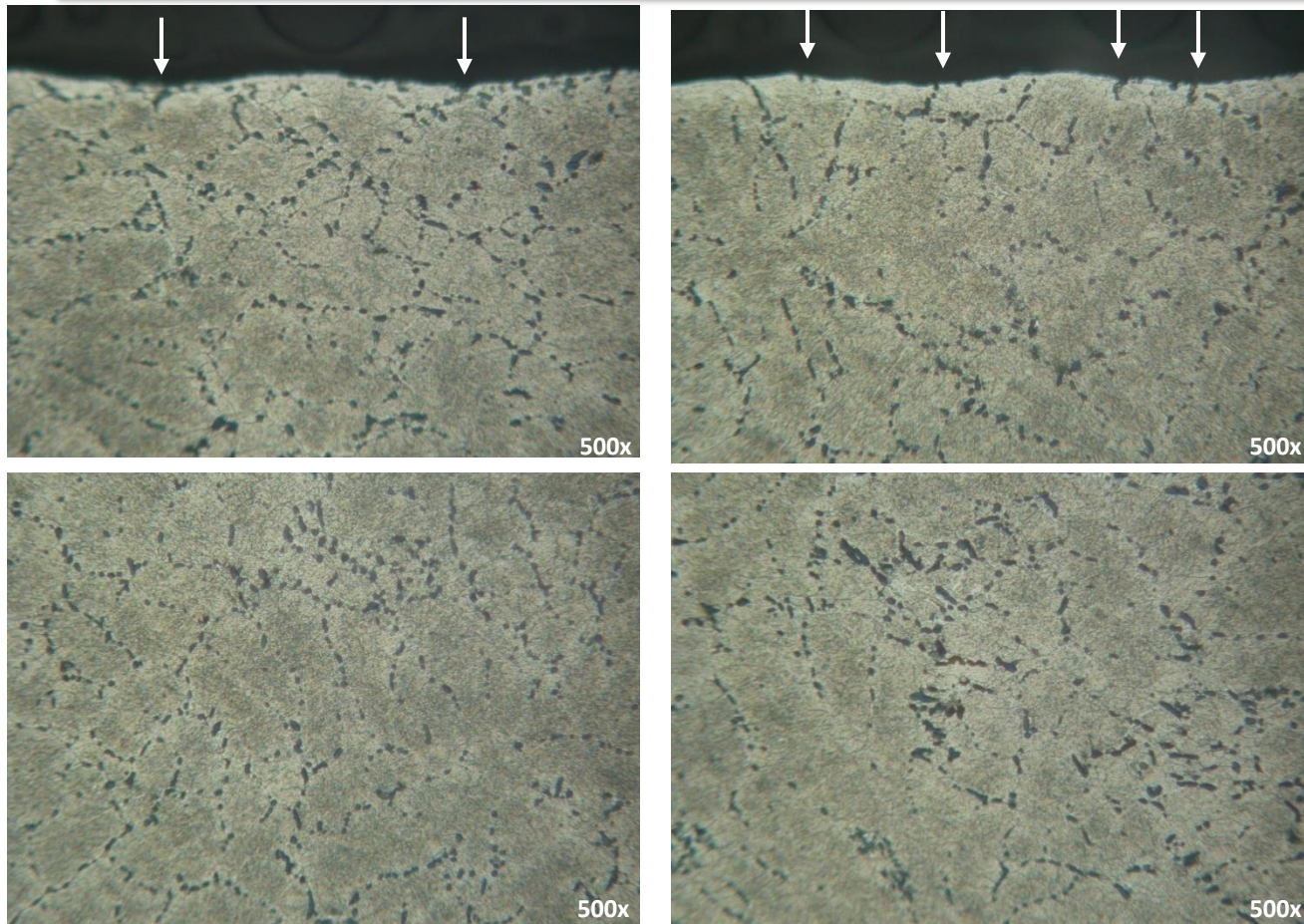
Missing particles that form several abandoned pits.



Microstructures obtained from specimen B after being etched, showing similar microstructures as that obtained from specimen A. All of the grey particles or precipitates that were observed in unetched specimen appeared black and formed islands of second phase particles or precipitates along the grain boundaries of the aluminum alloy 2618 matrix phase. Some of the second phase particles or precipitates that may have formed on the machined surface of the aileron block main bore area may have had left the machined surface to form several abandoned pits.



ROOT CAUSE FAILURE ANALYSIS OF A DEFECTIVE MACHINED AL-ALLOY AIRCRAFT AILERON BLOCK (continued)



Microstructures obtained from specimen B after being etched, showing similar microstructures as that obtained from specimen A. All of the grey particles or precipitates that were observed in unetched specimen appeared black and formed islands of second phase particles or precipitates along the grain boundaries of the aluminum alloy 2618 matrix phase. Some of the second phase particles or precipitates that may have formed on the machined surface of the aileron block main bore area may have had left the machined surface to form several abandoned pits .



Some broken disks that were retained on the fastener of the motor hub ring, the pump hub ring and the spacer pump side.

FAILURE ANALYSIS OF DISK PACK COUPLING (continued)

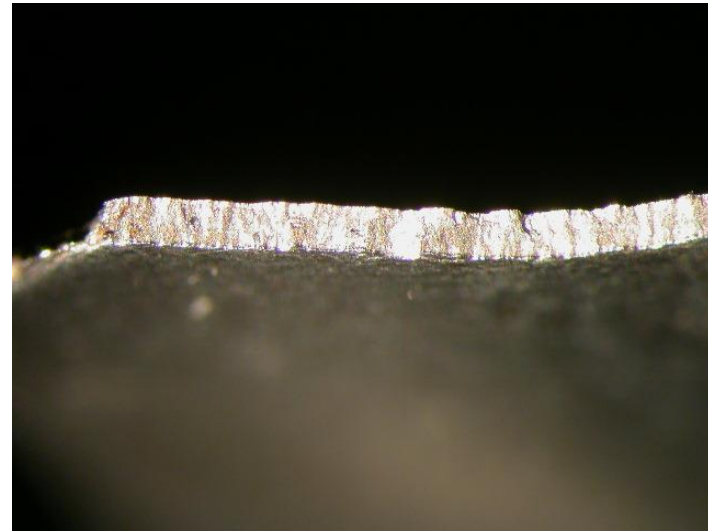
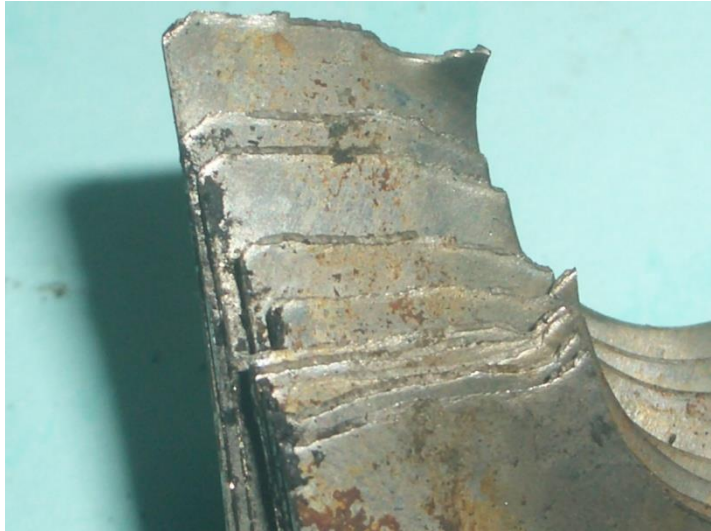


The as received disk pack coupling for failure analysis

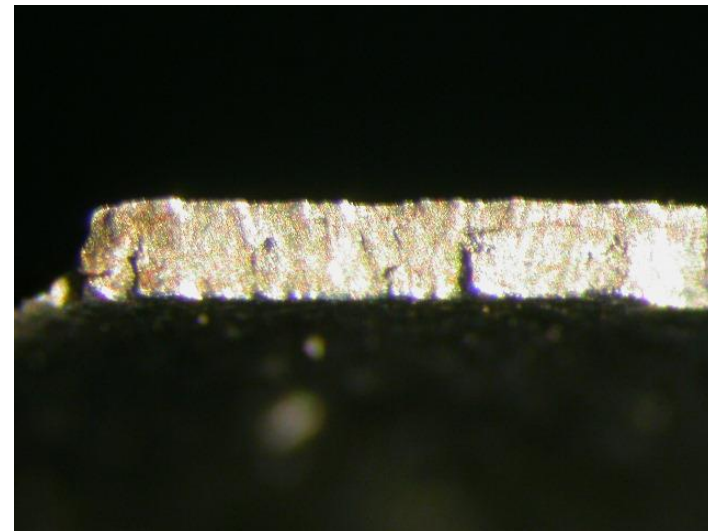
FAILURE ANALYSIS OF DISK PACK COUPLING (continued)



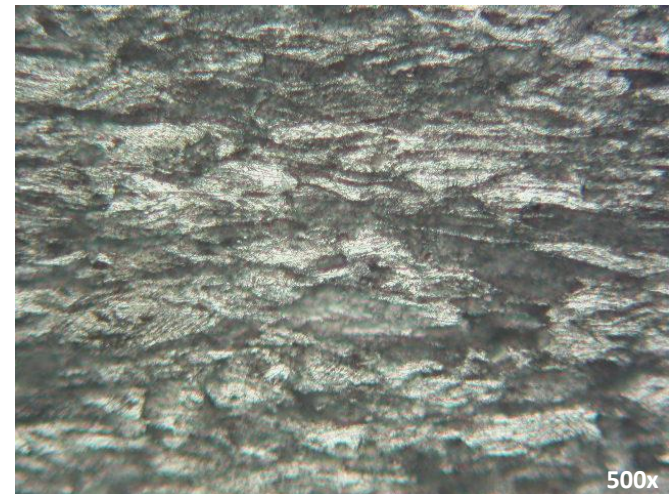
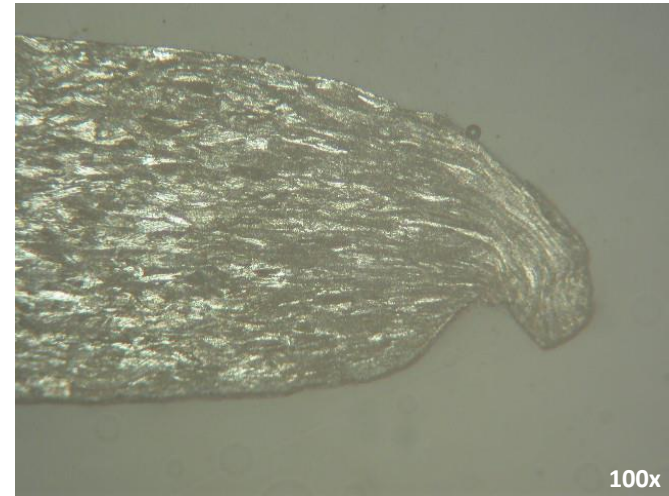
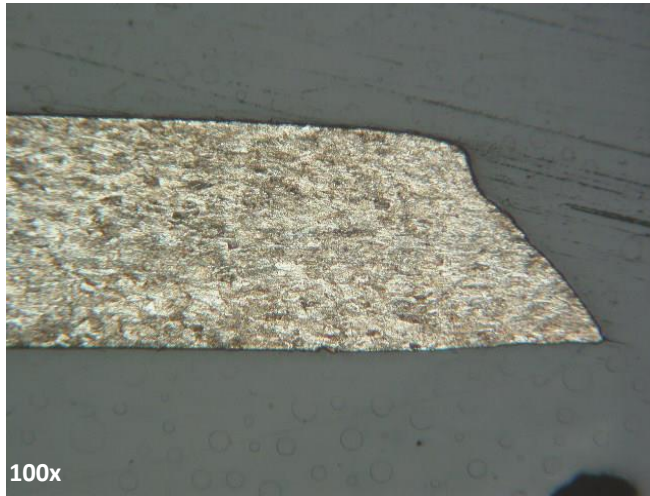
Macroscopic examination of the fracture surface of the broken disks (M Hub Ring A)



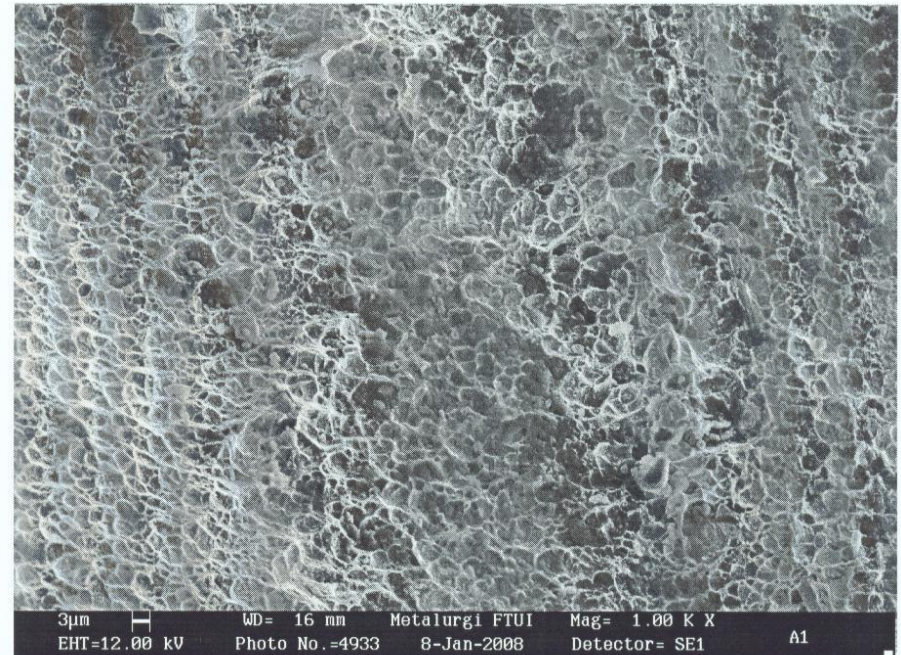
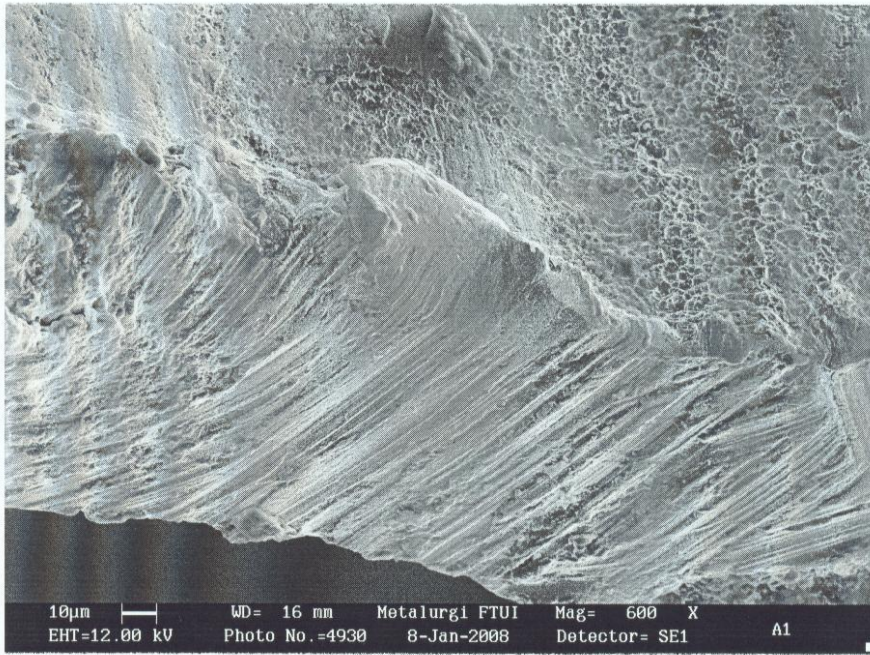
Macroscopic examination of the fracture surface of the broken disks (M Hub Ring A)



FAILURE ANALYSIS OF DISK PACK COUPLING (continued)



Microscopic examination of the cross section of the broken disk M Hub Ring A1



SEM fractograph of some fracture surface of the broken disk M Hub Ring A1

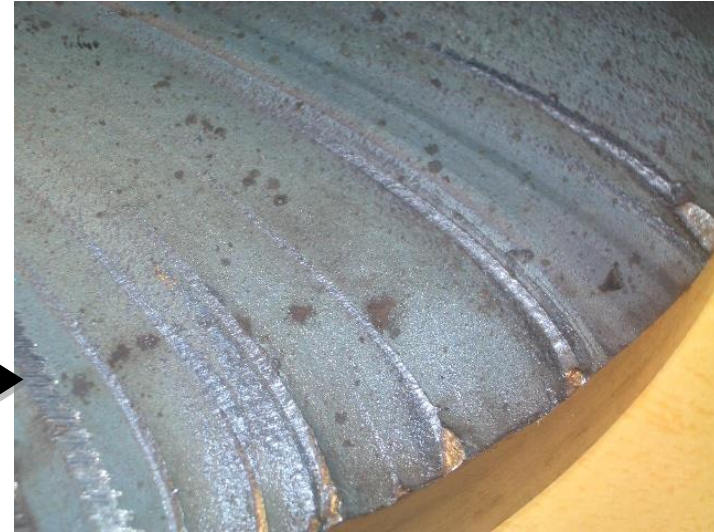
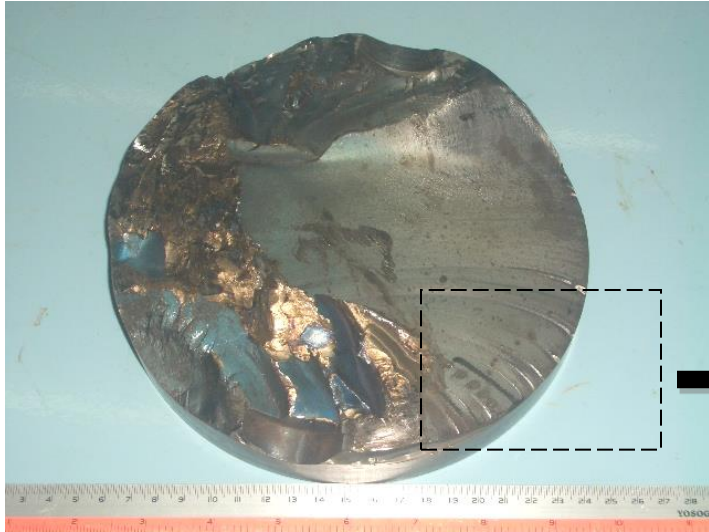
FAILURE ANALYSIS OF AN EXTRUDER GEAR PUMP SHAFT DUE TO FATIGUE



The fracture gear shaft that was photographed at the plant site.



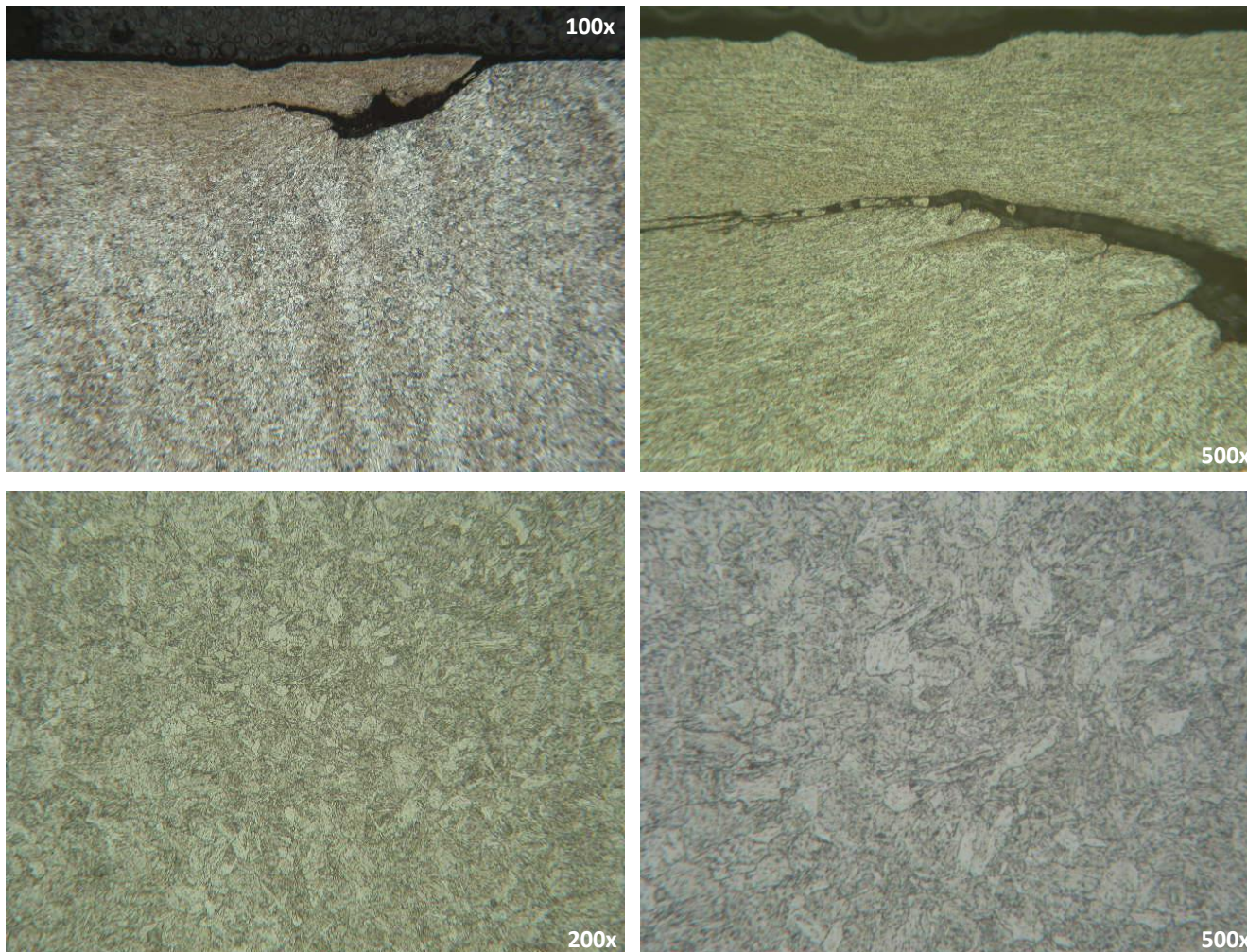
FAILURE ANALYSIS OF AN EXTRUDER GEAR PUMP SHAFT DUE TO FATIGUE (continued)



Close up view of the progressive flat fatigue fracture with curved beach marks

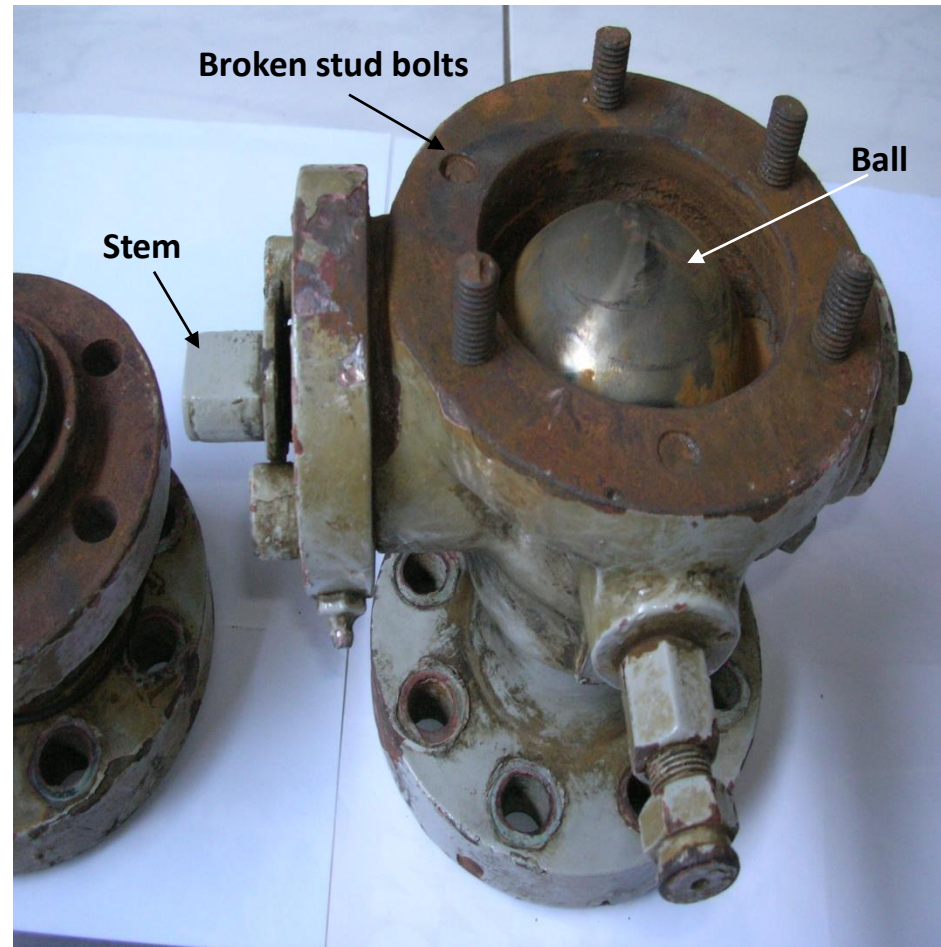
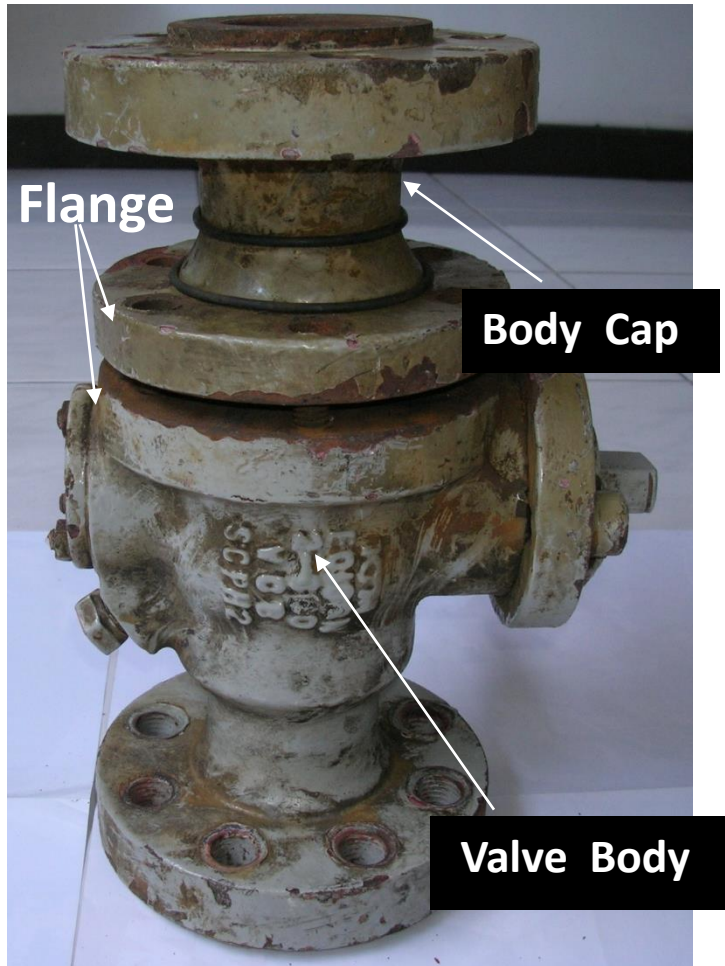


FAILURE ANALYSIS OF AN EXTRUDER GEAR PUMP SHAFT DUE TO FATIGUE (continued)



Microstructures obtained from a cross section located nearby the keyway 1 area, showing a homogenous and fine tempered martensite or bainite and no any significant defect was present.

FAILURE INVESTIGATION AND ANALYSIS OF FRACTURED STUD BOLTS OF A BYPASS BALL VALVE



FAILURE INVESTIGATION AND ANALYSIS OF FRACTURED STUD BOLTS OF A BYPASS BALL VALVE (continued)



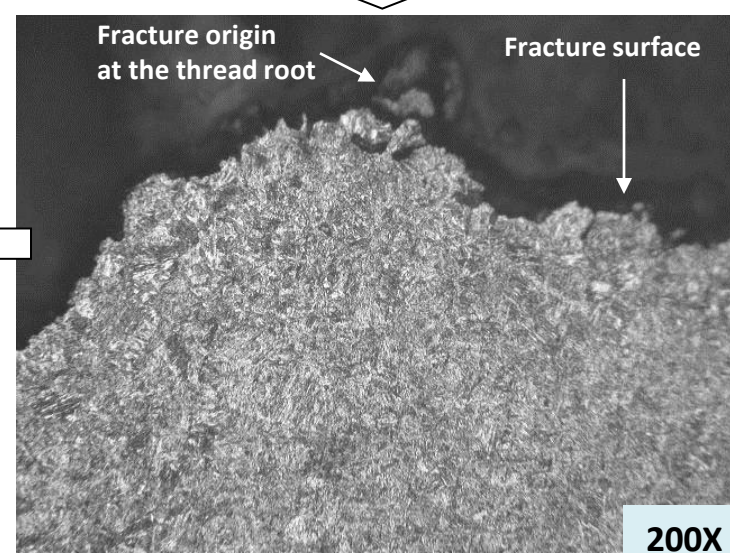
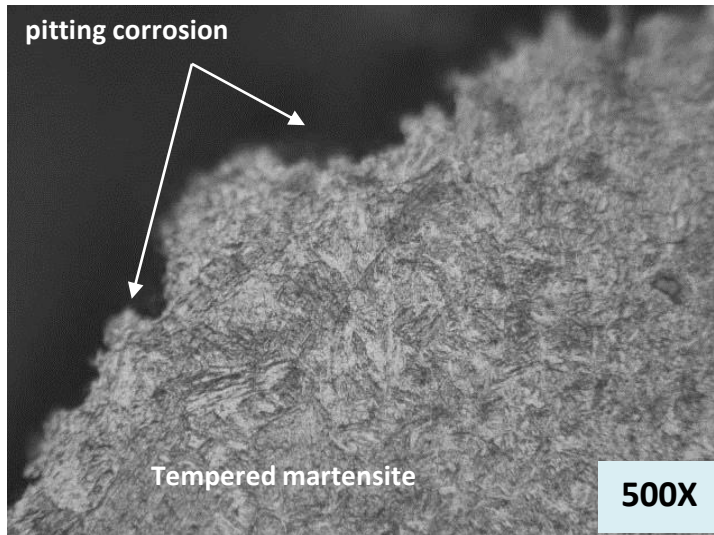
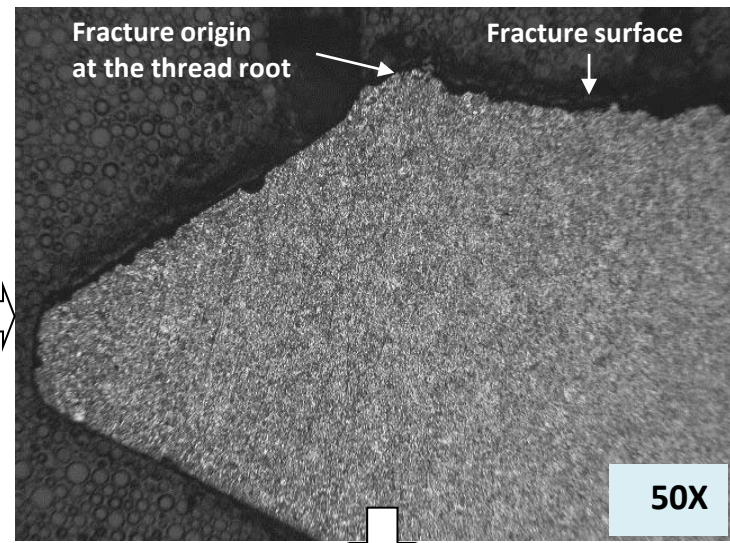
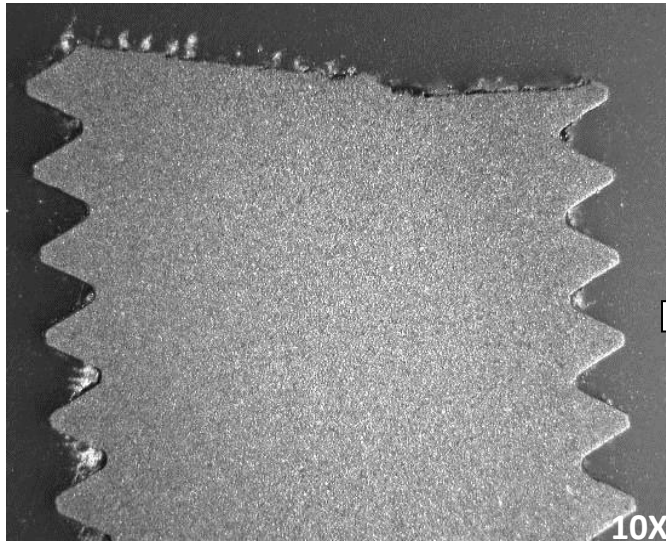
Close up view of the six broken stud bolts.

FAILURE INVESTIGATION AND ANALYSIS OF FRACTURED STUD BOLTS OF A BYPASS BALL VALVE (continued)

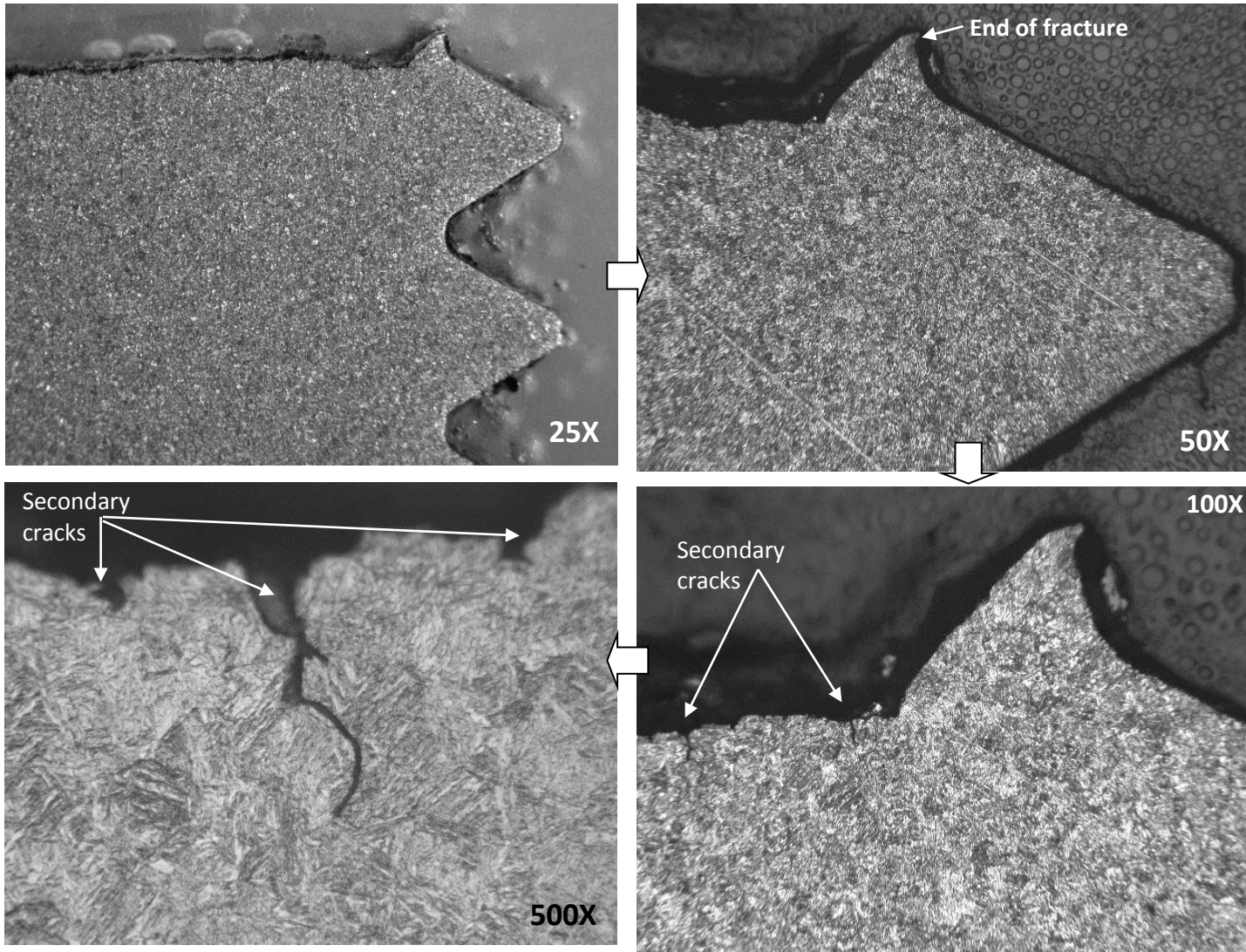


Fracture surfaces of the broken stud bolts showing chevrons or rays pattern.

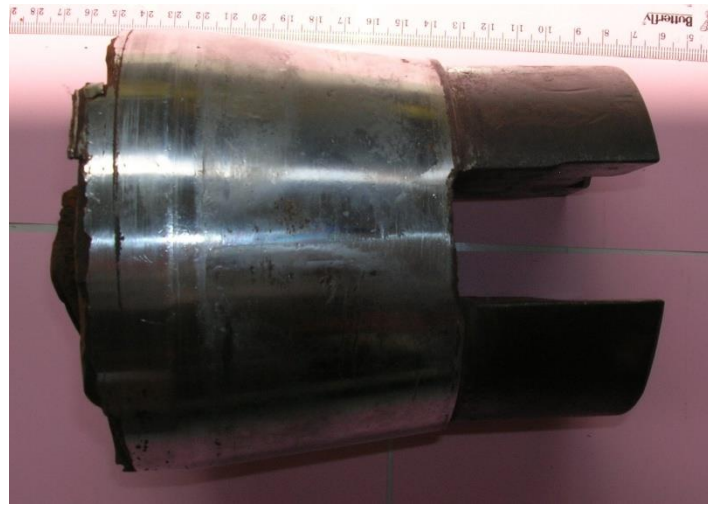
FAILURE INVESTIGATION AND ANALYSIS OF FRACTURED STUD BOLTS OF A BYPASS BALL VALVE (continued)



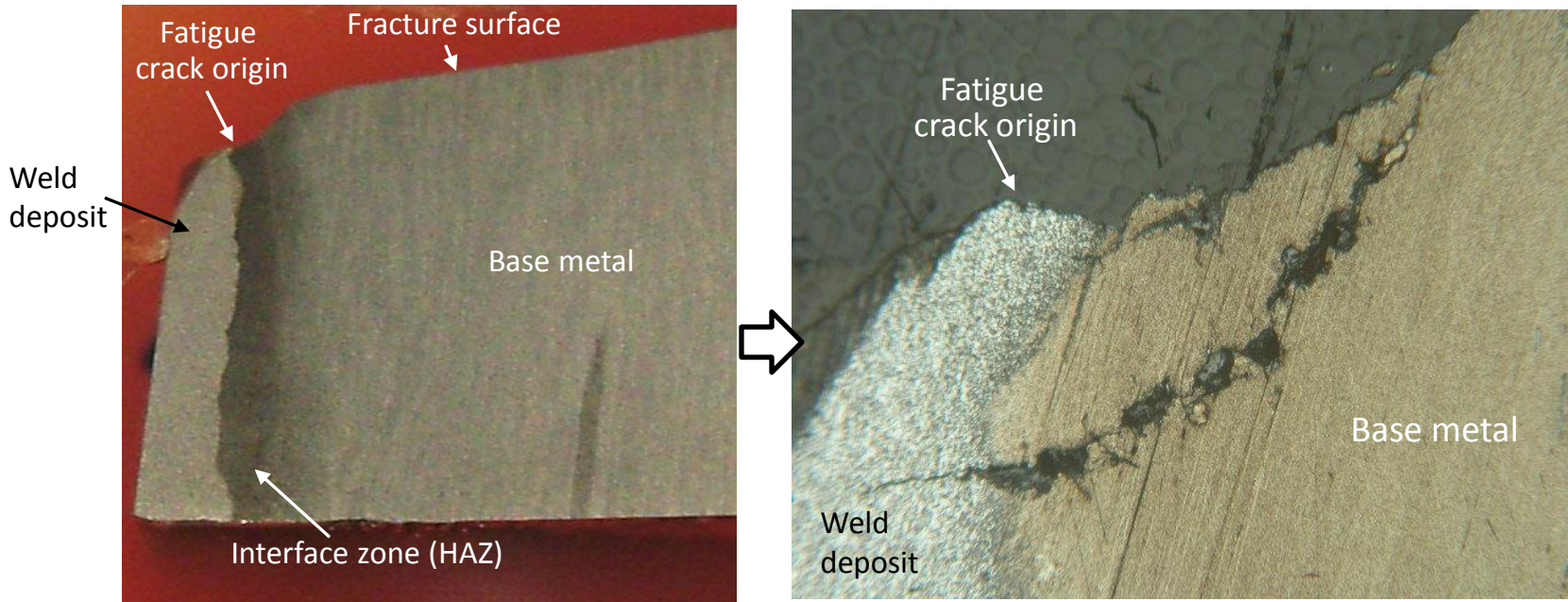
FAILURE INVESTIGATION AND ANALYSIS OF FRACTURED STUD BOLTS OF A BYPASS BALL VALVE (continued)



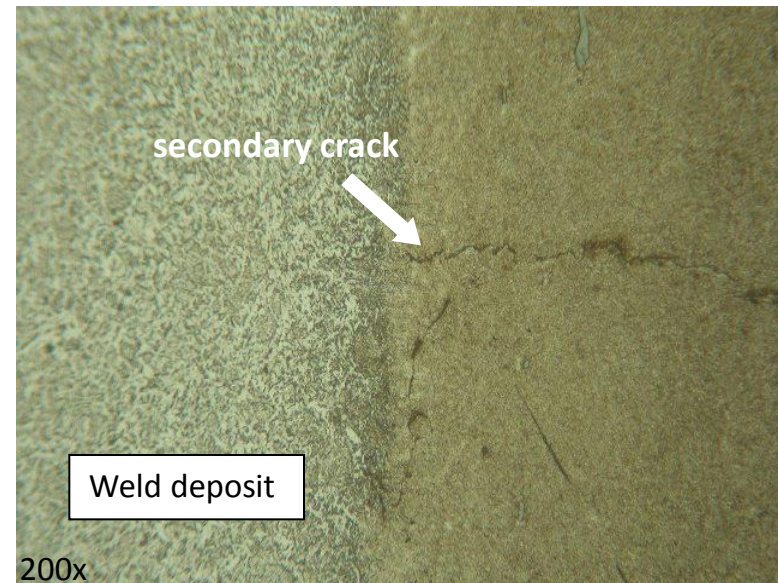
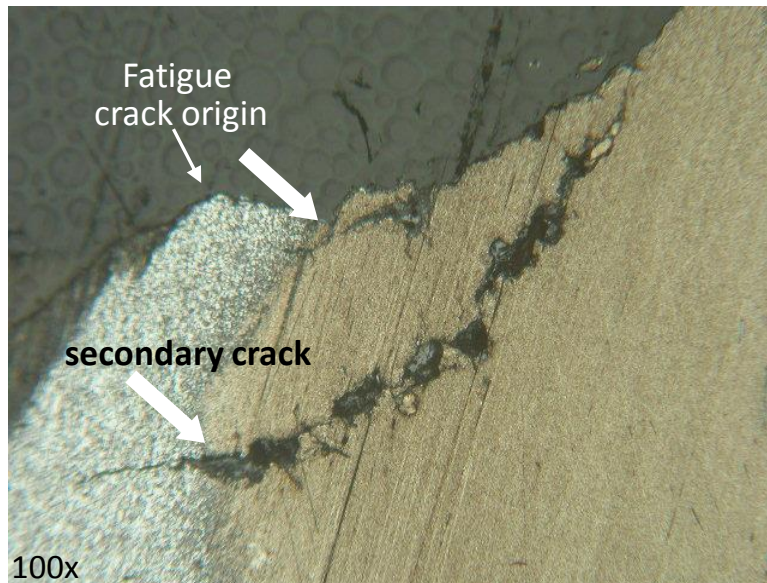
FAILURE ANALYSIS OF A BROKEN SHAFT OF SCR 3H ROLL MILL STAND



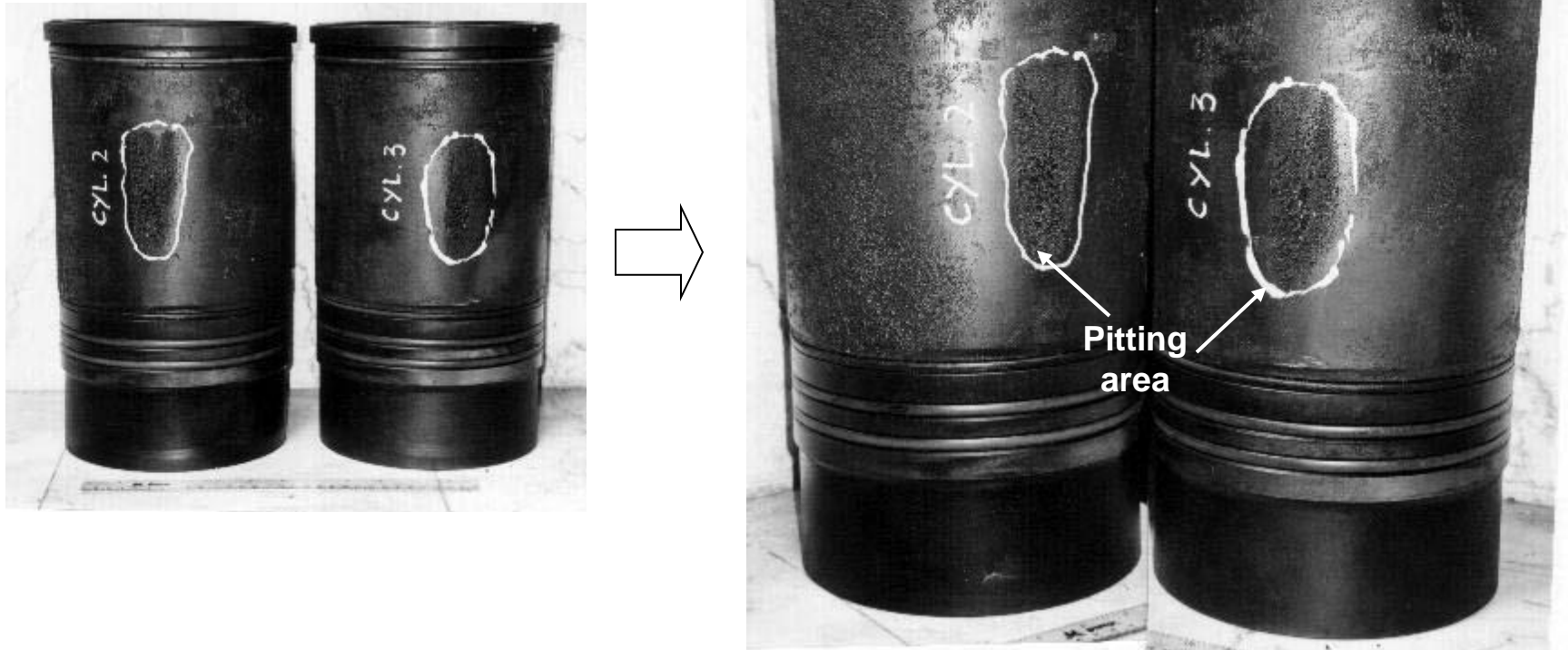
The as received fractured 3H roll mill stand shaft,
photographed from three different views.



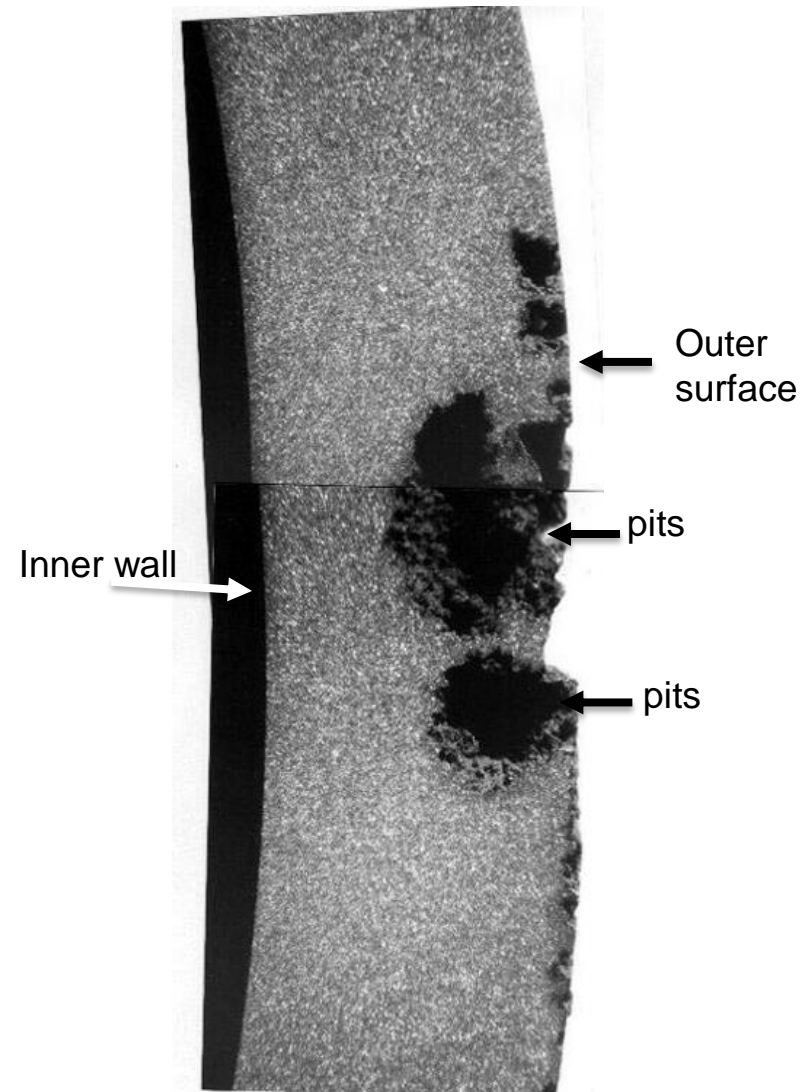
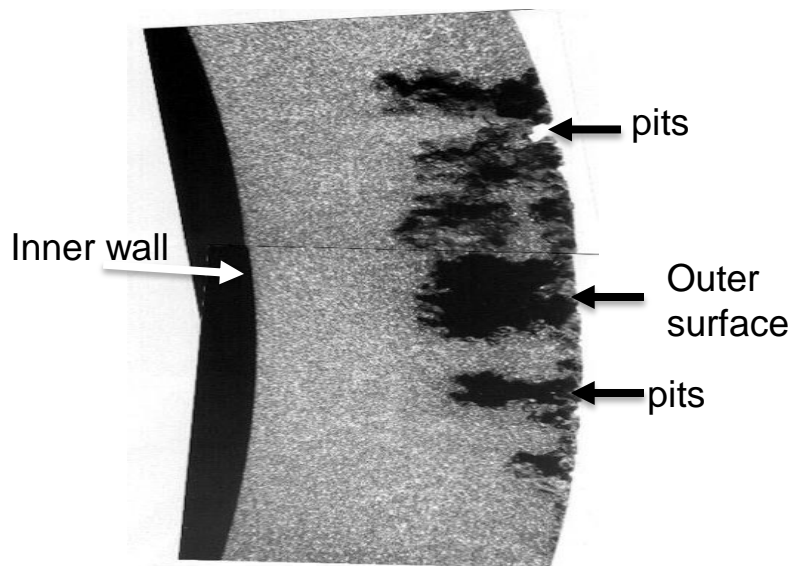
Longitudinal section of the fatigue fracture shaft showing its outer repaired weld metal deposit, interface zone (HAZ) and internal base metal part.



Microstructures showing some fatigue crack origin and secondary cracks (see arrows), originated from the outer weld deposit/ interface zone. This interface zone was considered as the heat affected zone (HAZ) of the repair weld. (This shaft was most likely rebuilt by welding)

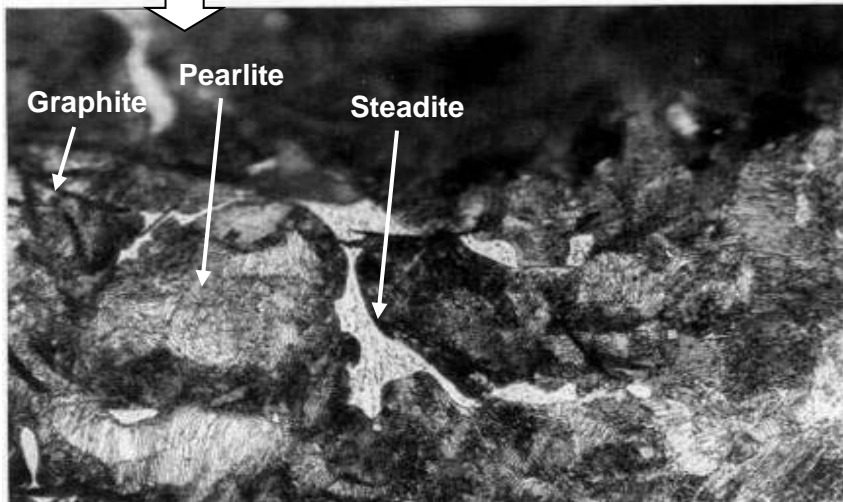
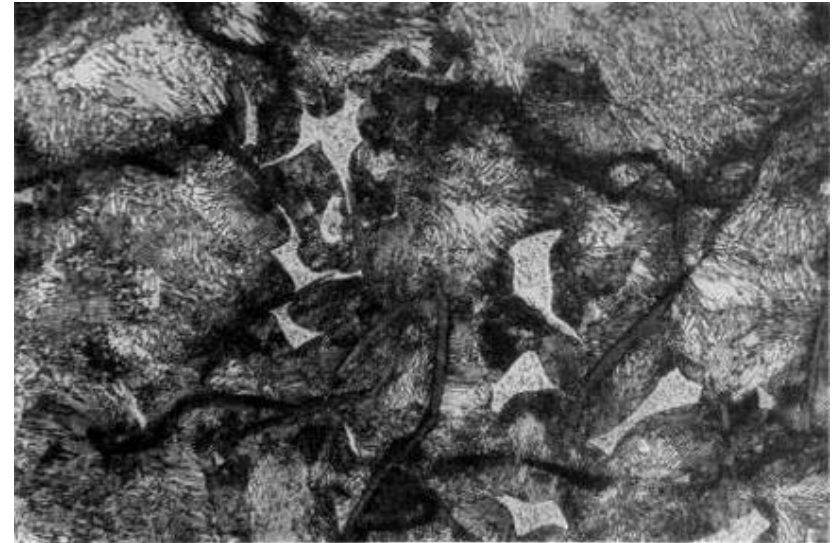
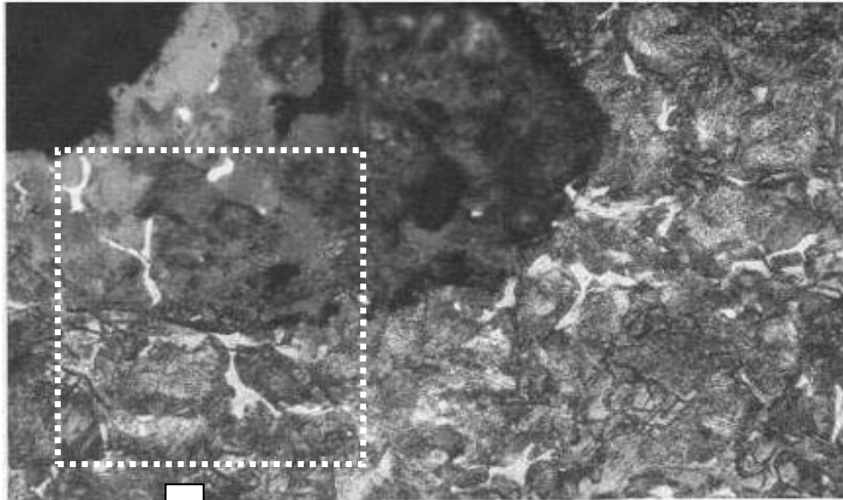


Photograph of two cylinder liners that had experienced erosion-cavitations



Macrostructures of the cross-section area of the cylinder liners no. 2 and no. 3 that had experienced erosion-cavitations.

FAILURE ANALYSIS OF CYLINDER LINERS OF DIESEL ENGINE DUE TO CAVITATION (continued)



Microstructures obtained from an area having with some pits of the cylinder liner no. 2, showing pearlite as matrix, flake graphite and steadite, typical of a pearlitic gray cast iron material containing high phosphor.



THANK YOU